National Library
of Canada

Acquisitions and
Bibliographic Services Branch

395 Wellington Street
Ottawa, Ontario
K1A 0N4

Bibliothèque nationale
du Canada

Direction des acquisitions et
des services bibliographiques

395, rue Wellington
Ottawa (Ontario)
K1A 0N4

Your file Votre référence

Our file Notre référence

NOTICE

The quality of this microform is heavily dependent upon the quality of the original thesis submitted for microfilming. Every effort has been made to ensure the highest quality of reproduction possible.

If pages are missing, contact the university which granted the degree.

Some pages may have indistinct print especially if the original pages were typed with a poor typewriter ribbon or if the university sent us an inferior photocopy.

AVIS

La qualité de cette microforme dépend grandement de la qualité de la thèse soumise au microfilmage. Nous avons tout fait pour assurer une qualité supérieure de reproduction.

S'il manque des pages, veuillez communiquer avec l'université qui a conféré le grade.

La qualité d'impression de certaines pages peut laisser à désirer, surtout si les pages originales ont été dactylographiées à l'aide d'un ruban usé ou si l'université nous a fait parvenir une photocopie de qualité inférieure.

Canada

Ultimate Strength and Buckling Behaviour of Stiffened Webs Used in Design of Steel Box Girder Bridges

Hong Chen

A Thesis

in

The Department

of

Civil Engineering

Presented in Partial Fulfillment of the Requirements
for the Degree of Master of Applied Science at
Concordia University
Montréal, Québec, Canada

September 1994

ISBN 0-612-01344-8

Canada

ABSTRACT

Ultimate Strength and Buckling Behaviour of Stiffened Webs
Used in Design of Steel Box Girder Bridges

Hong Chen

Results of an extensive parametric study on buckling behaviour and ultimate strength of box girder webs subjected to shear and combined shear and bending are reported in this thesis.

A theoretical model for analyzing the large deflection elasto-plastic response of the box girders with longitudinally unstiffened and stiffened webs is described.

Von Mises yield criterion and an associated flow rule were adopted and finite element method used to solve the plate equations. A total Lagrangian formulation was employed throughout this study associated with the full Newton method of iteration.

Comparisons of the predicted values using the present approach and previously published experimental and theoretical results confirm its soundness. Superiority of the discretely stiffened plate approach used in the present study for prediction of the buckling behaviour and ultimate strength of box girder

webs was proved by very good agreement of the former with the experimental results of physical models.

Realistic levels of residual stresses and initial geometric imperfections as well as a practical range of web subpanel aspect and slenderness ratios were considered in the parametric study.

Ultimate load curves applicable to design of box girders were defined for each type of stiffening. Based on results of the parametric study optimum position of longitudinal stiffeners was established.

It is concluded that the present study made a significant contribution towards a better understanding of buckling behaviour and ultimate strength of box girder webs.

To my wife Bing

and

my daughter Lucy

as well as

to my parents and my sister Mi

ACKNOWLEDGMENTS

The numerical investigation reported in this thesis was initiated under the supervision of Dr. E. Thimmhardy and Dr. M. M. Douglass and finalized under the co-supervision of Dr. E. Thimmhardy and Professor C. Marsh. I am deeply grateful to all of them for their guidance, criticism, constant encouragement and expert advice throughout the duration of the work. Special thanks are extended to Dr. E. Thimmhardy for the close working relationship which has been both professionally stimulating and personally joyful. I am also very pleased to record my gratitude to Professor C. Marsh who accepted to be my thesis co-supervisor after the sudden and tragic lost of Dr. M. M. Douglass in August 1992.

The financial support provided by the National Science and Engineering Research Council of Canada and Concordia University in carrying out this study is gratefully acknowledged.

Last but not least, special thanks are due to: my wife, Bing, for her invaluable support and patience; to my parents as well as my sister, Mi, for their continuous encouragement as well as to my recently born daughter, Lucy, who brought happiness and joy in our life.

TABLE OF CONTENTS

LIST OF TABLES

LIST OF FIGURES

NOTATIONS

a	length of plate panels between transverse stiffeners; side length of square plate panel
a/r	slenderness ratio
b	plate panel width
b/t	plate panel slenderness ratio
b_f	width of compression flange plate
C_{ijrs}	incremental material property tensor
e_{ij}	linear strain tensor
E	modulus of elasticity or Young's modulus
E_t	tangent modulus
F	yield function
h	depth of web plate
h_m	minimum depth of web subpanels
h_M	maximum depth of web subpanels
h_p	depth of web subpanel equal to h_m or h_M
h_p/t	slenderness ratio of web subpanel
H	hardening modulus
J_2	deviatoric stress tensor
L	length of cantilever box girder
M_r	factored bending moment resistance

M_u	ultimate bending moment resistance
M_y	bending moment required to produce yield in the extreme fibre of the compression flange
M_x, M_y, M_{xy}	plate moments per unit length
n	number of plate panel of stiffened plates
N_x, N_y, N_{xy}	membrane forces per unit length
p	applied uniform lateral load on plate panel; plate panel number
P	applied load on the tip of box girder
P_u	ultimate load
S_{ij}	second Piola - Kirchhoff stress tensor
S.S.	simply supported
t	thickness of plate panel
T.L.	total Lagrangian
V_r	factored shear resistance
V_u	ultimate shear resistance
V_y	yield shear force
w	thickness of web plate panel
w_c	central deflection of simply supported plates
Δ^0	initial deformation
Δ^0_p	initial out-of-plane deviation of plate panel
$\Delta^0_{p_m}$	initial out-of-plane deviation of smaller subpanel
$\Delta^0_{p_M}$	initial out-of-plane deviation of larger subpanel
Δ^0_s	initial out-of-straightness of stiffeners

δ	deflection
ν	Poisson's ratio
σ_a	average applied edge stress calculated by dividing the total applied load to the gross area of the stiffened plate
σ_{rc}	residual stress
σ_x	normal stress in x direction
σ_y	yield stress; normal stress in y direction
τ_{cr}	critical shear stress
τ_u	ultimate shear stress
τ_y	shear yield stress
ε_{ij}	Green-Laplace strain tensor

Matrix Notations

C^E	elastic stress - strain matrix
C^{EP}	elastic - plastic stress - strain matrix

CHAPTER 1

INTRODUCTION

1.1 Steel Box Girder Bridges — A Modern Type of Steel Bridges

Bridges have been and remain the great symbols of mankind's determination to remove all barriers in its pursuit to conquer the space.

In their continuous struggle to bring closer the peoples, communities and nations the bridge engineers have developed during the years new and better bridge types which allowed the efficient use of new materials and fabrication technologies. Among the latest developments, introduction of orthotropic steel deck concept and box girders in bridge design, represent the most important contributions which revolutionized the design of steel highway bridges.

The worldwide application and extensive use of orthotropic decks and box girder bridges are closely related to the post Second World War developments in welding technologies as well as the advances in structural theories which made possible the development of more efficient monolithic structures, in which plates are the principal elements.

Due to their efficiency, the orthotropic steel bridges became the favourite type of light-weight economical bridge construction for spans over 150 m. The

improved torsional resistance of single or multiple cell box girders proved highly advantageous especially when used in conjunction with the 'cantilever' type erection method for building bridges over great heights or wide rivers.

The Düsseldorf-Neus Bridge across the Rhine river with 103-206-103 m span box girders and a steel orthotropic deck opened to traffic in 1951, set this modern trend. Following this, many steel box girder bridges were built not only in Germany but also in other European countries.

In 1965, the first bridge of this type consisting of a single box girder was built in North America. It is the 690 m Concordia Bridge in Montreal, Canada. Following this in 1967, the first two steel box girder bridges having orthotropic decks were completed at nearly the same time in the USA. They were the San Mateo-Hayward Bridge in California and Poplar Street Bridge in St. Louis.

In the following years, the use of steel box girders in bridge construction has expanded rapidly all over the world and this is mainly due to the ideal distribution of metal resulting in great strength in bending and torsion. Such structures not only provide a saving in weight, but also reduce resistance to wind, improve aerodynamic stability, ease fabrication, construction and maintenance, and provide a graceful appearance.

Development of steel box girder bridges continued successfully until early 1970's when a series of collapses of steel box girder bridges occurred in Europe and Australia. Failure during erection of four large box girder bridges between 1969 and 1971 caused a general uneasiness about the reliability of the whole concept of the box girder as a structural element.

Based on official investigations on the causes of these accidents it was concluded that box girder bridges require more exact design, fabrication and erection methods and that they must be backed up by sufficient research.

In order to clarify and understand the behaviour of each component and of the whole box girder, extensive analytical and experimental research programs have been undertaken mostly in Europe [1 - 3].

Their preliminary conclusions were:

1. Thin, stiffened plates forming the flanges and webs of box girders require special analysis, taking into account, either explicitly or implicitly, the initial geometric imperfections and residual stresses produced during fabrication.
2. Classical linear plate buckling theory appears to be on the unsafe side in the design of steel box girder members, so that application of the ultimate strength theory of initial deformed stiffened panels should be considered in order to improve the existing situation. In this regard, an extensive research program on such panels must precede the development of design formulae.
3. The structural interaction between flange and webs of box girders is so different from plate girders that methods used in the design of plate girders cannot be extrapolated to box girder webs.
4. There appears to be insufficient knowledge of the ultimate capacity of complete or partially complete steel box girders and the proper evaluation of safety during construction and in-service depends on a sound understanding of behaviour at the ultimate states. To achieve this goal, more experimental research is needed.

The extensive experimental and theoretical investigations performed during the last twenty years on ultimate strength of steel box girders revealed that box girder design involves consideration of many effects which are of second order importance or non-existent in conventional single web plate girder design. Nonetheless, it represents an ideal way of building certain types of

bridges and none of the accidents which occurred, nor any research studies revealed any fundamental weakness of the box girder bridge concept.

1.2 Behaviour and Ultimate Strength of Steel Box Girder Components

Extensive use of box girders in design and construction of modern medium and long span steel bridges at national and international level is mainly related to application of welding to their fabrication. In the early stages of steel box girder design the effects of residual stresses and geometric imperfections induced during the fabrication process were overlooked; presently their deleterious effect on buckling behaviour and on the ultimate strength of box girder components has been clearly established and is considered either explicitly or implicitly in almost all bridge design codes.

Due to random variation of residual stressed and geometric imperfections their influence on overall buckling behaviour and ultimate strength of steel box girders and their components becomes an exceedingly complex problem to solve. For this reason, most of the experimental tests and analytical models were performed and developed for compression flanges which have been shown to be the most sensitive parts of the bridge structure [4]. Fewer tests and theoretical models have been focused on the webs and diaphragms [5, 6] and just a very few on complete steel box girders [1, 3, 4, 7].

Following the introduction of limit states design philosophy in bridge design codes at national and international level, the small displacement elasto-plastic models, that was the backbone of the linear plate theory, became unsuitable and has begun to be replaced by large displacement elasto-plastic models. The main advantage of the latter models is that they are more realistic

and account for the initial residual stresses and geometric imperfections induced in the real structures during fabrication and manufacturing processes.

In order to analyze the safety of steel box girder bridges and their components in the new context, it is necessary to consider and limit the magnitude of actual imperfections.

To define realistic values of tolerances, the magnitude of existing geometric imperfections of webs and compression flanges was investigated and statistically interpreted in both Europe [1 - 3, 7] and North America [4, 8].

Considering the results of the extensive experimental studies performed in Canada on ultimate strength and buckling behaviour of steel box girder bridges [4, 8], as well as theoretical investigations on ultimate load carrying capacity of their compression flanges [4, 9], an extension of the latter studies to the box girder webs was considered as absolutely necessary.

1.3 Aims and Scope of Thesis

The main goal of the research program performed and reported in this thesis was related to ultimate strength and buckling behaviour of stiffened webs used in design of Canadian box girder bridges. Being aimed at providing the necessary reliable data on which improvements of the existing design provisions can be drafted, three major criteria were considered. Firstly, an elasto-plastic finite element box girder model which accounts for both material and geometric nonliearities was developed and calibrated against the experimental models previously tested. Secondly, in order to generalize the limited experimental data to the wide range of stiffened webs currently used in box girder design, an extensive parametric study on the behaviour and ultimate strength of the transversely and longitudinally stiffened webs was performed. The study

considers the effects of: aspect and plate panel slenderness ratio; stiffener slenderness ratio; number of stiffeners; shear forces and bending moments; and initial geometric imperfections specific to Canadian bridges. Finally, ultimate load curves applicable to design of box girder webs with different stiffening systems are presented and discussed. Included also are comparisons of the ultimate shear resistance, predicted and calculated according to actual Canadian bridge provisions and recommendations for the design of webs stiffened with more than one stiffener for which presently no provision exists in the Canadian and international bridge design codes.

CHAPTER 2

ULTIMATE STRENGTH OF BOX GIRDER WEBS

2.1 Introduction

Design of medium and large box girder bridges implies in most cases the use of longitudinally and transversely stiffened webs in order to keep the web thickness within an economical range. Moreover, stiffeners increase the ultimate strength of girders by reducing nonlinear effects in the web and also help to provide sufficient strength and rigidity for transport and erection of the bridge girders.

Characteristically, these beams have wide stiffened flanges in which the flange plate thickness is comparable with that of webs. Consequently, the flange can only provide limited in-plane restraint to the longitudinal boundary of the outer web panel. This is in contrast to a plate girder, in which the much thicker and relatively narrow flange may provide considerable in-plane restraint.

For box girder webs stiffened longitudinally and transversely very little information is available about the interaction between the web subpanels and development of tension field. Referring to the former, the influence of the degree of in-plane boundary restraint on such behaviour is uncertain as is the extent to

which this restraint can be provided by an adjacent subpanel. For box girder webs subjected to combined shear forces and bending moments redistribution of longitudinal axial stresses is also affected by this behaviour.

For this type of webs in which the ultimate stages in the load carrying capacity usually involved some form of tension field, it is also unclear whether the tension field action can be developed in each subpanel, or whether, regardless of stiffener size, only a single tension field will be formed.

Understanding of orthogonally stiffened web behaviour is considered of major importance in providing a rational basis on which an ultimate strength theory can be formulated.

Derivation of a design procedure for stiffened webs, based on ultimate elasto-plastic behaviour, proves to be one of the most difficult tasks facing the code writers. The difficulties mainly arise because of the following factors;

1. The large variety of loading conditions encountered in practice, involving combination of bending moments, shear and axial forces in the plane of web.
2. The dependence of post-buckling resistance of web panels on the strength and stiffness of the boundaries. This applies particularly to the type of flanges, with a resulting interaction between design assumptions for webs and flanges.
3. The continuous change of stress distribution pattern in webs and flanges as the ultimate load carrying capacity of the girder approaches, resulting in shedding of bending stresses from webs to flanges.
4. The large variety of stresses acting on stiffeners under specified loading conditions.

Taking into account that ultimate load theories for transversely and orthogonally stiffened webs of plate and box girders are interrelated, the latter

mainly representing recent development of the former, a brief review of the theoretical and experimental work done in this area is presented in the following sections. Comments related to theoretical design provisions specified in international and national bridge design codes were also made and incorporated in the last section of this chapter.

2.2 Ultimate Strength of Transversely Stiffened Webs

To reduce the self-weight of the plate and box girders the web thickness is usually limited, with the consequence that the webs are normally of slender proportions.

In order to increase the buckling stress to satisfactory levels, transverse stiffeners are often employed to subdivide the web length into a number of smaller panels. The prime purpose of the stiffeners is to restrain the web panel boundaries from deflecting out-of-plane.

Even though until recently the design of plate girder web panels was based on the classical linear theory [10], it has been recognized for many years that web panels may exhibit a considerable post-buckling strength. This combined with the emergence of the limit state design philosophy, has led to the development of ultimate strength theoretical models for stiffened webs. These models, especially in their initial development stages, assumed that a tension field was developed in the panel once the critical shear buckling stress was exceeded, and this enabled load to be carried be a truss-type action. Capacity was then limited by yielding along a band across the web panel diagonal.

The ultimate strength tension field models, however, required the transverse stiffeners to carry considerable axial compressive forces.

Consequently, the stiffeners proportioned based on limiting elastic critical buckling stress levels were likely to be inappropriate.

The first ultimate strength model appropriate to conventional plate girders was developed by Basler [11-13] based on previously reported experimental results [14]. It was assumed that the girder flanges were unable to support the post-buckling tension field, and consequently, only a limited tension field developed between the transverse web stiffeners. It was indicated that the transverse stiffeners should satisfy two criteria. First, that the stiffeners had sufficient rigidity to enable the elastic critical buckling stress to be carried out by the panel. The second criterion was to ensure that the vertical component of the tension field force could be carried by the stiffeners.

Despite the limitations and consequences related to the collapse model in which the beam flanges are considered very flexible, Basler work represents a first and important contribution to the development of practical design provisions.

Subsequent tests performed by Rockey and Skaloud [15, 16] on plate girders subjected to shear showed that the flange rigidity had a major effect on the shear capacity of webs. Based on results of their experimental investigations, Rockey and Skaloud [16] developed empirical design formulas matching reasonably the test results.

Additional experimental and theoretical contributions to the subject were done by Chern and Ostapenko [17], Kamatsu [18], Porter et al. [19], Rockey et al. [20] and more recently by Horne and Grayson [21, 22].

Comparing the ultimate load capacity of tested plate girders with predicted theoretical values using some of the many models that have been proposed one can note in certain cases significant differences. These are partly due to the simplified assumptions considered in the ultimate strength models

and related to the angle and width of the tension band introduced in the theory. All models assuming the diagonal tension field anchored at the plate panel boundaries, cannot explain how an isolated panel with flanges having no bending strength can support high postbuckling forces. Arguing that postbuckling strength arises not by the action of diagonal tension, but by a nonuniform distribution of shear stresses along the boundaries, Marsh [23] suggested a different model in which the ultimate shear capacity of a plate girder is defined by the sum of the web and flange strength. Experimental investigation [24] as well as the parametric study performed on plate panels subjected to shear [25] confirm the validity of the Marsh model for shear webs of plate girders. Based on comparison with existing test results and other theoretical models Ajam and Marsh [26] developed design expressions able to predict the ultimate shear resistance of webs with no need for empirical adjustments. Similar expressions for the ultimate shear resistance of webs were also develop lately by Dubas [27] who modeled the web panel as diagonal strips in tension anchored by a corner zone carrying shear stresses only, which acted with the stiffeners in compression to form a "Pratt truss".

A theoretical model able to predict the stress variation and accompanying deformations of a web plate subjected to shear up to collapse load was developed more recently by Vilnay [28] who identifies three modes of the response of the shear webs: (i) the mode where the shear force is sustained by a uniformly distributed shear stress at the boundaries of the web, (ii) the mode where it is sustained by nonlinear distribution of shear stress at the boundaries, and (iii) the mode where a tensile band is developed.

Considering the importance of transverse stiffener rigidity on ultimate shear resistance of plate girders, Rahal and Harding [29] performed a parametric study on behaviour of transverse stiffeners used in plate girders subjected to

shear loading. Both material and geometric nonlinearities were considered in the numerical analysis. Showing that web panel capacity varies with the stiffener size the authors conclude that stiffener bending rigidity is of major importance for design. Based on results of the parametric study a simple analytical model is formulated and considered appropriate for use in design of transverse stiffeners [30].

Results of experimental and theoretical investigations on transverse stiffener behaviour and design were previously reported by Rockey et al. [31].

Taking into account that most of the plate girders used in civil engineering are subjected not only to shear but to combined shear and bending moment, extensive experimental and theoretical studies were performed during the last three decades on their ultimate strength and behaviour.

Among the most important early contributions, the experimental and subsequent theoretical studies of Ostapenko and Chern [32, 33] are worth noting.

Based on test results performed on twenty plate girders it was concluded that:

1. The interaction curve between moment and shear consists of two portions: web failure which occurs under dominant shear and flange failure which occurs under dominant moment.
2. The force in the flange for the flange failure mode results from superimposing effect of bending moment and the component of the force due to a partially developed tension field.

Subsequent studies aimed at providing the needed experimental data on which new design provisions could be drafted were done by Evans et al. [34]. Based on test results of fifty eight plate girders it is shown that the following additional factors must be considered in defining the ultimate load carrying capacity of plate girders subjected to combined shear and bending:

- Reduction of the buckling stresses in the web plate due to the presence of the bending stresses.
- Influence of bending stresses upon the magnitude of the membrane stresses required to produce yield in the web.
- Influence of load shedding from the web to the beam flanges as a consequence of buckling.
- Reduction of the plastic moment capacity of the flanges by the axial stresses arising from bending moments.

More recently, the experimental and theoretical studies performed by Horne and Grayson [21, 22] made new and valuable contributions to better understanding of ultimate strength and behaviour of plate girders subjected to combined shear and bending. In their studies the behaviour of web panels subjected to different combinations of applied boundary strains, as well as the influence of panel geometry on this behaviour was investigated.

Even though experimental and theoretical studies on transversely stiffened webs are related mostly to plate girders, some attempts in defining the affect of reduced flange thickness, specific to box girders, on ultimate strength of webs are to be noted. Among these contributions are the works of Rockey et al. [5], Horne and Grayson [21, 22], Puthli et al. [35] and Dowling et al. [1].

Presently, there is a general agreement that the relatively low bending stiffness of box girder flanges limits the applicability of the tension field concept to the girder webs, reason for which a modified Basler formula was proposed by Wolchuk and Mayrbaurl [36] for ultimate shear resistance of webs. Test results reported by Mele and Puhali [37] on box girders with webs without longitudinal stiffeners and low aspect ratio ($a/b = 2/3$) have demonstrated that proposed formula leads to a conservative solution.

2.3 Ultimate Strength of Orthogonally Stiffened webs

The slenderness limitations imposed on plate and box girder webs used for medium and long span bridges require the use of combined transverse and longitudinal stiffeners. Without this an uneconomical web thickness would be necessary.

The postbuckling behaviour of orthogonally stiffened plate girders is not fundamentally different from that of girders with only transverse stiffeners. Consequently, this section will be restricted only to those aspects of web behaviour not covered previously.

The fundamental role of both longitudinal and transverse stiffeners is to provide nodal lines for the buckling of the web subpanels. The present design provisions [38] for webs require the stiffeners to be designed such that they remain rigid until the ultimate limit load of the web is reached.

In the case of orthogonally stiffened webs, the ultimate capacity of the stiffened web plate frequently requires the determination of the load carrying capacity of the individual subpanels formed by the stiffeners. The capacity of the stiffened web is then defined based on the lowest subpanel ultimate resistance [27].

Regarding the optimum location of longitudinal stiffeners, it should be noted that this is mainly related to the type of in-plane loads and load combinations acting on the web.

In the case of pure shear, the stiffeners should be spaced equally so as to divide the web into equal subpanels, in which case the shear buckling capacities of the subpanels are equal.

When bending moments act in combination with the shear forces on the web, the stiffener spacing has to be adjusted so that the subpanels subjected to the highest compressive stresses are smaller than the others.

Taking into account that the ultimate strength of webs stiffened longitudinally and transversely depends on the web slenderness ratio, web aspect ratio, the axial and bending rigidity of girder flanges and the number of longitudinal stiffeners, experimental and theoretical studies have been performed during the last three decades in an attempt to develop simple, reliable ultimate resistance models to be used in design calculations.

Referring first to the ultimate load models developed for orthogonally stiffened webs subjected to shear, the following contributions are considered to be very important.

Assuming that each subpanel in an orthogonally stiffened web develops its own tension field after buckling, in the direction of the subpanel diagonal, Cooper [39, 40] developed one of the first ultimate shear models. Based on this model, the subpanel shear resistance is the sum of the shear at buckling load and the transverse component of its tension field; thus, the shear resistance of web is the sum of the individual shear resistance of the component web subpanels. The longitudinal stiffeners have to equilibrate the horizontal components of the tension field and consequently they are highly loaded.

Rockey et al. [5, 20, 41, 42], Porter et al. [19] and Mele and Puhali [37], suggest that a single tension field develops independently of the longitudinal stiffeners. The girder shear resistance can be defined using the same formula proposed earlier for transversely stiffened webs provided the critical shear stress is the one corresponding to the weakest subpanel. On this basis, it may be assumed that the main effect of the longitudinal stiffeners is to increase the buckling resistance of the web.

Recently, Ostapenko [43] presented a comparison between four ultimate strength models for longitudinal stiffened plate girders, using the same basic shear strength formulation as for transversely stiffened plate girder webs. The basic assumption used in this study was that the ultimate shear capacity of a plate girder consists of three components corresponding respectively to the critical buckling shear of the web plate, the tension field and frame action.

Ultimate resistance models for orthogonally stiffened plate girders subjected to combined shear and bending moments were developed by Rockey et al. [5, 20] and Evans et al. [34, 44]. Based on their studies interaction diagrams and simple design formulae for calculation of ultimate resistance of plate girders were developed.

Extending the investigations to box girder bridges, Dowling et al. [1] performed a series of experimental studies aimed at identifying the behaviour and ultimate strength of box girders subjected to shear and combined shear and bending. The effect of initial residual stresses and geometric imperfections on load carrying capacity of webs and compression flanges was monitored and reported for each box girder.

More recent experimental and numerical investigations on behaviour and ultimate strength of box girder webs subjected to shear and combined shear and bending moments were presented by Horne and Grayson [21, 22].

In their studies the interaction between adjacent subpanels down the depth of the girder web was considered. The influence of plate panel geometry on web behaviour was also investigated. The experimentally determined ultimate loads were compared with results of large defection elasto-plastic finite element analyses in which both material and geometric nonlinearities were included.

It is beyond the scope of this study to review in depth all the existing works related to ultimate strength of plate girders and the reader is referred for a fuller coverage to the references [27, 45- 48].

2.4 Limitations of Existing Codes

As shown earlier very little research information exists for buckling behaviour and ultimate strength of box girder webs stiffened transversely and orthogonally.

In particular there is a lack of experimental data against which numerical models can be calibrated and used in performing reliable parametric studies.

Even though some of the ultimate resistance models developed for plate girders have been incorporated in the bridge design codes, in most cases with some modifications able to satisfy the design criteria, there are no specific provisions for box girder webs at national [38, 49] and international levels [50], except the British one [51].

Referring only to Canadian bridge design codes CAN/CSA-S6-88 [38] and Ontario Highway Bridge Design Code [49] one can note, as stated in the commentaries to the former (Clause 7.18.3), that even for the plate girder webs the design provisions "are based on research conducted by Basler and Thurlimann [11-13]. Although more recent research [48, 52] indicates that the Basler-Thurlimann approach may be somewhat conservative, particular for girders with substantial flanges, incorporation of some of the new concepts in bridge design rules require further development work. The Basler-Thurlimann approach has been retained in this Standard for the present."

For design of very deep girders, the same clause specifies that transverse stiffeners used in conjunction with longitudinal stiffeners should be considered.

However design provisions are given for webs stiffened with only one longitudinal stiffener placed at a distance of 0.2h from the inner surface of the compression flange (Clause 7.18.5).

In both Canadian codes [38, 49] as well as the American one [50] there is no provision for designing webs with more than one longitudinal stiffener, though these are commonly used in box girders. Taking into account the lack of a reliable ultimate strength model for webs stiffened with more than one longitudinal stiffener, the recommendations for the plate girder webs that "design shall be based on a rational method of analysis" has practically no applicability to design.

Aiming at providing a set of reliable data on which design provisions for box girder webs stiffened with more than one longitudinal stiffener, a nonlinear finite element model was developed and calibrated against available experimental data as shown in Chapter 3. Further, this numerical model was used in performing the parametric study described in Chapter 4.

CHAPTER 3

NONLINEAR ANALYSIS OF STIFFENED WEBS USED IN BOX GIRDER BRIDGES

3.1 Objective of Present Study

The buckling behaviour and ultimate strength of stiffened webs of box girder bridges may be studied by either experimental or numerical methods. For stiffened web plates the geometric parameters governing their behaviour are: stiffener geometry and arrangement; aspect ratio of plate panels between stiffeners; plate panel slenderness ratio; stiffener slenderness ratio; initial geometric imperfections; and material nonlinearity.

If a deterministic approach is to be adopted for the analysis, all of these parameters must appear in the mathematical formulation. Due to the extreme complexity in the theoretical treatment of the effects of material and geometric nonlinearity on buckling behaviour and on the ultimate strength of stiffened web plates a closed-form solution does not exist. If an experimental program were to investigate the influence of each and all of these parameters, an enormous amount of time and money would be required. The approach generally adopted is to develop numerical models and check them against experimental results. Subsequently, numerical simulations using computer

programs are used to perform parametric studies and generalize the results of experimental studies.

In view of the fact that very little information is available on the ultimate load carrying capacity of box girder webs stiffened with more than one longitudinal stiffener, a parametric study on buckling behaviour of this structural component of box girders was considered necessary.

The finite element model developed and used in performing the parametric study simulated the box girder model tested previously [8]. Even though the decision to model the complete box girder led to a increased effort and computer time, this was considered the best solution for getting the most reliable information on web behaviour in relationship with stiffened compression flange rigidity and their interaction.

The major assumptions made in this study are:

- the material of both plates and stiffeners behaves in an ideal elastic perfectly plastic manner; strain hardening is not considered.
- neither lateral bending nor twisting of the longitudinal stiffeners can occur, thus the stiffener failure is assumed to occur through yielding with no associated local buckling. This is a reasonable assumption which complies with the general requirements that stiffeners must remain fully effective until the ultimate capacity of the box girder is reached.
- the shear stress in the stiffener is small, and does not influence stiffener yielding, i.e. only axial direct stresses contribute to stiffener yielding.
- local or overall buckling of the compression flange does not occur before ultimate load carrying capacity of box girder webs is reached.

Both geometric and material nonlinearities are considered in this numerical analysis. Plasticity in the plate and stiffeners is assumed to be governed by the von Mises yield criterion associated with the classical flow theory. The governing nonlinear equations are solved numerically in conjunction with specified boundary conditions using the finite element method. Total Lagrangian formulation is adopted and large displacements, large rotations but small strains are assumed in the analysis.

To accurately control the loading process and identify the peak shear forces and bending moments acting on the box girder, concentrated vertical loads were applied incrementally at the tip of the cantilever beams such that at the end of each increment the elasto-plastic rigidities could be calculated for use in the next increment.

The soundness of the present finite element model has been validated by comparison with the existing experimental data and other large deflection elasto-plastic analysis, using either the finite element formulation or alternative theoretical approaches.

In performing this study the finite element computer program ADINA available at Concordia University was used. Time dependent loads are applied to the structure in the ADINA program by means of time functions. Using this assumption in static analysis, time is only a convenient variable which defines different load intensities and correspondingly different configurations. In nonlinear analysis, the finite element system response in effectively evaluated using an incremental step-by-step solution of the equilibrium equations. In this case the basic approach is to assume that the solution for time t is known, and that the solution for the discrete time $t+\Delta t$ is required, where Δt is a suitable chosen time increment.

3.2 Basic Equations

In the total Lagrangian formulation all static and kinematics variables are referred to the initial configuration at time 0 and the basic virtual work expression using 2nd Piola-Kirchhoff stress and Green-Lagrange strain tensor is

$$\int_{0_V} {}^{t+\Delta t}_{0}S_{ij}\ \delta\ {}^{t+\Delta t}_{0}\varepsilon_{ij}\ {}^{0}dV = {}^{t+\Delta t}R \tag{3.1}$$

where

$${}^{t+\Delta t}R = \int_{t+\Delta t_V} {}^{t+\Delta t}f_i^B\ \delta u_i\ {}^{t+\Delta t}dV + \int_{t+\Delta t_S} {}^{t+\Delta t}f_i^S\ \delta u_i^S\ {}^{t+\Delta t}dS \tag{3.2}$$

An approximate solution to (3.1) can be obtained by linearizing this equilibrium equation of motion as

$$\int_{0_V} {}_0C_{ijrs}\ {}_0\varepsilon_{rs}\ \delta\ {}_0\varepsilon_{ij}\ {}^{0}dV + \int_{0_V} {}^{t}_{0}S_{ij}\ \delta\ {}_0\eta_{ij}\ {}^{0}dV = {}^{t+\Delta t}R - \int_{0_V} {}^{t}_{0}S_{ij}\ \delta\ {}_0e_{ij}\ {}^{0}dV \tag{3.3}$$

Term definition and further details regarding the finite element equilibrium equation used in ADINA program are given in references [53, 54].

3.3 Choice of Elements

The choice of element geometry used in the present analysis was based on a careful review of the finite elements available in the library of the ADINA program and some comparative tests. Finally, the eight-node shell element and three node isoparametric beam element have been proved to be the most suitable for discretization of the plate and stiffeners, respectively. Using this combination the analysis of stiffened plates is effectively performed with the current version of ADINA.

The eight-node shell element has six degrees of freedom per node corresponding to the local coordinate axes.

The beam element is a three-node isoparametric beam with six degrees of freedom per node. The element matrices are evaluated using Gauss or Newton-Cotes numerical integration. In elastic-plastic analysis, the stress-strain matrix is modified to include the effect of plasticity. This stress-strain matrix is based on the classical flow theory associated with the von Mises yield condition and is derived from the three-dimensional stress-strain law with the appropriate stresses and strain set to zero.

A more detailed discussion of the shell and isoparametric beam elements is given by Bathe [53].

3.4 Meshes

The accuracy achieved in a finite element analysis is related to the number of nodes used in defining the mesh. Refining the mesh of any structural component generally requires an increase in the number of elements in the other components. To define the optimum mesh size from the point of view of computing cost and accuracy of the results, two trials were performed using different numbers of nodes and configurations:

1. A simply supported square plate subjected to uniform lateral load (Figure 3.1).
2. A simply supported square plate with initial imperfections subjected to uniform axial compressive load (Figure 3.2).

3.4.1 Simply Supported Square Plate Subjected to Uniform Lateral Load

For the thin plate with simply supported edges and subjected to uniform lateral loads (Figure 3.1) a linear analysis was performed using the meshes and the three type of shell elements shown in Figure 3.1.(1), Figure 3.1.(2) and Figure 3.1.(3).

The theoretical linear solution for this problem is given by Timoshenko [55] and the expression for the central deflection is given by:

$$w_c = 0.00126\, pa^4 / D$$

where

p = uniform lateral load

a = side length

$$D = \frac{Et^3}{12(1-\nu^2)}$$

The stress expression at the top of plate in central area is given by:

$$\sigma_x = \sigma_y = -0.1386 \cdot \frac{pa^2}{t^2}$$

The results of central deflections and top surface stresses for the three types of meshes considered are given in Table 3.1. Comparing the central deflection and stresses determined from finite element analysis with those predicted using theoretical solution one can note that in each case a very close result is obtained. However, comparing the CPU time used in each case, the mesh with 4-node element is found to be the most efficient one.

3.4.2 Simply Supported Square Plate with Initial Imperfections Subjected to Uniform Axial Compressive Load

The square plate considered in the analysis is shown in Figure 3.2. The plate is simply supported on all edges and uniform axial compressive loads are applied at two opposite edges. Four different meshes and shell elements, as shown in Figure 3.2.(1) to Figure 3.2.(4), were used in order to define the optimum one. Using symmetry conditions, only one-quarter of the plate was modeled. The initial imperfection at the center of the plate was defined by:

$$w_o(x,y) = \frac{t}{100}\left(1-\frac{2x}{a}\right)\left(1-\frac{2y}{a}\right)$$

The above equation represents a linear approximation to the first buckling mode shape of the perfect plate. The load was applied in ten equal load steps and a geometrically nonlinear analysis with stiffness reformation and BFGS (Broyden-Fletcher-Goldfarb-Shanno) equilibrium iterations in each step was performed. Comparing the results given in Table 3.2 for the four type of meshes it is observed that the mesh with 8-node element is the most efficient one.

3.5 Constitutive Equations

The fundamental distinction between an elastic and elasto-plastic analysis lies in that in the latter the stress-strain relationship at time t depends on the stress and strain history. To define the inelastic response of the structure an incremental stress-strain relation must be established.

As previously shown, the basic equation (3.3) employed in this study to calculate the incremental displacements is the incremental virtual work equation of total Lagrangian formulation. Therefore, this formulation can be applied directly to describe the material behaviour.

Using the usual approach of flow theory, three other properties in addition to the elastic stress-strain relation must be specified to describe the elastic-plastic behaviour of a material:

1. a yield criterion, which defines the multiaxial stress state at the onset of plastic flow.

2. a flow rule, which provides the constitutive relations relating the incremental plastic strains to the current state of stress and the stress increments subsequent to yielding.

3. a hardening rule, which specifies the changes in the yield condition during plastic flow.

Details regarding the incremental theory of plasticity can be found in references [56-58].

For the isothermal conditions and isotropic hardening material considered in this study, the yield can be defined at time t as

$$ {}^{t}F\left({}^{t}\sigma_{ij}, {}^{t}k\right) = 0 \tag{3.4} $$

where ${}^{t}k$ is state variable which depends on the plastic strains ${}^{t}e_{ij}^{P}$. Using the normality principle and restricting the analysis to an associated flow rule, the function ${}^{t}F$ in equation (3.4) can be used to calculate the plastic strain increments

$$ de_{ij}^{P} = {}^{t}\lambda \frac{\partial {}^{t}F}{\partial {}^{t}\sigma_{ij}} \tag{3.5} $$

where ${}^{t}\lambda$ is a proportionality factor still to be determined. Since during plastic deformation ${}^{t}F = 0$, the differential of this function yields

$$ \frac{\partial {}^{t}F}{\partial {}^{t}\sigma_{ij}} d\sigma_{ij} + \frac{\partial {}^{t}F}{\partial {}^{t}e_{ij}^{P}} de_{ij}^{P} = 0 \tag{3.6} $$

where $d\sigma_{ij}$ and de_{ij}^{P} are differential increments in stresses and plastic strains.

To evaluate the stress increments the relation

$$d\sigma = C^{E}\left(de - de^{P}\right) \tag{3.7}$$

is used, where C^{E} is the elastic stress-strain matrix. Using for convenience the following notation

$${}^{t}q_{ij} = \frac{\partial^{t}F}{\partial^{t}\sigma_{ij}}; \qquad {}^{t}p_{ij} = \frac{\partial^{t}F}{\partial^{t}e_{ij}^{P}} \tag{3.8}$$

or in matrix form

$$\begin{aligned} {}^{t}q^{T} &= \left[{}^{t}q_{11}\ \ {}^{t}q_{22}\ \ {}^{t}q_{33}\ \ 2^{t}q_{12}\ \ 2^{t}q_{23}\ \ 2^{t}q_{31}\right] \\ {}^{t}p^{T} &= \left[{}^{t}p_{11}\ \ {}^{t}p_{22}\ \ {}^{t}p_{33}\ \ {}^{t}p_{12}\ \ {}^{t}p_{23}\ \ {}^{t}p_{31}\right] \end{aligned} \tag{3.9}$$

the scalar ${}^{t}\lambda$, can be defined based on (3.5) to (3.7) as

$${}^{t}\lambda = \frac{{}^{t}q^{T}C^{E}de}{{}^{t}p^{T}{}^{t}q + {}^{t}q^{T}C^{E}{}^{t}q} \tag{3.10}$$

Substitution of (3.5) and (3.10) into (3.7) yields

$$d\sigma = C^{EP}de \tag{3.11}$$

where the C^{EP} represents the instantaneous elastic-plastic stress-strain matrix:

$$C^{EP} = C^{E} - \frac{C^{E}{}^{t}q\left(C^{E}{}^{t}q\right)^{T}}{{}^{t}p^{T}{}^{t}q + {}^{t}q^{T}C^{E}{}^{t}q} \tag{3.12}$$

The above stress-strain relation depends on the yield function ${}^tF$ and consequently for each yield function ${}^tF$ assumed, related yield criteria can be derived.

In the case of the Von Mises yield criterion with isotropic hardening, applied for beam elements in this study, the yield function ${}^tF$ is given by

$$ {}^tF = J_2 - \frac{1}{3}{}^t\sigma_y^2 \tag{3.13} $$

where J_2 is the second invariant of the deviatoric stress tensor defined by

$$ J_2 = \frac{1}{2}\, {}^ts_{ij}\, {}^ts_{ij} \tag{3.14} $$

in which the ${}^ts_{ij}$ are the deviatoric stresses

$$ {}^ts_{ij} = {}^t\sigma_{ij} - \frac{{}^t\sigma_{mm}}{3}\delta_{ij}; \qquad {}^t\sigma_{mm} = \sum_m {}^t\sigma_{mm} \tag{3.15} $$

$$ \delta_{ij} = \begin{cases} 0 & \text{for} \quad i \neq j \\ 1 & \text{for} \quad i = j \end{cases} $$

and ${}^t\sigma_y$ is the yield stress at time t.

This yield stress is a function of the plastic work per unit volume ${}^tW_P$ defined as

$$ {}^tW_P = \int_0^{{}^te_{ij}^P} {}^t\sigma_{ij}\, de_{ij}^P \tag{3.16} $$

Evaluating ${}^tq_{ij}$ and ${}^tp_{ij}$ yields

$$ {}^tq_{ij} = {}^ts_{ij}; \qquad {}^tp_{ij} = {}^tH\, {}^t\sigma_{ij} \tag{3.17} $$

where

$$^{t}H=\frac{2}{3}\,^{t}\sigma_y\frac{d\sigma_y}{dW_p} \tag{3.18}$$

For strain hardening materials where data from simple axial tension tests are available

$$^{t}H=\frac{2}{3}\left(\frac{EE_t}{E-E_t}\right) \tag{3.19}$$

where E is the Young's modulus and E_t the tangent modulus.

3.6 Geometric Imperfections

Initial deformations of stiffened plates are included in nonlinear analysis of compression flanges and webs by specifying a continuous function $\Delta^0(X,Y)$ and $\Delta^0(X,Z)$ respectively, from which initial nodal displacement can be evaluated. This function has been defined to simulate closely the initial deformations of plate panels and stiffeners encountered in real bridges and is expressed as:

a) for the bottom flange of a box girder (Figure 3.3.a)

$$\Delta^0(X,Y)=(-1)^{p-1}\Delta_p^0\sin\left(\frac{\pi X}{a}\right)\cos\left(\frac{\pi Y}{b}\right)+\alpha^m\Delta_s^0\sin\left(\frac{\pi X}{a}\right) \tag{3.20.a}$$

where

$$\alpha=(2.5-Y/b)\quad\text{for}\quad p=n \qquad\qquad m=\begin{cases}0 & \text{for } 1\le p<n\\ 1 & \text{for } p=n\end{cases}$$

b) for the web of a box girder (Figure 3.3.b)

at $(h - h_M) \geq Z \geq 0$

$$\Delta^0(X,Z) = (-1)^k \Delta^0_{p_m} \sin\left(\frac{\pi X}{a}\right)\sin\left(\frac{\pi Z}{h_m}\right) - \alpha_m^k \Delta^0_s \sin\left(\frac{\pi X}{a}\right) \qquad (3.20.b)$$

at $h \geq Z > (h - h_M)$

$$\Delta^0(X,Z) = (-1)\Delta^0_{p_M} \sin\left(\frac{\pi X}{a}\right)\sin\left[\frac{\pi(Z-2h_m)}{h_M}\right] - \alpha_M \Delta^0_s \sin\left(\frac{\pi X}{a}\right) \qquad (3.20.c)$$

where

$$\alpha_m = (Z/h_m) \quad \text{for} \quad h_m \geq Z \geq 0; \quad k = \begin{cases} 0 & \text{for} \quad 2h_m \geq Z > h_m \\ 1 & \text{for} \quad h_m \geq Z \geq 0 \end{cases}$$

$$\alpha_M = [(Z-2h_m)/h_M] \quad \text{for} \quad h \geq Z \geq 2h_m$$

The coordinate axes and a plot of these functions are shown in Figure 3.3.a and Figure 3.3.b for the compression flange and web of box girder, respectively. In equation (3.20.a - 3.20.c) the first term defines the plate panel deformation while the second one the stiffener deformation effect.

Considering the wide range of practical geometric parameters considered in the present study a computer program was written to perform the necessary calculations of initial deformations at each node.

3.7 Residual Stresses

In the present study an idealized distribution consisting of two edge strips at tensile yield, in equilibrium with a central strip in uniform compression, is taken to represent the welding residual stresses in each plate panel (Figure 3.4). This distribution is modified to suit the finite element mesh. The residual force attributed to a node is determined by averaging the total force

under the idealized pattern acting on a width of plate equal to half the mesh length on either side of the node.

The idealized welding residual stresses are in equilibrium only in the case of perfectly flat plates. Consequently, for a plate with initial geometric imperfections, before the application of the external loads, these stresses and displacements must be relaxed until an equilibrium configuration is reached. This was done by calculating the out-of-balance loads and applying the full Newton method for iteration. The total deflection at the end of the run was compared with the required geometric imperfections. If the difference was greater than the preset value (5 percent) the initial geometric imperfections were factored and the run was repeated until the deflections were close to the required values. The effect of initial stresses is included in the element assemblage through the load vector R_I defined as

$$R_I = \sum_m \int_{V^m} B^{(m)^T} \tau^{I(m)} dV^{(m)} \tag{3.21}$$

where $\tau^{I(m)}$ is the element initial stress vector due to residual welding stresses and $B^{(m)^T}$ is the strain-displacement matrix.

3.8 Solution of Nonlinear Equations

To accomplish the objective of the present study where an incremental analysis had to be performed, the following basic equations were used at time $t+\Delta t$,

$$\Delta R = {}^{t+\Delta t}R - {}^{t+\Delta t}F = 0 \tag{3.22}$$

where ${}^{t+\Delta t}R$ represents the load vector due to the externally applied nodal loads, ${}^{t+\Delta t}F$ is the vector of nodal point forces that are equivalent to the element stresses and ΔR defines the out-of-balance load vector. The vectors ${}^{t+\Delta t}R$ and ${}^{t+\Delta t}F$ in equation (3.22) are both evaluated using the principle of virtual displacements.

The out-of-balance load vector ΔR corresponds to a load vector that is not balanced by element stresses, and hence an increment in the nodal point displacements is required. To update the nodal point displacements, iterations are carried out within each load increment. For the case when the Newton method [59-61] is applied, the iterative equations become

$$\Delta R^{(i-1)} = {}^{t+\Delta t}R - {}^{t+\Delta}F^{(i-1)} \tag{3.23}$$

$$\Delta \bar{U} = \left({}^{t+\Delta t}K^{-1}\right)^{(i-1)} \left({}^{t+\Delta t}R - {}^{t+\Delta t}F^{(i-1)}\right) \tag{3.24}$$

$${}^{t+\Delta}U^{(i)} = {}^{t+\Delta t}U^{(i-1)} - \Delta U^{(i)} \tag{3.25}$$

where ${}^{t+\Delta t}K^{(i-1)}$ is the tangent stiffness matrix in iteration i-1

Since an incremental analysis is performed with time (or load) steps of size Δt the initial conditions in this iteration are

$${}^{t+\Delta t}K^{(0)} = {}^{t}K \tag{3.26}$$

$${}^{t+\Delta t}F^{(0)} = {}^{t}F \tag{3.27}$$

$${}^{t+\Delta t}U^{(0)} = {}^{t}U \tag{3.28}$$

The equations (3.23 - 3.28) are obtained by linearizing the response of the finite element system about the conditions at time t. In each iteration performed in (3.24) an out-of-balance vector is calculated which yields an increment in

displacements obtained in (3.25). The iteration is continued until the out-of-balance load vector $\Delta R^{(i-1)}$ or the displacement increments $\Delta U^{(i)}$ are sufficiently small.

The full Newton method was applied for iteration of nonlinear systems of equations in this study. In the full Newton method a displacement vector increment which defines a "direction" for the actual displacement increment is evaluated as

$$\Delta \bar{U} = \left({}^{t+\Delta t}K^{-1}\right)^{(i-1)} \left({}^{t+\Delta t}R - {}^{t+\Delta t}F^{(i-1)}\right) \tag{3.29}$$

A detail description of the full Newton method is given in references [53, 54, 61] and the applications of this method in [62].

3.9 Validation of Finite Element Model

Prior to embarking on nonlinear analysis of stiffened plates used in box girder webs and compression flanges a series of tests were carried out on plate and stiffened plates using numerical formulation. Even though tests using different finite element configurations available in the ADINA program library were performed in the elastic range on plates subjected to in-plane and uniformly distributed lateral loads, for which the results were in very good agreement with the theoretical ones, only the numerical results from nonlinear elastic-plastic analyses are reported. To reduce the computing time the member symmetry was considered and only a quarter of the plate was analyzed. Four node shell elements with five degree of freedom per node were used throughout the test programs.

3.9.1 Plates in the Elastic Range

a. Simply supported plate with restrained edges subjected to uniformly distributed lateral load

The purpose of this test was to check the accuracy and reliability of the ADINA program in performing large deflection elastic analyses.

The classical solution of this problem was derived by Levy [63] who used a double trigonometric series to solve Von Karman's [64] large deflection equation.

Using the plate geometry and material properties given in Figure 3.5, a comparative study of the load-central deflection relationship was done using Levy's analytical solution and author's and Crisfield's [65] finite element solution. Referring to the finite element analysis it should be noted that in the latter, four node rectangular plate elements with five degree of freedom per node were considered.

As shown in Figure 3.5 a very good agreement exists between the three load-central deflection curves. However, larger discrepancies are noticed in the predicted stresses (Figure 3.6 and 3.7) and this is mainly related to the fact that stresses being derived from deflections are bound to be less accurate.

In performing the finite element analysis, constraints were used to model the uniform in-plane edge conditions. This analysis involved severe nonlinearities because the plate, initially only in bending action was subjected to increasing membrane action with increasing load. This resulted in a stiffening effect and the application of the BFGS method was required for iteration. Also, tight tolerances and small load steps had to be used i.e. 20 load steps up to the final load ratio $qa^4 / Et^4 = 400$. For every load step the stiffness was reformed and the BFGS method of equilibrium iteration employed.

b. Simply supported plate subjected to uniaxial in-plane compressive loads

The post-buckling behaviour of simply supported plates subject to uniform in-plane compression was previously investigated using analytical methods [63, 66 - 68]. Among the existing solutions for plates with initial geometric imperfections, the most accurate is considered that of Yamaki [67]. He used a double sine series, with four coefficients to solve Marguerre's fundamental equations.

The material properties and geometric characteristics pertinent to the plate used in this study are given in Figure 3.8. Initial geometric imperfections are induced as single half-sine waves in both directions and expressed mathematically as

$$w_0(x,y) = 0.1\ t \sin\frac{\pi x}{a} \sin\frac{\pi y}{a} \qquad (3.30)$$

where a is the side length of the square plate and t its thickness. The plate is uniformly compressed by imposing specified displacements along the loaded edges. Two boundary conditions related to the unloaded edges were considered. In one case the edge is free to pull in: in the other, the edges are constrained to remain straight. In each case the magnitudes of the applied in-plane loads can be evaluated by integrating the element stresses. Figure 3.8 presents comparatively the present results and those of Crisfield's and Yamaki's. All of them are depicted as curves plotting the average stress ratio (σ_a / σ_{cr}) versus central deflection ratio (w_c / t). As can be seen the computed displacement response in this study agrees very closely with the other two.

In performing this finite element analysis, similar procedures with those described in (3.9.1.a) were applied.

3.9.2 Plates in the Elastic-Plastic Range

a. Simply supported plate subject to uniformly distributed lateral load

The same plate as in 3.9.1 was tested in the elastic-plastic range. The results are shown in Figure 3.9 and compared with those of Marcal [69]. The latter employed the incremental or tangent stiffness approach using an Euler forward difference technique in defining the generalized displacements, approach specific to earlier stage of development of nonlinear analysis.

For reference, Levy's results were also plotted in Figure 3.9. The existing differences between these and those of Marcal are probably due to the finite element formulations used in each case especially in the plastic range. Unfortunately, the investigation of Marcal was terminated at an early stage and no comparison is possible after this with the present one which has been extended further.

b. Simply supported imperfect plates subject to uniaxial in-plane loads

Two plates of aspect ratio a/b = 0.875 with b/t ratio of 55 and 80 were tested under uniaxial in-plane compression. The unloaded edges were free to move and the initial imperfections were defined by only a single half-sine wave with

$$w_0(x,y) = 0.001\, b \sin\frac{\pi y}{b} \qquad (3.31)$$

These initial imperfections are introduced through the nodal coordinates, in the finite element program. The overall problem in these analyses was to define the behaviour of the plates as the uniform end shortening u is progressively increased, and in particular to find the ultimate load that the plates could

sustain. Material properties and geometric characteristics for the two plates are included in Figures 3.10 and 3.11, respectively. In each case the results are compared with the findings of the finite elements analyses performed by Crisfield [65] and Moxham [70] and experimental data reported by Moxham [71]. It is worth noting that Crisfield used Ilyushin yield criterion in his studies but in a modified form.

Figures 3.10 and 3.11, which plot the average edge stresses versus the average edge strains in plates with $\sigma_{rc} / \sigma_y = 0.0$, for b/t = 55 and b/t = 80, respectively, show a close agreement of the present results with those of the other two authors.

The small discrepancies noticed can be attributed to the different finite element formulations.

3.10 Nonlinear Analysis of Stiffened Compression Flange of Experimentally Tested Box Girder Model

3.10.1 Introduction

The satisfactory correlation of theoretical results derived for isolate components of box girders with the results of experiments performed on structures composed of assemblies of such members is a very difficult task. The assumptions used in developing the theoretical models relating to material properties, boundary conditions, etc. are generally over-simplifications of the real conditions. For example, in the case of compression flanges of the box girder tested previously and results reported by Thimmhardy [4, 8] the stiffened plate boundaries in theoretical model are considered to lie in the same plane, whereas the real plate boundaries almost certainly do not. Furthermore, the actual bottom flange, which is continuous over the transverse stiffener supports on two edges

and continuously connected with the webs on the other two, is idealized in the theory as an isolated stiffened plate with edge restraints only, approximating those provided by the flange continuity and web-flange joint. Regarding initial geometric imperfections, one should note that the assumed values are at best good approximations of the real deformations. In the case of residual stresses, for which the magnitude and distribution is very difficult to define, the idealized pattern used in the analysis of stiffened plates is a very simplified model of that which occurs in practice. It is useful to be aware of the existing differences between theoretical and experimental models, when considering the correlation of numerical and test results described in the remainder of this section.

3.10.2 Boundary Conditions

To simulate the compression flange situated between the webs and two adjacent transverse stiffeners of the box girder model, a simple support and non-deflecting edge were taken as the boundary condition. The former condition allows the plate panels to deform in the elastic buckling mode in which no rotational restraint is provided by the slender webs or adjacent panels in the transverse and longitudinal directions. The latter condition was assumed not only because of the difficulty in establishing the appropriate vertical spring stiffness to be used in representing the support provided by each web and transverse stiffener, but also because this idealization approximates closely the true situation. To model the restraint provided by transverse stiffeners, the tangential deformation was constrained along the loaded edges. For the unloaded edges there was no restraint against in-plane movement.

In the longitudinal direction uniform displacement was selected for the in-plane loading condition and applied normal to the end of the stiffened plate.

This was selected for three reasons. Firstly, in the critical buckling mode, symmetry dictates that this is the correct condition. Secondly, and more importantly, from the numerical analysis point of view, applying displacement rather than stress boundary conditions enables the unloading part of the average stress-average strain curve to be followed. Thirdly, stress boundary conditions other than zero stress value cannot readily be used where an elastic-plastic behaviour is analyzed because penetration of the yield surface could happen and this would conflict with one of the basic assumptions used in the development of constitutive equations in the plastic range Equation (3.6). Details regarding the boundary conditions specifically applied to each edge of the numerical model are given in Figure 3.12.

3.10.3 Initial Imperfections

Initial deformations of stiffened plates considered in this study were defined by Equation (3.20.a). The value of this developed equation consists in that it can closely simulate the pattern of initial geometric imperfections existing in the bottom flanges of box girder bridges as shown in Figure 3.3.a. In the finite element modelling plate panel deformations of $\Delta_s^0 / b = 1/165$ and out-of-straightness of stiffeners of $\Delta_s^0 / a = 1/500$, which closely approximate the values of imperfections measured in the bottom flange of the experimentally tested box girder model were used.

Residual compressive stresses $\sigma_{rc} = 0.15\sigma_y$ equivalent to the average measured stressed in the bottom flange of the box girder model were employed in the numerical analysis. The idealized rectangular distribution shown in Figure 3.4 was assumed and applied for each plate panel of the stiffened plate.

3.10.4 Material Properties

Considering the symmetry conditions, only a half of the stiffened plate was analyzed using the mesh shown in Figure 3.12.

The material properties used in this analysis are similar to those defined by test for the box girder model (Table 3.3), i.e. yield stress equal to 374 MPa and 377 MPa for the plate and longitudinal stiffeners, respectively. Additionally, it was assumed that the modulus of elasticity E=200 GPa, tangent modulus $E_T = 0.0$ and Poison's ratio $\nu = 0.3$.

3.10.5 Comparison of Experimental and Theoretical Results

The most convenient experimental value with which the theoretical results should be compared is the average membrane compressive stress in the plate determined at maximum load. This average stress calculated for the compression flange of the box girder model [4, 8] is compared with the predicted values in Figure 3.13. As can be seen good agreement is achieved between the predicted and experimentally determined ultimate loads, and this suggests that the simulated conditions were close to those of the physical model. There is thus full confidence that the finite element model, and associated procedures, can be used to perform valid parametric studies.

3.11 Nonlinear Analysis of Experimentally Tested Box Girder Model

3.11.1 Finite Element Modeling

In 1987 the results of ultimate load test on a large steel box girder model was first time reported in Canada by Korol et al. [8]. Figure 3.14.a shows typical box girder web layout and Figure 3.14.b presents a typical cross section of the

box girder model. To generalize the experimental results to the whole range of stiffened plates currently used in the design of stiffened flanges and webs of steel box girder bridges with geometries specific to Canadian and American practice, a large deflection nonlinear analysis of their buckling behaviour and ultimate strength was considered necessary. To perform this study, an elasto-plastic large deflection finite element model was developed and used to perform a parametric study on box girder behaviour in which both geometric and material nonlinearities were included.

Considering the symmetry conditions, only half of the steel box girder model was analyzed using the mesh shown in Figure 3.14.c.

The bottom flange plate and web plate were modeled by 8-node shell elements, while the top flange was modeled by 4-node shell elements.

All stiffeners were modeled by combinations of 4-node shell elements except the longitudinal stiffeners of the bottom flange where 2-node iso-beam elements were employed. The diaphragms shown in Figure 3.14.c were not modeled. However, their restraints on the adjacent members were simulated by constraints imposed on the connecting nodes.

Initial deformations of the bottom flange and the web of the box girder considered in this study were defined by Equation (3.20.a - 3.20.c) in which the value of the deformation was $\Delta_p^0 / b = 1/165$ for the bottom flange and web plates. The magnitude of out-of-straightness of longitudinal stiffeners of bottom flange and web was $\Delta_s^0 / a = 1/500$. Residual stresses of $\sigma_{rc} / \sigma_y = 0.0$ and $\sigma_{rc} / \sigma_y = 0.15$ were also considered in the finite element nonlinear analysis.

3.11.2 Comparison of Experimental and Theoretical Results

The results of the experimental tests and finite element analysis are presented in the form of overall load-deflection curves in Figure 3.15. Comparing the ultimate load predicted by numerical analysis in which residual stresses of $\sigma_{rc} / \sigma_y = 0.15$ were included, $P_u = 1530$ kN, with the experimentally determined ones of 1500 kN and 1450 kN one can see that a good agreement is achieved between the finite element analysis and experimental results.

As can be seen from Figure 3.15, small differences ranging from 2.0 to 4.2 percent exist between the finite element predicted ultimate loads in which $\sigma_{rc} / \sigma_y = 0.15$ and the experimentally determined collapse load. Based on these results as well as the previous ones it was concluded that the nonlinear finite element model is a valid and reliable one and can be used in performing the parametric studies described in Chapter 4.

Table 3.1 - Simply Supported Square Plate under Uniform Lateral Load.
Comparison of Theoretical and Numerical Analysis

CASE	Displacement w_c at center (mm)	$\frac{(w_c)_{th}}{(w_c)_{FE}}$	Stresses σ_x at center (MPa)	$\frac{(\sigma_x)_{th}}{(\sigma_x)_{FE}}$	CPU time used (sec)
Theoretical solution	-0.14544	1.000	-2.328	1.000	—
16 - Node Element	-0.14598	0.996	-2.353	0.989	8.14
8 - Node Element	-0.14576	0.998	-2.359	0.987	6.09
4 - Node Element	-0.14433	1.008	-2.330	0.999	0.96

Table 3.2 - Simply Supported Square Plate with Initial Imperfections under Uniform Axial Compressive Load. Comparison of Theoretical and Numerical Analysis

Type of Element n	Element Used	Displacement w_c at center (mm)	$\frac{(w_c)_1}{(w_c)_n}$	CPU time used (sec)
1	16 - Node Element	3.473	1.000	147.92
2	8 - Node Element	3.329	1.043	142.97
3	4 - Node Element	1.576	2.204	7.39
4	16 - Node Single Element	3.116	1.115	15.71

Table 3.3 - Material Properties and Plate Thickness of Box Girder Model Components

Component	Plate Thickness		Yield Stress	Ultimate Stress
	Nominal (mm)	Measured	(MPa)	(MPa)
Top Flange	25	25.8	352	521
Bottom Flange	8	8.4	374	460
Web	5	5.2	383	482
Longitudinal Stiffeners of Bottom Flange	—	—	377	510
Longitudinal Stiffeners of Webs	—	—	371	493

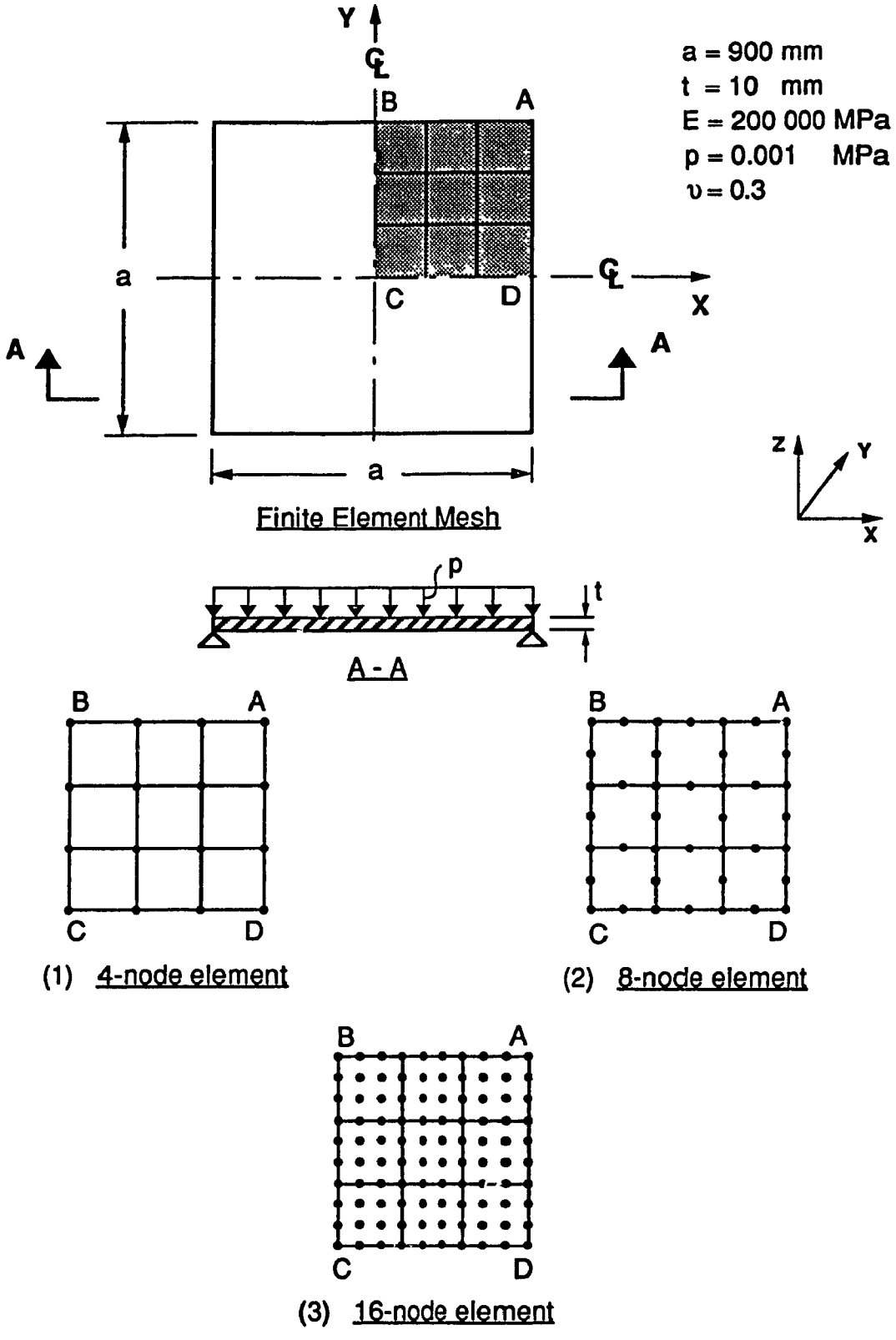

Figure 3.1 Simply Supported Square Plate under Uniform Distributed Lateral Load

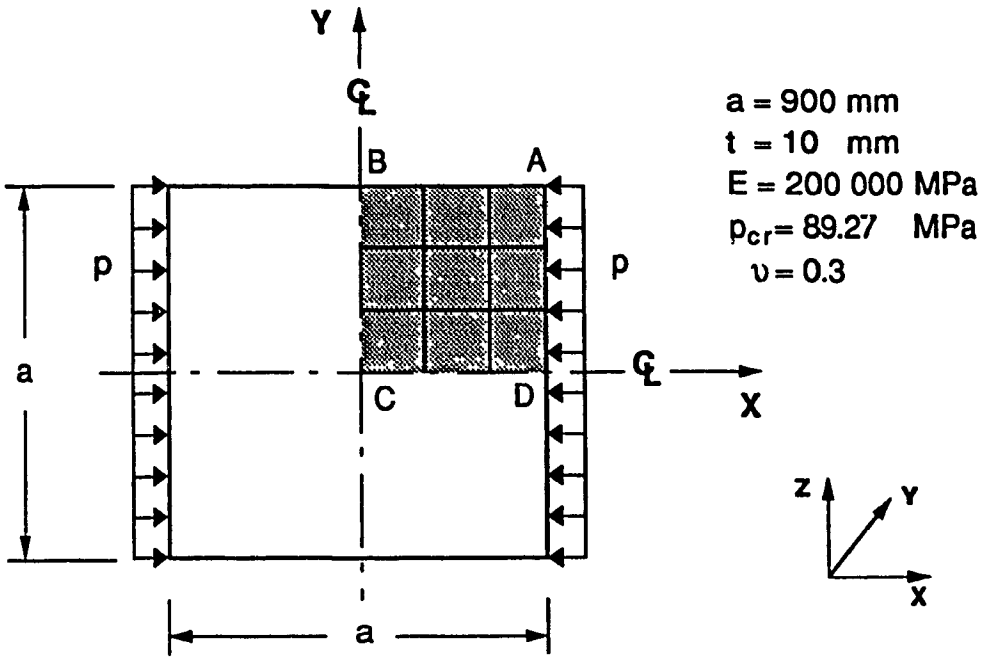

Finite Element Mesh

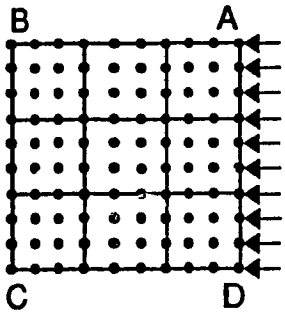

(1) 16-node element

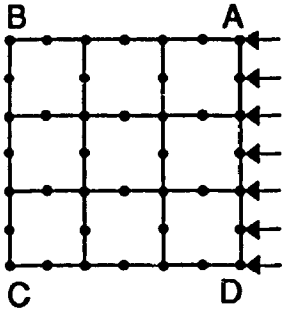

(2) 8-node element

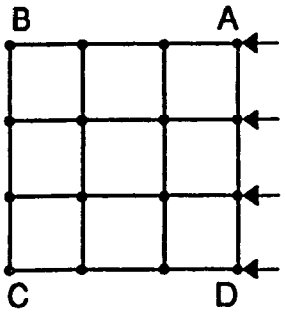

(3) 4-node element

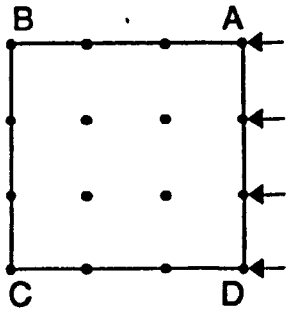

(4) 16-node single element

Figure 3.2 Simply Supported Square Plate under Uniform Axial Compressive Load

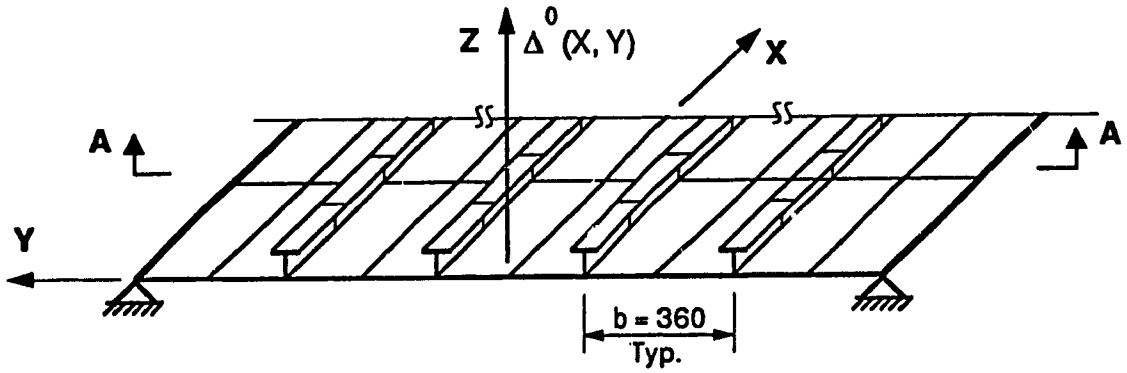

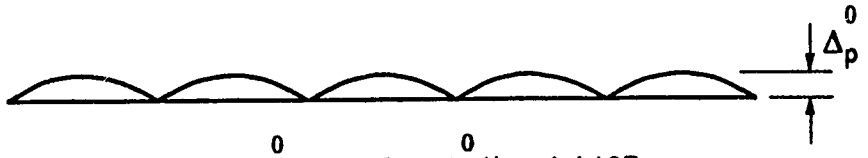

a. $\Delta_s^0/a = 0.0$; $\Delta_p^0/b = 1/165$

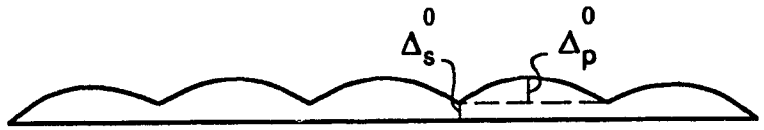

b. $\Delta_s^0/a = 1/500$; $\Delta_p^0/b = 1/165$

Section A - A

$$\Delta^0(X,Y) = (-1)^{p-1}\Delta_p^0 \sin\left(\frac{\pi X}{a}\right)\cos\left(\frac{\pi Y}{b}\right) + \alpha^m \Delta_s^0 \sin\left(\frac{\pi X}{a}\right)$$

Where

$$\alpha = (2.5 - Y/b) \text{ for } p = n; \qquad m = \begin{cases} 0 & \text{for } 1 \le p < n \\ 1 & \text{for } p = n \end{cases}$$

Figure 3.3.a Initial Geometric Imperfections of Bottom Flange of Box Girder

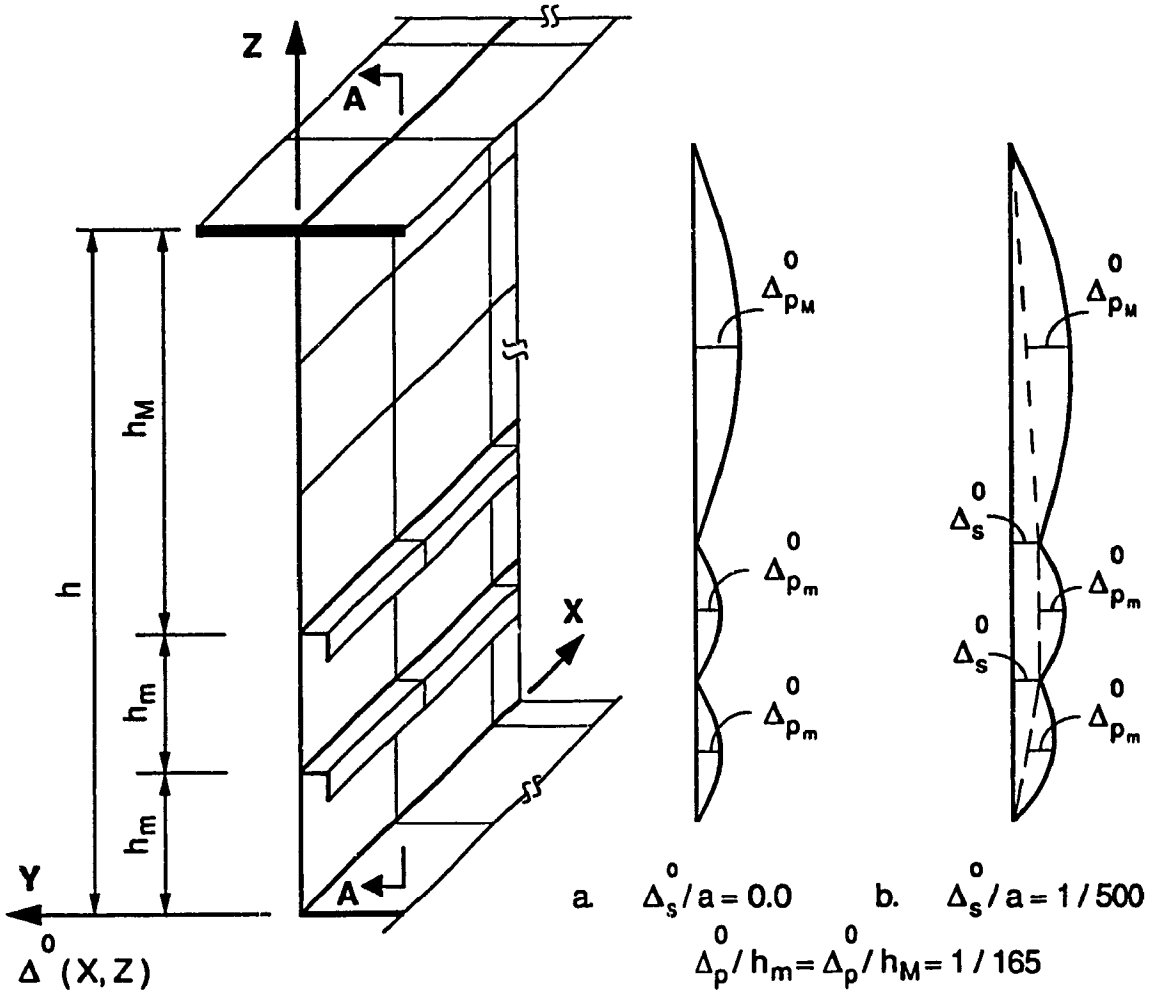

For $(h - h_M) \geq Z \geq 0$

$$\Delta^0(X,Z) = (-1)^k \Delta^0_{p_m} \sin\left(\frac{\pi X}{a}\right) \sin\left(\frac{\pi Z}{h_m}\right) - \alpha_m^k \Delta^0_s \sin\left(\frac{\pi X}{a}\right)$$

For $h \geq Z > (h - h_M)$

$$\Delta^0(X,Z) = (-1) \Delta^0_{p_M} \sin\left(\frac{\pi X}{a}\right) \sin\left[\frac{\pi(Z - 2h_m)}{h_M}\right] - \alpha_M \Delta^0_s \sin\left(\frac{\pi X}{a}\right)$$

where

$$\alpha_m = (Z/h_m) \quad \text{for } h_m \geq Z \geq 0 \qquad k = \begin{cases} 0 & \text{for } 2h_m \geq Z > h_m \\ 1 & \text{for } h_m \geq Z > 0 \end{cases}$$

$$\alpha_M = [(Z - 2h_m)/h_M] \quad \text{for } h \geq Z > 2h_m$$

Figure 3.3.b Initial Geometric Imperfections of Box Girder Webs

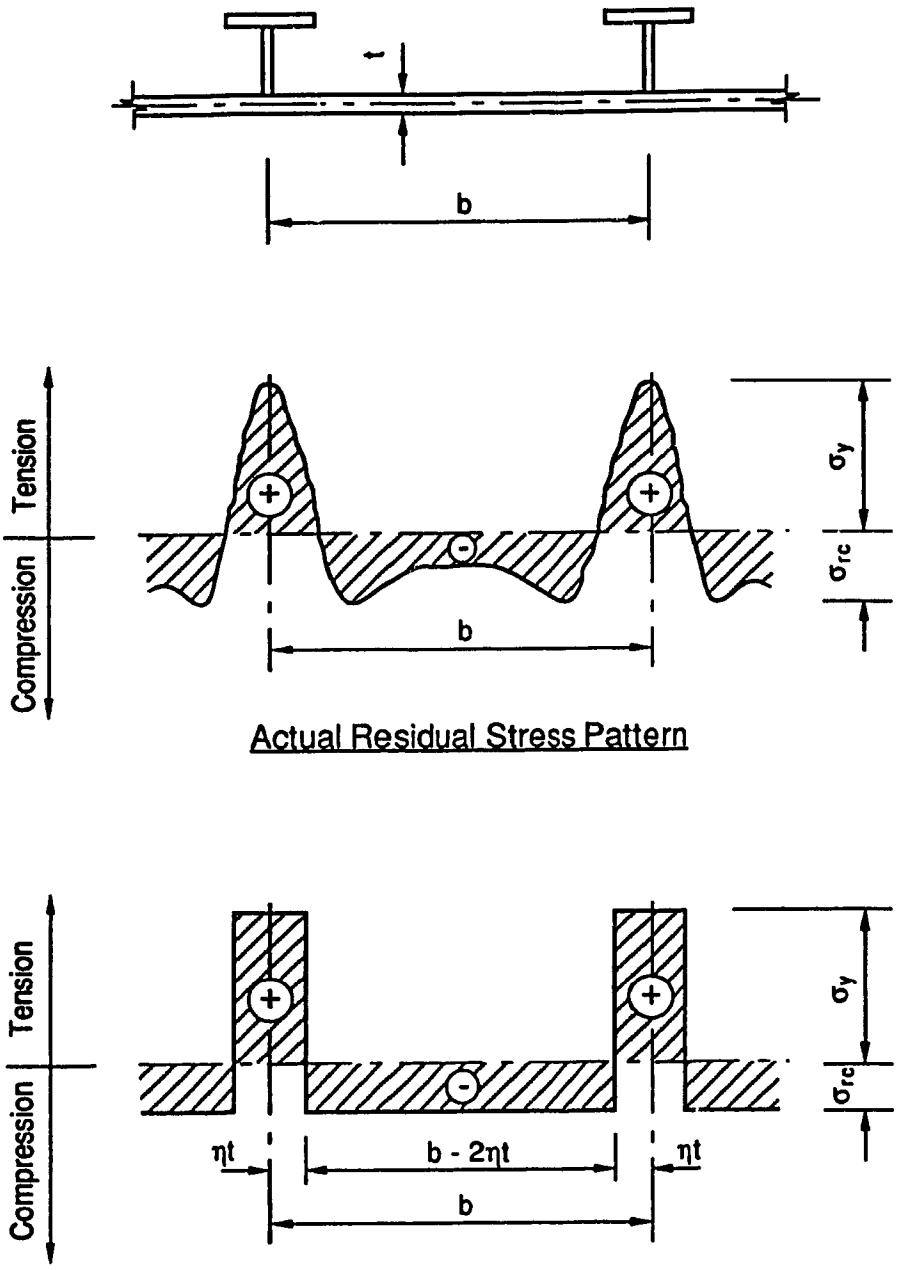

Figure 3.4 Residual Stress Distribution in Stiffened Plates

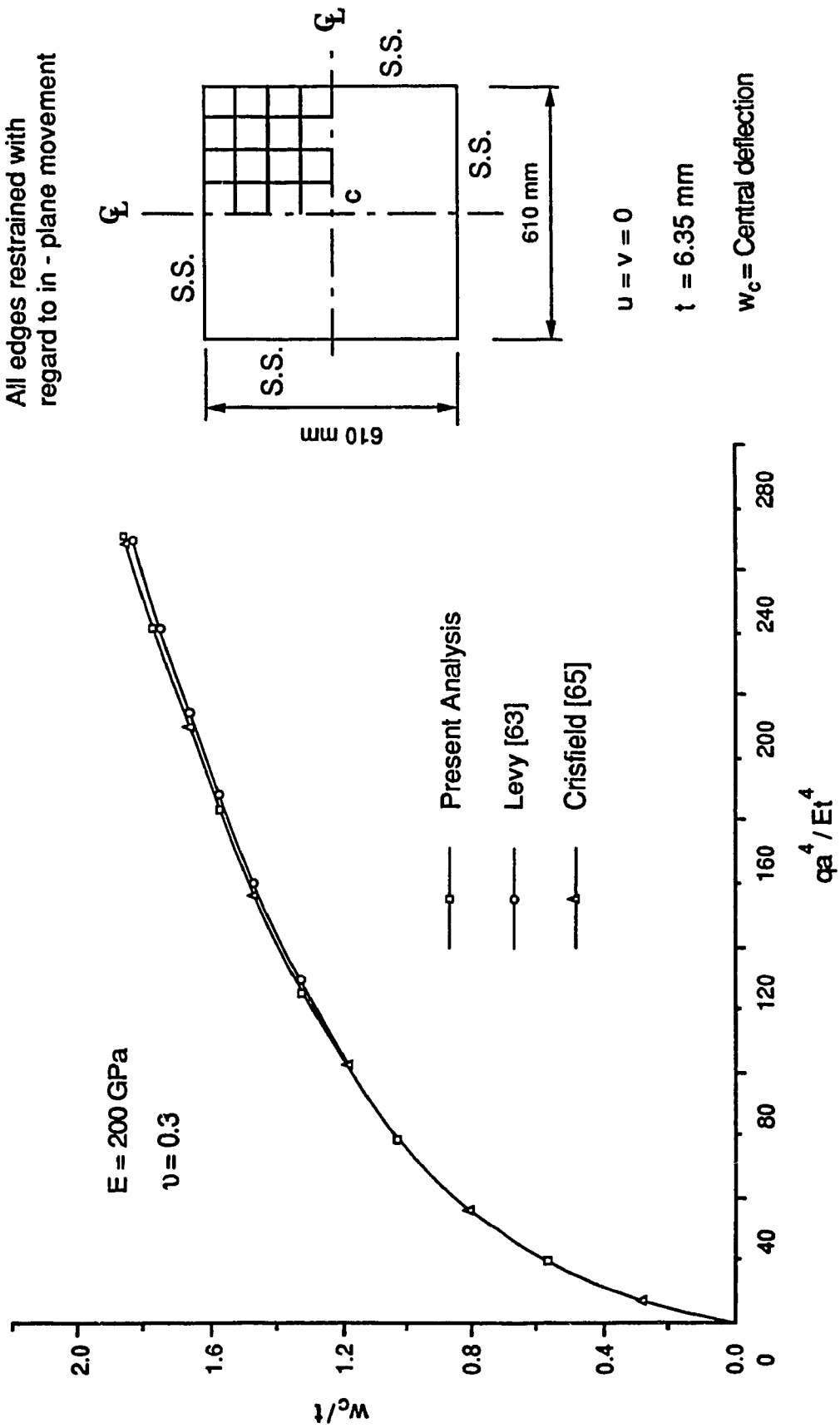

Figure 3.5 Restrained Elastic Plate. Behaviour under Uniform Lateral Load

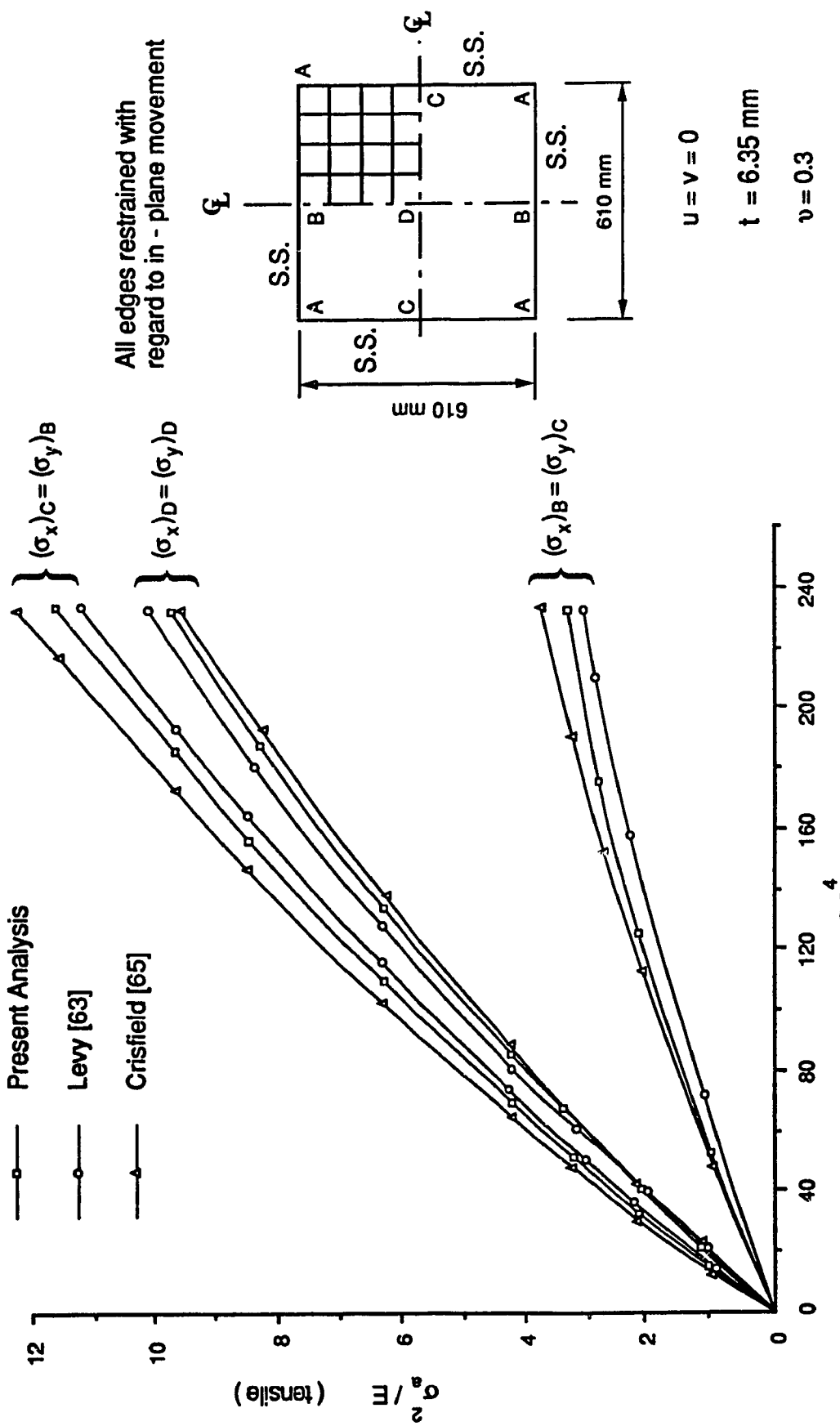

Figure 3.6 Restrained Elastic Plate under Uniform Lateral Load. Membrane Stresses

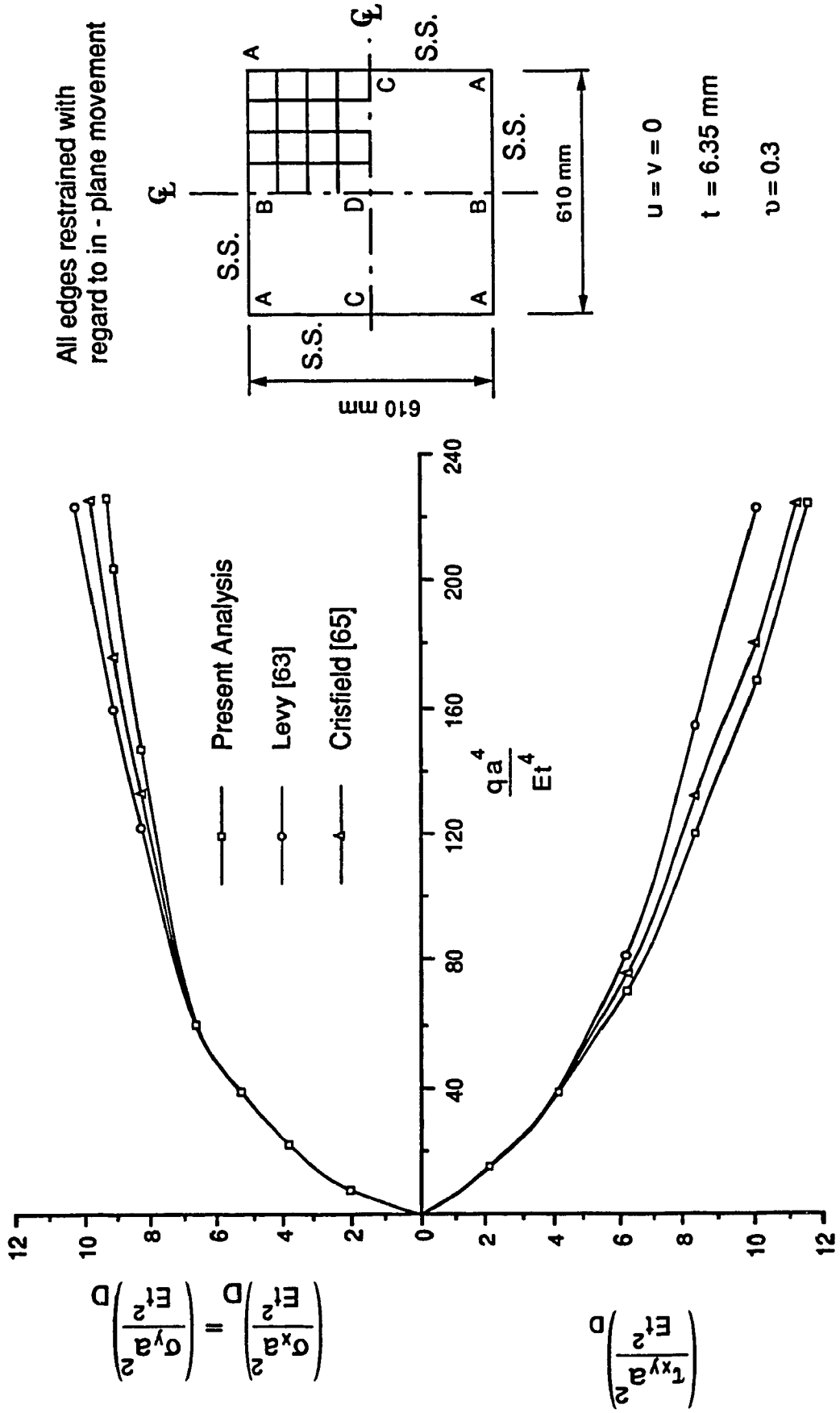

Figure 3.7 Restrained Elastic Plate under Uniform Lateral Load. Bending Stresses

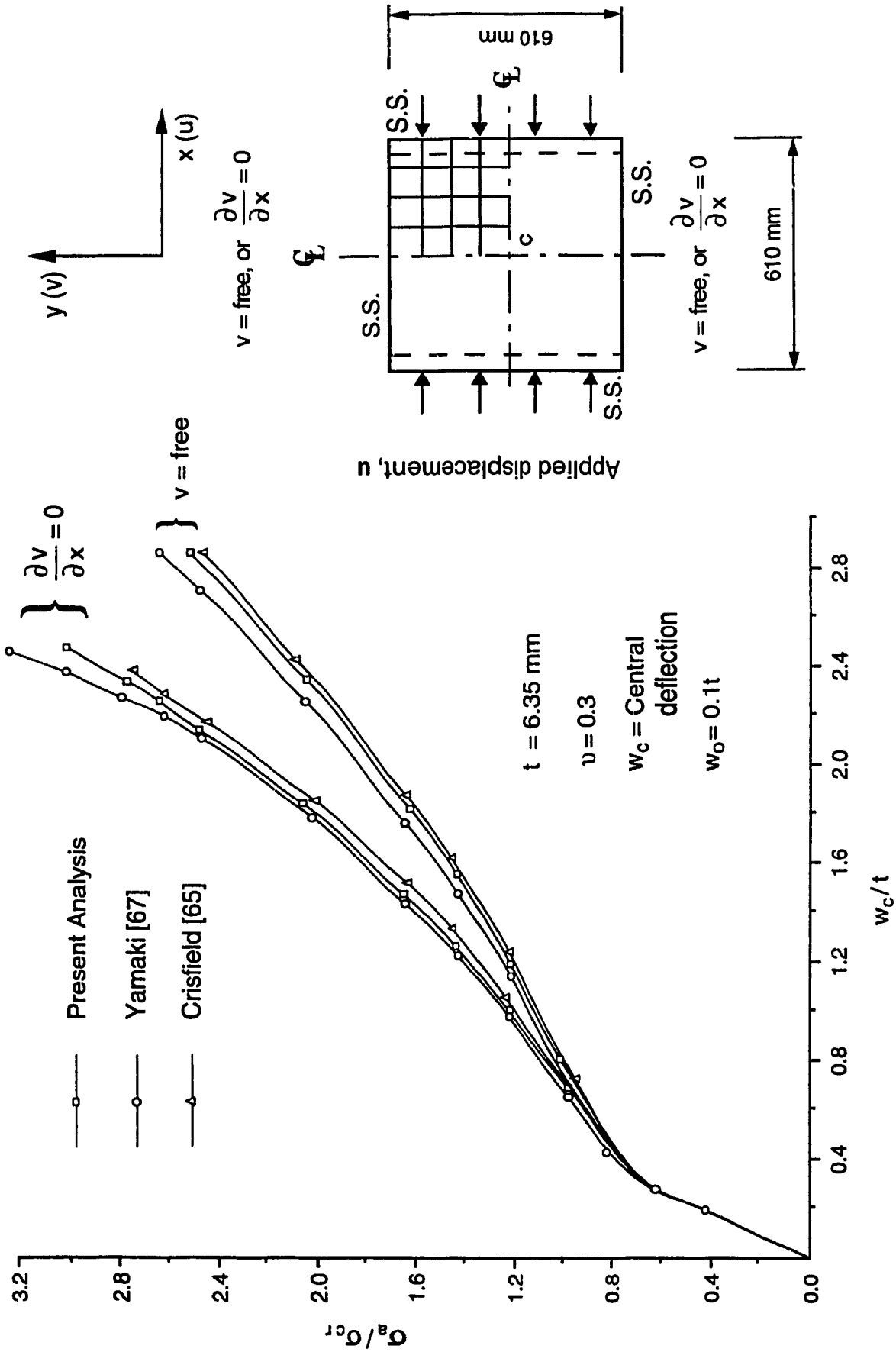

Figure 3.8 In - Plane Load - Central Deflection Relationship. Imperfect Elastic Plate

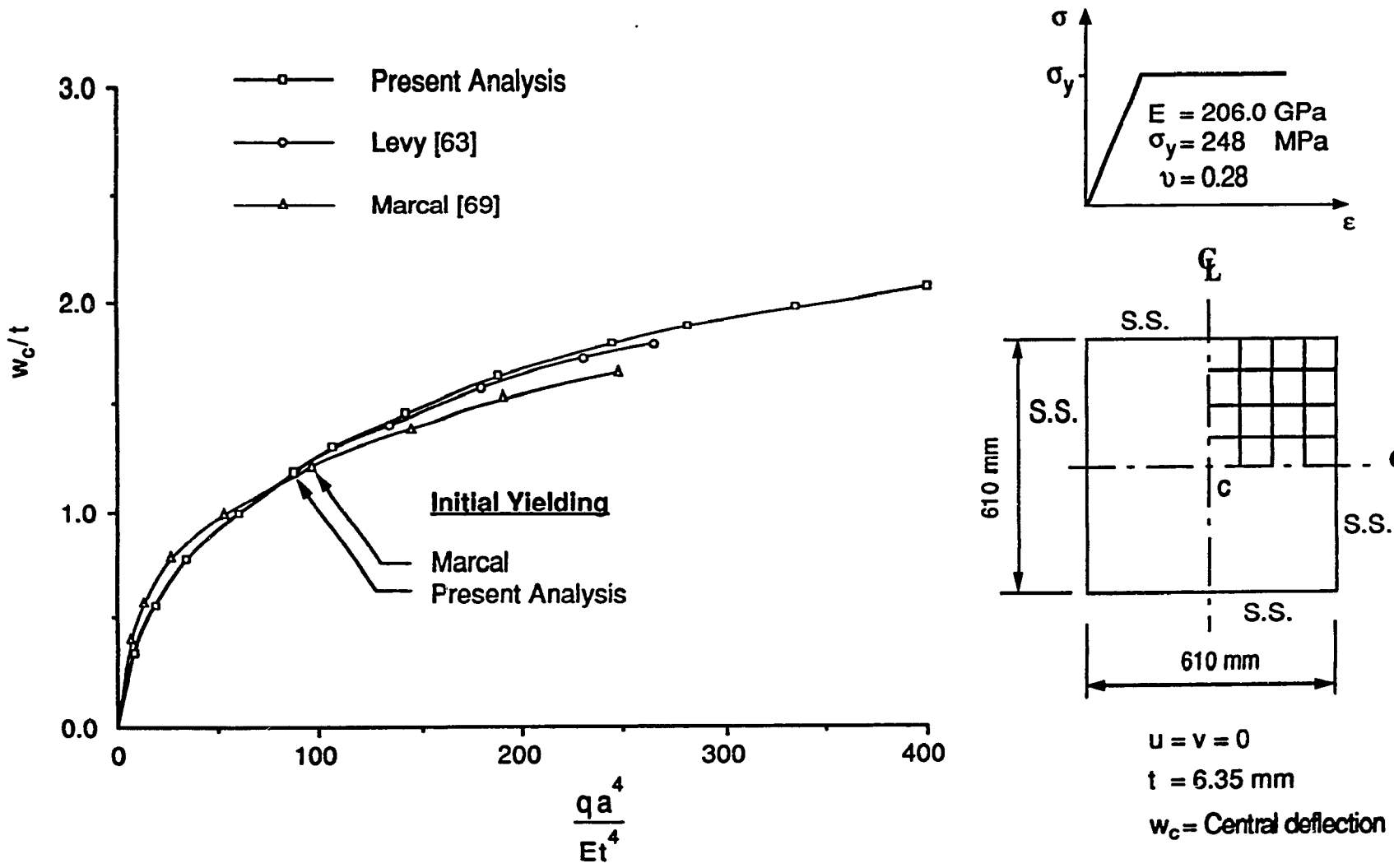

Figure 3.9 Restrained Plate Under Uniform Lateral Load.
Elastic - Plastic Behaviour

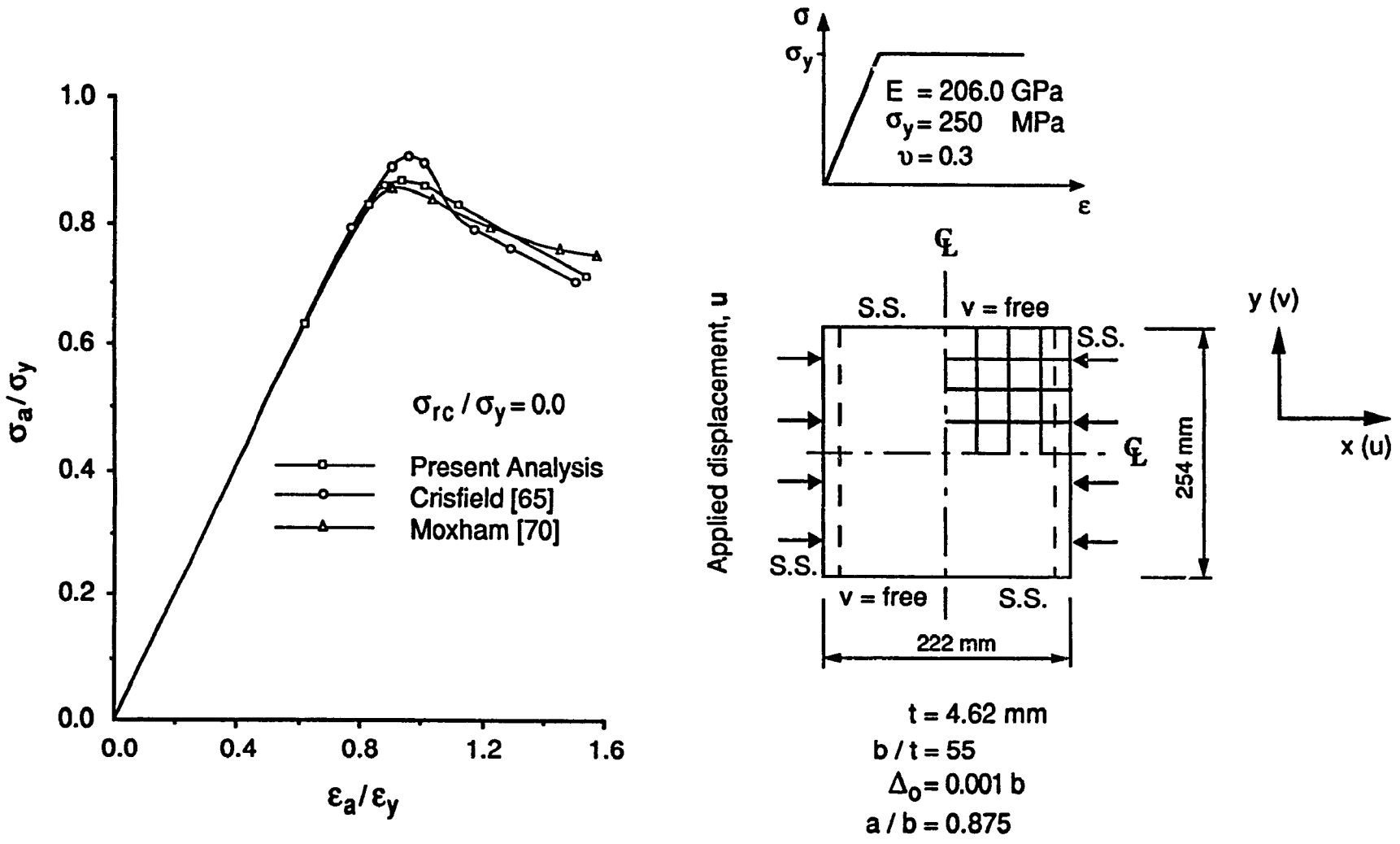

Figure 3.10 Average Stress - Average Strain Relationship. Simply Supported Plate Subjected to In - Plane Compression

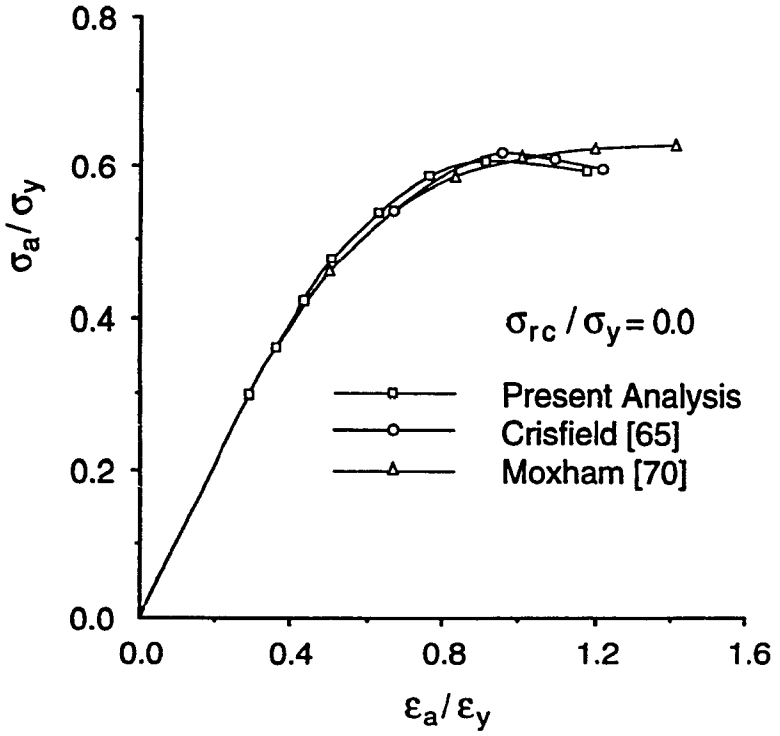

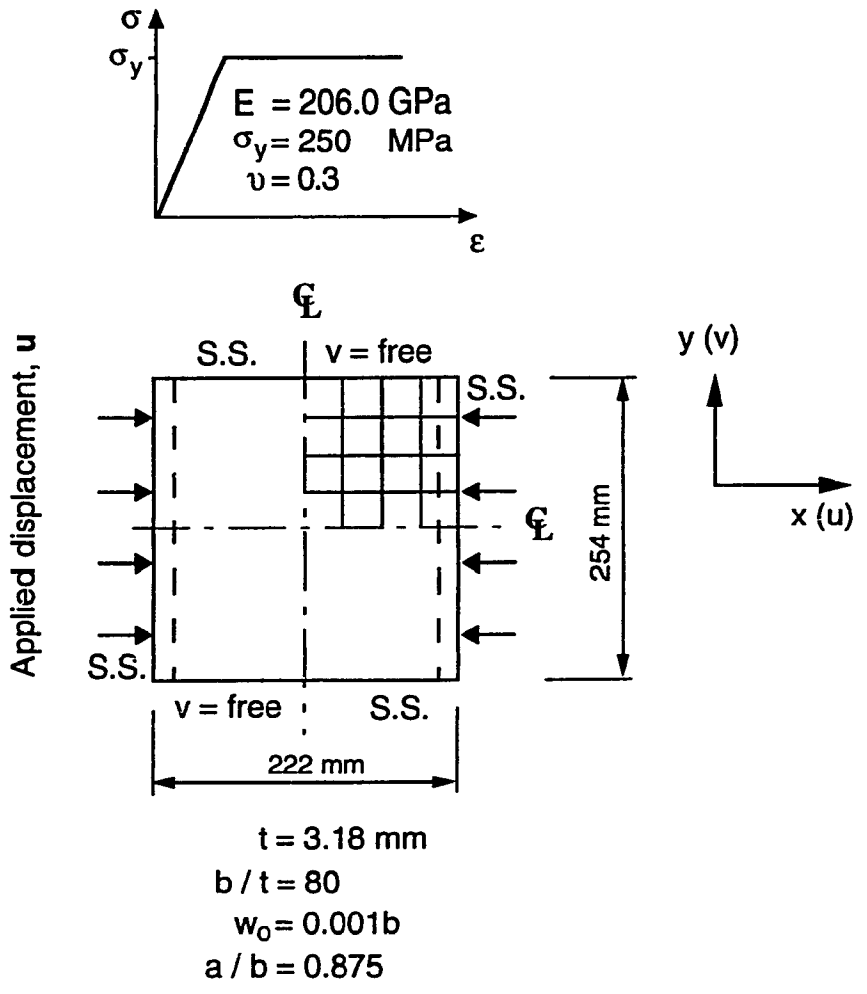

Figure 3.11 Average Stress - Average Strain Relationship. Simply Supported Plate Subjected to In - Plane Compression

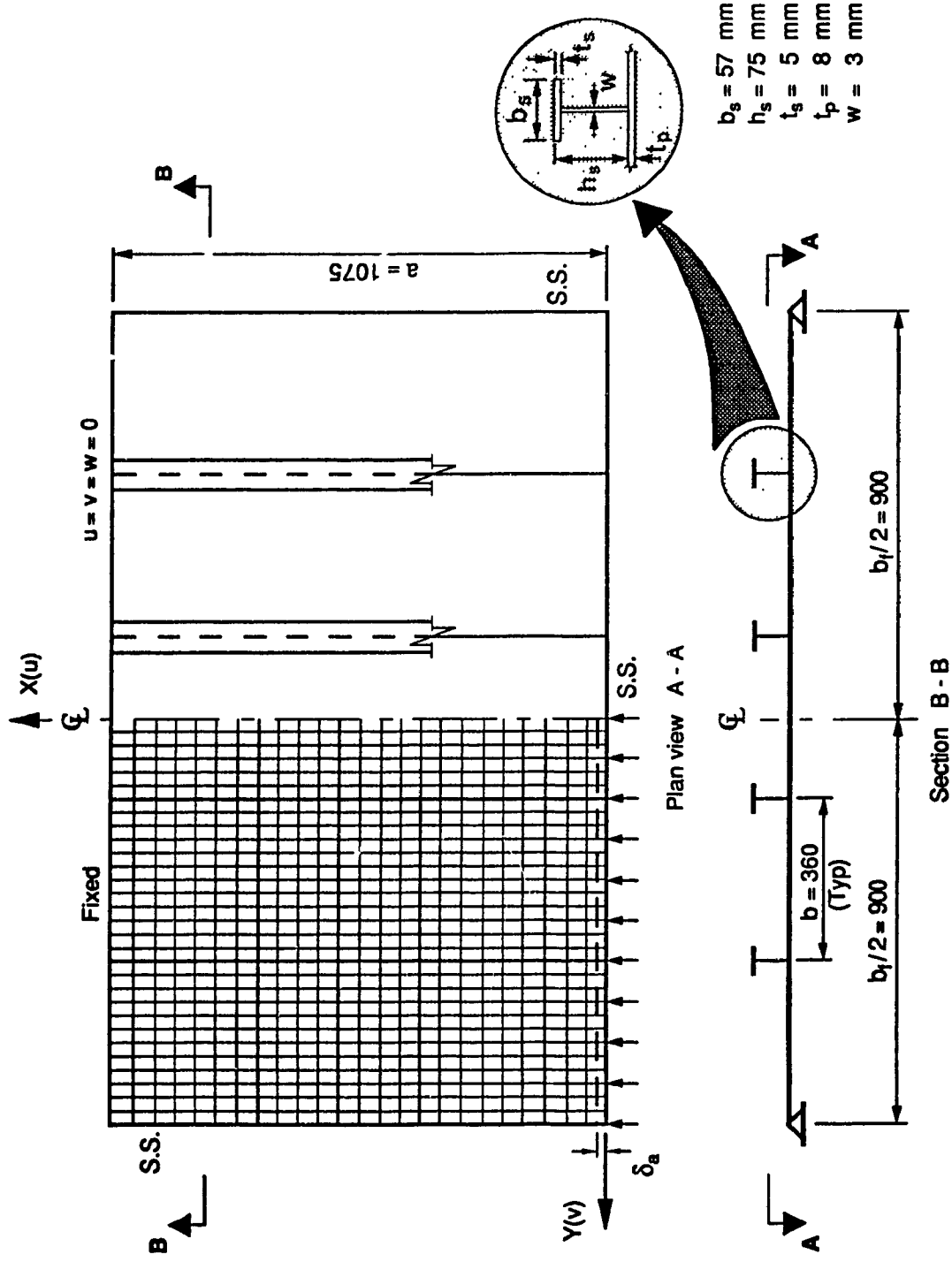

Figure 3.12 Mesh and Boundary Conditions Used in Numerical Analysis of Bottom Flange of Steel Box Girder Model

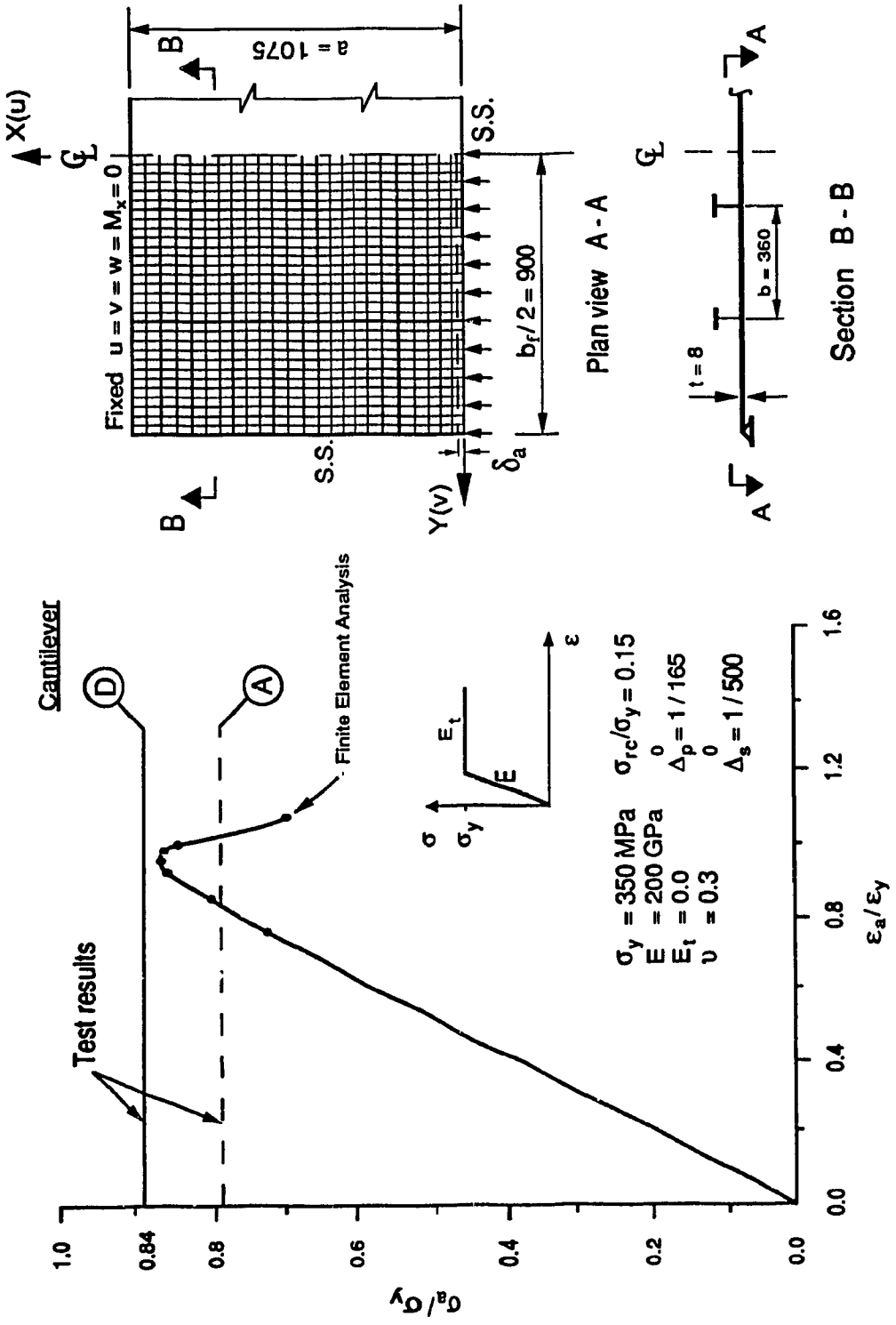

Figure 3.13 Behaviour of Simulated Compression Flange of Steel Box Girder Model Under Uniform Edge Displacement

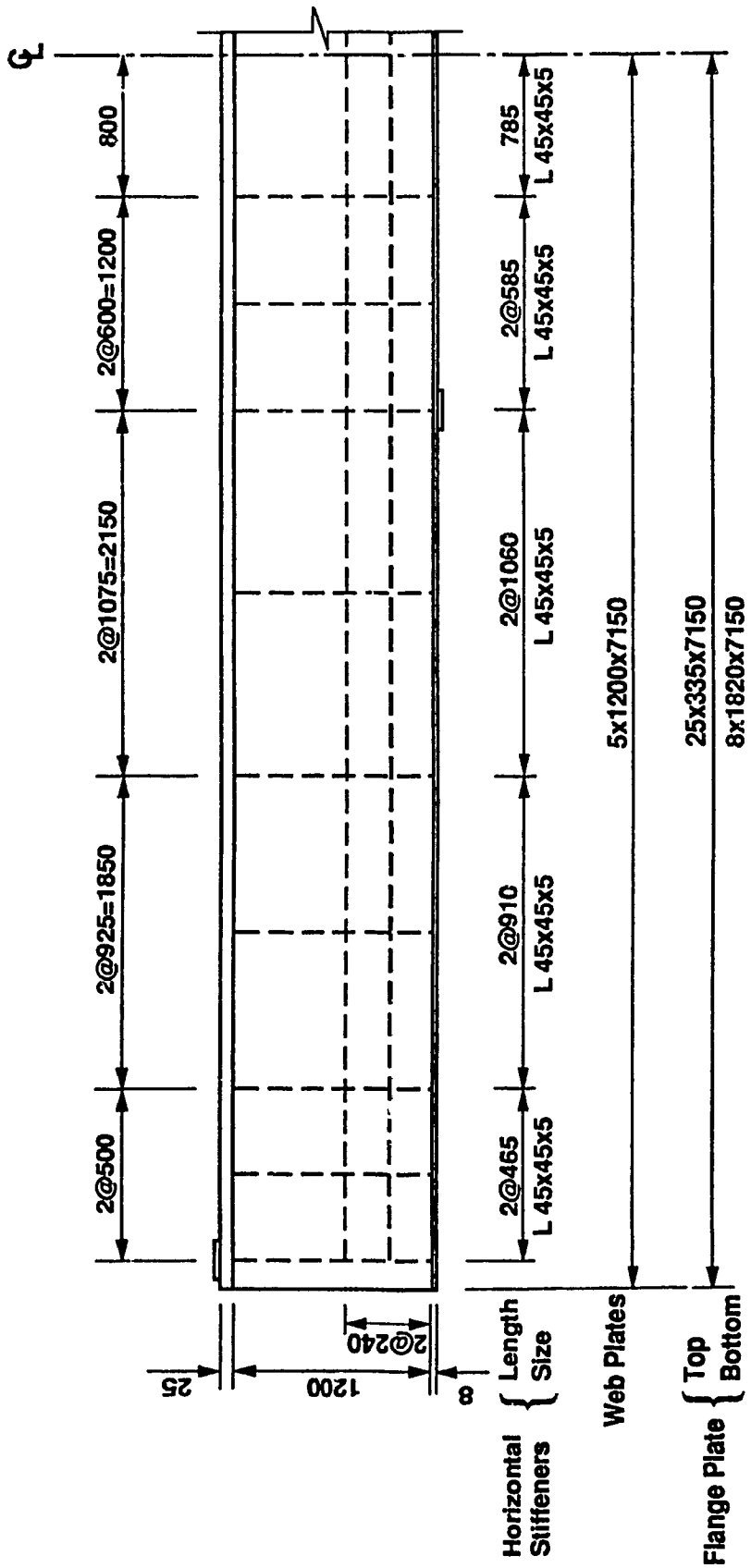

Figure 3.14.a Elevation of Box Girder Model

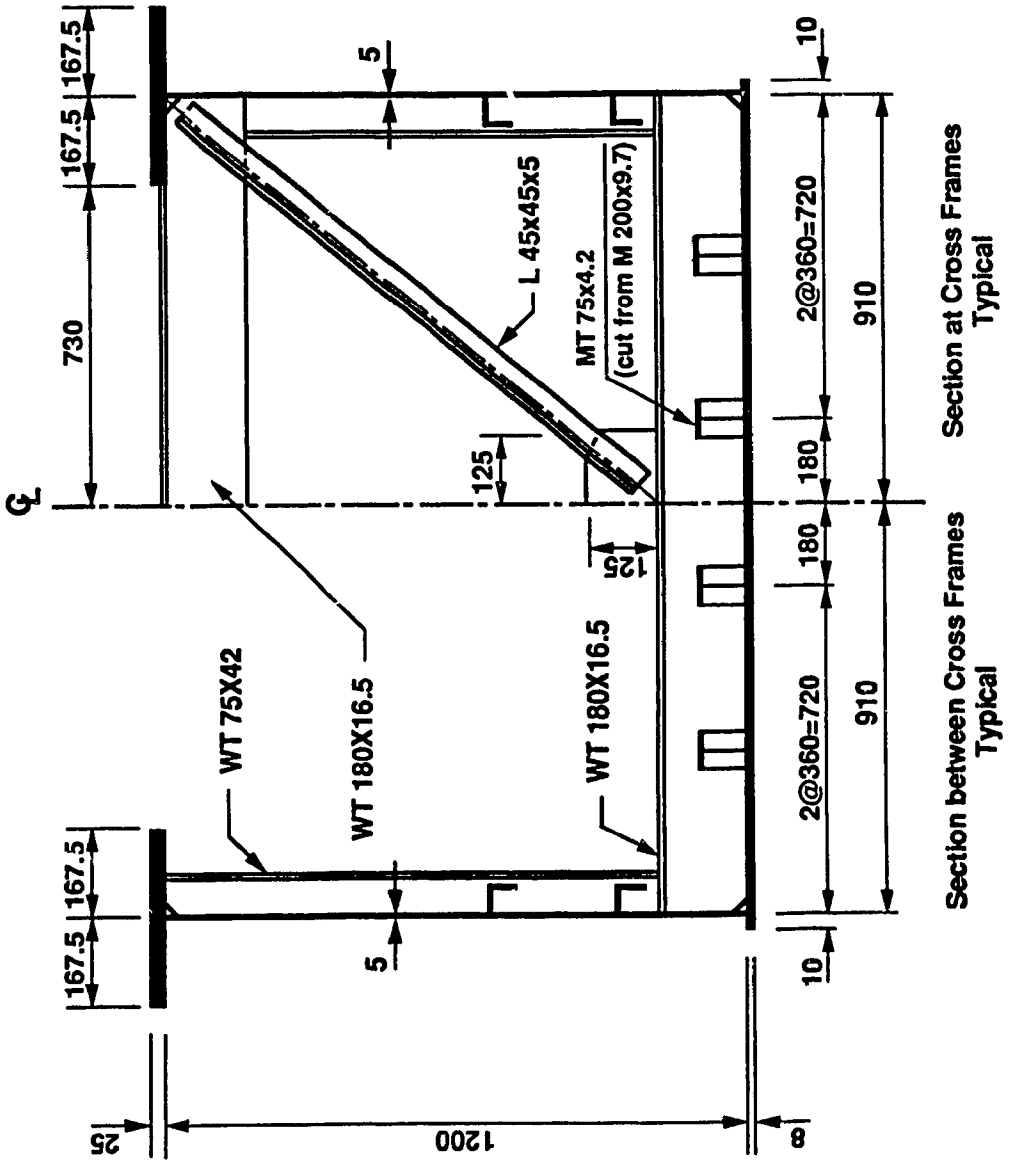

Figure 3.14.b Box Girder Model. Cross Section

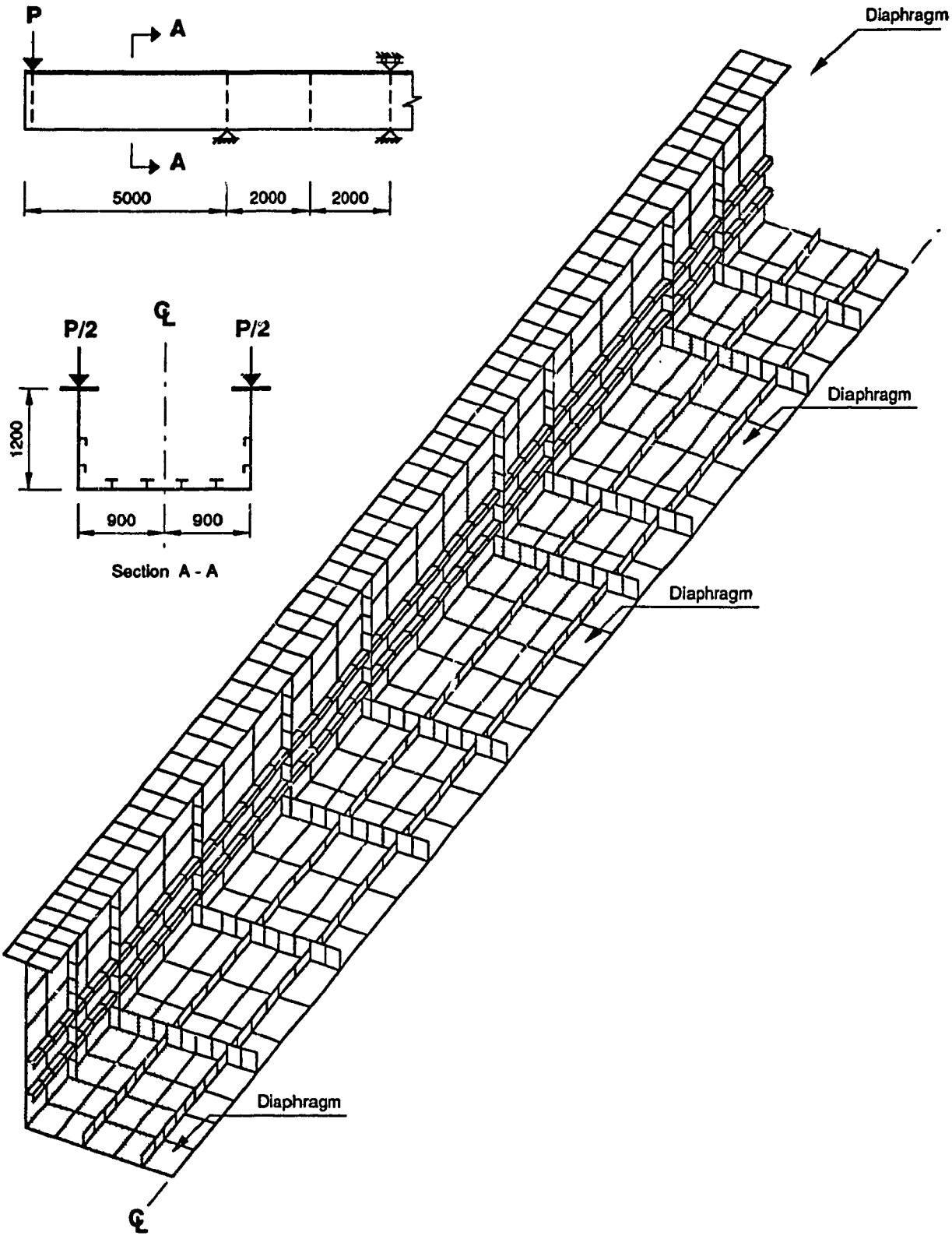

Figure 3.14.c Steel Box Girder Model. Finite Element Discretization

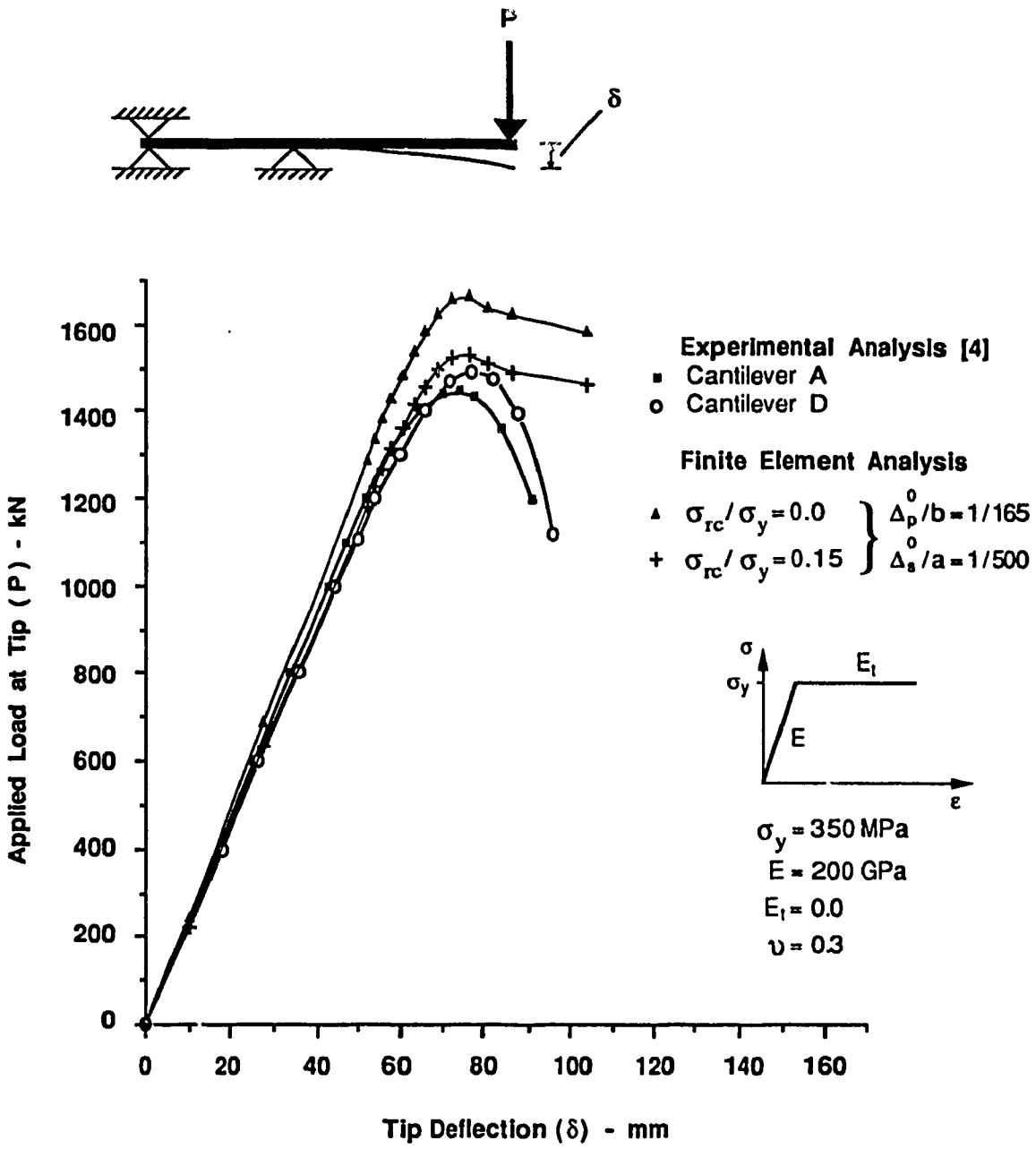

Figure 3.15 Steel Box Girder Model.
Load - Deflection Curves from
Experimental and Numerical Analysis

CHAPTER 4

PARAMETRIC STUDY

4.1 Introduction

Design of medium and large box girder bridges in which orthogonally stiffened webs are extensively used implies in many cases the use of more than one longitudinal stiffener. However, as mentioned previously in Chapter 2 the present North American code provisions [38, 49, 50] provide design specifications for webs stiffened with only one longitudinal stiffener, and recommend the use of "a rational method of analysis" when more than one longitudinal stiffener is required.

To fill this gap a parametric study on buckling behaviour and ultimate strength of box girder webs stiffened with more than one longitudinal stiffener was considered necessary. However, taking into account that even for one longitudinal stiffener the present design provisions relate to plate girders and not enough information exists for box girder webs , it was decided to include this type of web stiffening also in the parametric study. Additionally, for reference purposes box girder webs stiffened only transversally were included in the study.

In performing the study the following parameters were used: magnitude of shear forces and bending moments acting on the web panels; longitudinal web stiffening system which included up to three longitudinal stiffeners; position of longitudinal stiffeners within the web depth; web aspect ratio; web slenderness ratio; initial out-of-plane deformation of web panels; out-of-straightness of longitudinal stiffeners; and slenderness ratio of longitudinal stiffeners.

As discussed further in this chapter, the range of geometric parameters considered in this study was limited mostly to practical values encountered in design of steel box girder bridges.

The transverse stiffeners considered in all finite element analyses are similar to those used in the experimentally tested box girder model and designed such that they remain straight until the ultimate load carrying capacity is reached.

Taking into account the large number of parameters as well as their possible combinations, a preliminary parametric study aiming at defining the numerical data to be used in plotting shear force - bending moment interaction diagrams as well as particular parameters to be used further in the major part of the research work was undertaken.

In performing the preliminary parametric study the finite element model calibrated against the experimental one and described in Chapter 3 was used throughout. However, to suit the loading conditions considered in the analysis the finite element mesh shown in figure 3.14.c has been adjusted accordingly as described further in section 4.2.

Based on results of the preliminary study a reduced number of geometric parameters was considered in the main parametric study. These parameters were considered as the minimum required to perform a reliable study on

ultimate strength and buckling behaviour of box girder webs stiffened longitudinally with one and more longitudinal stiffeners.

To reduce the computing time, the existing symmetry of each box girder was considered and consequently only one half was modeled and analyzed.

The material properties used in this study are as follows: yield stress $F_y = 350$ MPa, modulus of elasticity E = 200000 MPa, tangent modulus $E_t = 0.0$, Poisson's ratio $\upsilon = 0.3$.

In both preliminary and main parametric studies, initial geometric imperfections specific to Canadian built box girder bridges [72] were considered for both web plate and stiffeners.

4.2 Preliminary Parametric Study

4.2.1 Geometric Parameters

Taking into account that the box girder webs can be subjected to a large number of shear force and bending moment combinations, the main objective of the preliminary study was to define the necessary data based on which shear force - bending moment interaction curves could be plotted. This study has also been considered in defining the governing combinations to be used in the major part of the study. In performing this part of the parametric study, three cantilever beams loaded as shown in Figure 4 1 were considered. Although the overall cross section geometric properties of the experimentally tested box girders [4, 8] were maintained, only three types of web stiffening shown in Figure 4.2 were used in order to define the affect of web/subpanel slenderness ratios on ultimate strength and buckling behaviour of webs and overall box girder. They correspond to the longitudinal web stiffening type 1.(ii), 2.a.(ii) and 3.c.(ii) as defined in Figure 4.2 and Table 4.1.

Complying with the existing Canadian bridge design provisions [38, 49] which require the use of longitudinal stiffeners for webs with slenderness ratio $3150 / \sqrt{F_y} < h / w \leq 6000 / \sqrt{F_y}$, only webs with $h / w = 300 = 5612 / \sqrt{350}$, i.e. close to the upper limit, were used in the preliminary study.

The remaining parameters considered in the preliminary parametric study are also defined in Table 4.1.

4.2.2 Initial Geometric and Material Imperfections

As shown in Table 4.1., the initial geometric imperfections considered in the preliminary study are the out-of-plane deformations of web and compression flange plate panels as well as out-of-straightness of stiffeners. Their magnitudes representing respectively 1/165 of the plate panel depth/width and 1/500 of the stiffener length, are considered representative for Canadian box girder bridges [72] and consequently used throughout the parametric study.

Residual stresses $\sigma_{rc} = 0.10\sigma_y$ similar to those measured in box girder bridges built in Canada [4] and applied as described in section 3.7 were initially considered in both webs and compression flanges of box girder models. However, after several trials it was found that residual stresses considered in box girder webs have a minor effect on their ultimate strength even though the stiffness of the web subpanels was reduced in the early stages of loading. These findings which are in line with those reported previously by Horne and Grayson [21] and Harding et al. [73] led to the decision not to include further the residual stresses in box girder webs and this reduced considerably the computer time.

4.2.3 Discussion of Results

a. Box Girder Type A

The webs of plate and box girders are primarily designed to resist shear forces acting on them. Consequently the first part of the preliminary study dealt with ultimate strength and buckling behaviour of box girder webs subjected primarily to shear ($M_u / M_y \approx 0.2$).

In performing the study the box girder finite element model was loaded as shown in Figure 4.1.a.

Using the finite element mesh given in Figure 4.3 to perform the numerical analysis, lateral and vertical displacements as well as stresses developed in the web at each nodal point were defined at each incremental load until the peak load was reached. However, considering the objective of this study, only load - deflection curves are plotted in Figure 4.4 for the three types of web stiffening previously defined in section 4.2.2. The corresponding ultimate loads are listed in Table 4.2.

Referring to Figure 4.4 and results of the numerical analysis based on which the local deflection curves were plotted, the loads corresponding to the beginning of the nonlinear behaviour are: 439 kN for box girder webs without longitudinal stiffeners (Type 1.(ii)), 684 kN for web with one longitudinal stiffener (Type 2.a.(ii)) and 972 kN for web with two longitudinal stiffeners (Type 3.c.(ii)). These loads which corresponding to the elastic shear buckling stress of webs are compared in Table 4.3 using the former as reference. As shown in the table, the elastic critical buckling stress of webs in shear increases by 102 and 122 percent for the web stiffening Type 2.a.(ii) and Type 3.c.(ii), respectively. However, when the elastic shear buckling stress of web Type 3.c.(ii)

is compared with that of box girder with web stiffening Type 2.a.(ii) an increase of only 10 percent is noted (Table 4.3).

Comparing also the ultimate loads given in Table 4.2 for each type of web stiffening, one can see from Table 4.3 that the increase in ultimate load carrying capacity of longitudinally stiffened webs with respect to the longitudinally unstiffened one represents 3.2 and 10.7 percent for type 2.a.(ii) and type 3.c.(ii), respectively. From comparison of the ultimate resistance of the box girder webs with two (Type 3.c.(ii)) and one longitudinal stiffener one can note that in the former the load carrying capacity increases by 7.3 percent.

Referring to Table 4.3 where the effect of longitudinal stiffeners on buckling resistance of webs is shown, one can see that the elastic values are changed radically due to the presence of stiffeners while the increase in the ultimate shear capacity represents less than 11 percent.

From Figure 4.4 which defines the behaviour of each box girder under load, one can see that practically a plateau is developed once the ultimate load is reached.

As expected in the case of longitudinally stiffened webs, the subpanel of maximum slenderness ratio buckles in the early loading stages. However, the restraint provided by the adjacent smaller subpanels leads to the increased ultimate loads. At the peak load, when the ultimate shear resistance of the web is reached, increased deformations of the large web panel are noticed. Subsequent loading leads to steadily increased local and overall deformations as illustrated in Figure 4.5 for the box girder model with web stiffening type 3.c.(ii) subjected to ultimate load P_u = 1694 kN.

b. Box Girder Type B

To provide the necessary data to be used in plotting the shear force - bending moment interaction diagrams, the cantilevered box girders of intermediate length shown in Figure 4.1.b were considered. The cantilever length of 3075 mm was defined such that $0.5 < M_u / M_y \leq 0.6$.

In performing the nonlinear finite element analysis the mesh illustrated in Figure 4.6 was used. Based on numerical analysis in which the applied loads were incrementally increased until the ultimate load were reached load - deflection curves as shown in Figure 4.7 were plotted for each type of web stiffening defined previously in section 4.2.2.

Referring to the load - deflection curves, one can note that for this type of box girders the nonlinear behaviour starts at 519 kN for web stiffening type 1.(ii), 936 kN for type 2.a.(ii) and 1122 kN for type 3.c.(ii).

Comparing the above loads one can see from Table 4.3 that the use of one longitudinal stiffener (Type 2.a.(ii)) leads to an increase of 80 percent in the elastic buckling resistance. When two longitudinal stiffeners (Type 3.c.(ii)) are used, the shear resistance increases by 116 percent.

For the present study the ultimate resistance of the webs is of first importance. The ultimate loads corresponding to the three types of web stiffening and listed in Table 4.2 are compared in Table 4.3. As shown for this type of box girder, the addition of each stiffener leads to an increase of ultimate load of 4.9 percent.

For the box girder type B the comments previously made on the box girder type A and related to the affect of web stiffening on buckling resistance of webs also apply.

However, relatively small deformations of the small subpanels are noticed up to the box girder collapse.

For this type of box girder it is worth noting, as shown in Figure 4.8 for web stiffening type 3.c.(ii) that at the ultimate load of P_u = 1608 kN buckling of the most loaded web panel subjected to combined action of shear and bending triggered the buckling of the adjacent panel mainly loaded in shear.

c. Box Girder Type C

To determine the behaviour and ultimate resistance of a box girder web subjected to a combination of shear force and a large bending moment ($0.6 < M_u / M_y \leq 1.0$) finite element model was loaded as shown in Figure 4.1.c.

Using the mesh shown in Figure 4.9, the finite element analysis gave load - deflection curves, up to the collapse load, shown in Figure 4.10 for the three types of web stiffening defined in section 4.2.2.

As shown in the figure, the nonlinear behaviour starts at 549 kN for web stiffening type 1.(ii), 961 kN for web stiffening type 2.a.(ii) and 1139 kN for web stiffening type 3.c.(ii).

A comparison of these loads, as well as of the ultimate loads defined in Table 4.2 for the longitudinally stiffened webs with respect to the longitudinally unstiffened web, is given in Table 4.3.

Referring to Table 4.3 one can note that the elastic shear buckling stress of the box girder model with webs stiffened by one (Type 2.a.(ii)) and two (Type 3.c.(ii)) longitudinal stiffeners is increased by 75 and 107 percent, respectively, when compared with that of webs unstiffened longitudinally (Type 1.(ii)).

A comparison of the ultimate load given in Table 4.2 for the three types of web stiffening is done the increases are 6.9 and 10.6 percent for web stiffening type 2.a.(ii) and 3.c.(ii), respectively as shown in Table 4.3.

Referring to the behaviour of box girders under load, one can see from Figure 4.10 that their behaviour at the peak load is totally different from that of box girder type A and B. In all three cases a sudden reduction in load carrying capacity occurs after the peak load is reached and this is similar to that noticed during the experimental tests (Figure 3.15).

As soon as the ultimate shear buckling resistance of the web is reached (Figure 4.10), excessive deformation of the box girder webs occur and this is followed by buckling of the bottom flange which leads to the overall collapse. As a typical example, the behaviour of box girder model with web stiffening type 3.c.(ii) at ultimate load P_u = 1383 kN is shown in Figure 4.11.

4.2.4 Shear Force - Bending Moment Interaction

The ultimate shear and bending resistance of the three types of box girder with longitudinally unstiffened and stiffened webs are given in Table 4.2 in nondimensional form and expressed as V_u / V_y and M_u / M_y, respectively.

Using the shear forces and bending moments listed in Table 4.2, interaction curves were plotted as illustrated in Figure 4.12.a. From this figure one can note that the effect of bending moments on shear resistance of box girder webs is very small up to $M_u / M_y = 0.6$. After this, a continuous decrease of web shear resistance occurs with the increase of applied bending moment.

For reference, the shear - moment interaction curve specified in Clause 7.10.2 of Canadian bridge design code CAN/CSA-S6-M88 [38] for transversely stiffened webs of plate girders is also included in Figure 4.12.a. For convenience

this curve was plotted in terms of the yield shear and moment as used in defining the interaction curves for web stiffening types considered in this study.

Comparing the interaction curve for unstiffened longitudinally webs (Type 1.(ii)) with that specified by the Canadian standard CAN/CSA-S6-M88 one can note that for the box girder webs subjected to bending moments $M_u / M_y \leq 0.6$ the predicted ultimate strengths are higher than those specified by the code by only 9 and 5 percent for web stiffening type 1.(ii) and type 2.a.(ii), respectively. However, in the case of box girder webs subjected to combined action of shear forces and large moments, the predicted and prescribed ultimate resistance is almost identical.

As shown in Figure 4.12.a and Table 4.2, the most significant changes in interaction curves plotted for box girder webs occur at $0.62 \leq M_u / M_y \leq 0.68$ for the three types of web stiffening. These values are different from $M_u / M_y = 0.75$, specified in the design provisions for plate girders [38], a new interaction equation is proposed:

$$0.625 \frac{M_f}{M_r} + 0.625 \frac{V_f}{V_r} \leq 1.0 \qquad (4.1)$$

which closely agrees with the predicted curves for unstiffened and stiffened longitudinal webs in thin box girder webs where $V_f / V_r > 0.6$ (Figure 4.12.b).

The changes in numerical values used in the proposed interaction formula reflect the behaviour at ultimate load of box girder webs in which, as shown by numerical analysis, the shear - force interaction starts prior to that considered in the plate girders. As many time stated by other investigators, but not proved until the present study, this is the result of the relatively small amount of support against in-plane and out-of-plane movement provided to the web by the thin flange of box girders, compared with the restraint offered by the thicker and narrower flanges of corresponding plate girders.

As shown in the main parametric study, the reduced thickness of the compression flange affects the magnitude and distribution of stresses at ultimate load at the web - compression flange junction as well as anchoring points of the tension-field. Consequently, a reviewed tension-field theory which accounts for the reduced stiffness of the compression flanges must be developed for box girder bridges.

Aiming at providing a set of reliable data related to the contribution of the compression flanges to the ultimate strength and behaviour of box girder webs, a more detailed parametric study was considered necessary as discussed further in section 4.3.

4.3 Main Parametric Study

4.3.1. General

In view of the large number of geometric parameters as well as shear - moment combinations required to be considered in defining the ultimate strength and behaviour of longitudinally stiffened webs used in box girder design, a decision had to be made regarding the research area on which an extensive study ought to be performed. Considering the results of the preliminary parametric study on one side, and the lack of information on the tension-field developed at the ultimate loads in web panels of box girders subjected to shear and combined effect of shear and moment on the other, it was decided to focus the attention on box girder webs subjected to shear. The main reason in taking this decision was the existence of a large amount of experimental and theoretical data on ultimate strength and buckling behaviour of plate girder webs with which the results of the parametric study can be compared. However, an increased number of geometric parameters was

considered necessary in this main part of the parametric study as discussed in section 4.3.1.

To determine the ultimate resistance and behaviour of webs subjected to shear, only box girders type A loaded as shown in Figure 4.1.a were considered in this part of the parametric study.

4.3.2 Parameter Definition

To find the optimum position of longitudinal stiffeners for each of the web stiffening systems illustrated in Figure 4.2, in which one to three longitudinal stiffeners were used, including the recommended value of 0.2h (Clause 7.18.5.1 [38]). This led to the eight subpanel slenderness ratios listed in Table 4.4 as compared to two used in the preliminary study. In addition, for reference purposes box girders webs stiffened only transversely (Type 1.(ii)) were also considered in this study. As shown in the same table, these parameters were used in conjunction with three different subpanel slenderness ratios of which two, h/w = 240 and 300, are in the range of $3150/\sqrt{F_y} < h/w \leq 6000/\sqrt{F_y}$ specified by Clause 7.18.3.3 and 7.18.5.2 [38].

The third one having a slenderness ratio h/w = 400, which is above the specified upper limit, was considered necessary for understanding the local and overall behaviour of slender box girder webs at the ultimate loads.

As previously done, the above parameters were used in combination with those related to the slenderness ratio of the web stiffener, out-of-plane deformation of web and compression flange as well as out-of-straightness of longitudinal stiffeners also defined in Table 4.4.

Residual stresses of $\sigma_{rc} = 0.10\sigma_y$ were considered only in the compression flange for the reasons discussed in section 4.2.2.

Combination of the above parameters led finally to twenty seven finite element box girder models with meshes shown in Figure 4.13 and used in performing the nonlinear analysis discussed in detail in section 4.3.3.

To improve the accuracy of predicted ultimate loads and behaviour of box girder webs the use of a refined mesh was considered necessary. However, due to the restriction imposed by the ADINA program on number of elements, the simply supported part of the cantilevered box girders used in the parametric study (Figure 4.1.a) had to be eliminated and replaced by a fixed support. This led to the finite element mesh illustrated in Figure 4.13, in which 1824 four-node shell elements were employed. Constraints on the nodes at the cantilever end were imposed such that the fixed boundary conditions assumed in the analysis were satisfied.

Comparison of load - deflection curves plotted previously in Figure 4.4 for box girder type A with those defined using the refined mesh and fixed boundary conditions showed good agreement. Consequently only the latter was employed in performing the main parametric study.

4.3.3. Discussion of Results

The ultimate loads and corresponding nondimensionalized shear forces (V_u / V_y) and bending moments (M_u / M_y) predicted for all box girders with web stiffening systems shown in Figure 4.13 and longitudinal stiffener spacing used in this part of the parametric study are given in Table 4.5.

To define the contribution of each subpanel to the overall box girder shear resistance, their individual ultimate shear resistance as well as web panel resistance are listed in Table 4.6. Included in the table are predicted and calculated values. The former represent the average of the shear stresses

developed within each subpanel at ultimate load. The latter were calculated by extending the provisions of Clause 7.10.2 [38] for transversely stiffened webs to web subpanels and assuming each stiffener rigid enough to provide development of tension-field within each panel. Although this assumption is not strictly correct and fully applicable to box girder webs, as shown further, it was considered acceptable taking into account the lack of specific provisions for calculation of ultimate shear stresses in web plates stiffened transversely and longitudinally. As shown in Table 4.6, this assumption led in the case of some web subpanels to a difference between the calculated and predicted shear capacity of maximum 14 percent.

Average predicted and calculated ultimate shear resistance for the web stiffened transversely and longitudinally was also included in Table 4.6. If the former represents the average of the ultimate shear strengths of the component web subpanels, it should be noted that the latter was calculated considering the elastic critical bucking shear stress of the large subpanel in conjunction with tension-field post-buckling stress corresponding to box girder webs stiffened only transversely.

Even though detailed information related to stress distribution and pattern of deformations developed in box girder webs during the loading process up to the peak load is available, only the results of box girders with web thickness of 4 mm, for which slenderness ratio $h/w = 300 = 5120/\sqrt{350}$ is close to the specified upper limit of $h/w = 6000/\sqrt{F_y}$, are presented and discussed in detail in this thesis.

For box girder with web thickness of 3 mm (h/w=400) and 5 mm (h/w=240) the ultimate shear and bending resistance only is given in Table 4.5. For the same webs, the corresponding predicted and calculated individual

subpanel ultimate shear resistance together with their average values defined as above, are also listed in Table 4.6.

The overall main parametric results presented in Table 4.5 and 4.6 are finally used in defining the optimum stiffening system corresponding to each web panel slenderness ratio.

A. Web Stiffening Type 1.(ii)

Using the finite element mesh illustrated in Figure 4.13.A with the loading and boundary conditions shown in Figure 4.14, nonlinear finite element analyses were performed first for box girders with webs stiffened only transversely. Web thickness of 4 mm as shown in Figure 4.2.A corresponding to h/w = 300 was used in the analysis and the ultimate loads given in Table 4.5 determined.

As mentioned in section 4.3.1, these loads are to be used as reference loads in defining the increase in box girder capacity provided by the different web stiffening systems considered in this study.

As illustrated in Figure 4.14 which depicts the load - deflection curve for the unstiffened webs type 1.(ii), the nonlinear behaviour starts in the early stages of the loading (P = 345 kN) and increases steadily until the ultimate load carrying capacity is reached (P_u = 1327 kN). The shear stresses corresponding to this ultimate load and overall ultimate shear resistance $V_u = 0.67V_y$ defined in Table 4.5, compares closely with the specified ultimate shear resistance calculated based on Clause 7.10.1 [38] and given in Table 4.6.

The overall behaviour and ultimate strength of box girder is governed by web buckling. This is clearly indicated in Figure 4.15 by the web deformation at the ultimate load.

As illustrated in Figure 4.16 and 4.17, the elastic buckling of the web occurs at P = 215 kN which practically corresponds to the theoretical value. However, this does not significantly affect the overall box girder behaviour which ceases to be linear at P = 345 kN. As shown in these figures, deflection of the large web panel increases steadily under the applied load and reaches the maximum value of 13 mm at the ultimate load (P_u = 1327 kN) in section A. The presence of initial deformations has little effect on web buckling behaviour where a change in the mode shape from one sine wave to two sine waves became visible right from the beginning of the loading.

Variation of the superimposed membrane and bending stresses σ_x acting on the inner side of the web at the ultimate load is shown in Figure 4.18. The distribution of the membrane stresses developed at sections A and B for increasing loading, up to the box girder failure, are given in Figure 4.19 and 4.20, respectively.

As shown in both figures, the nonuniform distribution of stresses starts at the early stages of loading. At the ultimate load the maximum tensile stress reaches 158 MPa in areas adjacent to the web panel diagonal.

Distribution of shear stresses in the same sections are shown in Figure 4.21 and Figure 4.22, respectively. A change from uniform to non-uniform stress distribution can be noticed almost immediately after the occurrence of the elastic buckling (P = 345 kN) and this trend continue until the ultimate load is reached. In the final stages the variation of shear stress distribution increases and this is related to the extensive development of the web buckles as shown in Figure 4.16 and Figure 4.17.

As illustrated in both figures the maximum shear stresses, developed in the web after elastic shear buckling occur at 0.3h (section A) and 0.2h (section B) from the inner surface of the compression and tension flange, respectively. In

section A (Figure 4.21) this stress pattern remain unchanged until the ultimate load is reached. However, in section B (Figure 4.22) the stress distribution changes at $P = 0.94\,P_u$ (1242 kN) to the one in which the maximum shear stresses develop at the tension flange - web connection.

The difference in distribution and magnitude of the shear stresses illustrated in Figure 4.21 and 4.22 confirms for the first time the concern of previous investigators related to the effect of reduced stiffness of thin compression flanges on ultimate shear strength and buckling behaviour of box girder webs. As shown in the latter, the increased restraint provided by the thicker flange leads to the occurrence of constantly higher shear stresses at its junction with the web as compared with stresses developed in section A at web - compression flange connection.

The shear and membrane stresses developed in the mid-plane of the web do not reach the yield limit. However, due to plate bending plastic deformations occur on web surfaces (Figure 4.18).

B. Web Stiffening Type 2.a.(ii)

Using the mesh shown in Figure 4.13.B for the web with one longitudinal stiffener at $h_m = 0.2h$ (Figure 4.2.B) complying with Clause 7.18.5.1 of the Canadian bridge code [38], the load - deflection curve given in Figure 4.23 is obtained. The nonlinear behaviour of the web occurs at an early stage (P = 417 kN). Further increase in the applied load produces a continuous reduction in web stiffness as illustrated by the increased nonlinear behaviour until the ultimate web capacity is reached (P_u = 1520 kN). As shown in Table 4.5 for this ultimate load the overall ultimate shear resistance is $V_u / V_y = 0.75$.

From Table 4.6 and Figure 4.24 one can see that the load carrying capacity of the web 2.a.(ii) was governed by buckling resistance of the large subpanel (2) for which $\tau_u / \tau_y = 0.70$ while the small subpanel (1) was able to carry almost 98 percent of the subpanel shear yield load.

From Figure 4.25 and 4.26 which depicts the deflection of box girder web at section A and B, respectively, one can see that the elastic buckling occurs also at P = 229 kN. Under subsequent loading, deflection of the large web subpanel increases steadily under the applied load and reaches the maximum value of 18 mm at the ultimate load (P_u = 1520 kN) in section A. As shown in both figures, the pattern of deflected web prior to the failure load is defined by a two wave sinusoidal curve increasing steadily in amplitude as the load increases. As shown, the buckling mode shape is not affected by the initial deformations of the web panels considered in the analysis (Figure 3.3.b). At the ultimate load a change of the mode shape to three wave sine curves define the buckled shape of the web. However, the deflections of small panel do not increase significantly under the applied loads, behaviour which leads to the increased local buckling resistance previously discussed.

The distribution of the superimposed membrane and bending stresses action in longitudinal direction (σ_x) on the inner surface of the web subjected to ultimate load is presented in Figure 4.27. From this figure and Figure 4.24 one can see that at the ultimate load an incipient twisting of the longitudinal stiffener occurs in association with out-of-plane deformation of web (Figure 4.25).

The longitudinal stiffeners were designed to conform to Clause 7.18.5.3 and supposedly ought to remain straight until the ultimate load is reached. However, as shown above and subsequently for other types of web stiffening, the longitudinal stiffeners of box girder webs designed based on the actual

provisions do not perform accordingly and general start to buckle before the ultimate loads are reached.

Even though several tests aimed at defining the optimum size of the longitudinal stiffeners able to satisfy their assumed behaviour were conducted, for consistency of the work and comparison of results, only stiffeners designed based on actual code provisions are used throughout this study.

Variation of mid-plane membrane stresses (σ_x) in sections A and B of the box girder web during the loading process are shown in Figure 4.28 and 4.29, respectively. From both figures one can see that at each load increment the membrane stresses at sections A and B increase steadily up to 223 MPa and 213 MPa, respectively along the tension band developed within the large subpanel. However, due to increased buckling resistance of the small subpanel, practically no membrane stresses (σ_x) develop along its depth (Figure 4.28). This leads to the conclusion that in this section the small subpanel is subjected to almost pure shear and failure occurs by yielding in shear as shown in Figure 4.30.

Comparing Figure 4.18, where the peak tension stress is at the junction of the transverse stiffener with the box girder web and compression flange, with Figure 4.27, it is seen that in the latter the peak tension stress is at junction of the transverse stiffener with the web and the longitudinal stiffener.

Significant changes in shear stress magnitude and distribution are to be noted for longitudinally stiffened webs Type 2.a.(ii) when compared with unstiffened one (Type 1.(ii)). These changes are visible at section A (Figure 4.30) and section B (Figure 4.31) and relate to increased shear stresses developed at the longitudinal stiffener level. Even though the trend in shear stress distribution along the web depth remains similar to that previously discussed for Type 1.(ii), there is a significant increase of area affected by large shear stresses (Figure 4.30).

However, as previously noted for Type 1.(ii) webs, the maximum shear stresses in section A are smaller than those in section B until the last stages of loading. Shear stresses in section A at web - compression flange junction remain also smaller than those developed in the adjacent areas until the collapse load is reached.

Although at ultimate load the shear stresses reach the yield point in both sections, the web area on which these high stresses act is much larger in section A (Figure 4.30) than section B (Figure 4.31), and this should be related as previously to the affect of inner compression flange on shear buckling resistance of box girder webs.

Deformation of the top and bottom flanges of the box girder were negligible prior to and after the ultimate load was reached (Figure 4.24).

C. Web Stiffening Type 2.b.(ii)

For the box girder with webs stiffened by one longitudinal stiffener at $h_m = 0.3\,h$ (Figure 4.2.B) the mesh shown in Figure 4.13.C was used with the loading and boundary conditions given in Figure 4.1.a.

The load - deflection curve for web stiffening Type 2.b.(ii) is plotted in Figure 4.32. Nonlinear behaviour starts at P = 535 kN and continuous up to the ultimate load $P_u = 1520$ kN. As shown in Table 4.5 the ultimate load for web stiffening type 2.b.(ii) corresponds to an overall ultimate shear resistance of $V_u / V_y = 0.76$. From Table 4.6 and Figure 4.33 the load carrying capacity of the web 2.b.(ii) was again governed by the shear resistance of the large subpanel (2) for which $\tau_u / \tau_y = 0.70$ while the small subpanel (1) was able to carry almost 90 percent of its yield ultimate resistance.

The occurrence of elastic buckling of box girder web at P = 233 kN is clearly noticed in Figure 4.34 and 4.35 which depicts the deflection of web at section A and B, respectively. As shown, deflection of the large web subpanel increases steadily under the applied load and reaches the maximum value of 14 mm at the ultimate load (P_u = 1520 kN) in section A. However, unlike that of web stiffening type 2.a.(ii), the small subpanel of web type 2.b.(ii) exhibits large deformations especially in the final stages of the loading and in areas close to section A. At ultimate load, as shown in the Figure 4.33 and Figure 4.34, buckling of both the large and the small subpanel occurs. Maximum deflections of 12.0 mm and 10.6 mm are noticed in section A and B, respectively.

Buckling of the small subpanel practically restricts any further increase of the applied load and this leads to a plateau similar to that noticed in the case of unstiffened webs (Figure 4.14).

Distribution of superimposed membrane and bending stresses acting on the inner surface of web subjected to the ultimate load is shown in Figure 4.36.

Distribution of normal membrane stresses (σ_x) under incremental loading is shown in Figure 4.37 for section A and Figure 4.38 for section B. From these figures one can see that prior to the ultimate load the web behaviour is similar to that of Type 2.a.(ii). However, at the ultimate load as illustrated in Figure 4.36 and Figure 4.37 the smaller panel also buckles and develops a nonuniform distribution of normal stresses (σ_x).

Shear stress distribution as shown in Figure 4.39 and 4.40 tend to be more uniform than in the case of box girder Type 2.a.(ii) especially in the early loading stages due to the increased buckling resistance of the upper subpanel. In general the stress pattern remain similar to that previously discussed for Type 2.a.(ii), even though the same changes occur.

D. Web Stiffening Type 3.a.(ii)

Taking into account that practically no design provisions exist for web stiffened by two longitudinal stiffeners it was decided to vary the stiffener spacing between 0.13h to 0.27h. This range was considered practical and large enough to provide the data on which to base on which the optimum web stiffening system.

The first box girder considered in this part of the parametric study is Type 3.a.(ii) with two longitudinal stiffeners spaced at 0.13h (Figure 4.2.C). To perform the finite element nonlinear analysis the finite element mesh shown in Figure 4.13.D was used.

From Figure 4.41 which depicts the load - deflection one can see that at P = 486 kN the box girder ceases to behave linearly. Subsequent loading leads to increased nonlinear behaviour until the ultimate load carrying capacity of P_u = 1593 kN is reached. This correspond to the ultimate shear resistance of V_u / V_y = 0.78 (Table 4.5).

As shown in Figure 4.42 and Table 4.6 the overall box girder behaviour is governed by the buckling resistance of the larger subpanel (3) for which V_u / V_y = 0.72. The two small subpanels carry almost their ultimate shear load.

As can be seen from Figure 4.43 and 4.44 which depicts the deflection of web at section A and B, respectively, the elastic buckling of web occurs at 231 kN which represents 80 percent of the theoretical critical load. This reduction in elastic buckling load predicted numerically is related to the initial deformations considered in this study (Table 4.4). At P = 486 kN the nonlinear behaviour of box girder starts.

As illustrated in Figure 4.43 and 4.44, deflection of large subpanel increases steadily under the applied load and reaches 26 mm in section A at the ultimate load.

Figure 4.45 presents the envelope of normal stresses developed on the inner surface of web at the ultimate load.

Distribution of mid-plane membrane stresses in section A (Figure 4.46) and B (Figure 4.47) shows that the stress magnitude and pattern is almost identical to that illustrated in Figure 4.28 and 4.29 for Type 2.a.(ii) with a difference of only 5 percent in ultimate loads. This indicates that adding stiffeners in an already stiffened zone has little effect.

The same observation applies when the shear stress magnitude and distribution illustrated in Figure 4.48 and 4.49 are compared to Figure 4.30 and 4.31. The main difference is that, due to the increased shear buckling resistance provided by the two longitudinal stiffeners, slightly higher stresses develop in the two subpanels of box girder web Type 3.a.(ii). At the ultimate load, the shear stresses at section A (Figure 4.48) reach the yield stress over the depth of the stiffened zone.

E. Web Stiffening Type 3.b.(ii)

For the box girder with web stiffening Type 3.b.(ii), the second in the series of web stiffened by two longitudinal stiffeners, the spacing was 0.17h (Figure 4.2.C).

Using the mesh shown in Figure 4.13.E, the load - deflection curve in Figure 4.50 was obtained. The box girder behaves linearly up to P = 568 kN, and nonlinearily up to the ultimate load P_u = 1621 kN. As shown in Table 4.5 this corresponds to $V_u / V_y = 0.80$.

The ultimate shear resistance of the large subpanel (3) $V_u / V_y = 0.70$ governs the overall web resistance while the small subpanels provide almost the yield shear resistance (Table 4.6). This compares closely with the calculated value given in Table 4.6 except that corresponding to subpanel (3) for which the numerically predicted load carrying capacity is under the specified one by 5 percent.

Deflections of the web at section A and B are illustrated in Figure 4.52 and 4.53, respectively. They replicate almost the pattern of box girder Type 3.a.(ii) and consequently the previous observations apply.

Similarities extend to Figure 4.45 which depicts the distribution of normal stresses developed on the inner surface of the web as well as Figure 4.55 and 4.56 showing the variation of mid-plane membrane stresses in section A and B, respectively.

There are no significant changes in the shear stress distribution shown in Figure 4.57 and 4.58 when compared with Figure 4.48 and 4.49, respectively.

The ultimate shear resistance of box girders 3.a.(ii) and 3.b.(ii) differ by only 2 percent (Table 4.5 and 4.6).

F. Web Stiffening Type 3.c.(ii)

A box girder with longitudinal web stiffeners spaced at 0.2h (Figure 4.2.c) was considered for Type 3.c.(ii).

Using the mesh shown in Figure 4.13.F, the load - deflection curve in Figure 4.59 was obtained. The behaviour is linear up to P=647 and nonlinear up to the ultimate load P_u = 1642 kN.

Box girder web shear resistance corresponding to the ultimate load is $V_u / V_y = 0.81$ (Table 4.5) while the ultimate shear resistance of the large

subpanel (3) governing the overall web resistance (Figure 4.60) is $V_u / V_y = 0.70$ (Table 4.6). Subpanel (2) and (1) provide 96 and 100 percent yield shear resistance. These compare closely with the calculated values given in Table 4.6 except that corresponding to subpanel (3) for which a difference in the load carrying capacity of 8 percent is noticed.

The pattern of web deformations (Figure 4.61 and 4.62) is almost identical to that of box girder web Type 3.a.(ii) and 3.b.(ii) prior to failure load and the comments made on Type 3.a.(ii) apply. However, at the ultimate load, as shown in Figure 4.60 and 4.61, local buckling of the small subpanel (2) and distortion of the longitudinal stiffener occur.

Similar observations extend to distribution of mid-plane membrane stresses in section A (Figure 4.64) and section B (Figure 4.65) up to P=1582 kN when compared with corresponding figures previously discussed for box girder Type 3.a.(ii) and 3.b.(ii). However, at the peak load $P_u = 1642$ kN the stress distribution in section A shows the occurrence of tensile stresses at the level of the upper longitudinal stiffener. This sudden change from compression to tension is related to the occurrence of local buckling of the subpanel (2). No changes occur at the ultimate load in section B.

Closed similarities exist also in distribution of shear stresses developed prior to the collapse load in section A (Figure 4.66) and section B (Figure 4.67) of this girder and the other two previously discussed. However, at the ultimate load shear yielding of the small panel extends beyond the upper longitudinal stiffener.

No such changes occur in section B (Figure 4.67).

G. Web Stiffening Type 3.d.(ii)

The fourth box girder considered in this series (Type 3.d.(ii)) has spacing of longitudinal stiffeners at 0.23h (Figure 4.2.C).

Using the finite element mesh shown in Figure 4.13.G the load - deflection curve shown in Figure 4.68 was obtained. The behaviour is linear up to P = 909 kN and nonlinear until the failure load P_u = 1657 kN.

A comparison of this curve with those plotted for Type 3.a.(ii) to Type 3.c.(ii) reveals that a shorter plateau develops after the ultimate load is reached.

At the ultimate load the web shear resistance is V_u / V_y = 0.83 (Table 4.5) and the corresponding ultimate shear resistance of subpanel (3), (2) and (1) is 0.71, 0.94 and 0.97, respectively (Table 4.6). These compare closely with the calculated values given in Table 4.6 except that corresponding to subpanel (3) for which the load carrying capacity is 10 percent higher.

The web deformations in sections A and B are illustrated in Figure 4.70 and 4.71, respectively. This is similar to the deformation of box girder web Type 3.d.(ii).

The observation extends also to Figure 4.72 which shows the normal stresses acting on the inner surface of the web.

The distribution of membrane stresses in section A (Figure 4.73) and section B (Figure 4.74) prior to and at the ultimate load clearly illustrates the almost identical behaviour with the other box girder in this series.

Similarities are also seen between the shear stress distributions shown in Figures 4.75 and 4.76 and Figures 4.66 and 4.67 for box girder Type 3.c.(ii). However, in the former (section A) the increased subpanel slenderness ratio prevents the shear stresses reaching the yield at the web - compression flange connection.

H. Web Stiffening Type 3.e.(ii)

The fifth box girder used to define the efficiency of the second longitudinal stiffener on ultimate strength and buckling behaviour of box girder web is Type 3.e.(ii). For this, the longitudinal stiffeners were spaced at 0.27h (Figure 4.2.C).

Using the mesh shown in Figure 4.13.H the load - deflection curve in Figure 4.77 was obtained. The nonlinear behaviour starts at P=1243 kN and increases steadily up to the failure load P_u = 1730 kN.

Comparing this curve with the previous ones, one can see a reduction in load carrying capacity after the ultimate load is reached. This behaviour is mainly due to the reduced shear resistance of the small subpanels which buckle before reaching the yield stress.

At the ultimate load the web shear resistance is $V_u / V_y = 0.88$ (Table 4.5) and the corresponding ultimate shear resistances of subpanel (3), (2) and (1) are 0.75, 0.97 and 0.95, respectively (Table 4.6). These compare closely with the calculated values given in Table 4.6 except that corresponding to subpanel (3) for which the numerically predicted load carrying capacity is lower by 9 percent.

As shown above and Figure 4.78 the buckling resistance of the large subpanel (3) controls the overall box girder web resistance but is also affected by the reduced local buckling resistance of the adjacent small subpanels.

The pattern of web deformations occurred during the incremental loading in section A and B are shown in Figure 4.79 and 4.80, respectively. In general, prior to ultimate load, the deformations of web are similar to those of Type 3.a.(ii) to 3.d.(ii). As shown, prior to reaching the peak load the only subpanel which buckles is the large one. However, at the ultimate load the two lower

subpanels buckle suddenly as illustrated in Figure 4.79 and no further reserve exists.

Variation of normal stresses on the inner face of the stiffened web is given in Figure 4.81. Distribution of membrane stresses is illustrated in Figures 4.82 and 4.83 for the two sections considered.

As can be seen in the former, a very small increase in stress magnitude occurs prior to failure in the small subpanels. However, a sudden change can be noticed at the ultimate load, triggered by their buckling.

In the latter, an almost linear variation of stresses develops on three quarters of the web depth prior to failure, with a nonlinear one after the buckling.

Shear stresses plotted in Figure 4.84 and 4.85 presents an almost uniform distribution in the early loading stages. Afterwards a nonlinear distribution different from the previous ones develops. As shown, in Figure 4.84, the maximum shear stress occurs at the upper stiffener level but extend across the central subpanel. The yield shear is reached first at P=1640 kN and with further increase in load it extends to the adjacent subpanels.

An unusual stress distribution is also noticed in section B (Figure 4.85) where maximum shear stresses develop between the stiffeners and at 0.13h from the inner face of the tension flange. At ultimate load, yield shear resistance is reached only at the junction of web - tension flange. However, stresses representing 97 percent of the yield stress occurs in the central subpanel.

I. Web Stiffening Type 4.(ii)

In case of many long span box girder bridges the flanges and adjacent areas of webs can be subjected to stresses which alternate between tension and compression.

Consequently longitudinal stiffening of webs is required in both lower and upper areas.

To study the behaviour of such webs a box girder with the web stiffened by two longitudinal stiffeners in the lower part and one stiffener in the upper part of one the web (Figure 4.2.D) was used. Only stiffeners spaced at 0.2h were considered in this study.

Using the mesh illustrated in Figure 4.13.I the load - deflection curve presented in Figure 4.86 was obtained. This shows that linear behaviour extends much above the previous values reaching P = 1455 kN. The nonlinear behaviour provides a long plateau at the ultimate load P_u = 1797 kN and, as is to be expected, the reduced panel width results in higher elastic and ultimate loads.

At the ultimate load the web shear resistance is $V_u / V_y = 0.90$ (Table 4.5) and the corresponding ultimate shear resistance of subpanel (4), (3), (2) and (1) is 1.0, 0.76, 1.0 and 1.0, respectively (Table 4.6). These compare closely with the calculated values given in Table 4.6 except that corresponding to subpanel (3) for which the numerically predicted load carrying capacity is lower by 11 percent.

As shown above and in Figure 4.87 the box girder web resistance is governed by the large subpanel resistance.

The increased linear behaviour as well as high ultimate load is directly related to small deformations of the web during the loading process as illustrate in Figure 4.88 and 4.89 for section A and B, respectively. No change in the buckling mode occurs even at the ultimate load.

From Figure 4.90 which presents the distribution of normal stresses on the inner surface of the web, one can see that at the ultimate load the maximum tensile stresses develops along the large subpanel diagonal. At this loading stage twisting of the longitudinal stiffeners (Figure 4.87) occur mainly due to increased deformations of the web subpanels (Figure 4.88 and 4.89). However, as shown in Figure 4.88 and 4.89 no lateral displacement of stiffeners is noticed up to the collapse load.

Due to the reduced subpanel slenderness ratio the membrane stresses in the small subpanels of section A (Figure 4.91) and section B (Figure 4.92) vary linear and increase very slowly up to the ultimate load. At failure load, a sudden increase of tensile stresses occurs especially along the large subpanel diagonal.

At ultimate load the yield shear stresses at section A (Figure 4.93) extend across all three small subpanels with the average shear stress in the large panel of 76 percent of the yield shear stress.

In section B (Figure 4.94) the shear stresses developed in the areas adjacent to the upper stiffener increase more rapidly and reach the yield shear stress prior to the failure load. At the ultimate load yield stresses extend up to the web - tension flange connection.

The behaviour of box girder webs type 4.(ii) which allowed development of 90 percent of its yield shear resistance is mainly due to almost ideal support provided by longitudinal stiffeners to the small subpanel boundaries which allowed them to yield without buckling. This explains also the development of large plateau noticed in Figure 4.86.

4.4 Discussion of Parametric Study

In discussing the predicted behaviour and ultimate buckling resistance of thin box girder webs reference will be made to the loading conditions used in performing the parametric studies.

a. Box girders subjected to shear

As shown in the main parametric study the behaviour and ultimate shear resistance of box girder webs is affected by the reduced thickness of the compression flange. The reduced support provided by this flange leads to a switch of the area where tensile stresses develop from junction of transverse stiffener - web - compression flange considered in plate girders, to junction of transverse stiffener - web - longitudinal stiffeners.

The data on the ultimate strength of box girder webs listed in (Table 4.6), is presented diagrammatically in Figure 4.95. In this figure the predicted and calculated ultimate shear resistance of each of the nine types of web stiffening is given for web slenderness ratios of: i) $h/w = 400$; ii) $h/w = 300$ and iii) $h/w = 240$.

Comparing the ultimate shear resistance predicted by numerical analysis with that calculated based on code provisions, for longitudinally stiffened webs, the former are above the latter by a maximum of 9 percent, except for webs with $h/w = 240$ (Figure 4.95.c) Type 3.a.(iii) and 4.(iii) where they are below by 1 and 6 percent, respectively.

For unstiffened webs the predicted strength for $h/w = 400$ are below the calculated one by 13 and 1 percent respectively. For $h/w = 240$ the former is above the latter by 3 percent.

Finally one can conclude that, under the assumptions made in calculation of ultimate shear resistance, the code provisions for plate girder webs can be used also for box girder webs. However, care should be taken for box girders with stiffened webs in the range of the specified lower limit $h / w = 3150 / \sqrt{F_y}$ such as Type 3.e.(iii) and 4.(iii) for which the code provisions seems to underestimate the ultimate load carrying capacity.

Even though the optimum spacing of longitudinal stiffeners for webs subjected to shear is that corresponding to equal subpanel depth, different spacings were used in performing the present parametric studies. This was done considering the practical loading conditions encountered in box girder design where in almost all cases the webs are subjected to the combined action of shear and bending, and not shear only.

For this type of webs longitudinal stiffeners are provided in the web area subjected to bending induced compressive stresses as discussed further in section 4.4.b.

b. Box girders subjected to combined shear and bending

Based on results of the preliminary parametric study it was shown that in the case of box girder webs subjected to combined action of shear forces and bending moments for which $V_u / V_y > 0.6$ the interaction starts at $M_u / M_y = 0.6$, and not at $M_u / M_y = 0.75$ as considered for plate girders. Although a more detailed parametric study is considered necessary to confirm the findings, it appears that the behaviour and ultimate strength of box girder webs stiffened longitudinally and subjected to combined shear and bending is even more affected than that of webs subjected to shear forces only. For such box girders the interaction between the web and compression flange behaviour at the

ultimate load must also be considered especially when their individual buckling resistance approaches simultaneously the critical values. In such cases the boundary conditions assumed in design of box girder components cease to be satisfied.

In an attempt aimed at defining a interaction curve which matches the results of parametric study a new interaction formula is proposed specifically for box girder webs.

Table 4.1 Parameters Used in the Preliminary Parametric Study

Parameter	Notation	Value
1. Out-of-Plane Deformation of Plate Panels		
a. Web	Δ_p^0 / h_p	1/165
b. Compression flange	Δ_p^0 / b	1/165
2. Out-of-Straightness of Stiffeners (Webs & Flanges)	Δ_s^0 / a	1/500
3. Web Panel Slenderness Ratio	h / w	300
4. Web Subpanel Slenderness Ratio		
a. Maximum	h_M /w	180 240 300
b. Minimum	h_m /w	60 60 0
5. Slenderness Ratio of Web Stiffeners	a / r	53.7
6. Number of Web Stiffeners	n_s	0 1 2
7. Web Stiffener Spacing	h_m /h	0.00 0.20
8. Length of Cantilevered Box Girder (mm)	L	1075 3075 5000

Table 4.2 Ultimate Shear and Bending Resistance of Box Girders Used in the Preliminary Study

Web Stiffening Type			Box Girder Type	P_u (kN)	V_u / V_y	M_u / M_y
1		ii	A	1531	0.74	0.23
2	a	ii		1580	0.77	0.23
3	c	ii		1694	0.81	0.25
1		ii	B	1465	0.72	0.62
2	a	ii		1535	0.75	0.65
3	c	ii		1608	0.80	0.68
1		ii	C	1251	0.64	0.86
2	a	ii		1338	0.67	0.92
3	c	ii		1383	0.70	0.95

Note:

For box girder type and web stiffening type see Figure 4.1 and Figure 4.2, respectively.

Table 4.3 Effect of Web Stiffening System on Box Girder Resistance. Preliminary Study

Web Stiffening Type		Box Girder Type					
		A		B		C	
		Resistance					
		Elastic	Ultimate	Elastic	Ultimate	Elastic	Ultimate
$\frac{2.a.(ii)}{1.(ii)}$	%	102	3.2	80	4.9	75	6.9
$\frac{3.c.(ii)}{1.(ii)}$	%	122	10.7	116	9.8	107	10.6
$\frac{3.c.(ii)}{2.a.(ii)}$	%	10	7.3	19.9	4.8	18.5	3.4
1.(ii)	kN	439	1531	519	1465	549	1251

Note:

For box girder type and web stiffening type see Figure 4.1 and Figure 4.2, respectively.

Table 4.4 Parameters Used in the Main Parametric Study

Parameter	Notation	Value
1. Out-of-Plane Deformation of Plate Panels		
a. Web	Δ_p^0 / h_p	1/165
b. Compression flange	Δ_p^0 / b	1/165
2. Out-of-Straightness of Stiffeners	Δ_s^0 / a	1/500
3. Web Panel Slenderness Ratio	h/w	240 300 400
4. Web Subpanel Slenderness Ratio		
a. Maximum	h_M /w	176 to 400
b. Minimum	h_m /w	32 to 120
5. Slenderness Ratio of web Stiffener	a / r	53.7
6. Number of Web Stiffeners	n_s	0 1 2 3
7. Web Stiffener Spacing	h_m /h	0.00 0.13 0.17 0.20 0.23 0.27 0.30

Table 4.5 Ultimate Shear and Bending Resistance of Box Girders Type A Used in the Main Study

Web Stiffening Type			Stiffening Spacing h_m /h	P_u (kN)	V_u /V_y	M_u /M_y
1		i	0.00	800	0.54	0.12
		ii		1327	0.67	0.20
		iii		1812	0.73	0.27
2	a	i	0.20	1072	0.70	0.16
		ii		1520	0.75	0.22
		iii		1960	0.78	0.29
	b	i	0.30	1089	0.70	0.16
		ii		1520	0.76	0.22
		iii		2007	0.80	0.30
3	a	i	0.13	1198	0.77	0.18
		ii		1593	0.78	0.24
		iii		2015	0.81	0.30
	b	i	0.17	1214	0.78	0.18
		ii		1621	0.80	0.24
		iii		2054	0.82	0.30

Table 4.5 — continued

Web Stiffening Type			Stiffening Spacing h_m /h	P_u (kN)	V_u /V_y	M_u /M_y
3	c	i	0.20	1196	0.76	0.18
		ii		1642	0.81	0.24
		iii		2096	0.84	0.31
	d	i	0.23	1159	0.77	0.17
		ii		1657	0.83	0.24
		iii		2158	0.87	0.32
	e	i	0.27	1177	0.79	0.17
		ii		1730	0.88	0.26
		iii		2240	0.91	0.33
4		i	0.20	1303	0.86	0.19
		ii		1797	0.90	0.27
		iii		2303	0.94	0.34

Note:

For web stiffening type see Figure 4.2.

Table 4.6 Comparison of Ultimate Shear Resistance of Web Panels Box Girder Type A

Web Stiffening Type			Plate Panel Number	h_p/h	h_p/a	h_p/w	Normalized Ultimate Shear Resistance (τ_u/τ_y)	
							Code CSA-S6-M88	Finite Element Analysis
1		i	1	1.00	1.12	400.0	0.67	0.54
		ii	1	1.00	1.12	300.0	0.68	0.67
		iii	1	1.00	1.12	240.0	0.70	0.73
2	a	i	1	0.20	0.22	80.0	0.97	0.90
			2	0.80	0.89	320.0	0.67	0.65
			Average	–	–	–	0.68*	0.70
		ii	1	0.20	0.22	60.0	1.00	0.98
			2	0.80	0.89	240.0	0.69	0.69
			Average	–	–	–	0.70*	0.75
		iii	1	0.20	0.22	48.0	1.00	0.97
			2	0.80	0.89	192.0	0.72	0.74
			Average	–	–	–	0.73*	0.78
	b	i	1	0.30	0.34	120.0	0.89	0.76
			2	0.70	0.78	280.0	0.71	0.67
			Average	–	–	–	0.69*	0.70

Table 4.6 — continued

Web Stiffening Type			Plate Panel Number	h_p/h	h_p/a	h_p/w	Normalized Ultimate Shear Resistance (τ_u/τ_y)	
							Code CSA-S6-M88	Finite Element Analysis
2	b	ii	1	0.30	0.34	90.0	0.94	0.90
			2	0.70	0.78	210.0	0.73	0.70
			Average	–	–	–	0.72*	0.76
		iii	1	0.30	0.34	72.0	1.00	0.94
			2	0.70	0.78	168.0	0.76	0.75
			Average	–	–	–	0.76*	0.80
3	a	i	1	0.13	0.15	53.3	1.00	1.00
			2	0.13	0.15	53.3	1.00	0.99
			3	0.73	0.82	293.3	0.70	0.69
			Average	–	–	–	0.68*	0.77
		ii	1	0.13	0.15	40.0	1.00	1.00
			2	0.13	0.15	40.0	1.00	0.99
			3	0.73	0.82	220.0	0.72	0.71
			Average	–	–	–	0.71*	0.78
		iii	1	0.13	0.15	32.0	1.00	1.00
			2	0.13	0.15	32.0	1.00	0.98
			3	0.73	0.82	176.0	0.75	0.74
			Average	–	–	–	0.75*	0.81

Table 4.6 — continued

Web Stiffening Type			Plate Panel Number	h_p/h	h_p/a	h_p/w	Normalized Ultimate Shear Resistance (τ_u/τ_y)	
							Code CSA-S6-M88	Finite Element Analysis
3	b	i	1	0.17	0.19	66.7	1.00	1.00
			2	0.17	0.19	66.7	1.00	0.97
			3	0.67	0.74	266.7	0.72	0.68
			Average	–	–	–	0.69*	0.78
		ii	1	0.17	0.19	50.0	1.00	1.00
			2	0.17	0.19	50.0	1.00	0.99
			3	0.67	0.74	200.0	0.75	0.70
			Average	–	–	–	0.73*	0.80
		iii	1	0.17	0.19	40.0	1.00	1.00
			2	0.17	0.19	40.0	1.00	0.98
			3	0.67	0.74	160.0	0.78	0.74
			Average	–	–	–	0.77*	0.82
	c	i	1	0.20	0.22	80.0	0.97	0.90
			2	0.20	0.22	80.0	0.97	0.88
			3	0.60	0.67	240.0	0.75	0.68
			Average	–	–	–	0.70*	0.77

Table 4.6 — continued

Web Stiffening Type			Plate Panel Number	h_p/h	h_p/a	h_p/w	Normalized Ultimate Shear Resistance (τ_u/τ_y)	
							Code CSA-S6-M88	Finite Element Analysis
3	c	ii	1	0.20	0.22	60.0	1.00	1.00
			2	0.20	0.22	60.0	1.00	0.96
			3	0.60	0.67	180.0	0.78	0.70
			Average	–	–	–	0.75*	0.81
		iii	1	0.20	0.22	48.0	1.00	1.00
			2	0.20	0.22	48.0	1.00	0.96
			3	0.60	0.67	144.0	0.81	0.74
			Average	–	–	–	0.80*	0.84
	d	i	1	0.23	0.26	93.3	0.93	0.92
			2	0.23	0.26	93.3	0.93	0.94
			3	0.53	0.60	213.3	0.78	0.63
			Average	–	–	–	0.72*	0.77
		ii	1	0.23	0.26	70.0	1.00	0.97
			2	0.23	0.26	70.0	1.00	0.94
			3	0.53	0.60	160.0	0.81	0.71
			Average	–	–	–	0.78*	0.83

Table 4.6 — continued

Web Stiffening Type			Plate Panel Number	h_p/h	h_p/a	h_p/w	Normalized Ultimate Shear Resistance (τ_u/τ_y)	
							Code CSA-S6-M88	Finite Element Analysis
3	d	iii	1	0.23	0.26	56.0	1.00	0.98
			2	0.23	0.26	56.0	1.00	0.98
			3	0.53	0.60	128.0	0.84	0.78
			Average	–	–	–	0.85*	0.87
	e	i	1	0.27	0.30	106.7	0.91	0.85
			2	0.27	0.30	106.7	0.91	0.91
			3	0.47	0.52	186.7	0.81	0.69
			Average	–	–	–	0.74*	0.79
		ii	1	0.27	0.30	80.0	0.97	0.95
			2	0.27	0.30	80.0	0.97	0.97
			3	0.47	0.52	140.0	0.84	0.75
			Average	–	–	–	0.82*	0.86
		iii	1	0.27	0.30	64.0	1.00	0.96
			2	0.27	0.30	64.0	1.00	0.99
			3	0.47	0.52	112.0	0.87	0.84
			Average	–	–	–	0.92*	0.91

Table 4.6 — continued

Web Stiffening Type			Plate Panel Number	h_p /h	h_p /a	h_p /w	Normalized Ultimate Shear Resistance (τ_u /τ_y)	
							Code CSA-S6- M88	Finite Element Analysis
4		i	1	0.20	0.22	80.0	0.97	0.98
			2	0.20	0.22	80.0	0.97	0.96
			3	0.40	0.45	160.0	0.84	0.70
			4	0.20	0.22	80.0	0.97	1.00
			Average	–	–	–	0.78*	0.86
		ii	1	0.20	0.22	60.0	1.00	1.00
			2	0.20	0.22	60.0	1.00	1.00
			3	0.40	0.45	120.0	0.87	0.76
			4	0.20	0.22	60.0	1.00	1.00
			Average	–	–	–	0.89*	0.90
		iii	1	0.20	0.22	48.0	1.00	1.00
			2	0.20	0.22	48.0	1.00	1.00
			3	0.40	0.45	96.0	0.92	0.86
			4	0.20	0.22	48.0	1.00	0.98
			Average	–	–	–	1.00*	0.94

Note:

* Ultimate shear resistance calculated considering the elastic critical buckling shear stress in conjunction with the tension-field post-buckling stress corresponding to box girder webs stiffened only transversely.

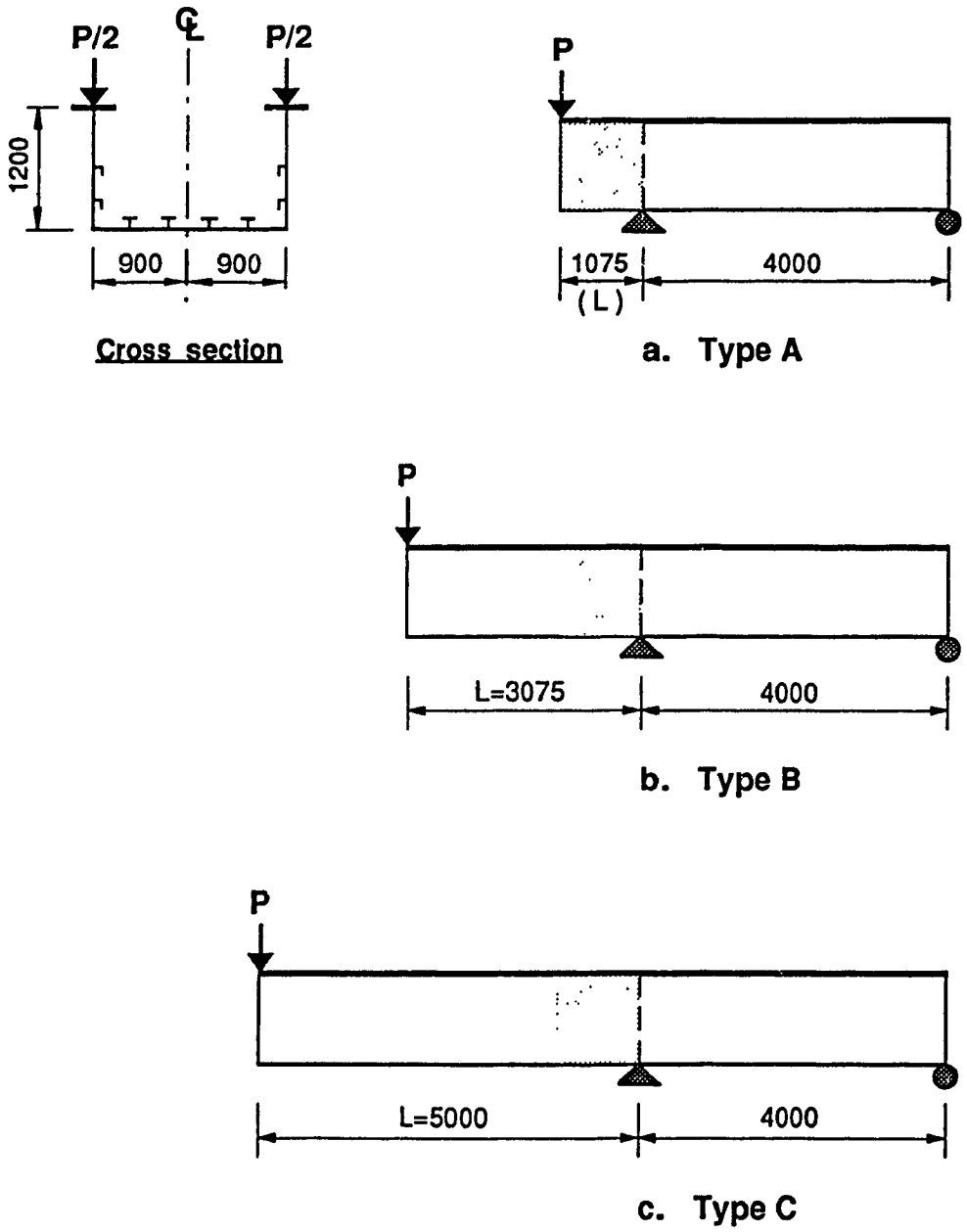

Figure 4.1 Type of Box Girders Used in the Parametric Study

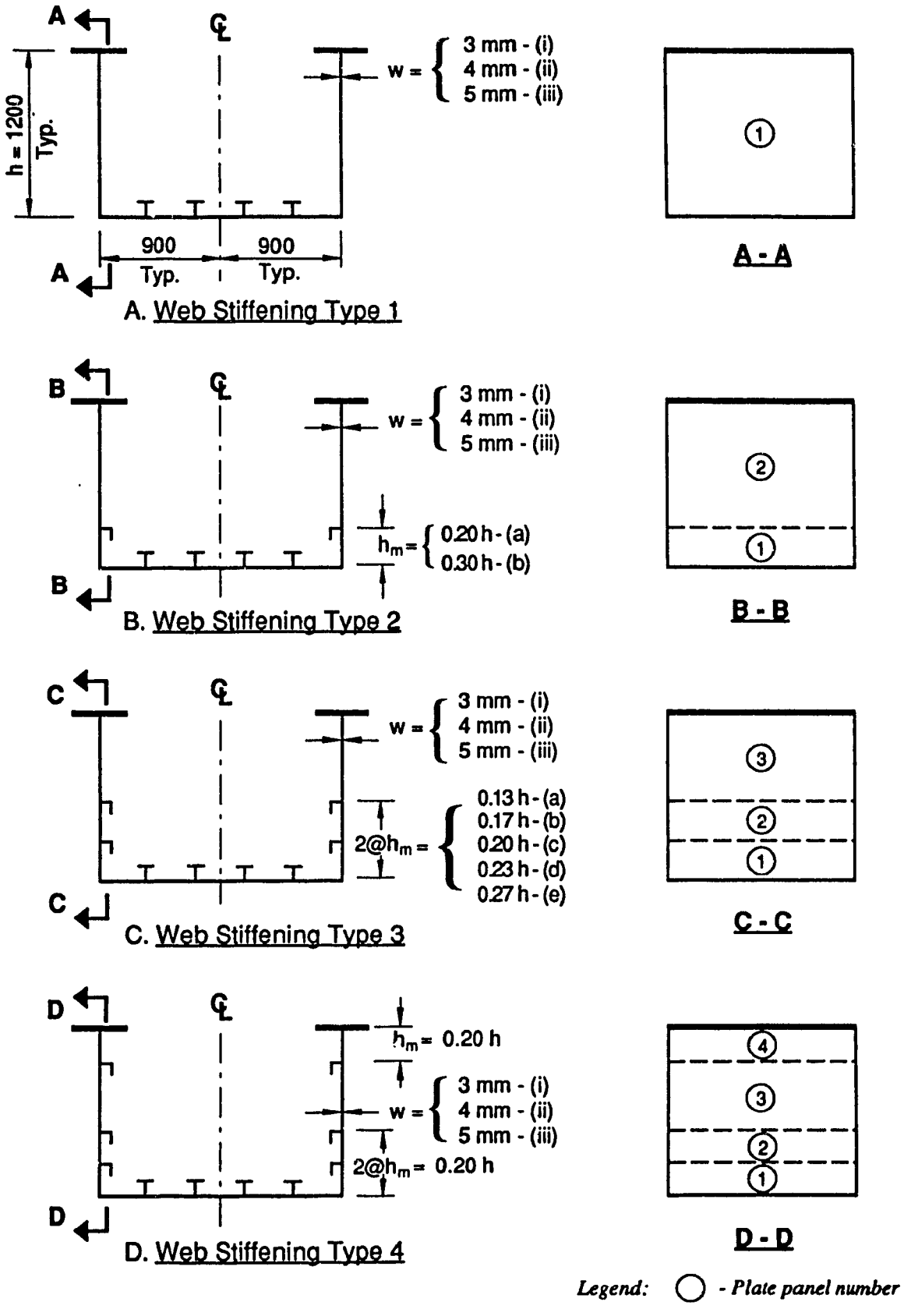

Figure 4.2 Longitudinal Web Stiffening Types

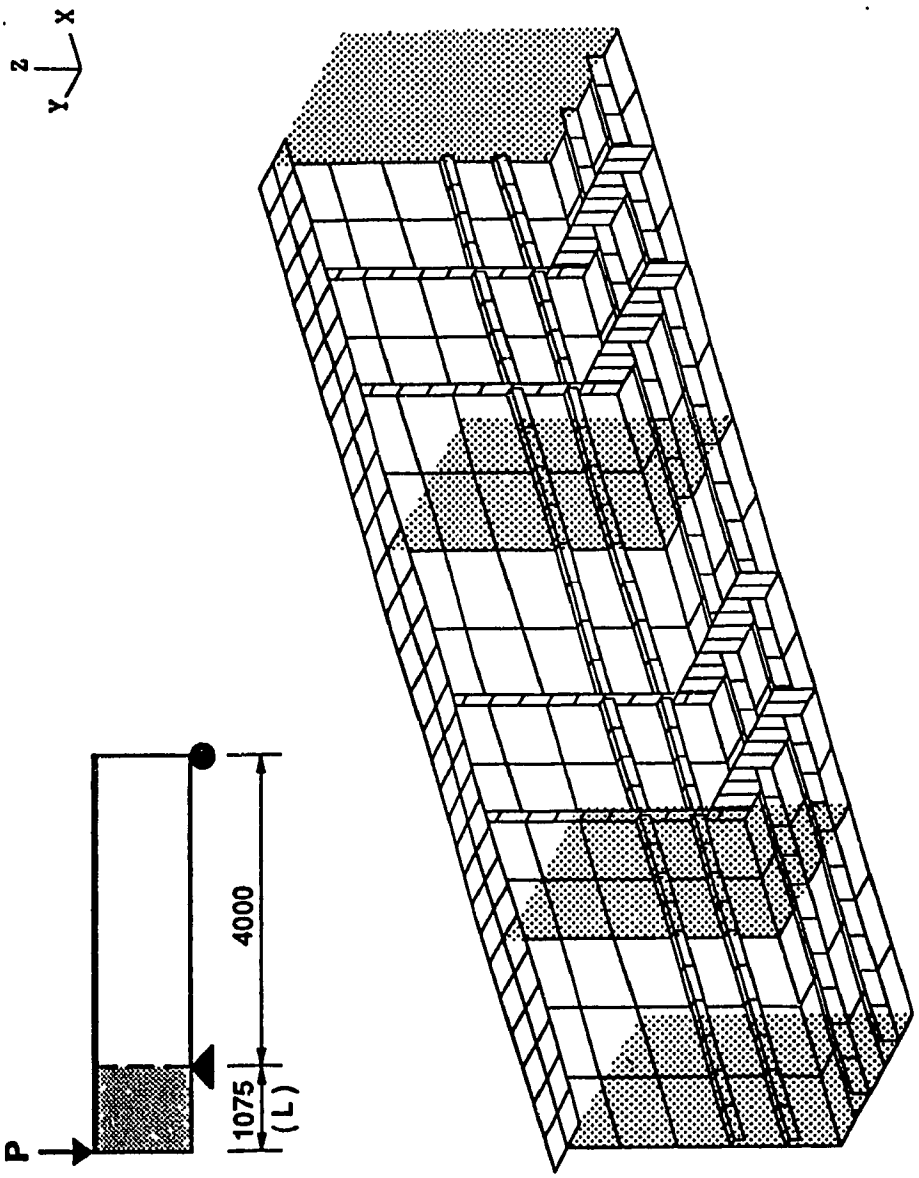

Figure 4.3 Finite Element Model
Box Girder Type A. Web Stiffening Type 3.c.(ii)

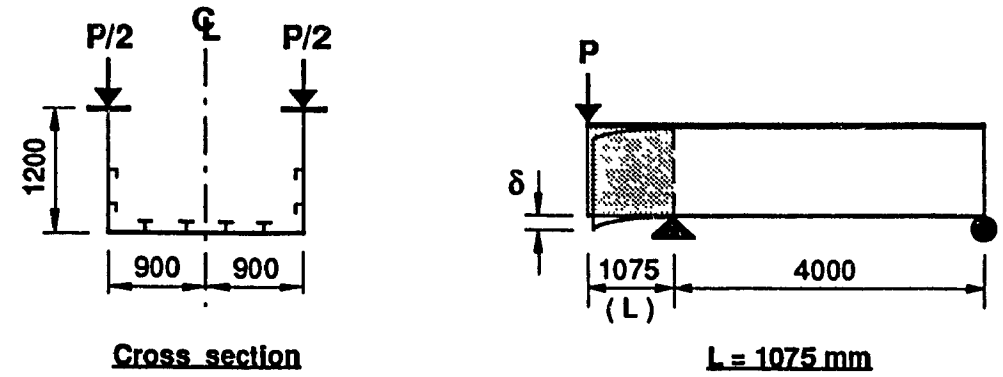

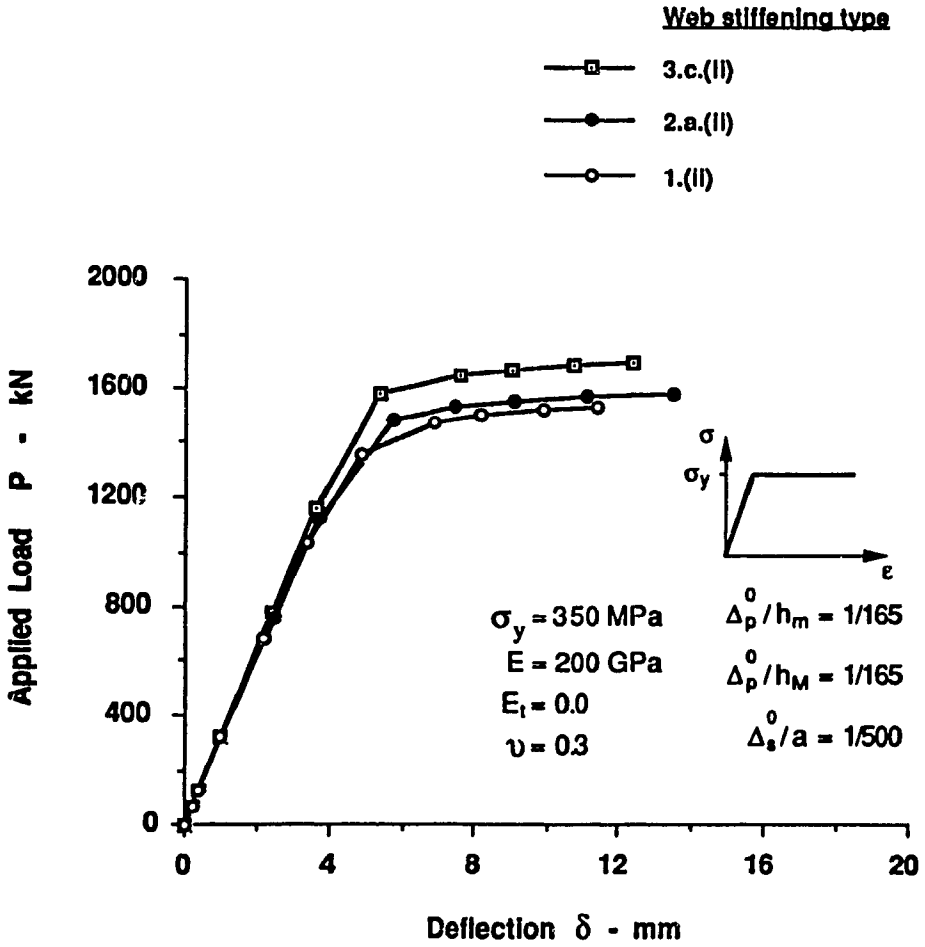

Figure 4.4 Load - Deflection Curves.
Box Girder Type A.

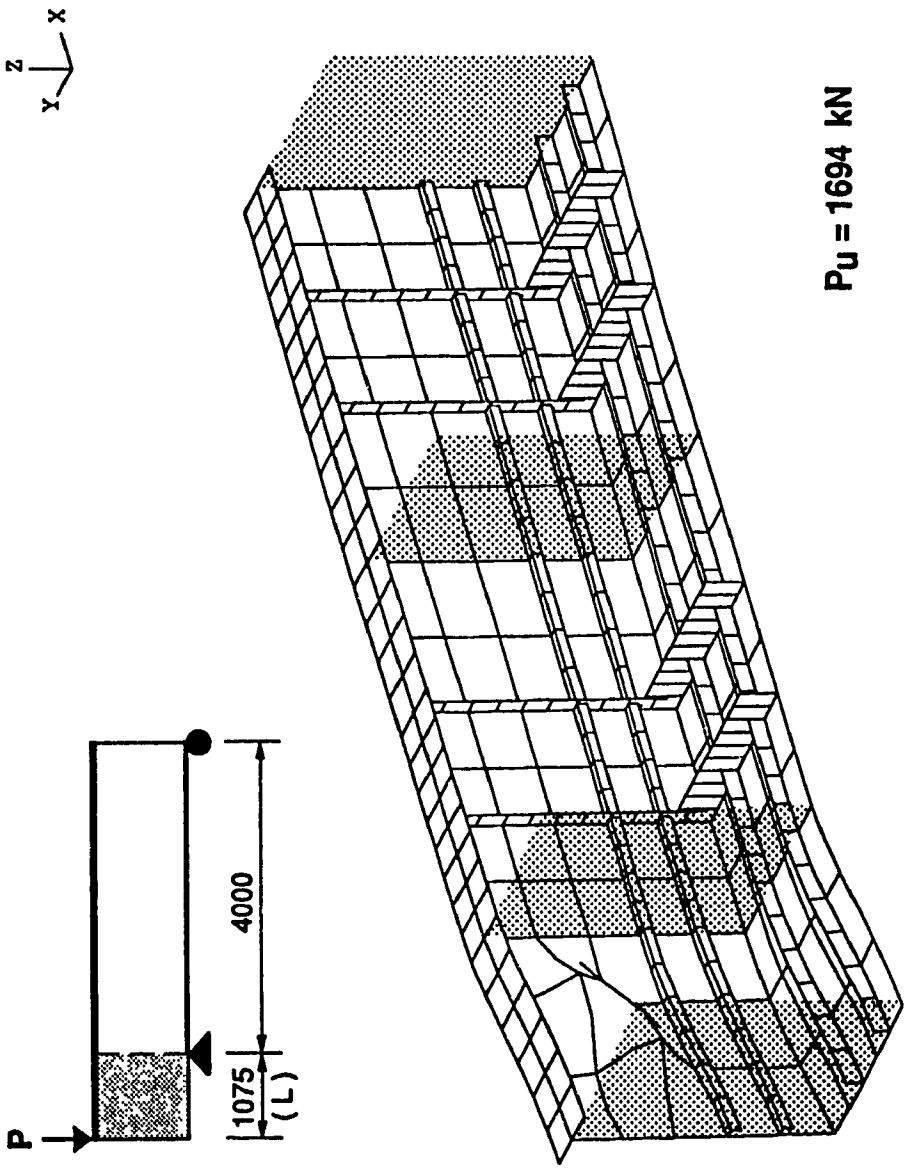

Figure 4.5 Failure of Box Girder Type A with Web Stiffening Type 3.c.(ii)

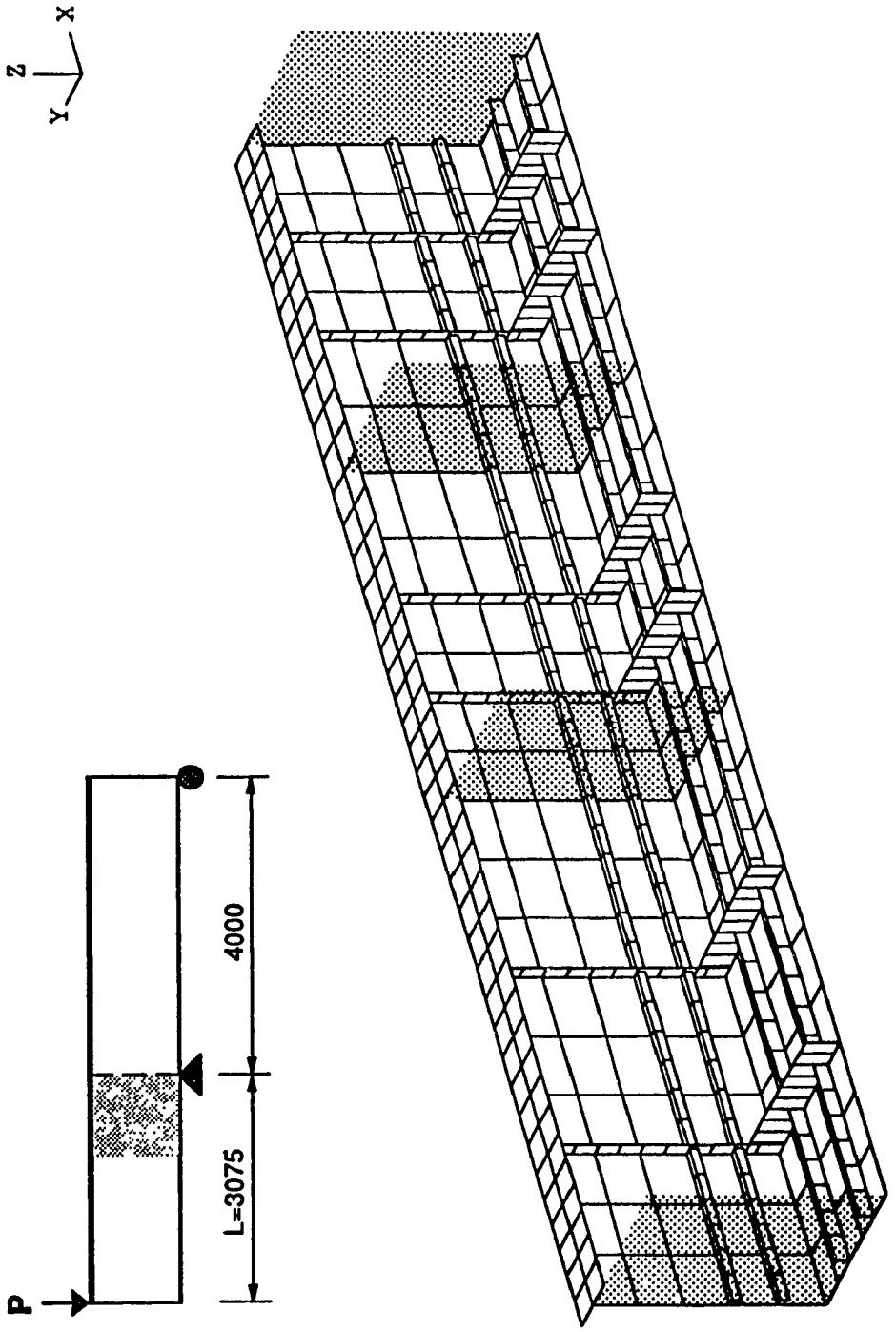

Figure 4.6 Finite Element Model
Box Girder Type B. Web Stiffening Type 3.c.(ii)

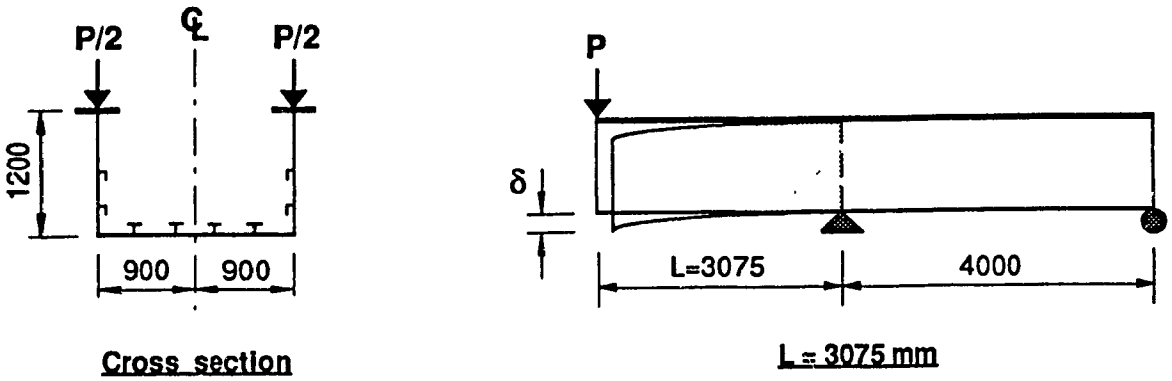

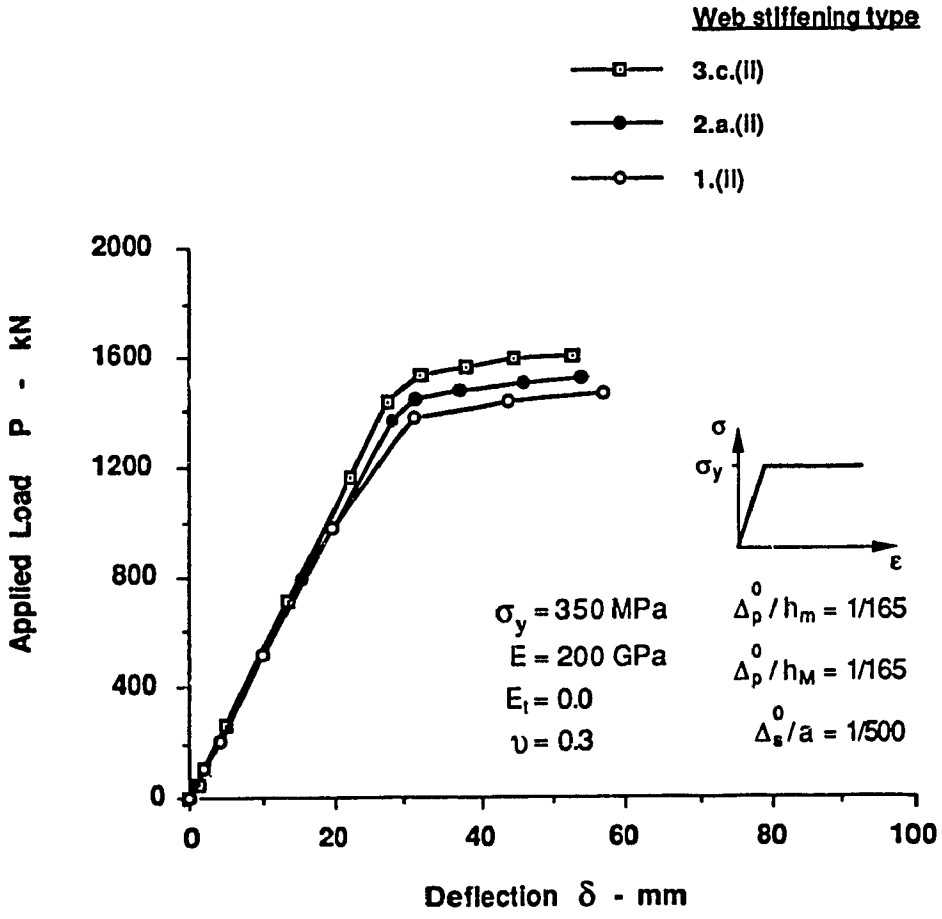

Figure 4.7 Load - Deflection Curves.
Box Girder Type B.

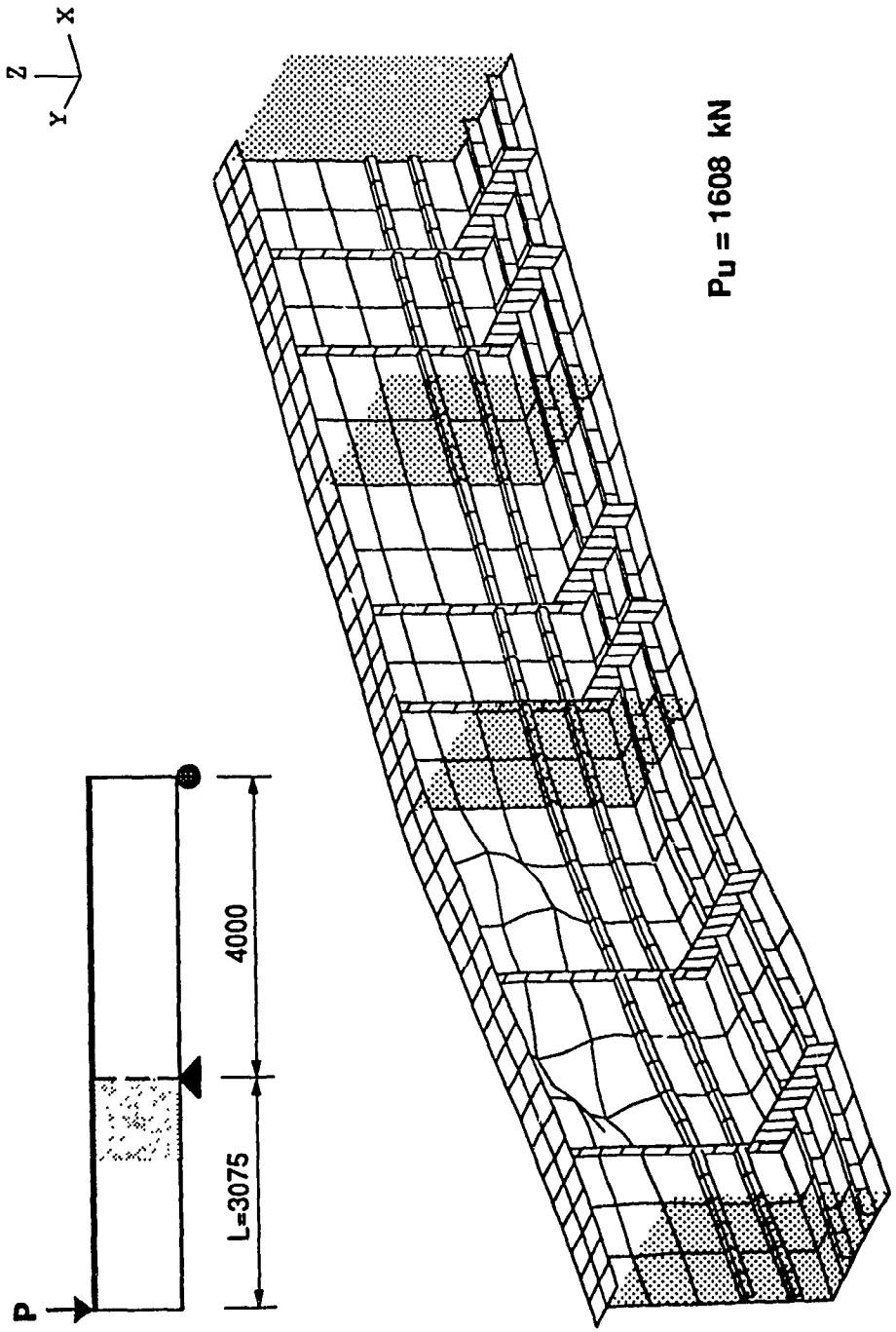

Figure 4.8 Failure of Box Girder Type B with Web Stiffening Type 3.c.(ii)

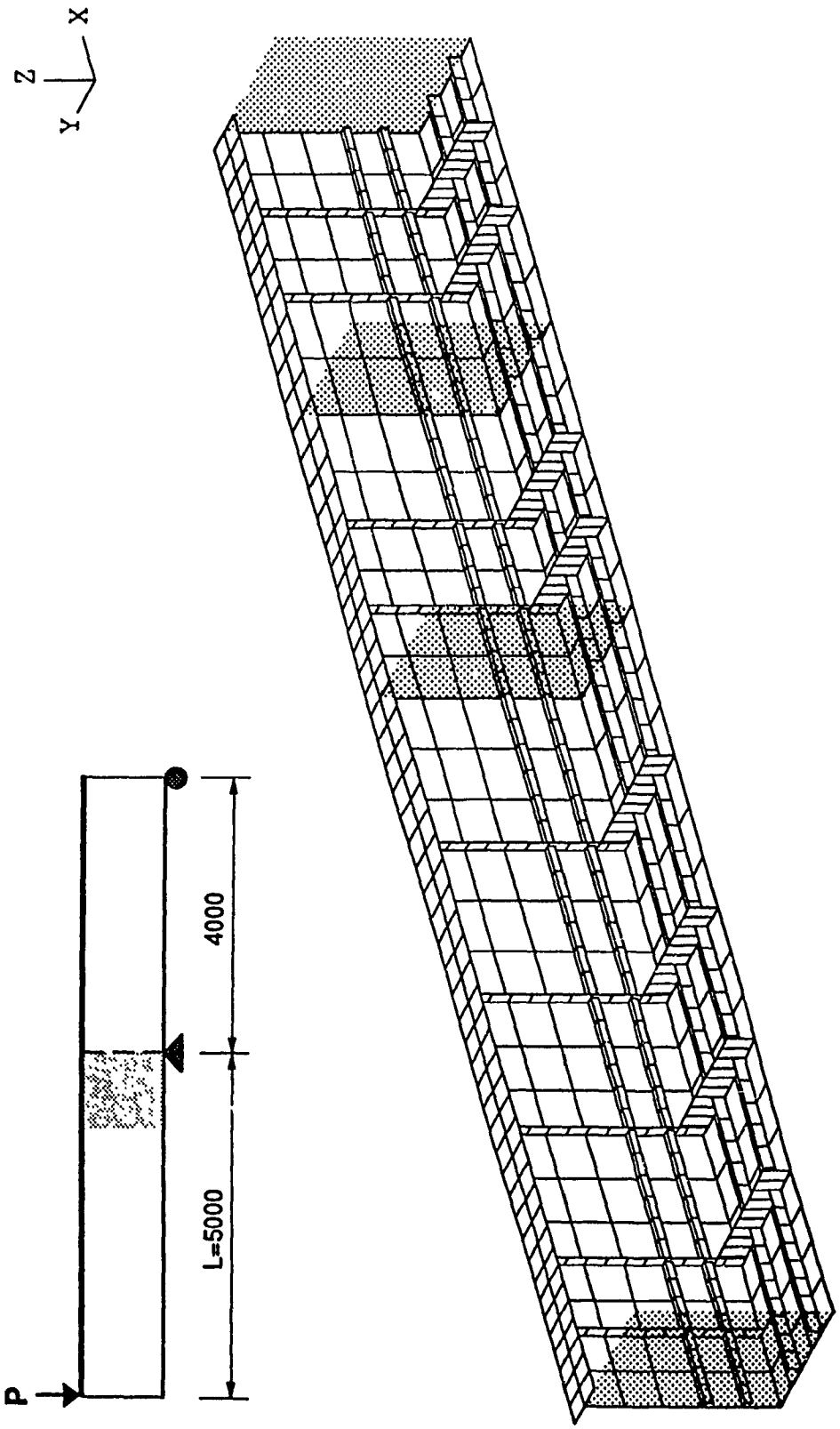

Figure 4.9 Finite Element Model
Box Girder Type C. Web Stiffening Type 3.c.(ii)

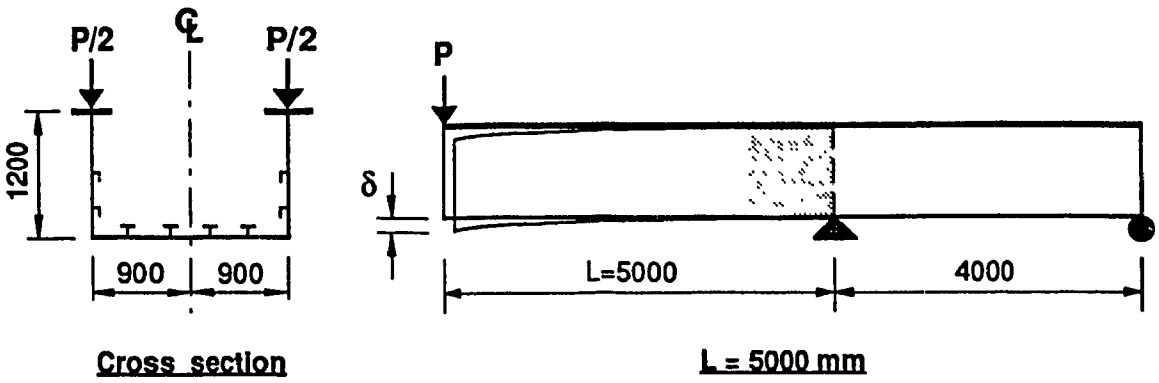

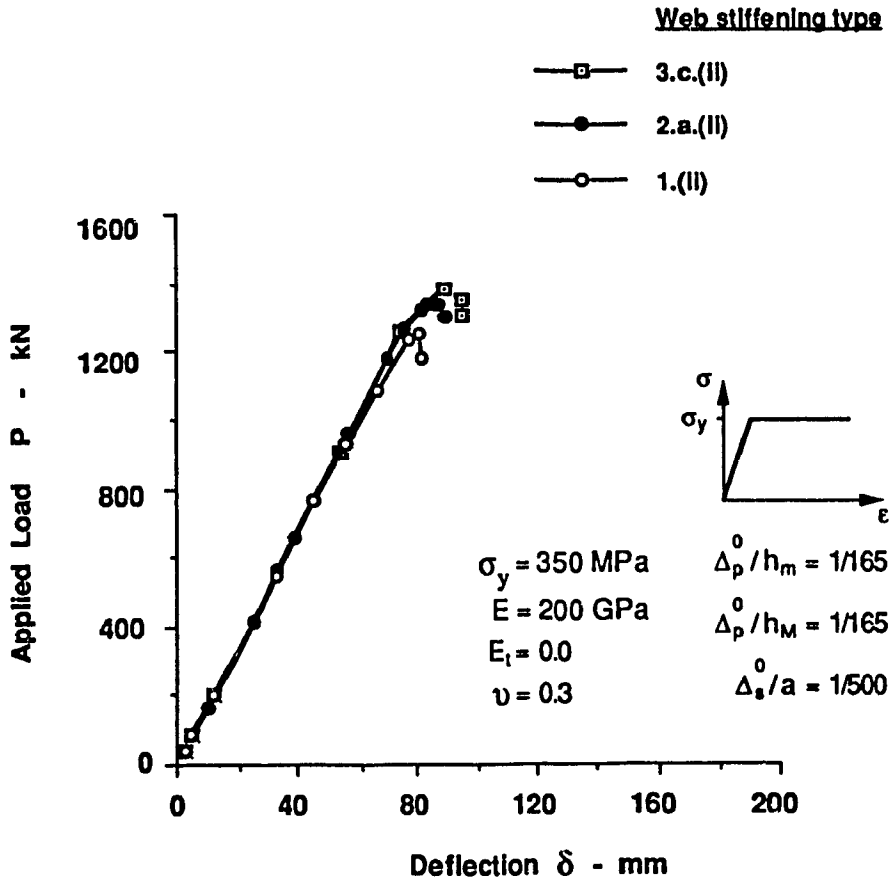

Figure 4.10 Load - Deflection Curves.
Box Girder Type C.

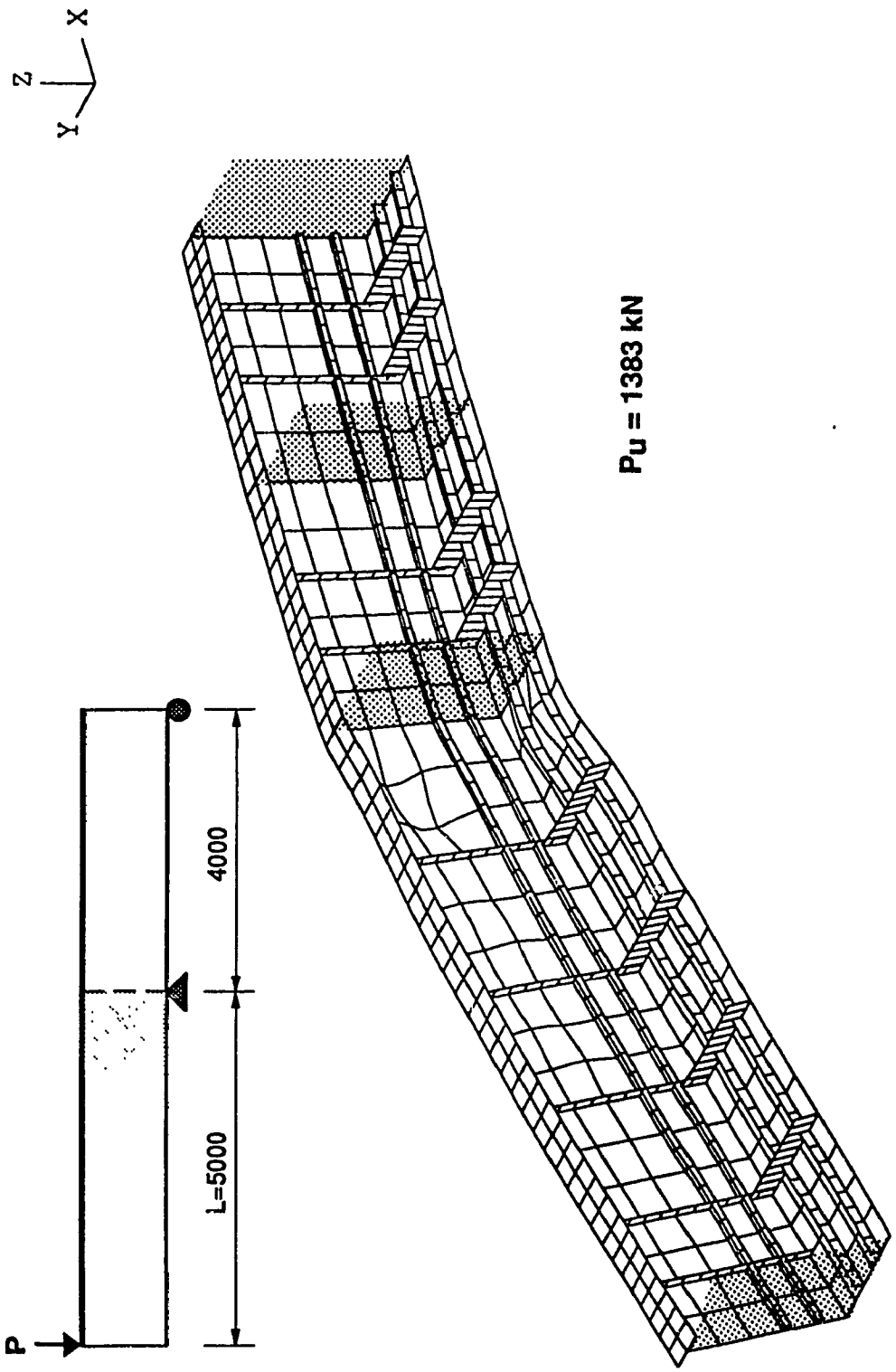

Figure 4.11 Failure of Box Girder Type C with Web Stiffening Type 3.c.(ii)

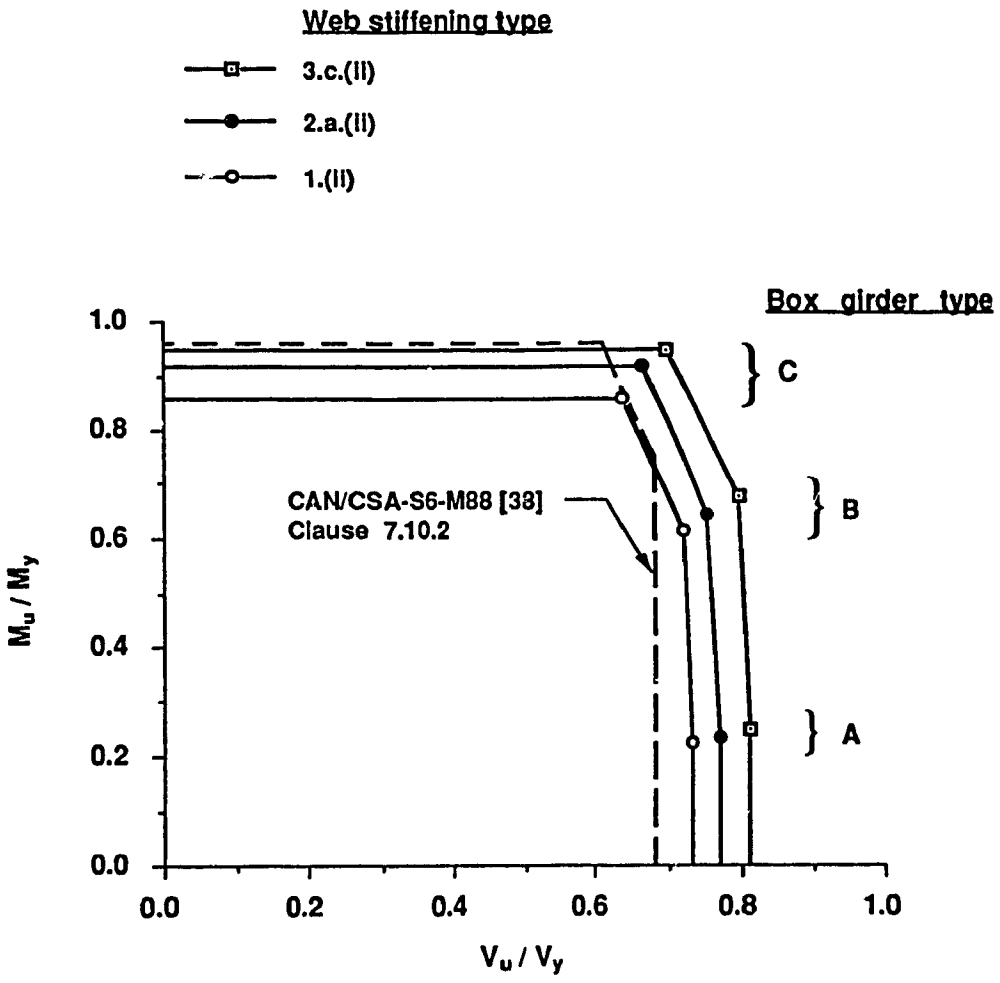

Figure 4.12.a Interaction Diagrams for Box Girder Webs.
Ultimate Shear Resistance Versus Ultimate Bending Moment

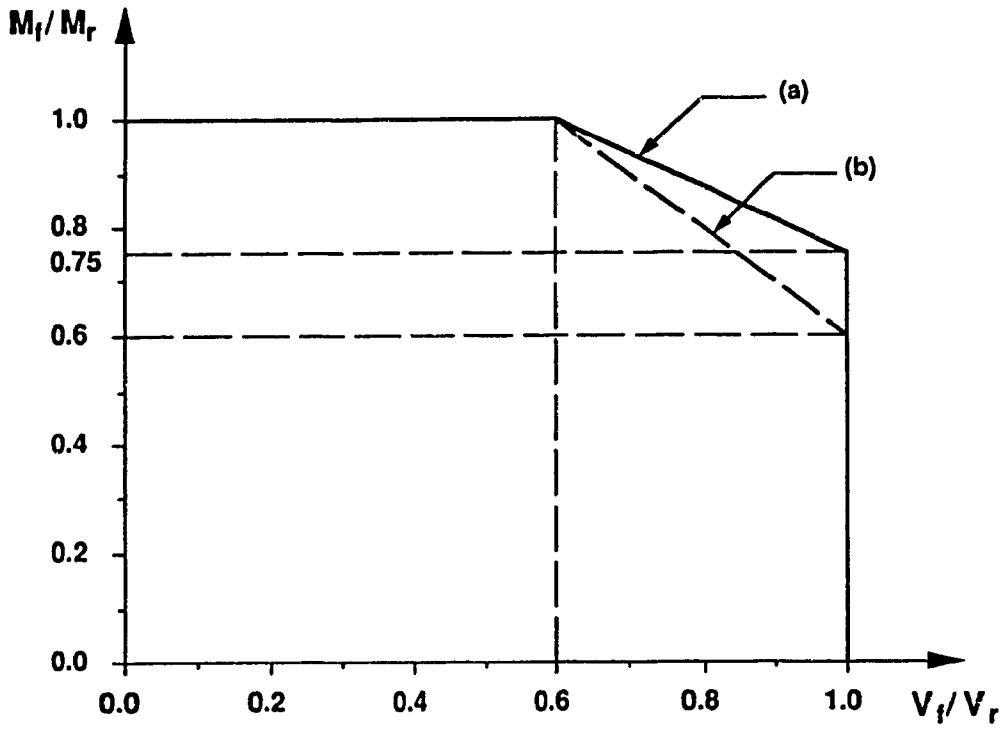

a. Transversely stiffened plate girder webs - Clause 7.10.2 [38]

$$0.727\frac{M_f}{M_r}+0.455\frac{V_f}{V_r}=1.0 \qquad \text{for: } V_f/V_r > 0.6$$

b. Transversely and longitudinally stiffened box girder webs - Proposal

$$\text{b.}\quad 0.625\frac{M_f}{M_r}+0.625\frac{V_f}{V_r}=1.0 \qquad \text{for: } V_f/V_r > 0.6$$

Figure 4.12.b Shear - Moment Interaction

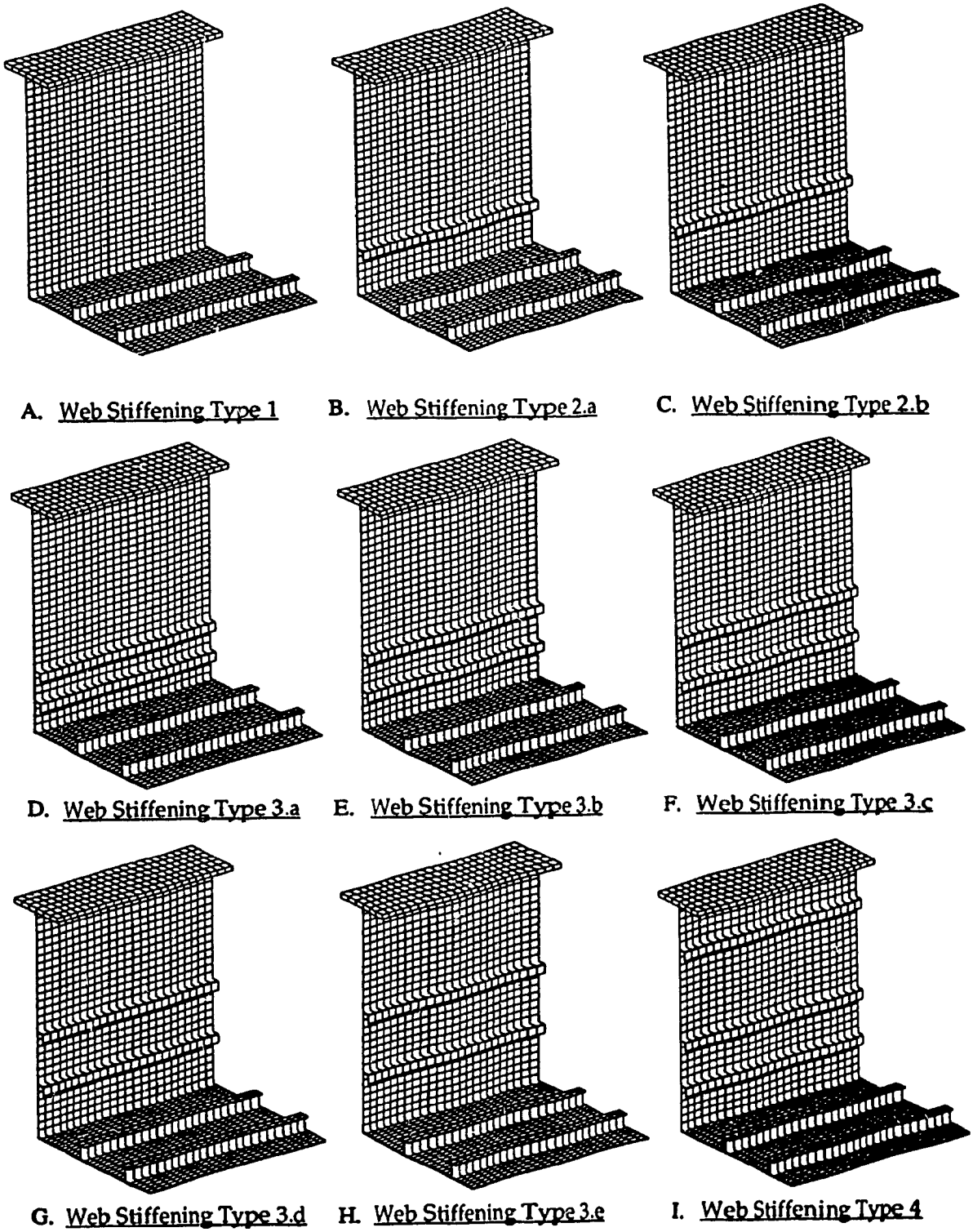

A. Web Stiffening Type 1 B. Web Stiffening Type 2.a C. Web Stiffening Type 2.b

D. Web Stiffening Type 3.a E. Web Stiffening Type 3.b F. Web Stiffening Type 3.c

G. Web Stiffening Type 3.d H. Web Stiffening Type 3.e I. Web Stiffening Type 4

Figure 4.13 Box Girder Type A
Finite Element Models

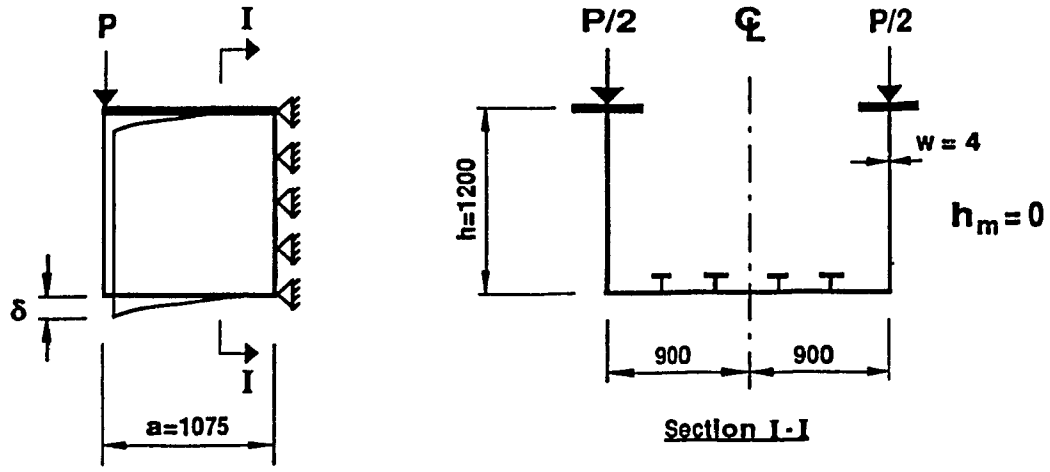

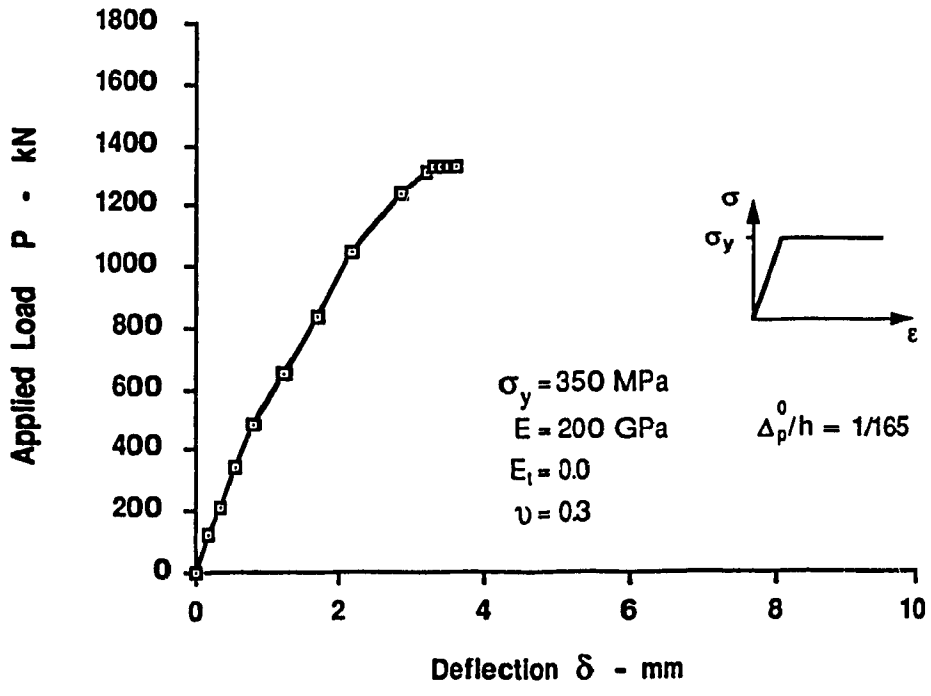

Figure 4.14 Load - Deflection Curve for Box Girder Type A. Web Stiffening Type 1.(ii)

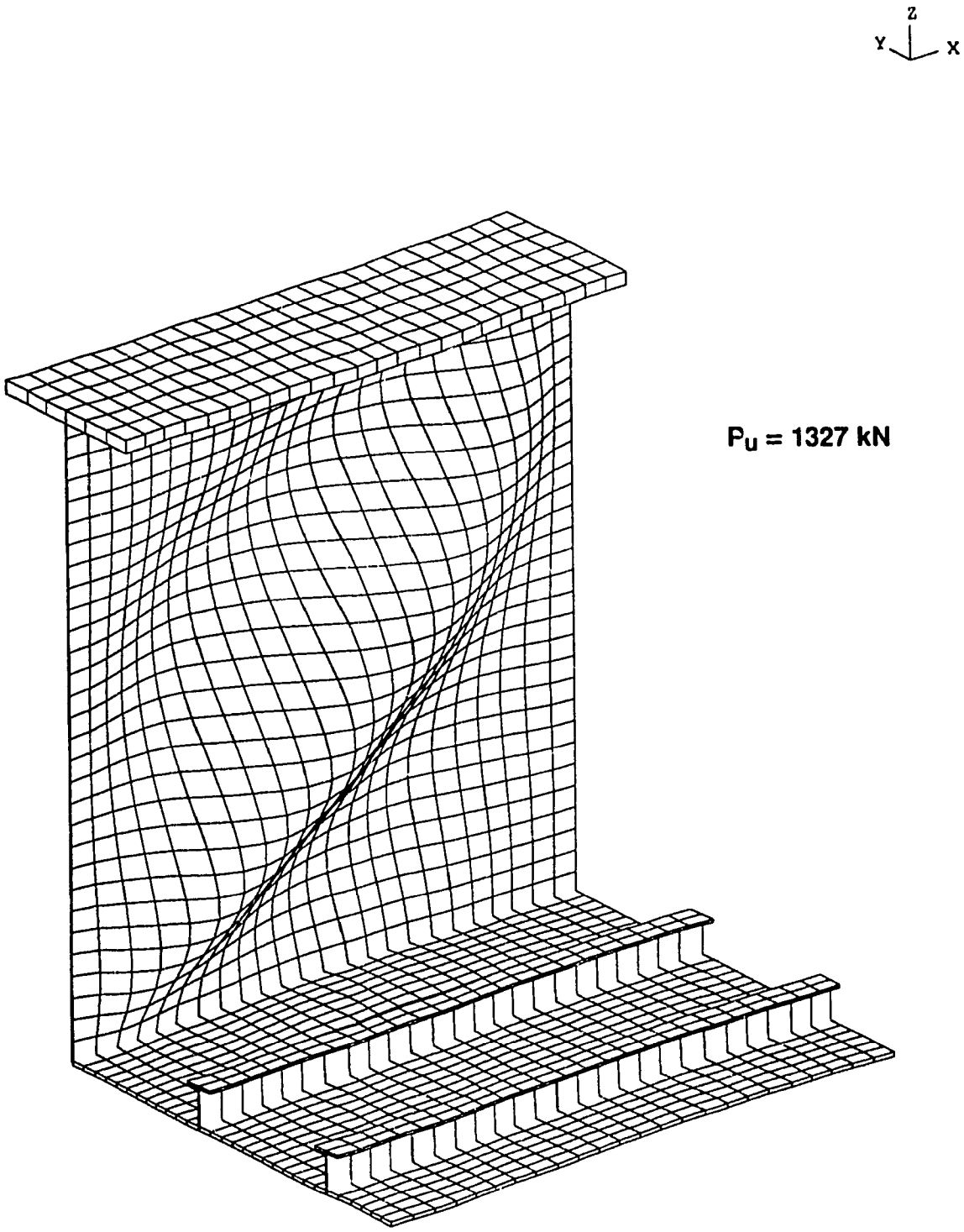

Figure 4.15 Web Buckling of Box Girder Type A.
Web Stiffening Type 1.(ii)

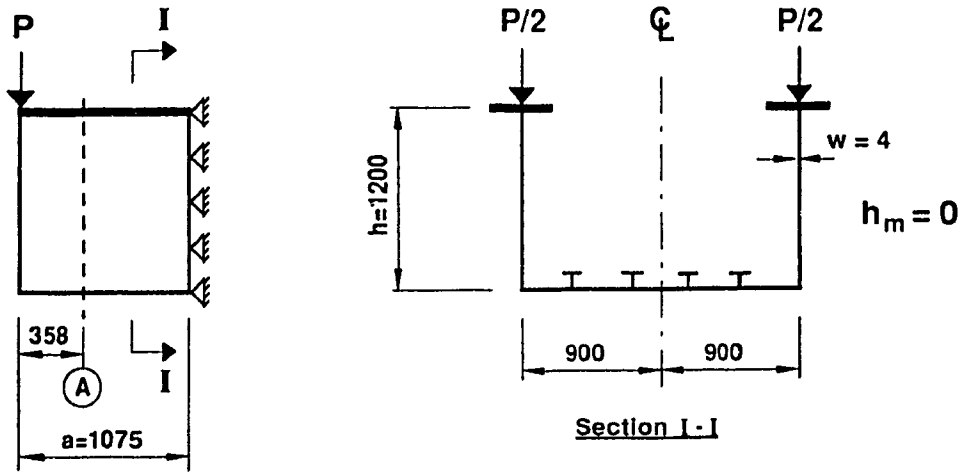

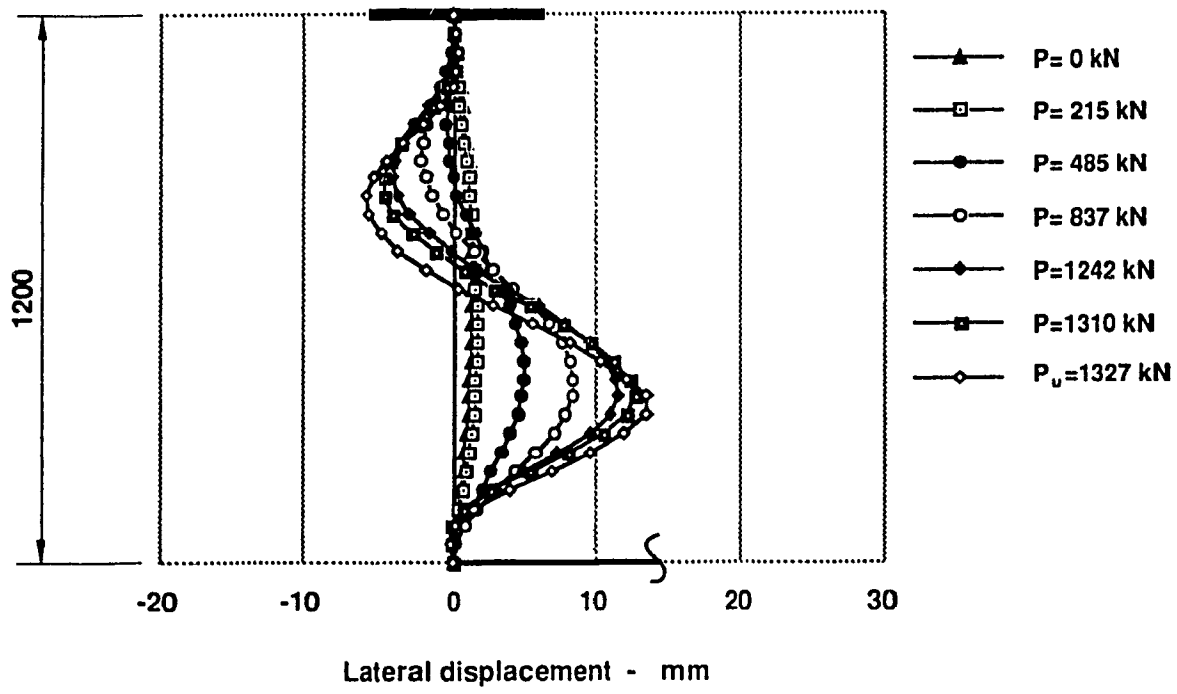

Figure 4.16 Deflection of Web under Loading - Section A
Box Girder Type A. Web Stiffening Type 1.(ii)

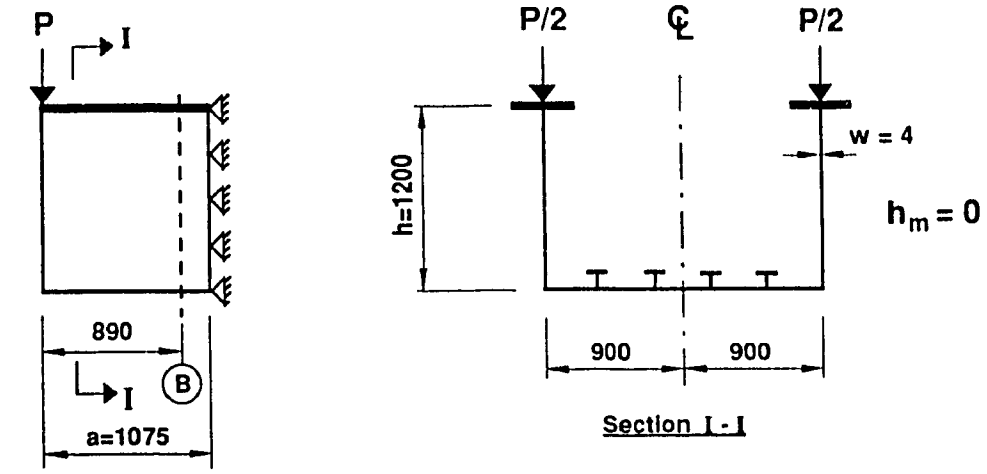

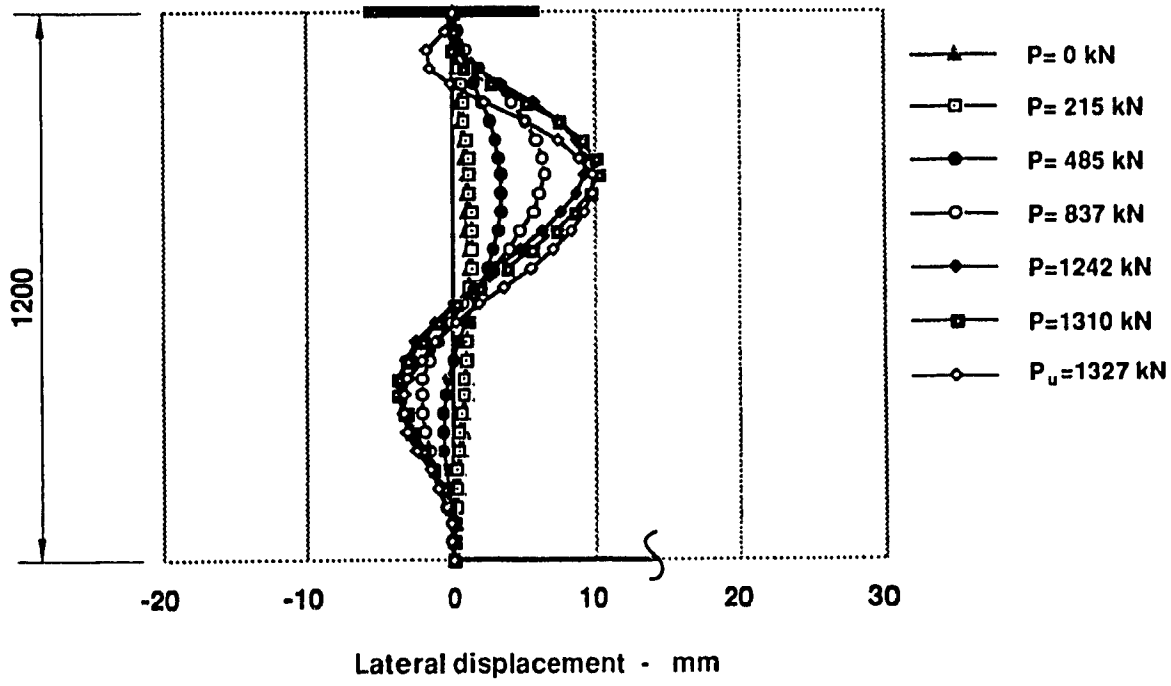

Figure 4.17 Deflection of Web under Loading - Section B
Box Girder Type A. Web Stiffening Type 1.(ii)

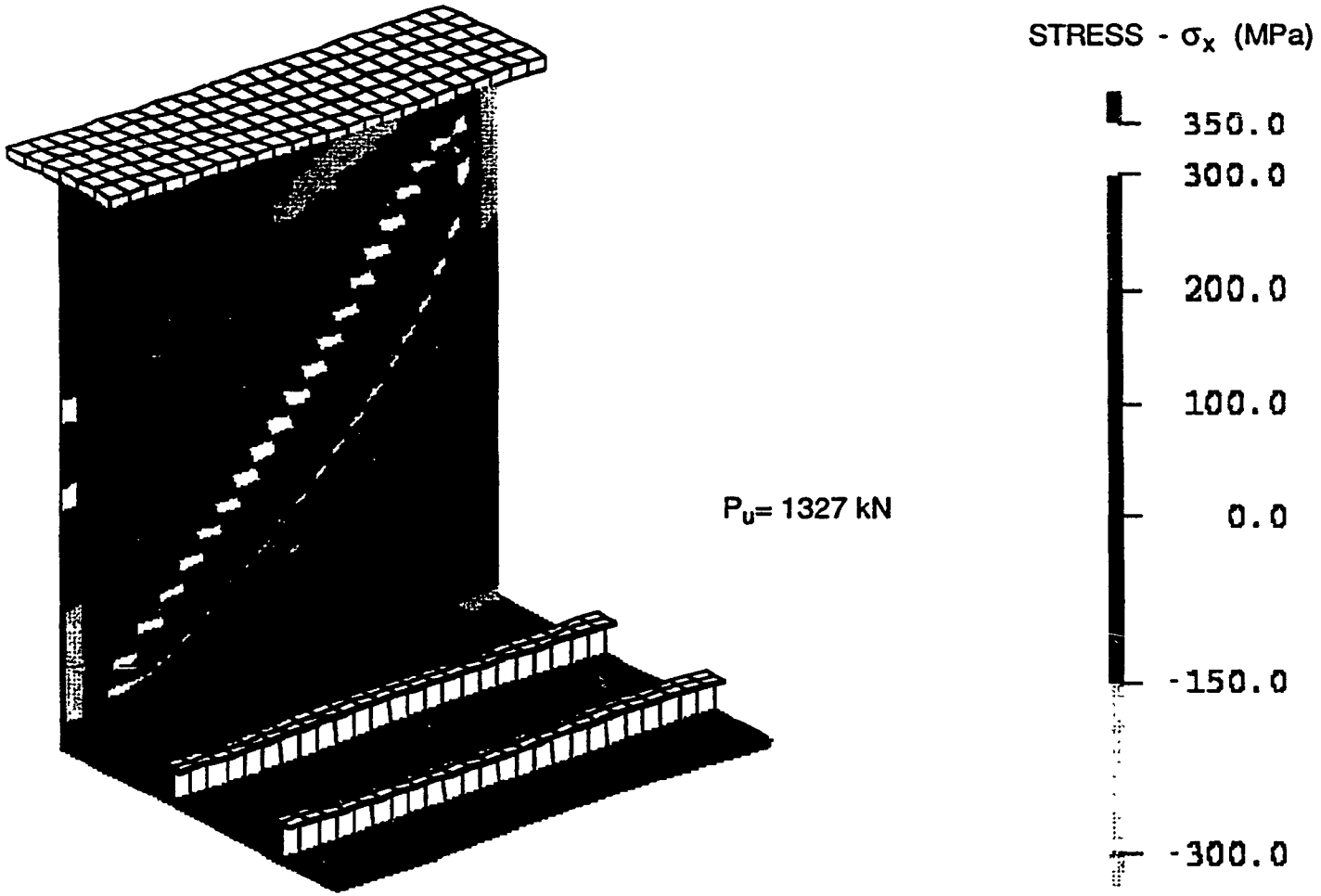

Figure 4.18 Normal Stress Distribution
Box Girder Type A. Web Stiffening Type 1.(ii)

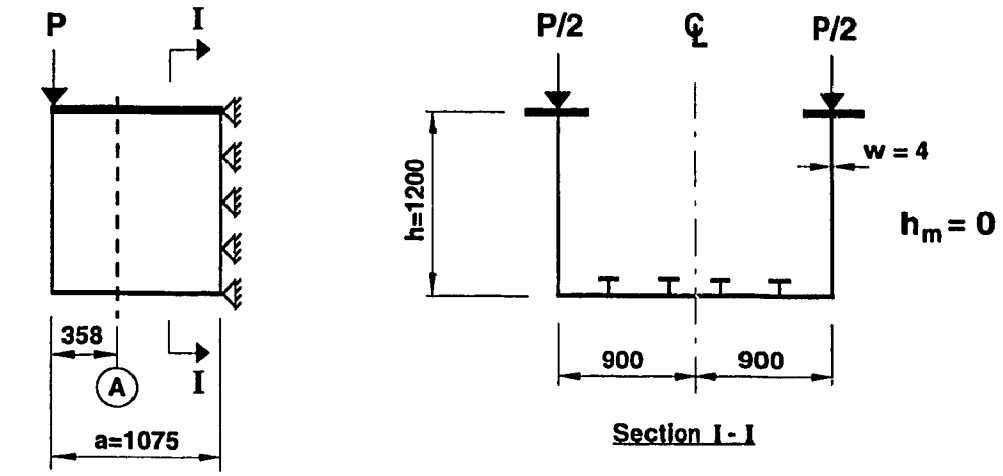

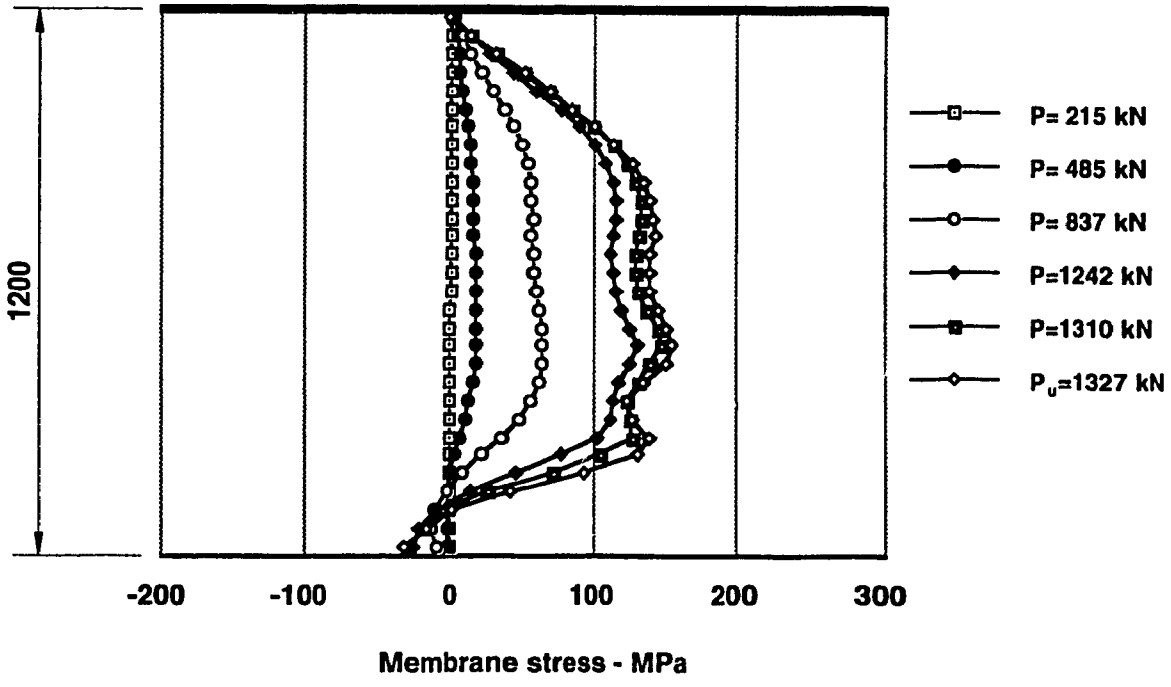

Figure 4.19 Distribution of Membrane Stresses - σ_x in the Web at Section A Box Girder Type A. Web Stiffening Type 1.(ii)

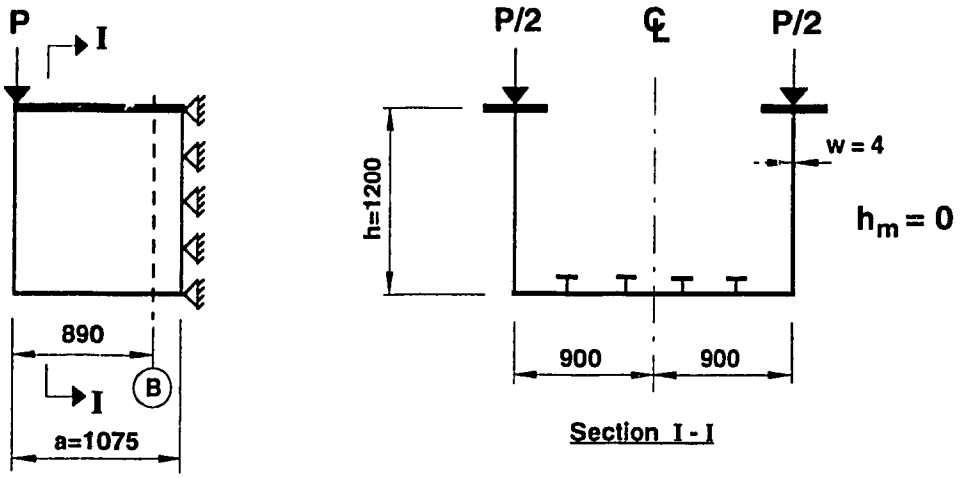

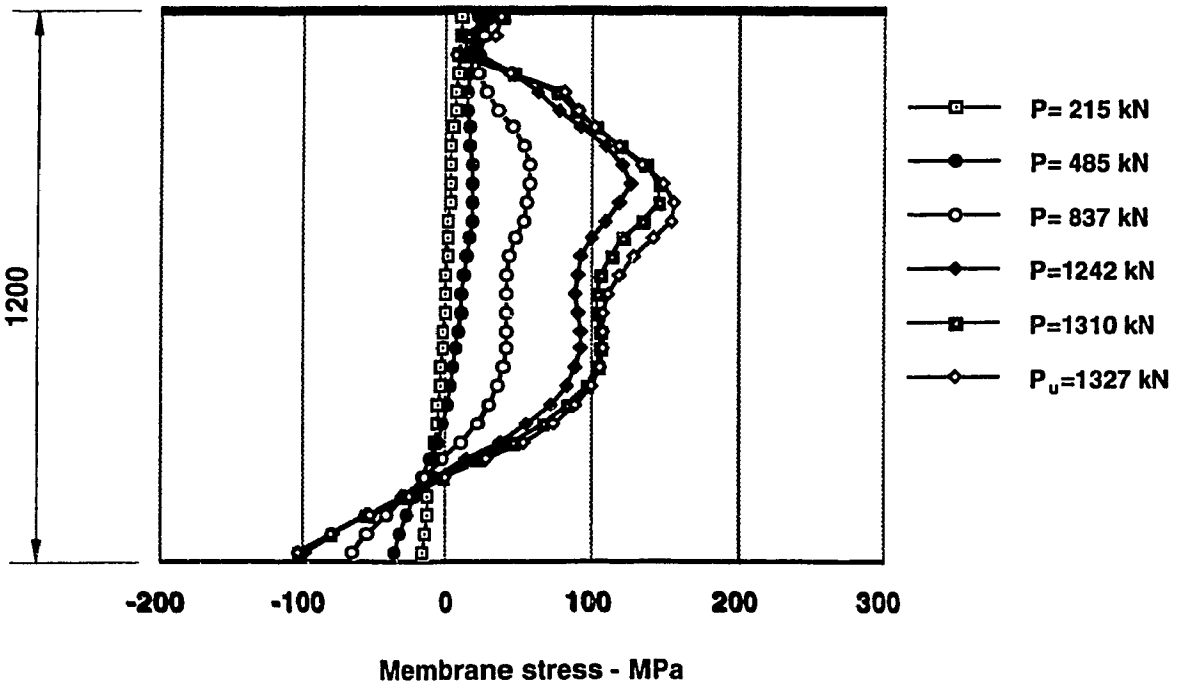

Figure 4.20 Distribution of Membrane Stresses - σ_x in the Web at Section B Box Girder Type A. Web Stiffening Type 1.(ii)

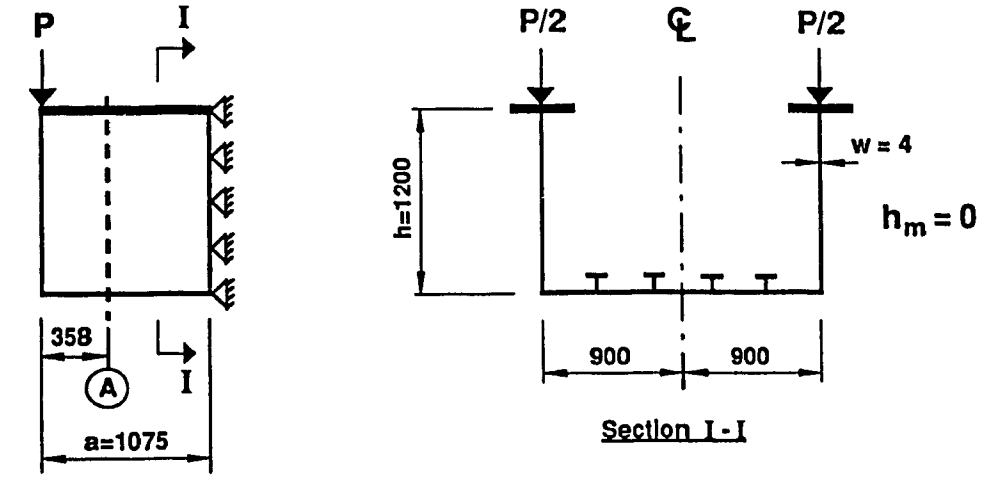

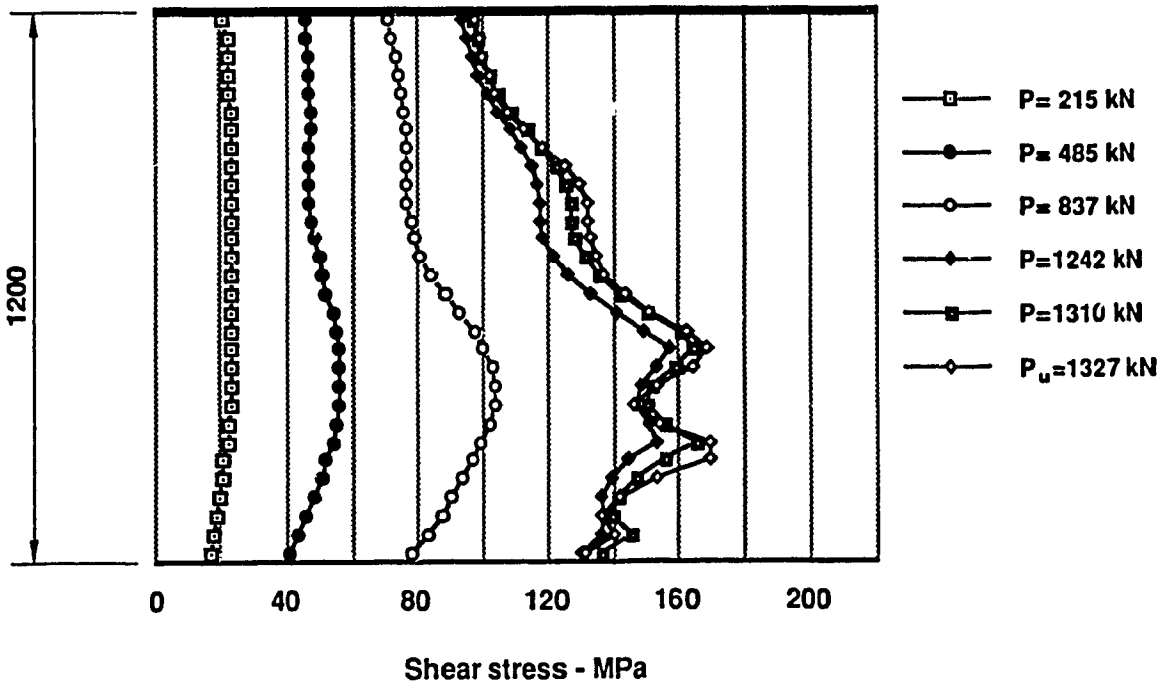

Figure 4.21 Distribution of Shear Stresses in the Web at Section A Box Girder Type A. Web Stiffening Type 1.(ii)

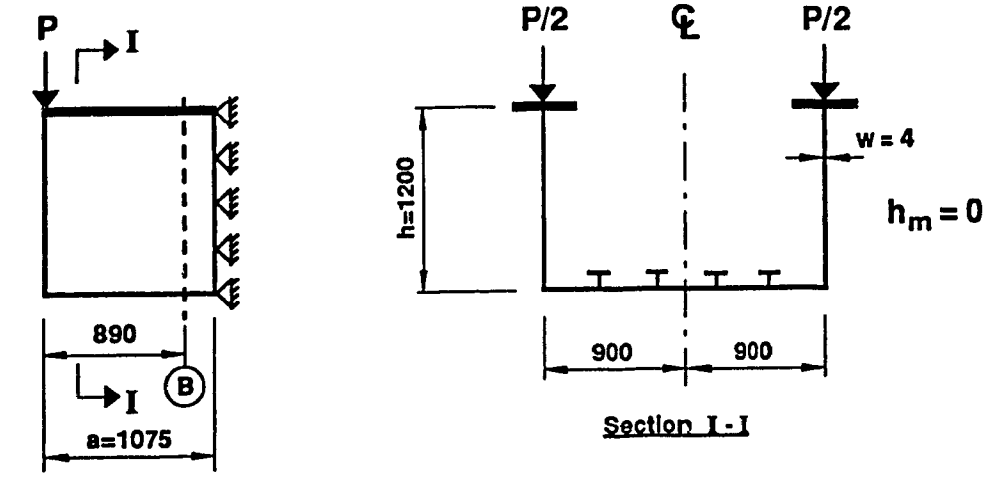

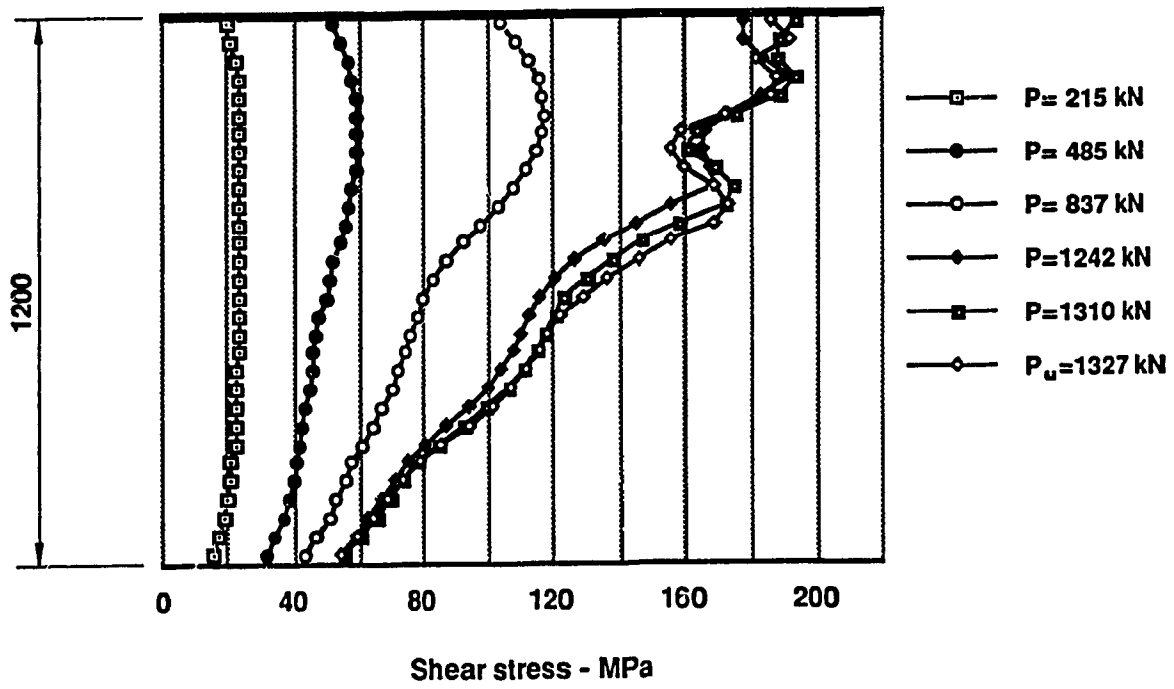

Figure 4.22 Distribution of Shear Stresses in the Web at Section B Box Girder Type A. Web Stiffening Type 1.(ii)

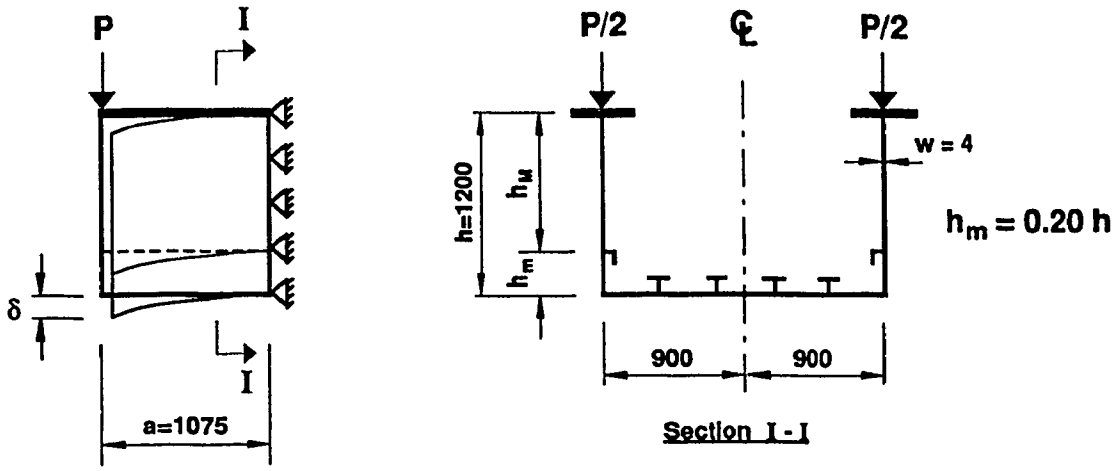

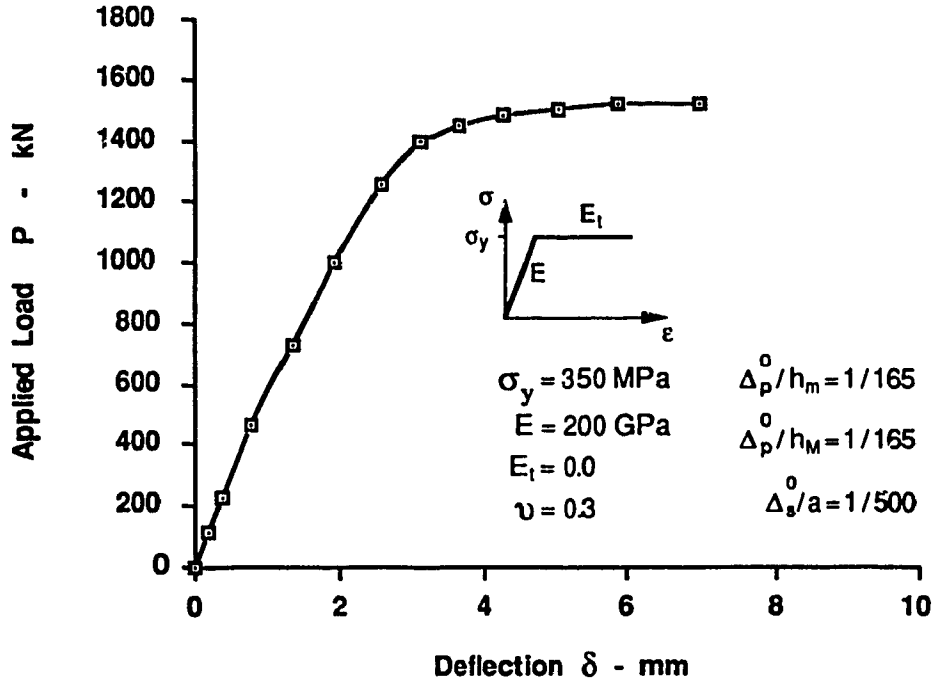

Figure 4.23 Load - Deflection Curve for Box Girder Type A. Web Stiffening Type 2.a.(ii)

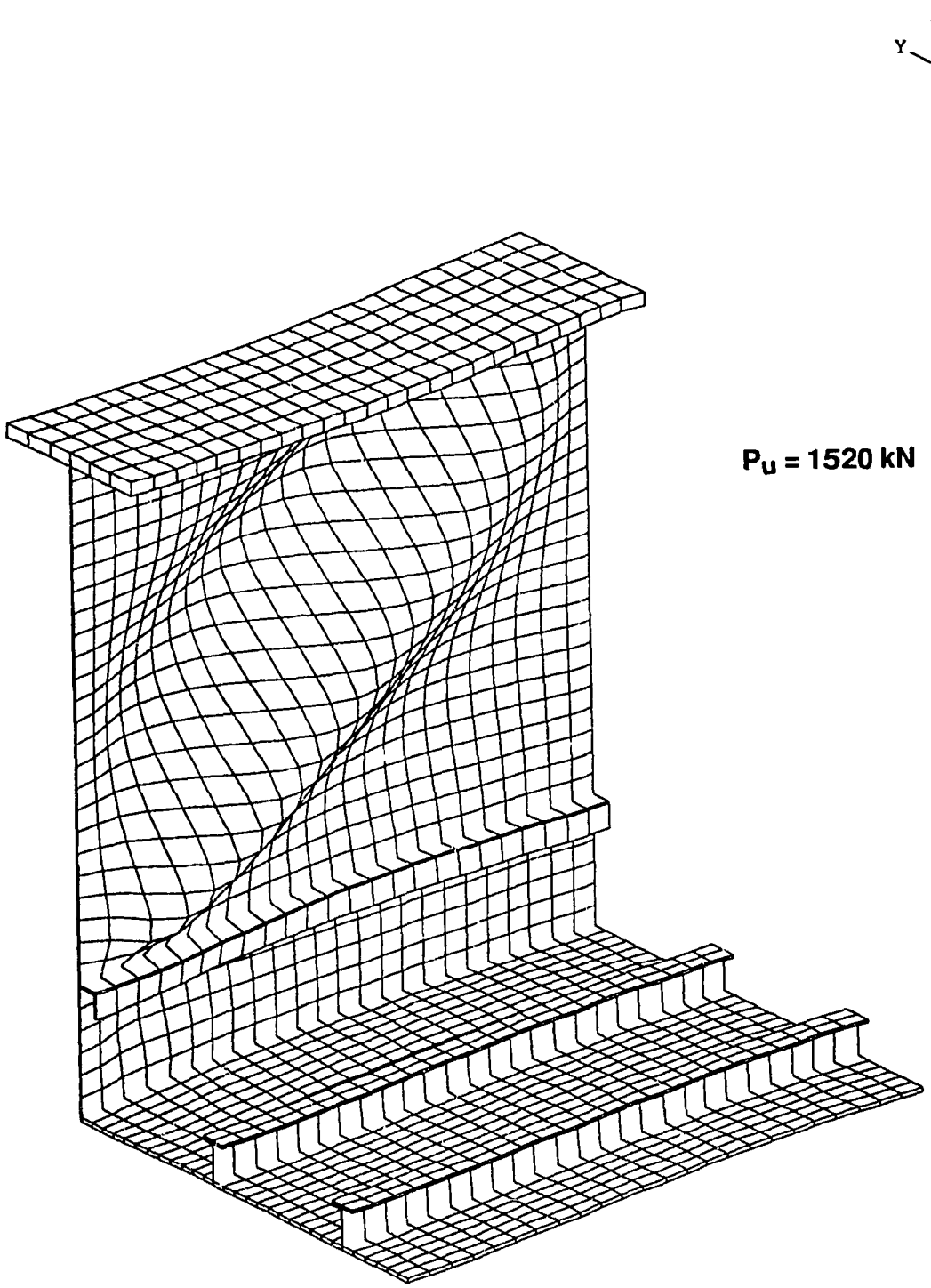

Figure 4.24 Web Buckling of Box Girder Type A.
Web Stiffening Type 2.a.(ii)

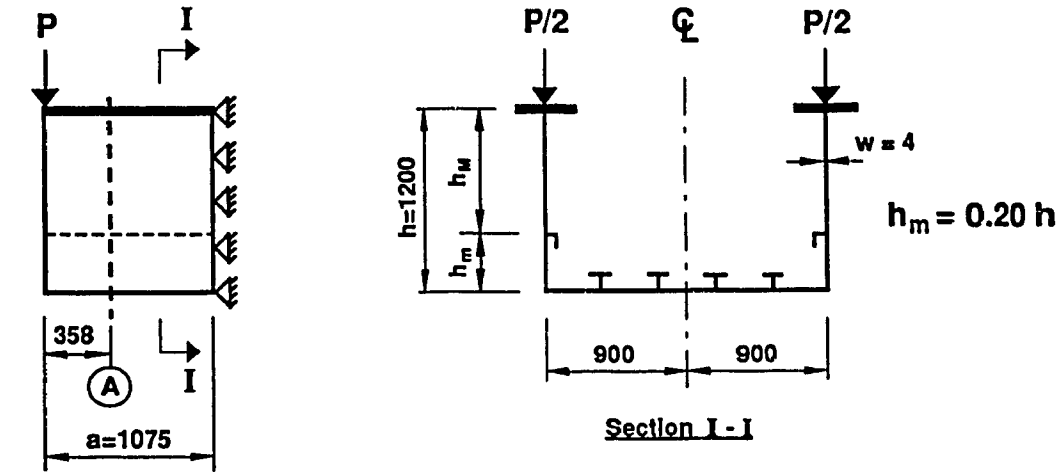

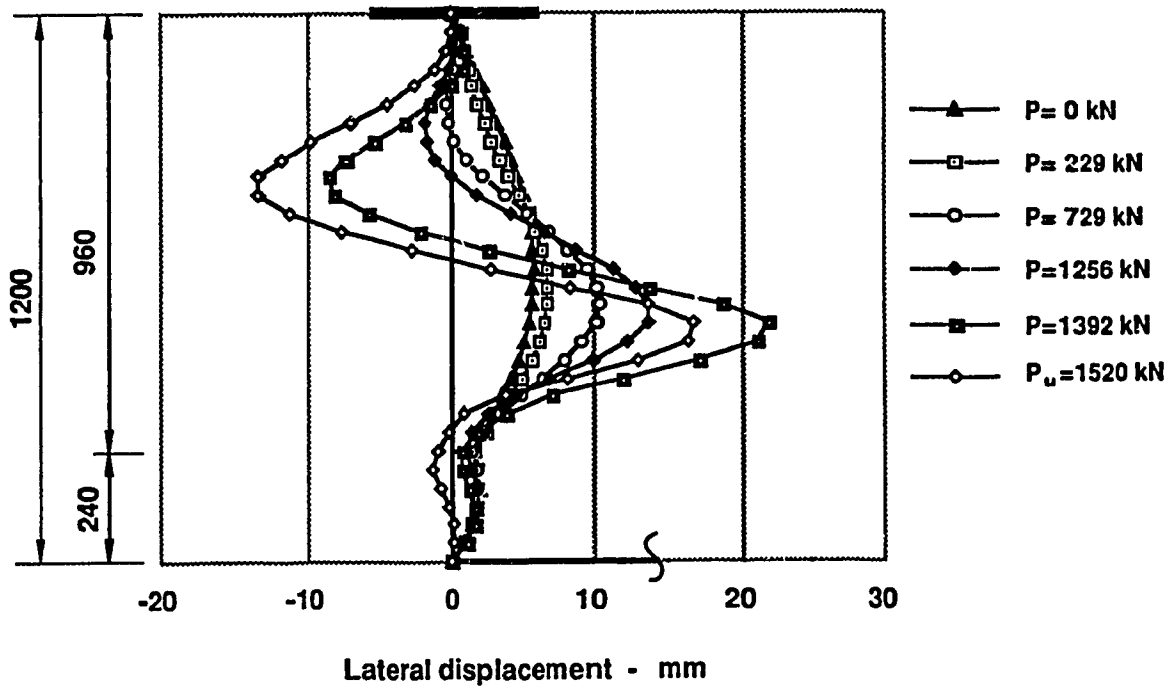

Figure 4.25 Deflection of Web under Loading - Section A
Box Girder Type A. Web Stiffening Type 2.a.(ii)

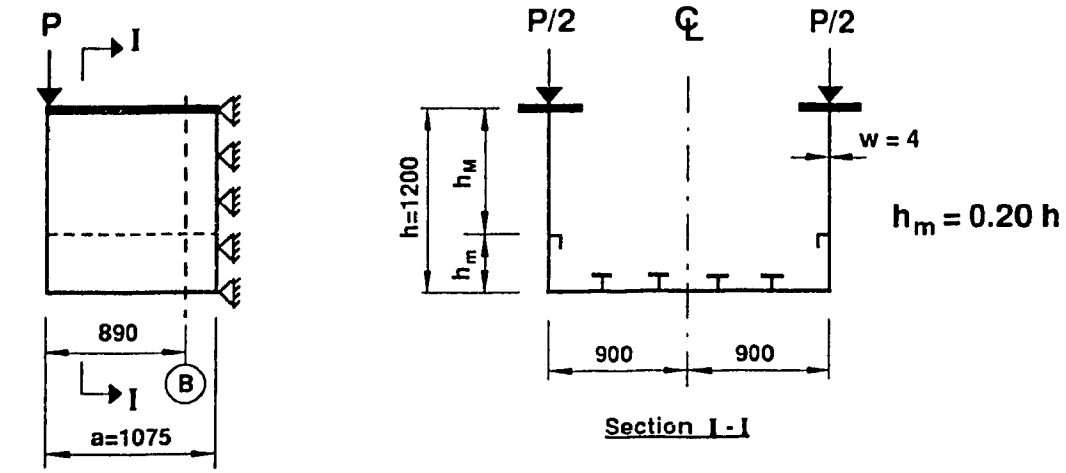

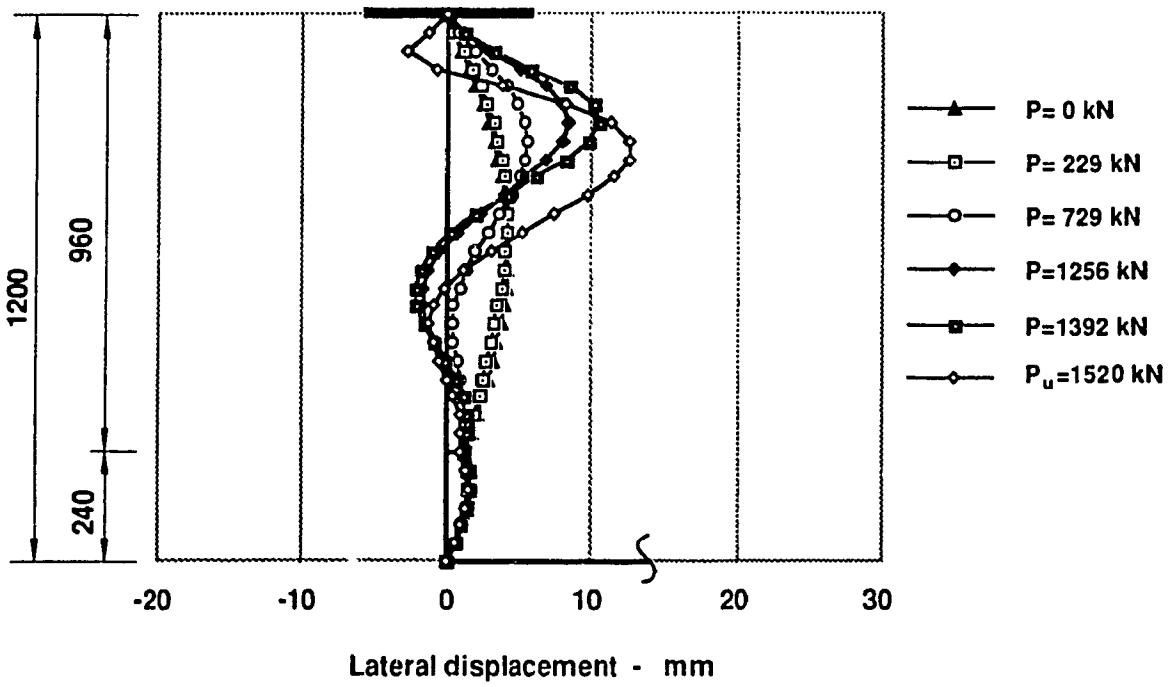

Figure 4.26 Deflection of Web under Loading - Section B
Box Girder Type A. Web Stiffening Type 2.a.(ii)

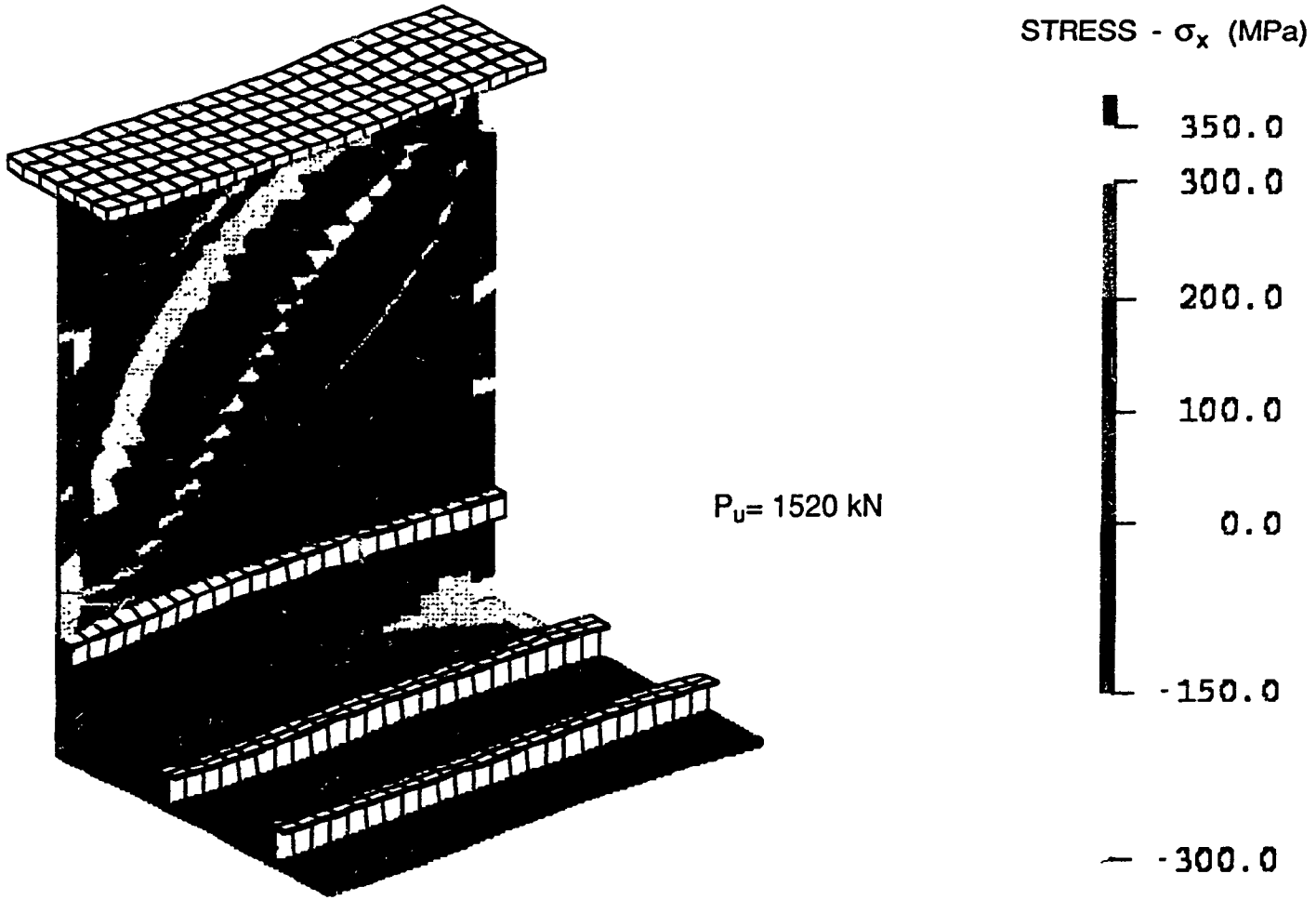

Figure 4.27 Normal Stress Distribution
Box Girder Type A. Web Stiffening Type 2.a.(ii)

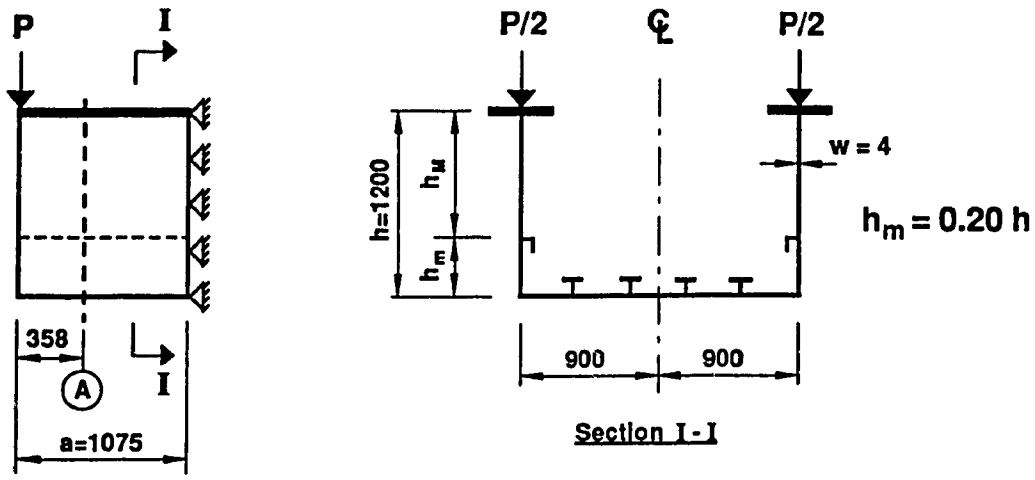

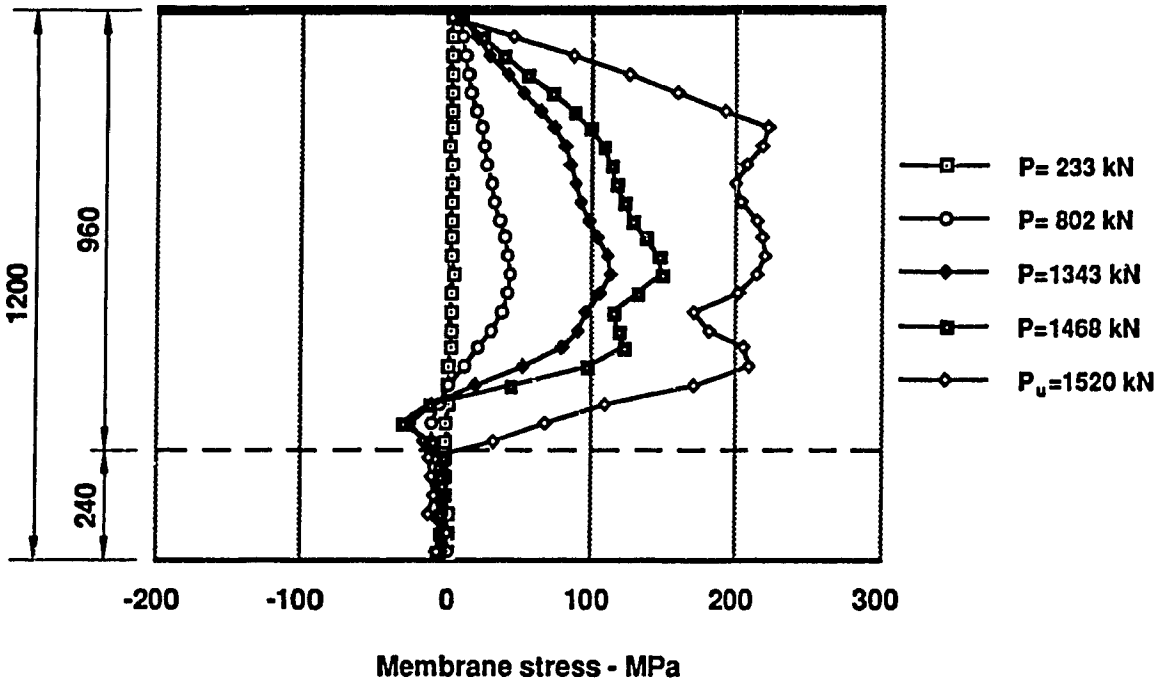

Figure 4.28 Distribution of Membrane Stresses - σ_x in the Web at Section A Box Girder Type A. Web Stiffening Type 2.a.(ii)

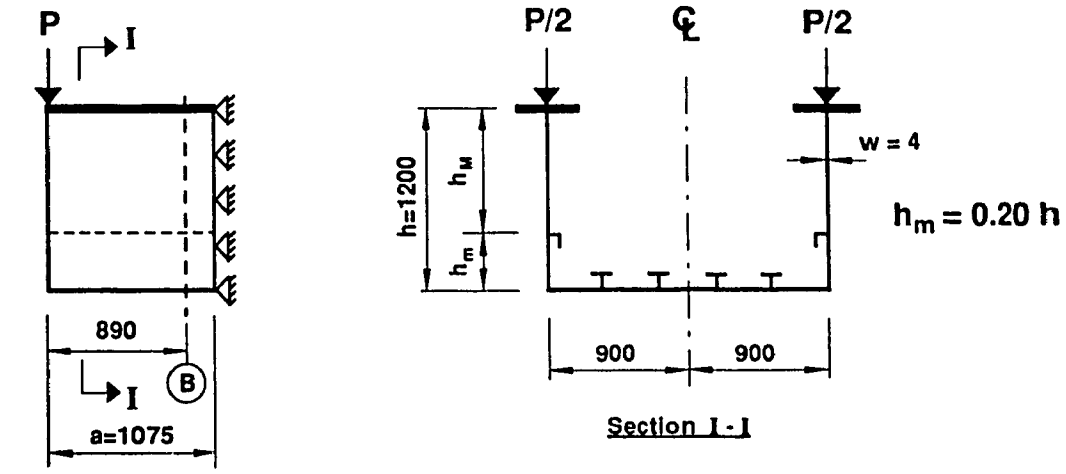

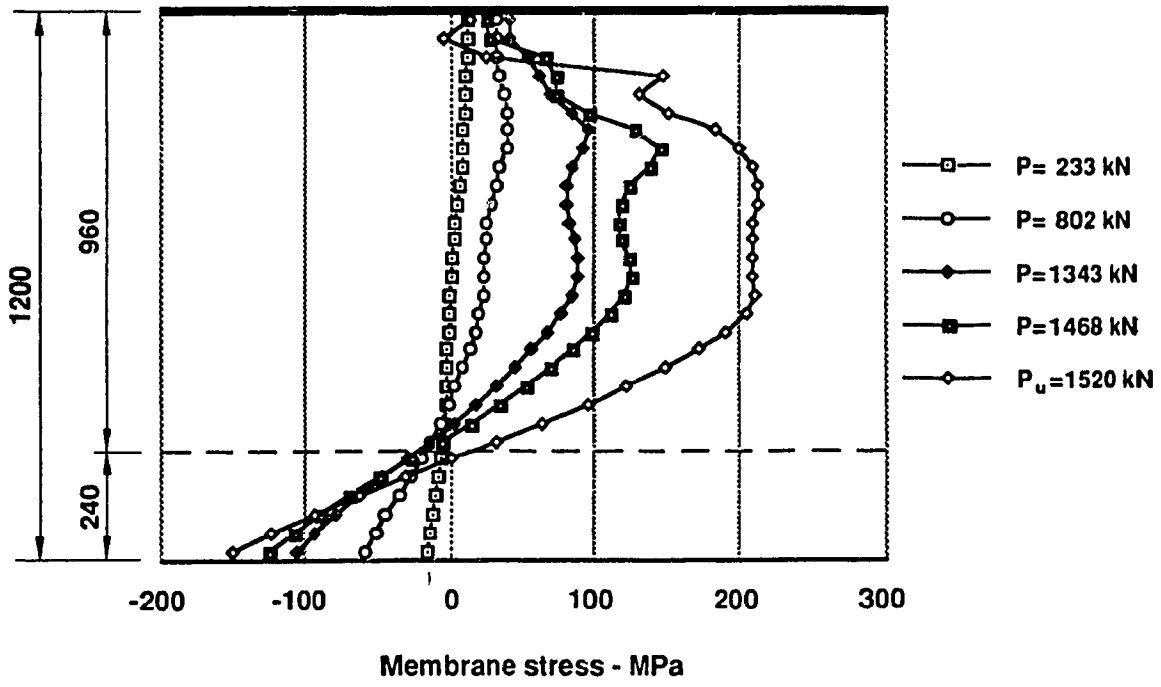

Figure 4.29 Distribution of Membrane Stresses - σ_x in the Web at Section B Box Girder Type A. Web Stiffening Type 2.a.(ii)

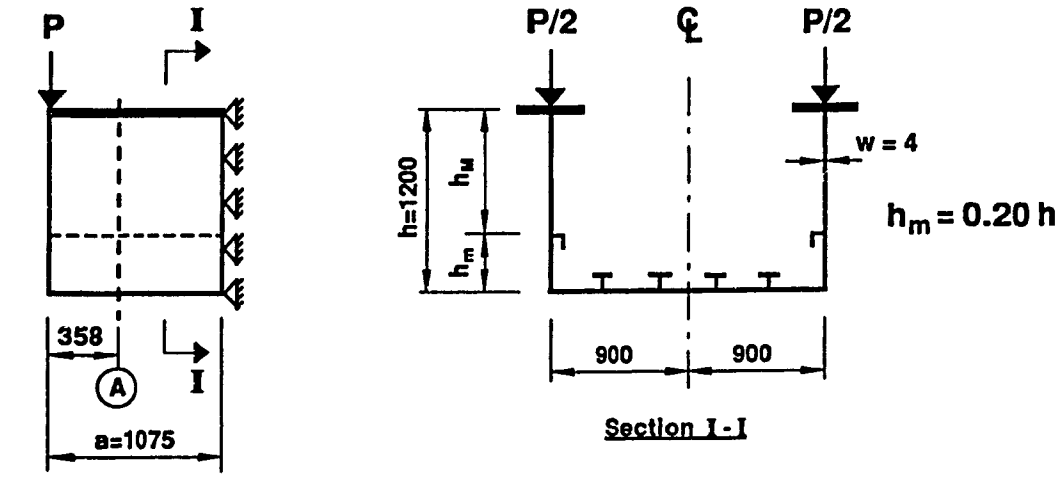

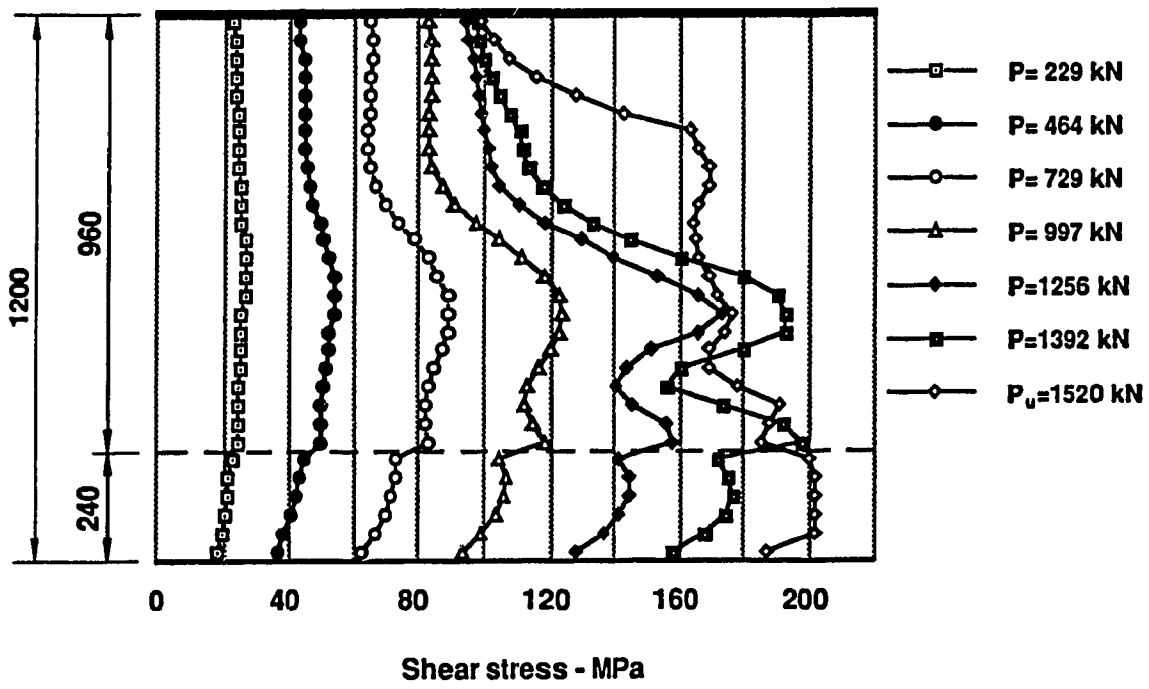

Figure 4.30 Distribution of Shear Stresses in the Web at Section A
Web Stiffening Type 2.a.(ii)

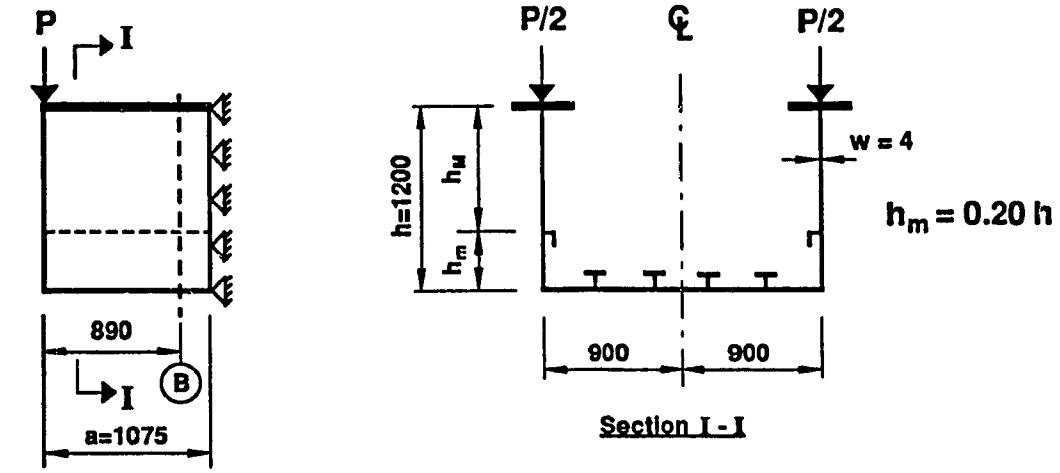

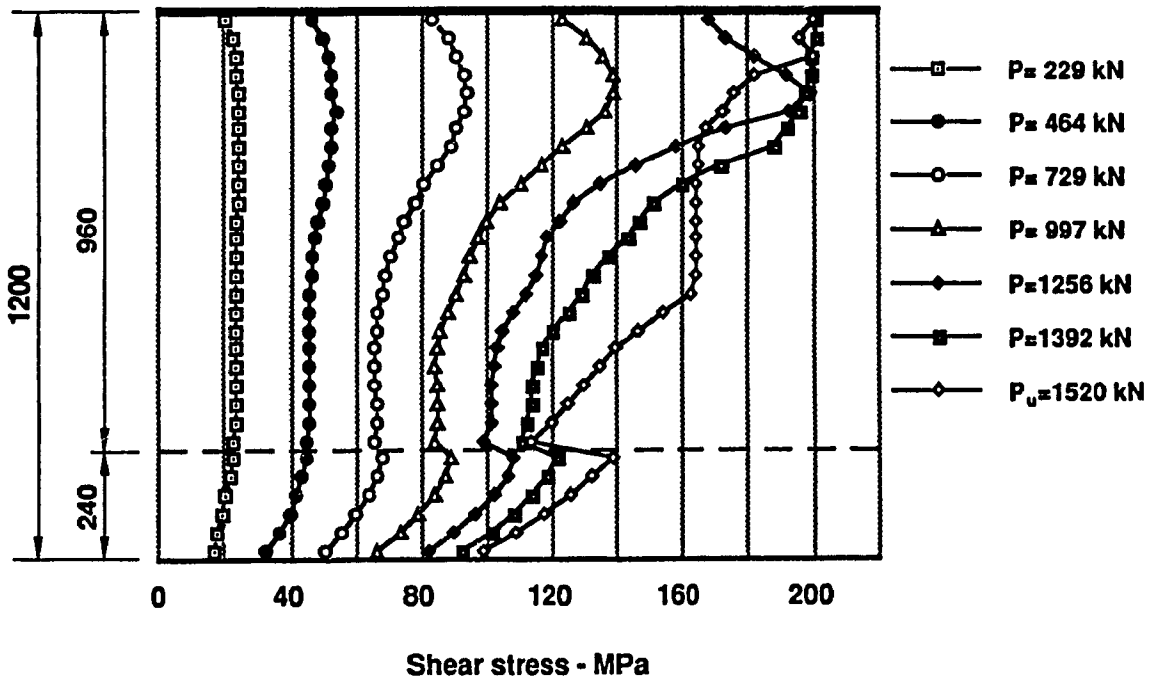

Figure 4.31 Distribution of Shear Stresses in the Web at Section B
Web Stiffening Type 2.a.(ii)

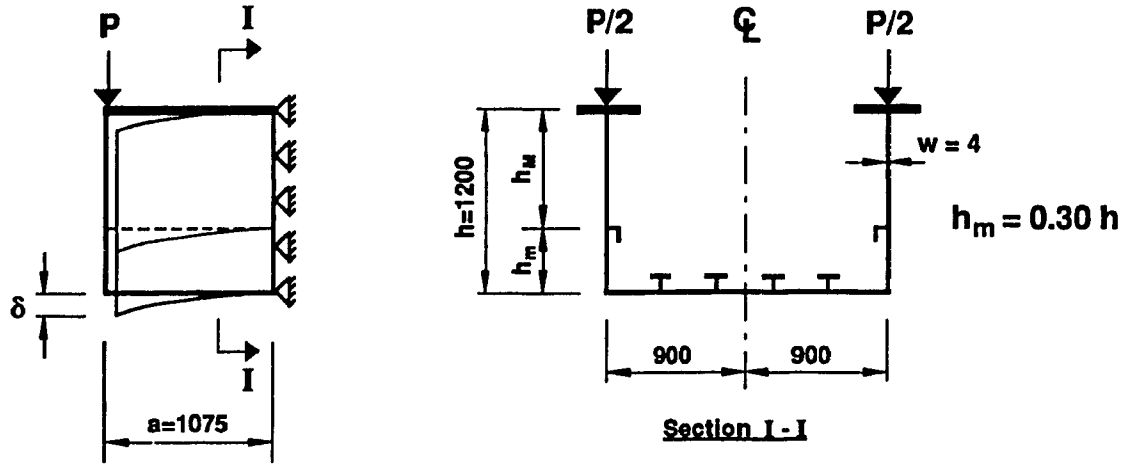

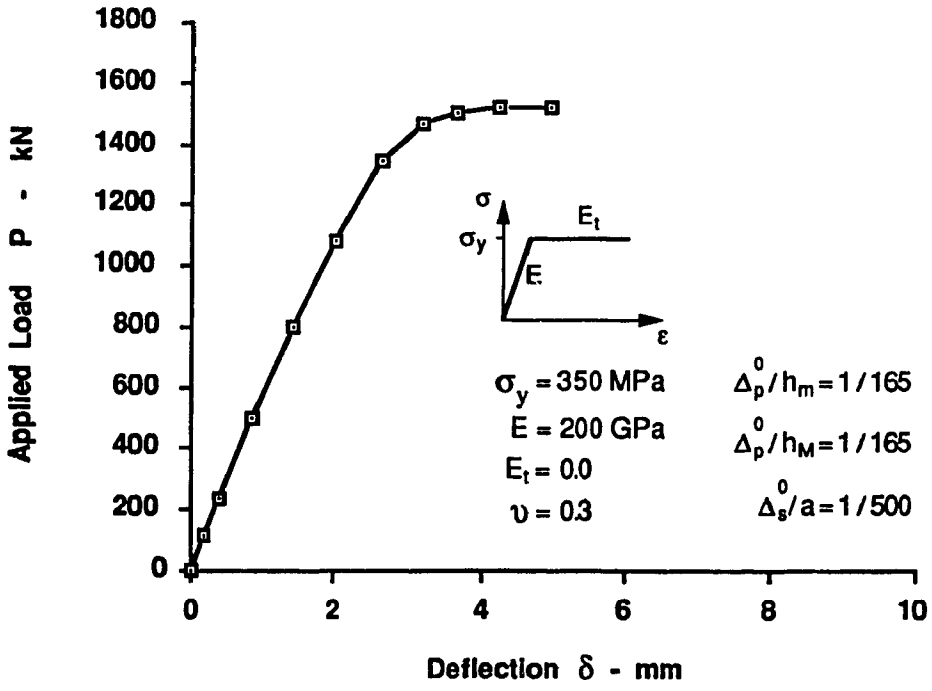

Figure 4.32 Load - Deflection Curve for Box Girder Type A. Web Stiffening Type 2.b.(ii)

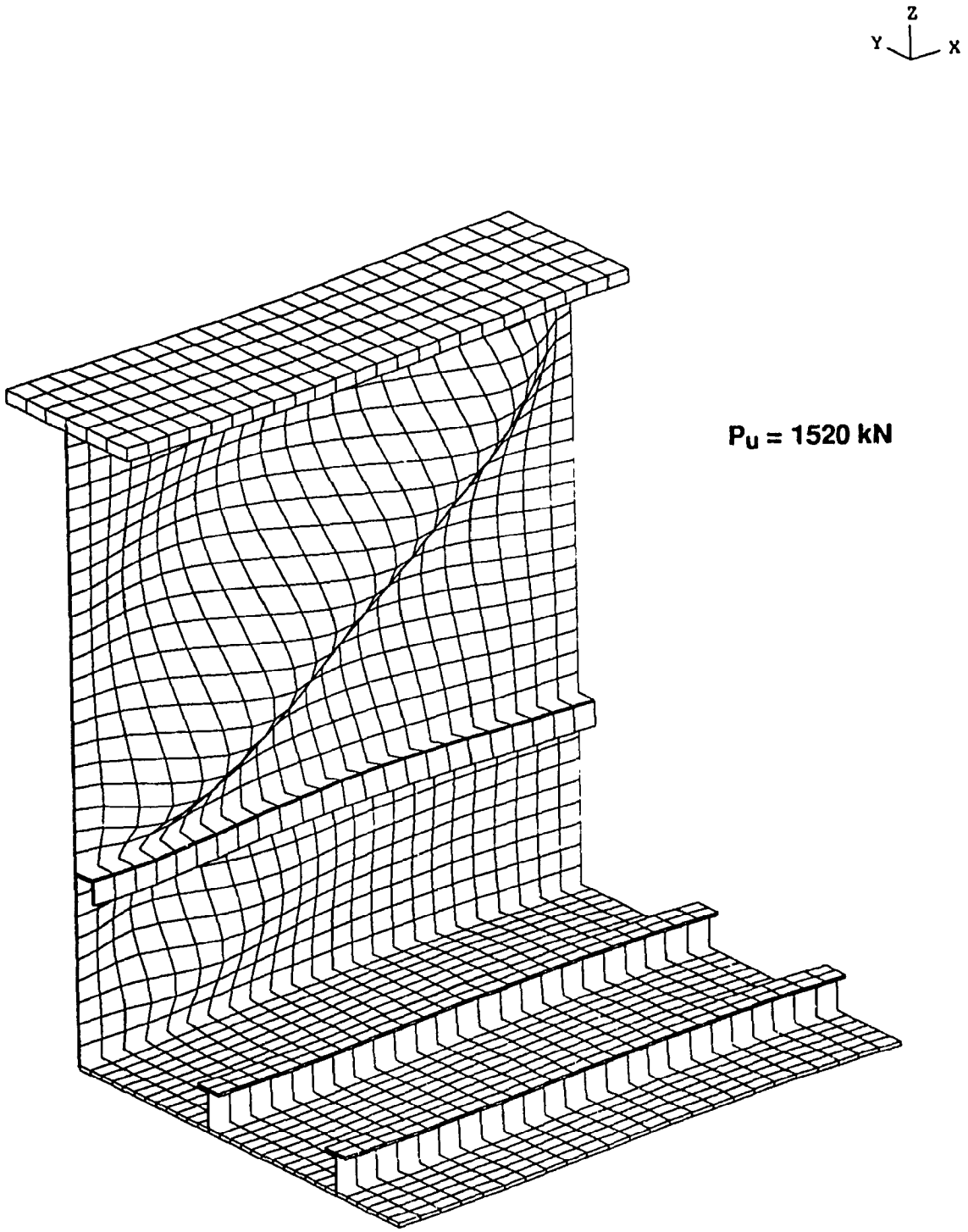

Figure 4.33 Web Buckling of Box Girder Type A.
Web Stiffening Type 2.b.(ii)

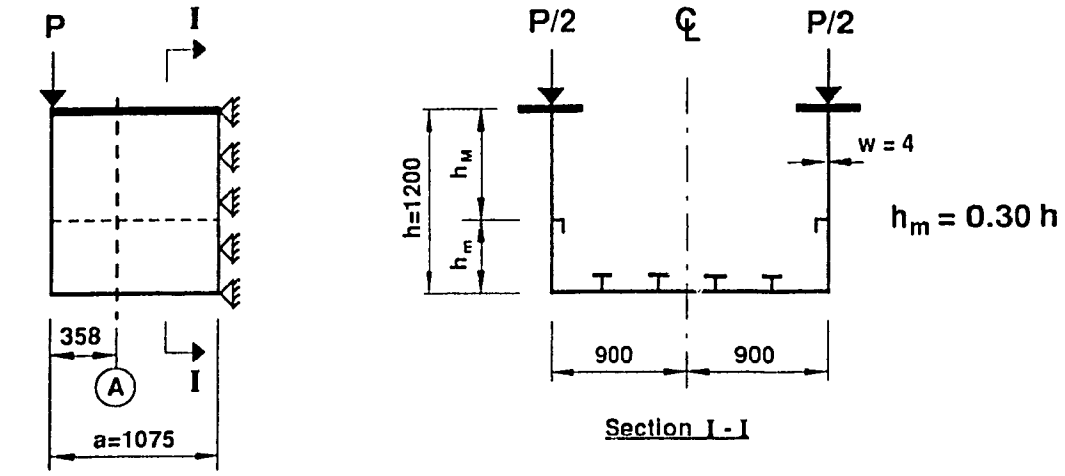

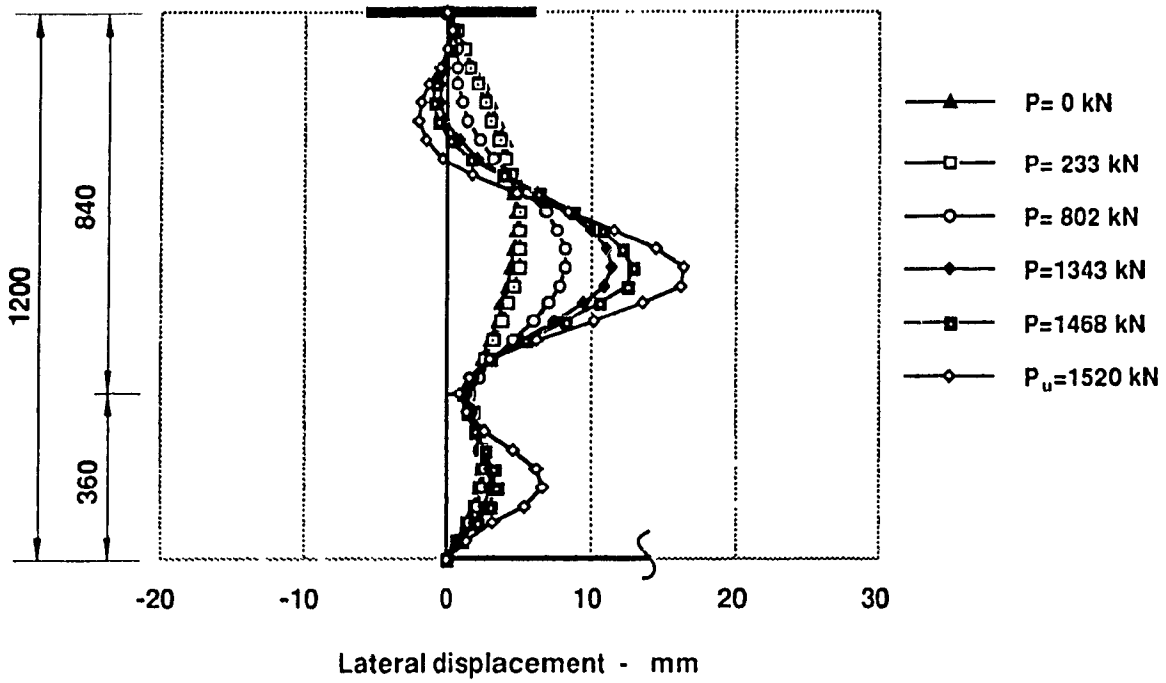

Figure 4.34 Deflection of Web under Loading - Section A
Box Girder Type A. Web Stiffening Type 2.b.(ii)

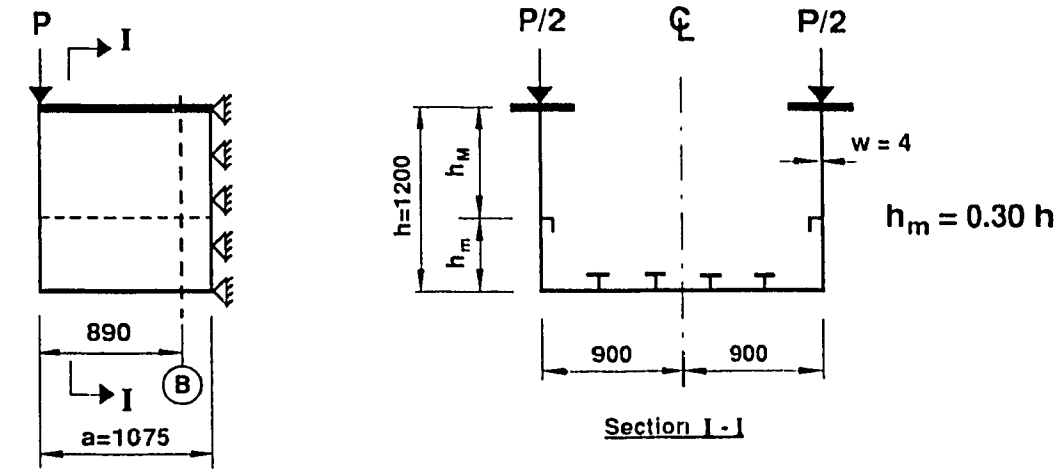

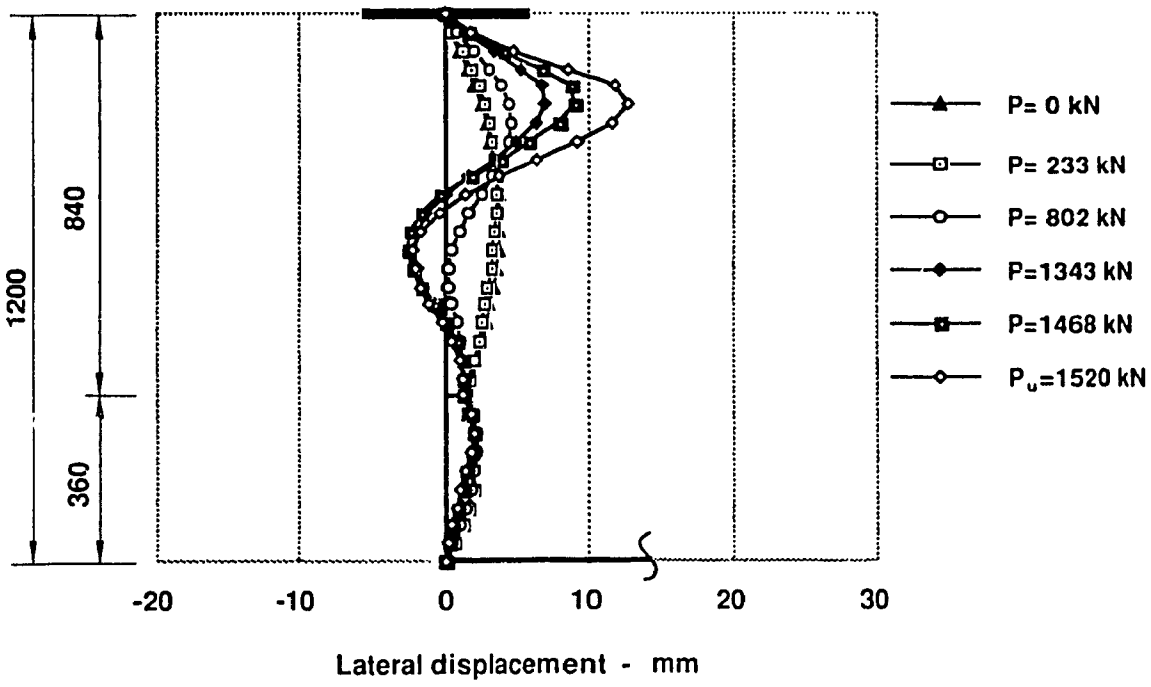

Figure 4.35 Deflection of Web under Loading - Section B
Box Girder Type A. Web Stiffening Type 2.b.(ii)

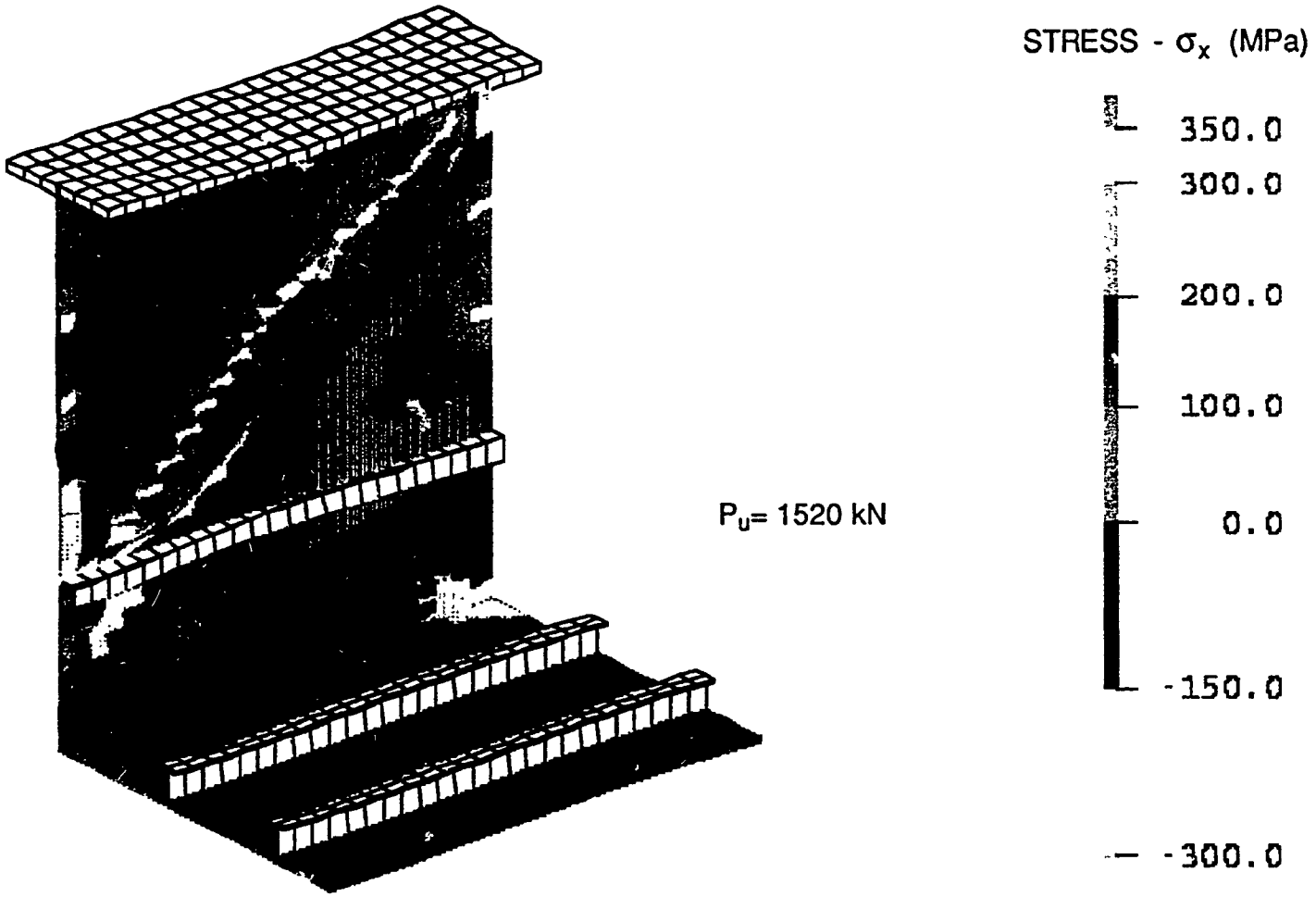

Figure 4.36 Normal Stress Distribution
Box Girder Type A. Web Stiffening Type 2.b.(ii)

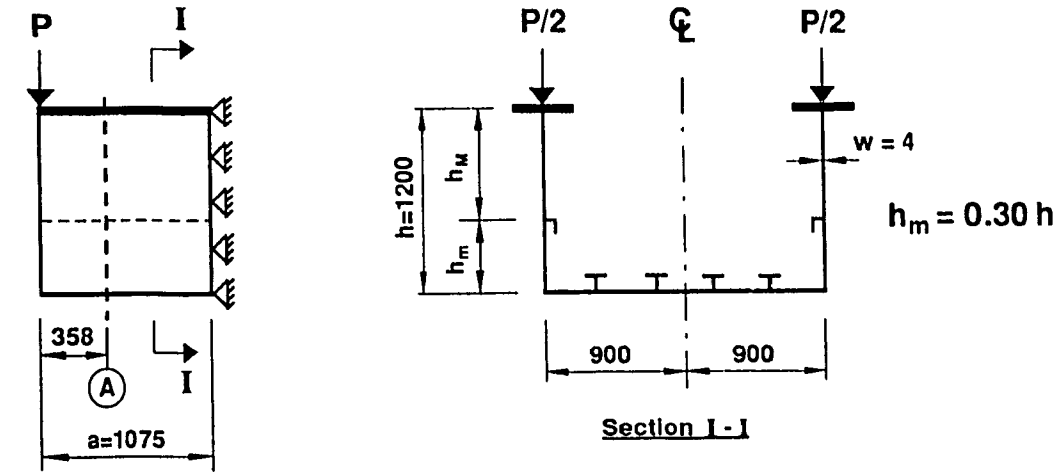

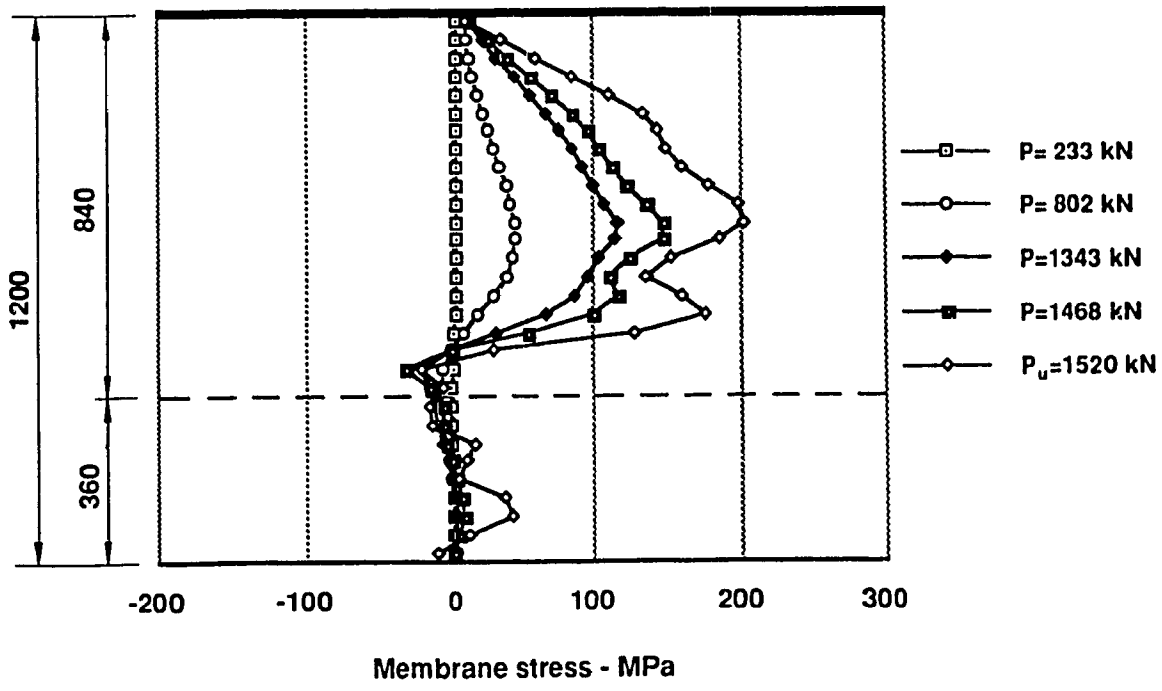

Figure 4.37 Distribution of Membrane Stresses - σ_x in the Web at Section A Box Girder Type A. Web Stiffening Type 2.b.(ii)

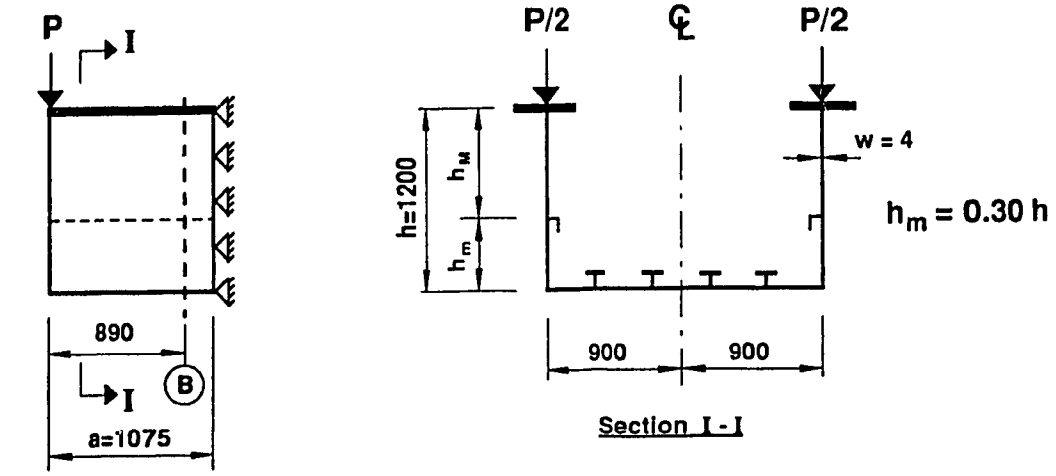

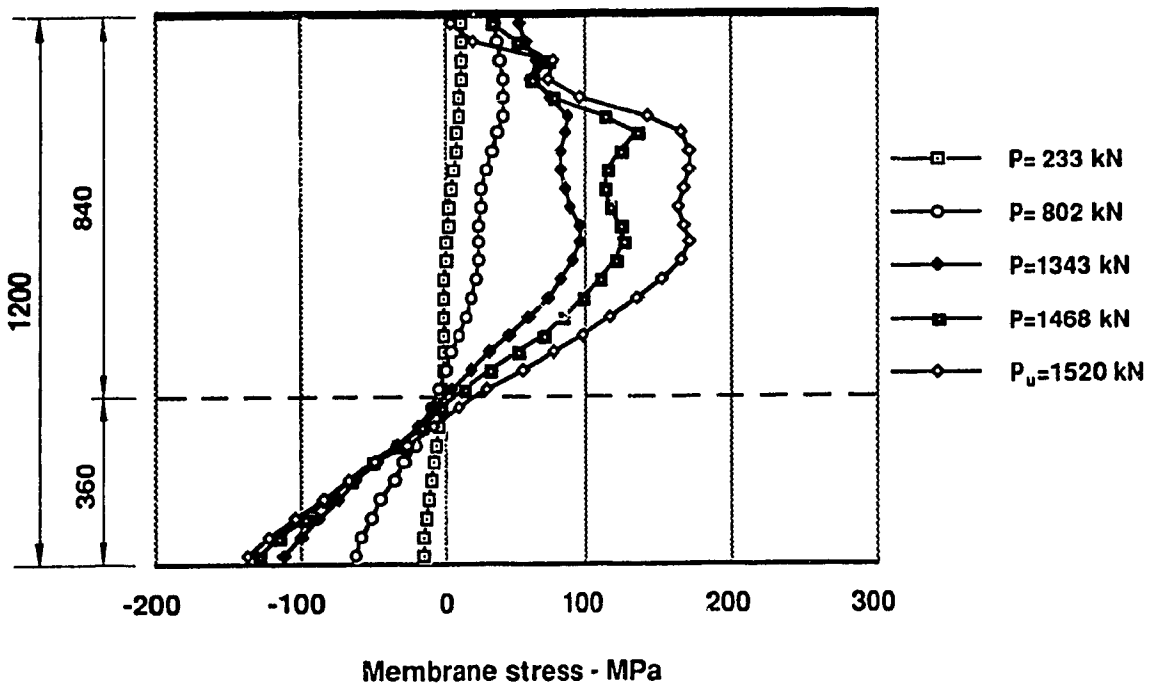

Figure 4.38 Distribution of Membrane Stresses - σ_x in the Web at Section B Box Girder Type A. Web Stiffening Type 2.b.(ii)

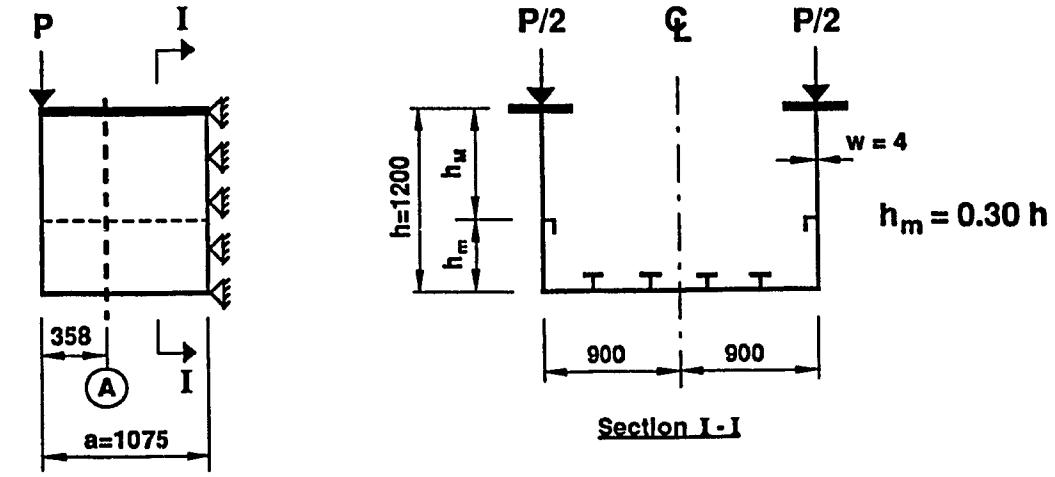

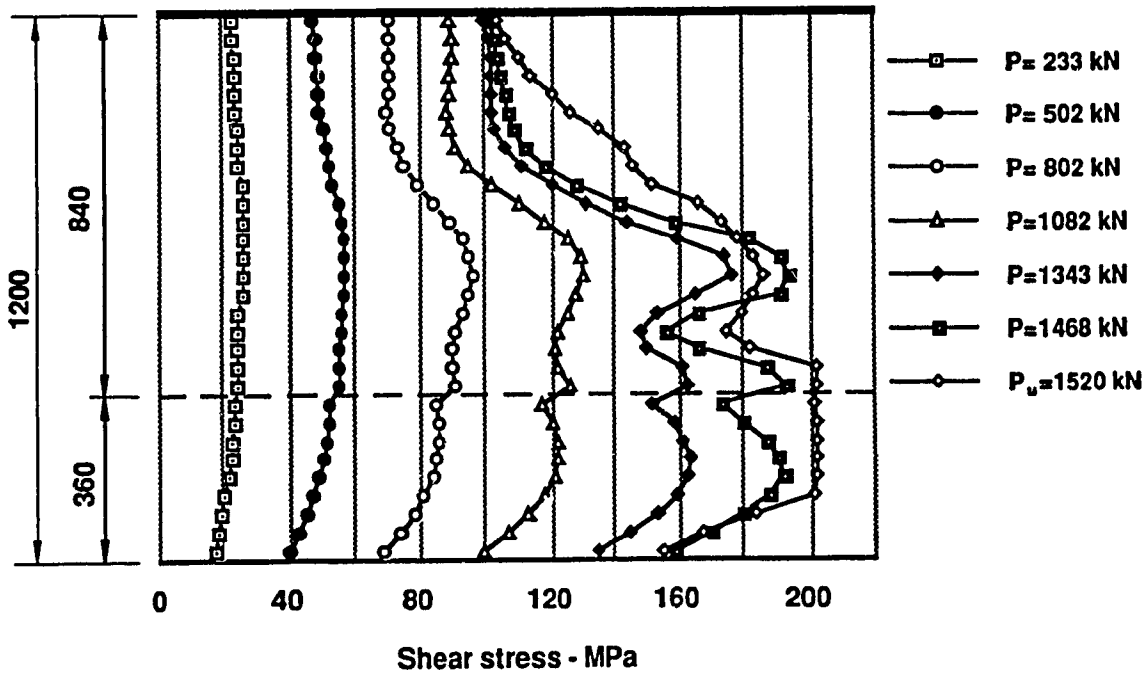

Figure 4.39 Distribution of Shear Stresses in the Web at Section A Box Girder Type A. Web Stiffening Type 2.b.(ii)

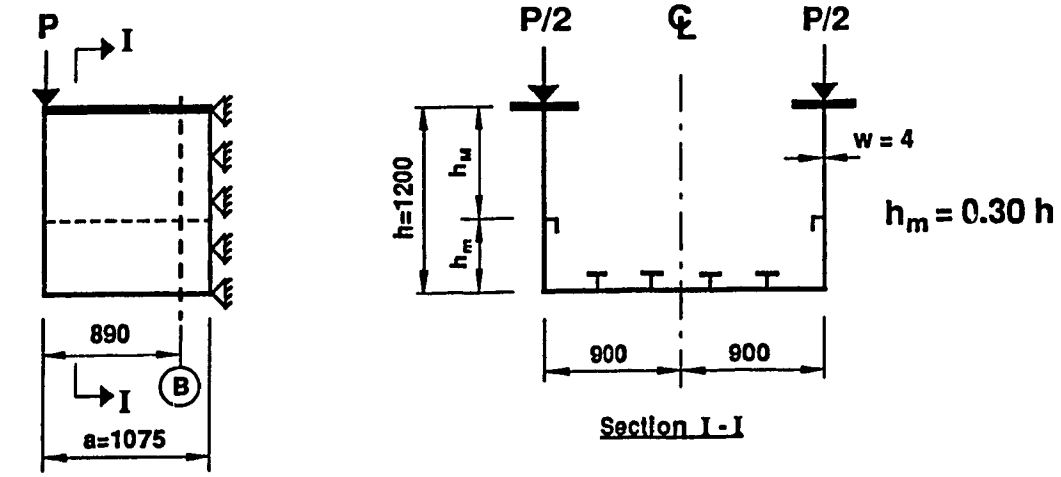

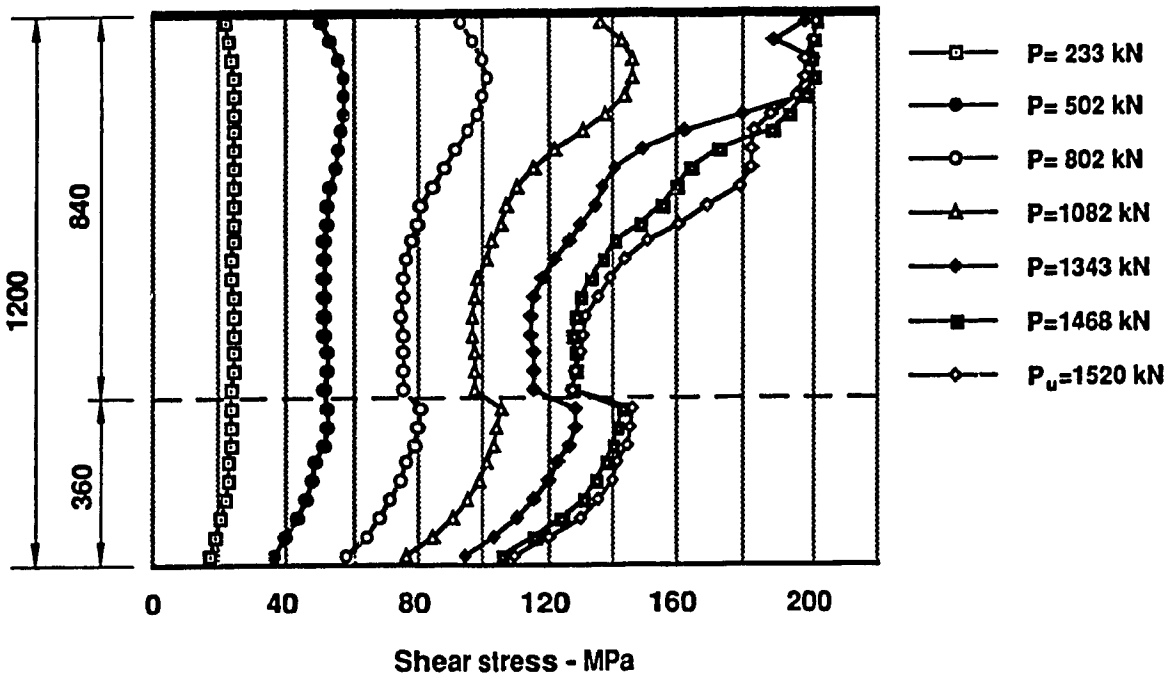

Figure 4.40 Distribution of Shear Stresses in the Web at Section B Box Girder Type A. Web Stiffening Type 2.b.(ii)

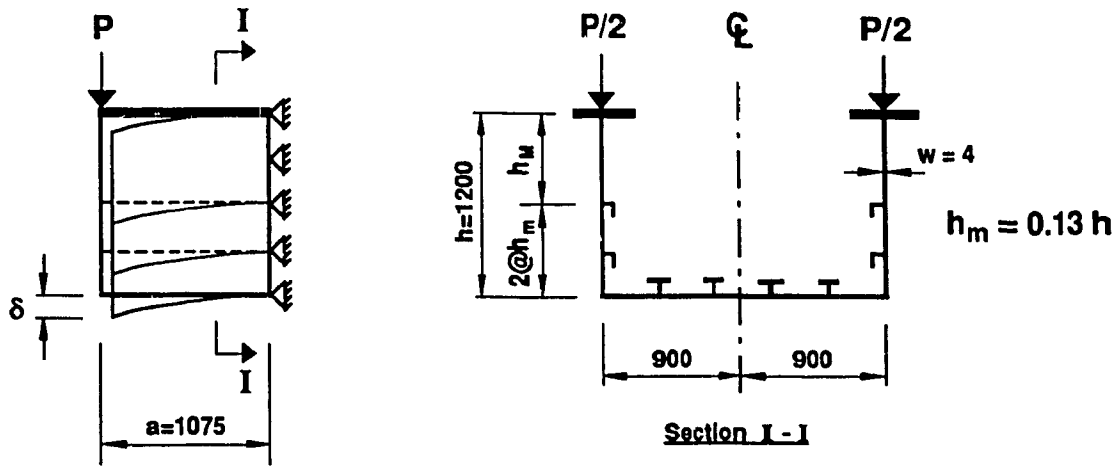

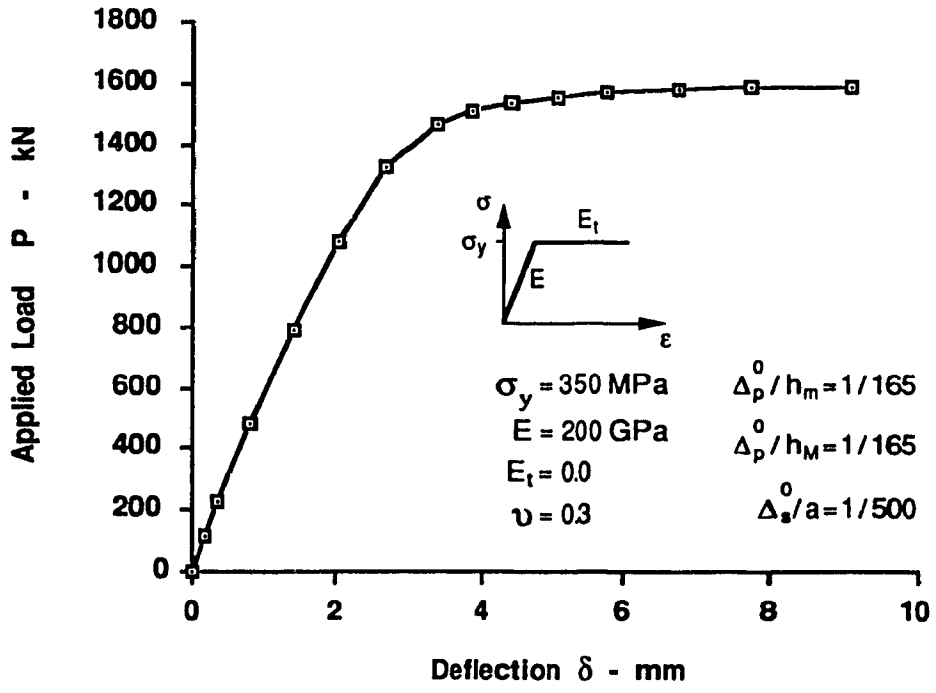

Figure 4.41 Load - Deflection Curve for Box Girder Type A. Web Stiffening Type 3.a.(ii)

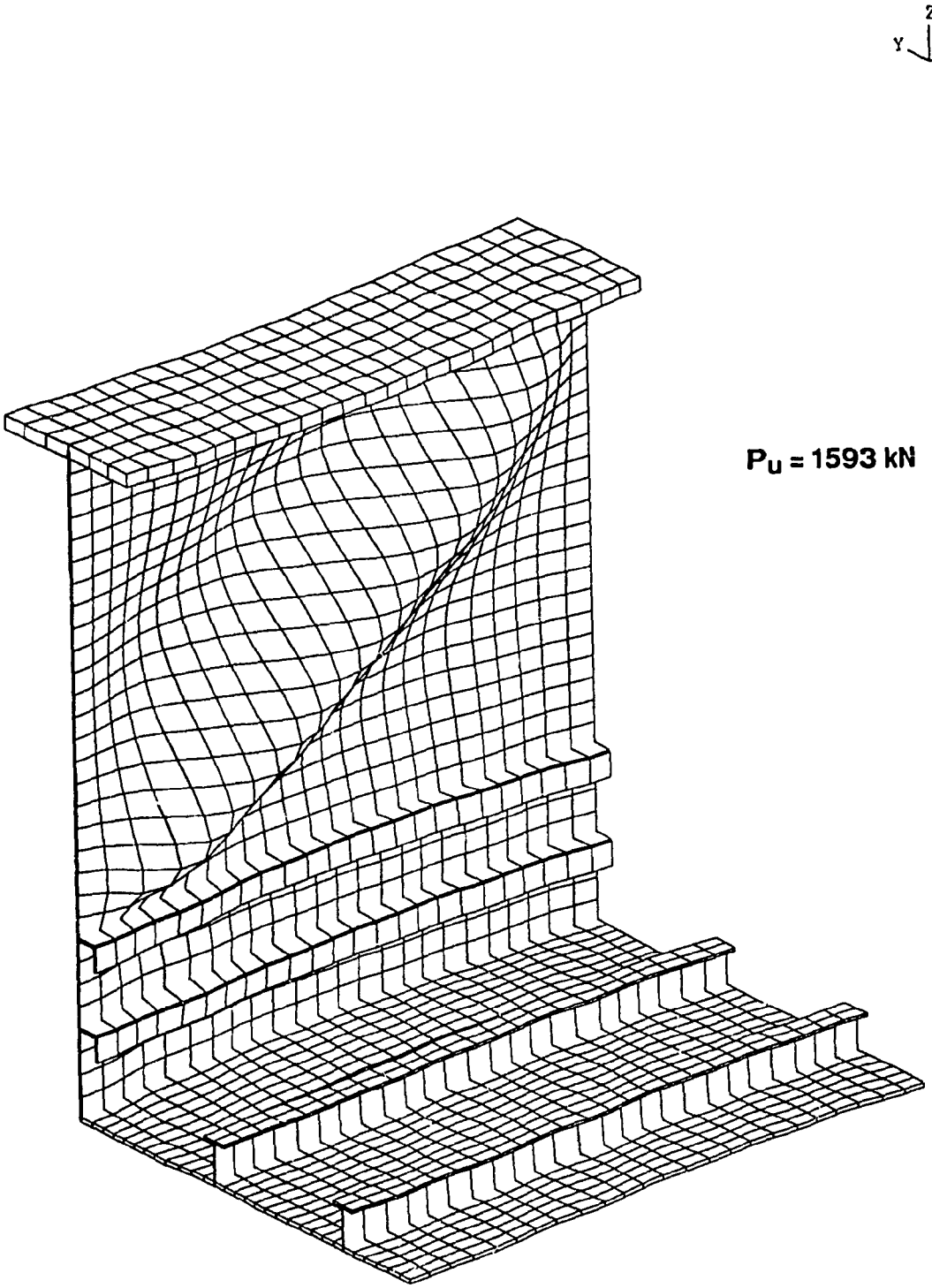

Figure 4.42 Web Buckling of Box Girder Type A.
Web Stiffening Type 3.a.(ii)

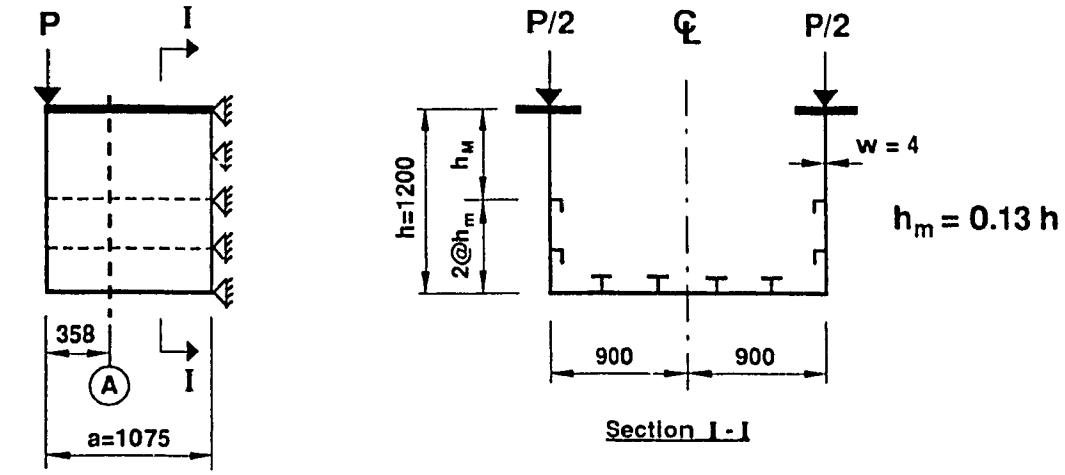

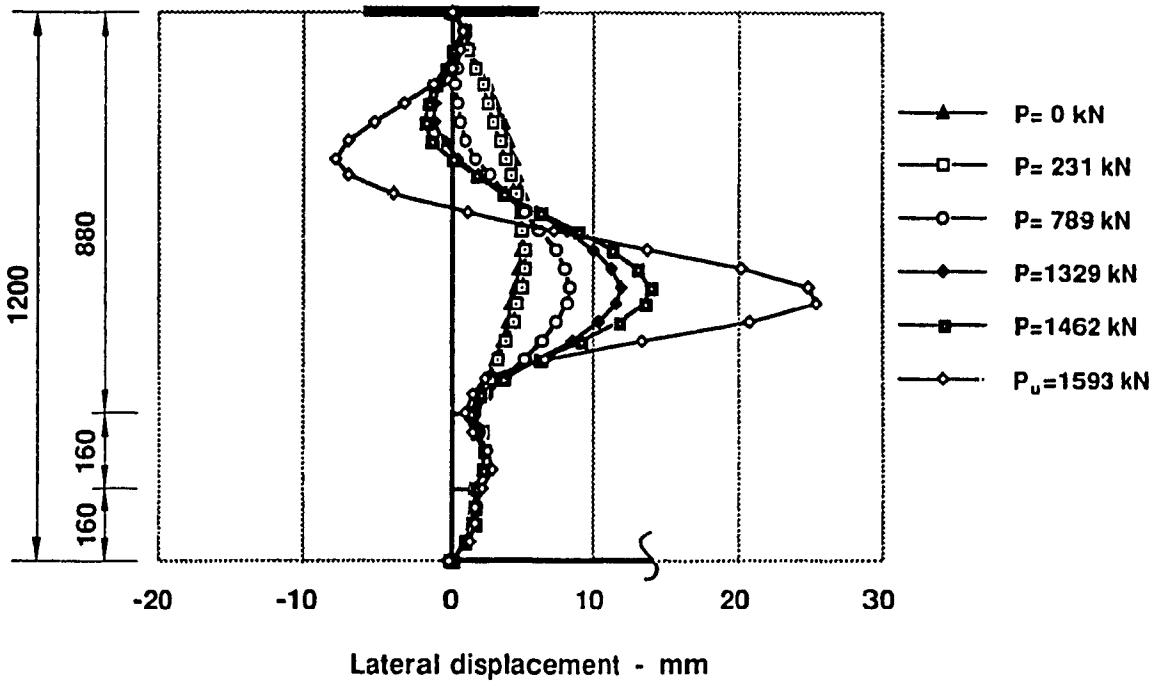

Figure 4.43 Deflection of Web under Loading - Section A
Box Girder Type A. Web Stiffening Type 3.a.(ii)

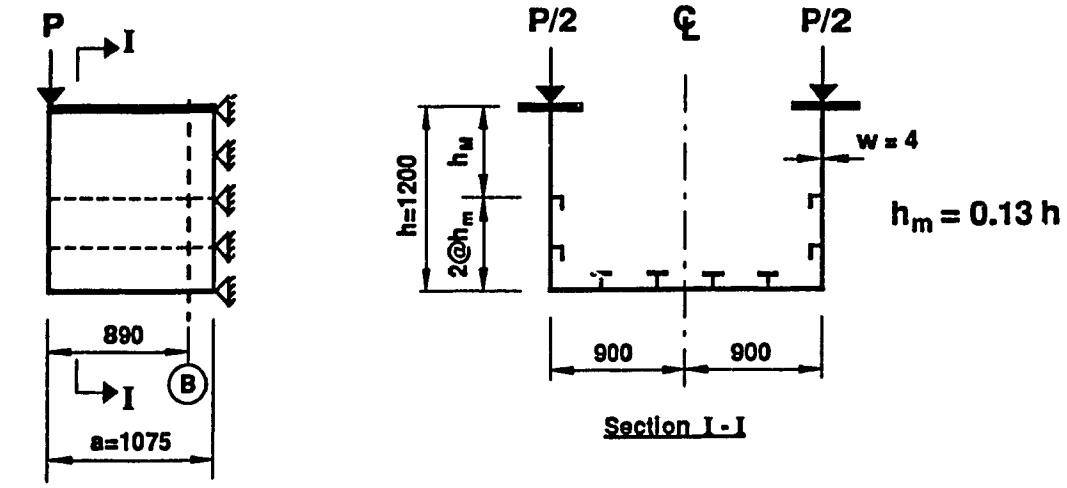

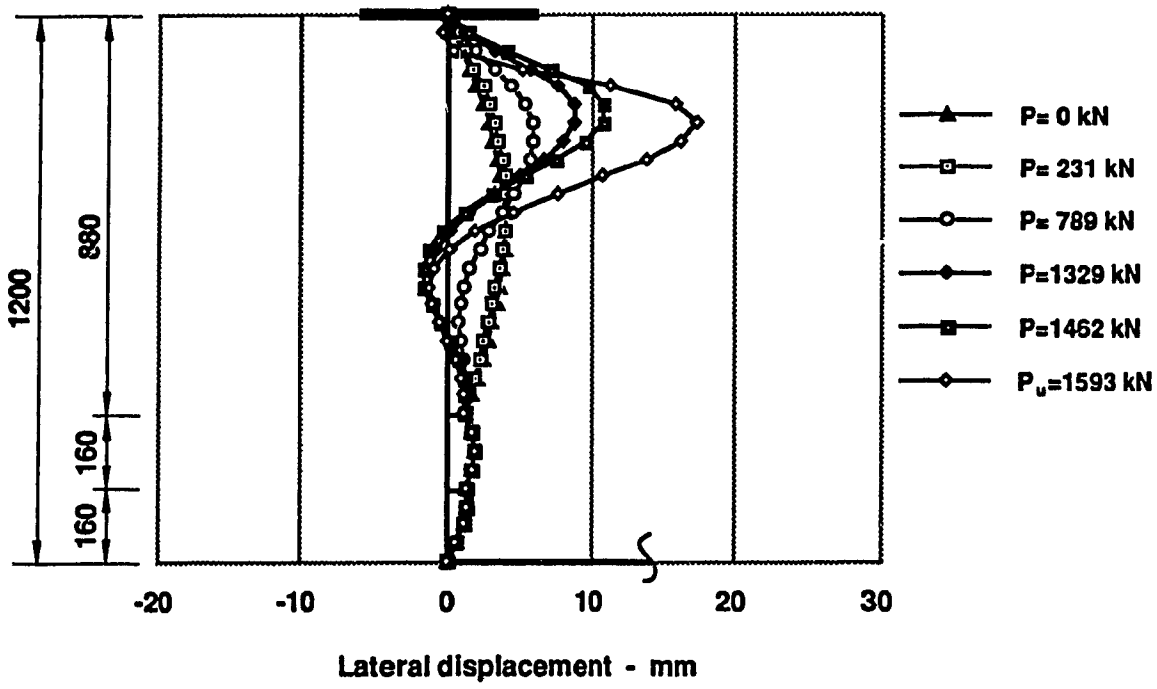

Figure 4.44 Deflection of Web under Loading - Section B
Box Girder Type A. Web Stiffening Type 3.a.(ii)

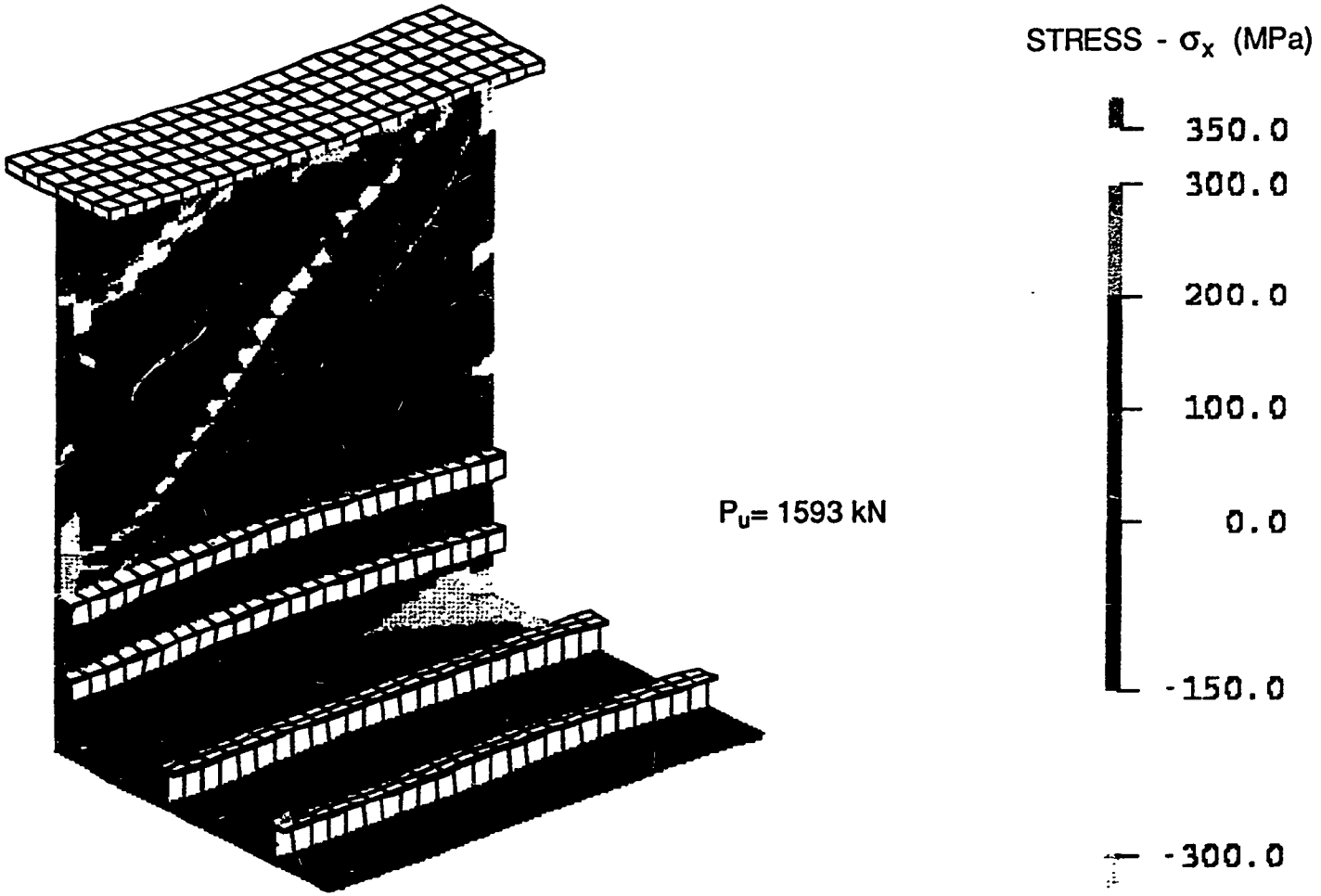

Figure 4.45 Normal Stress Distribution
Box Girder Type A. Web Stiffening Type 3.a.(ii)

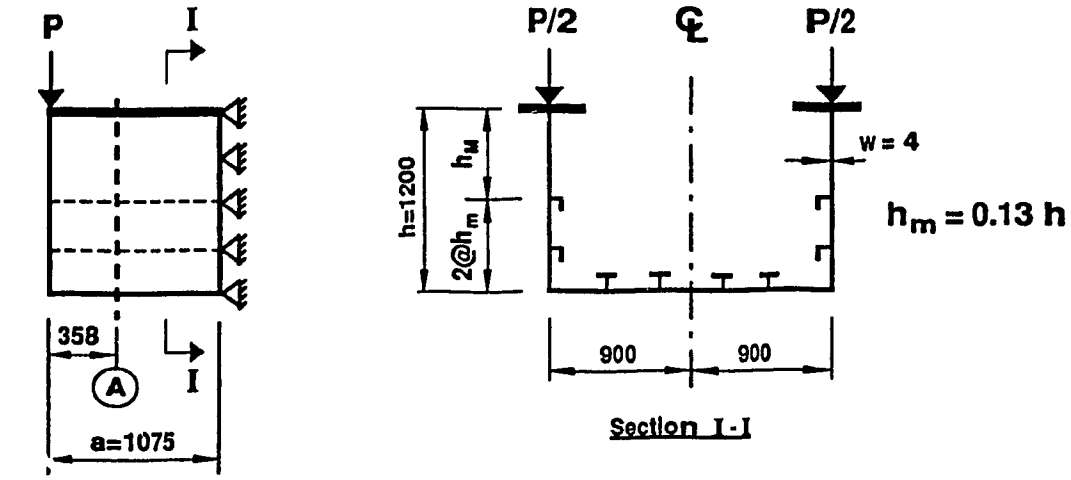

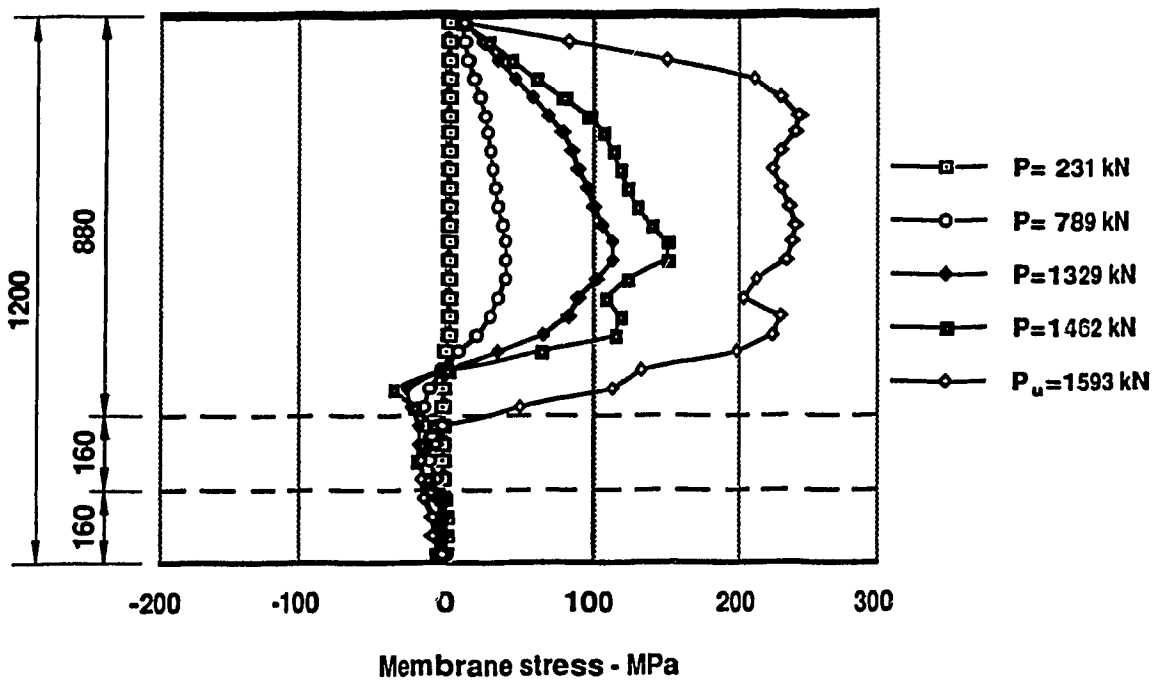

Figure 4.46 Distribution of Membrane Stresses - σ_x in the Web at Section A Box Girder Type A. Web Stiffening Type 3.a.(ii)

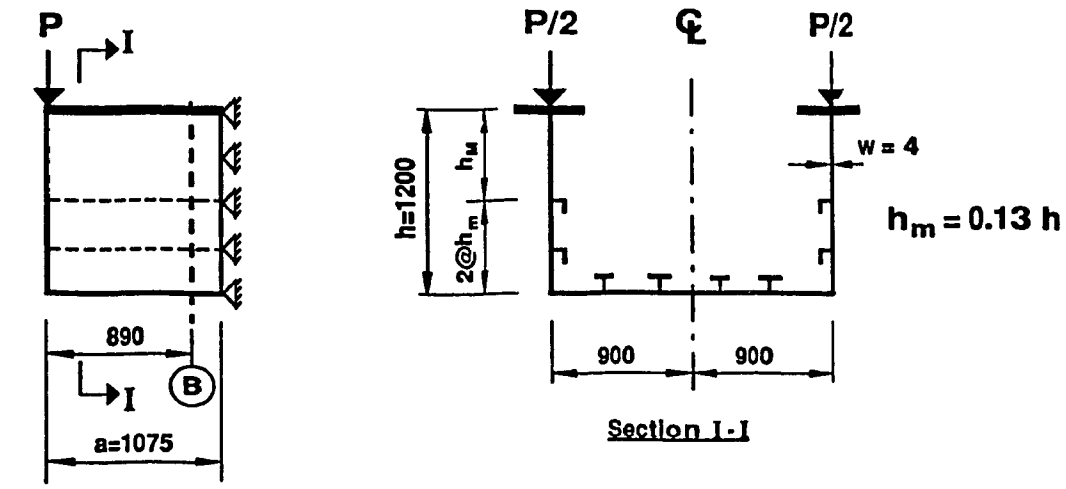

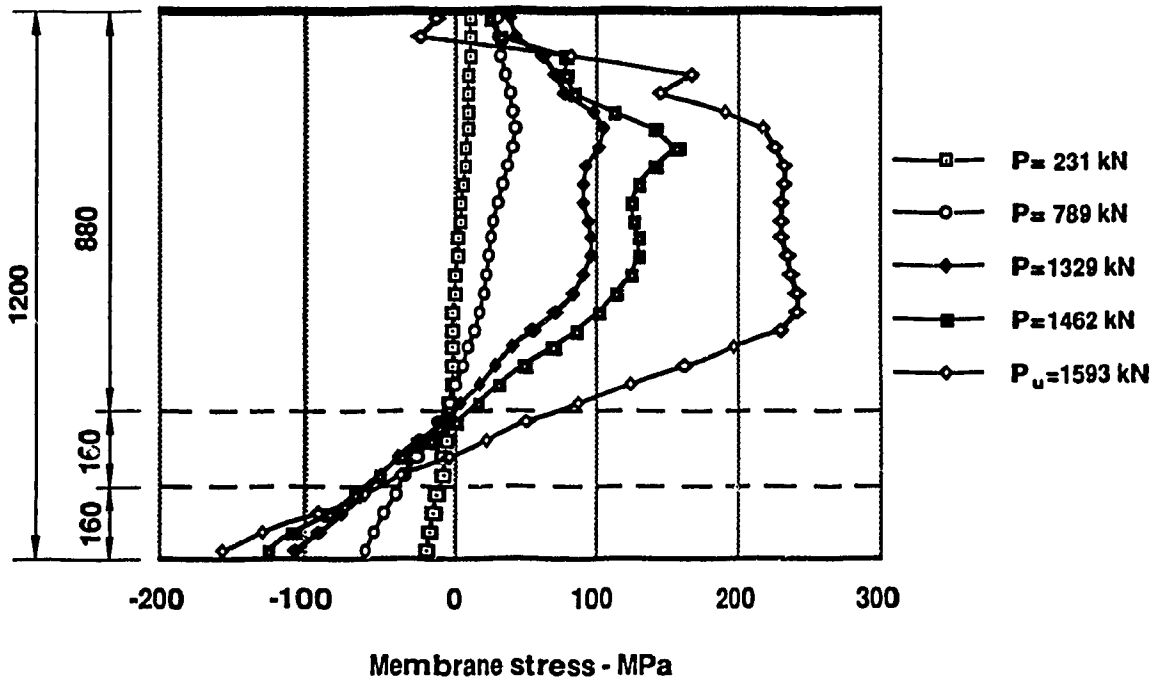

Figure 4.47 Distribution of Membrane Stresses - σ_x in the Web at Section B Box Girder Type A. Web Stiffening Type 3.a.(ii)

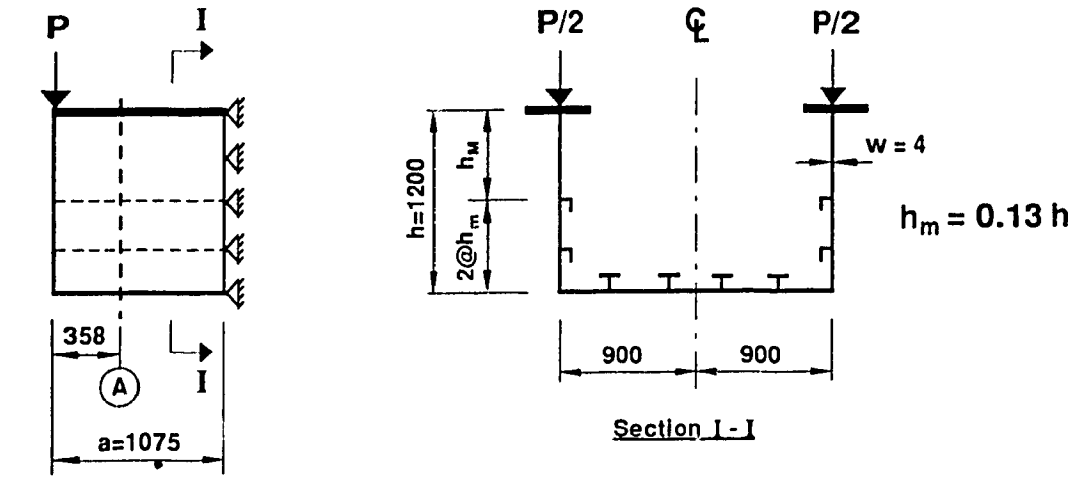

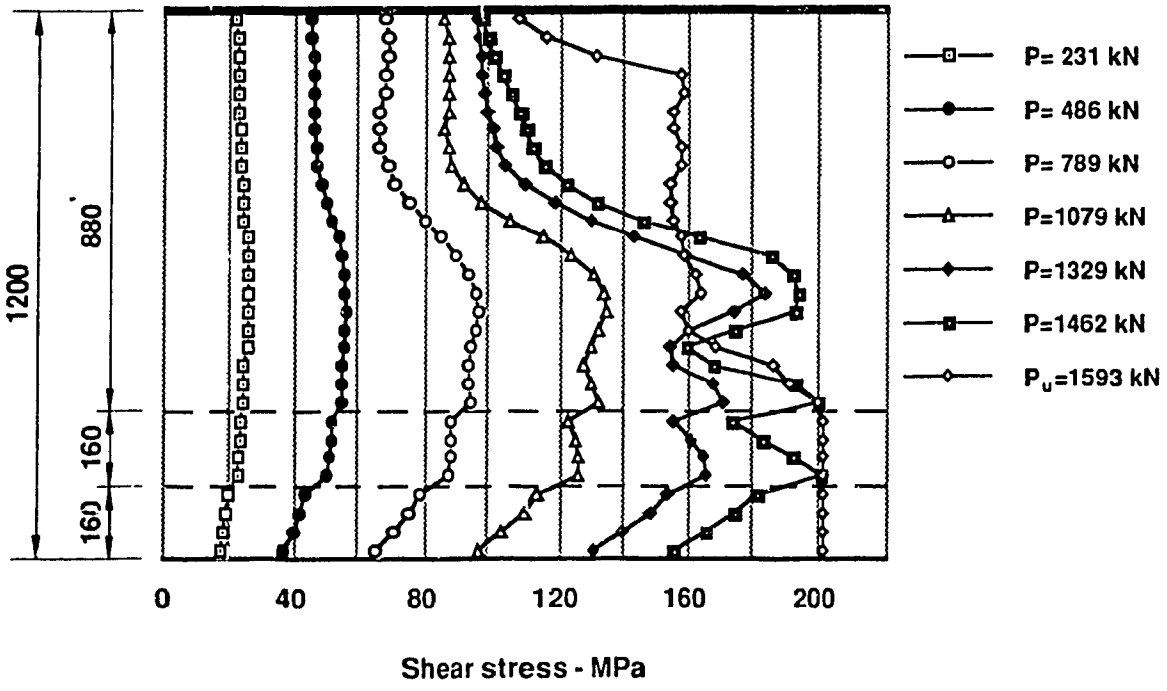

Figure 4.48 Distribution of Shear Stresses in the Web at Section A Box Girder Type A. Web Stiffening Type 3.a (ii)

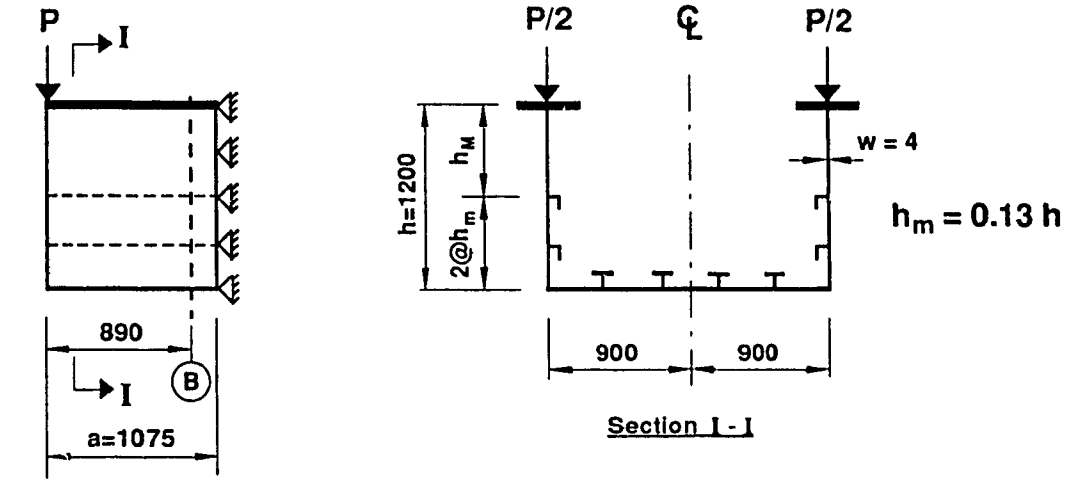

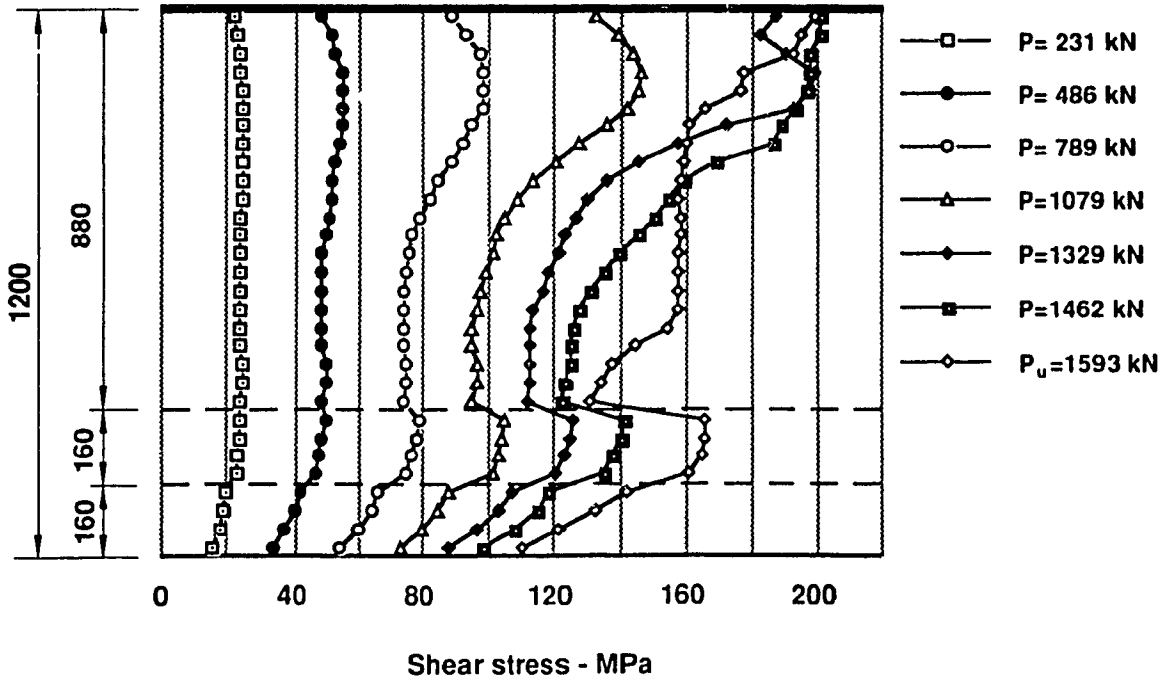

Figure 4.49 Distribution of Shear Stresses in the Web at Section B
Box Girder Type A. Web Stiffening Type 3.a (ii)

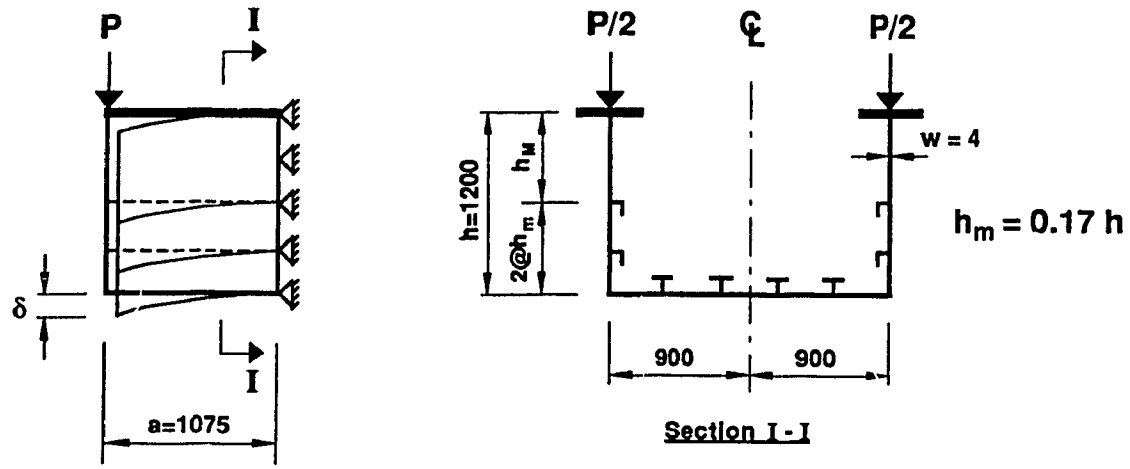

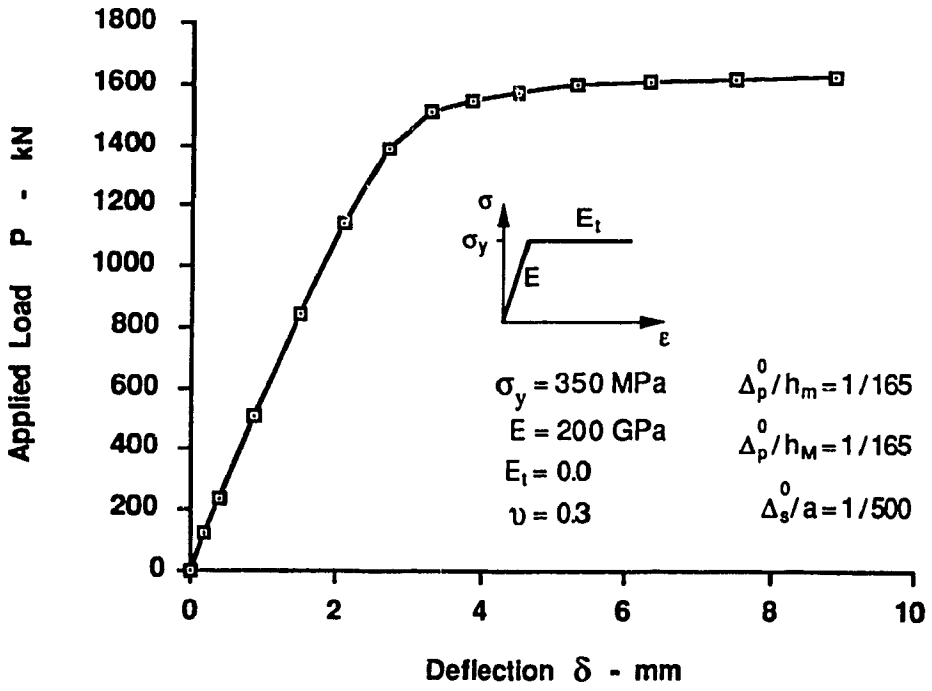

Figure 4.50 Load - Deflection Curve for Box Girder Type A. Web Stiffening Type 3.b.(ii)

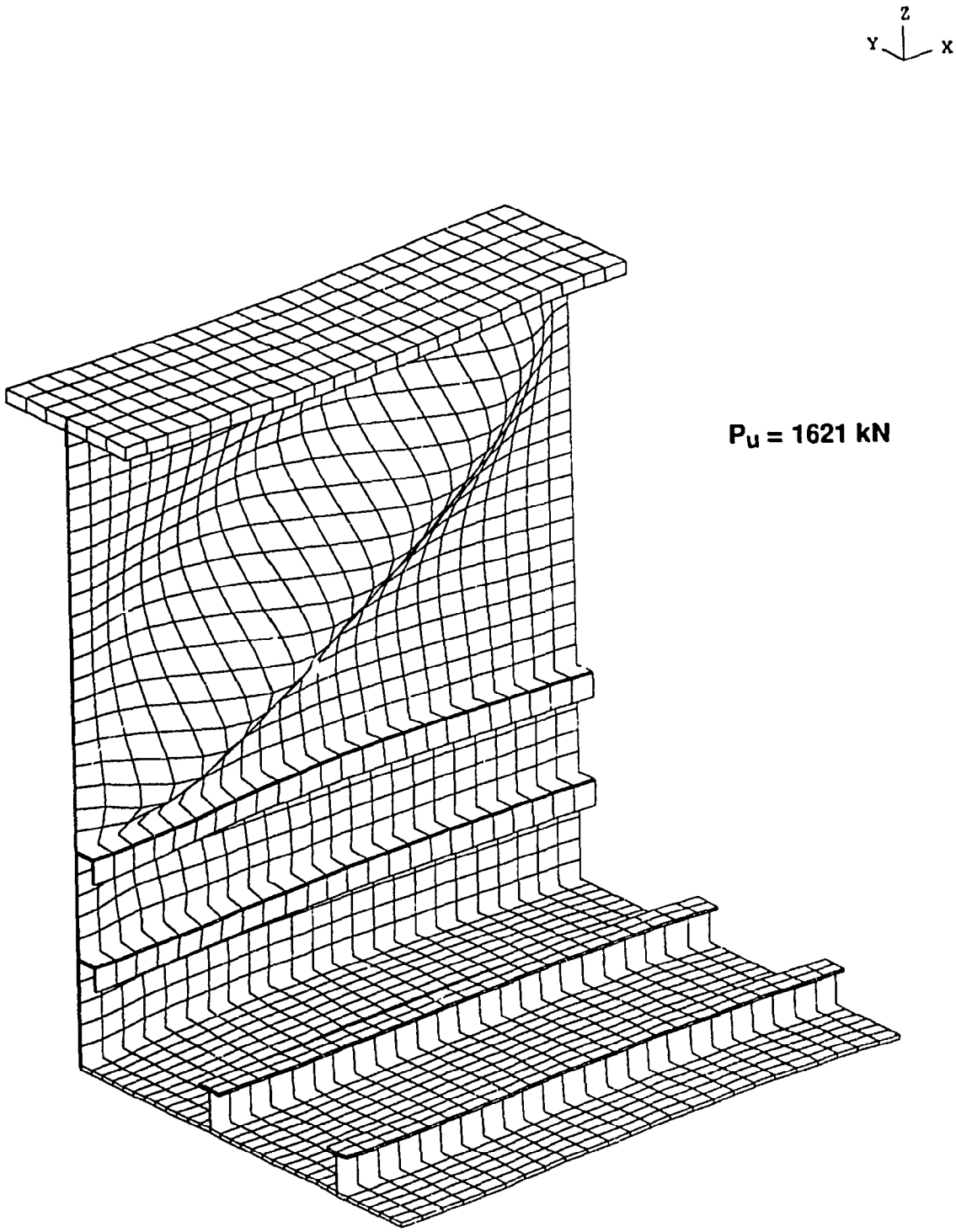

Figure 4.51 Web Buckling of Box Girder Type A.
Web Stiffening Type 3.b.(ii)

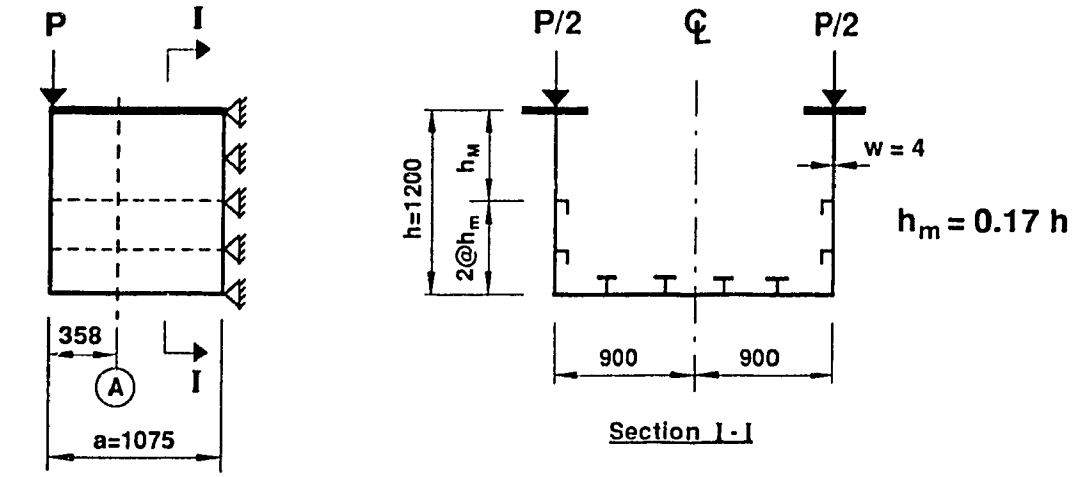

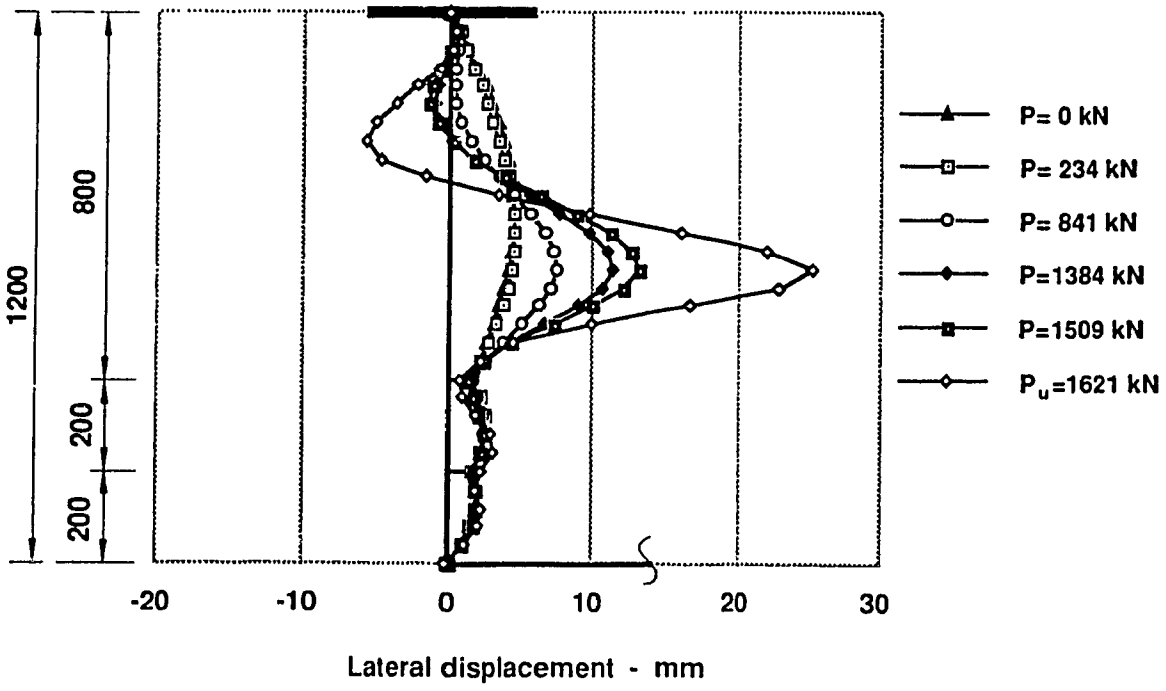

Figure 4.52 Deflection of Web under Loading - Section A
Box Girder Type A. Web Stiffening Type 3.b.(ii)

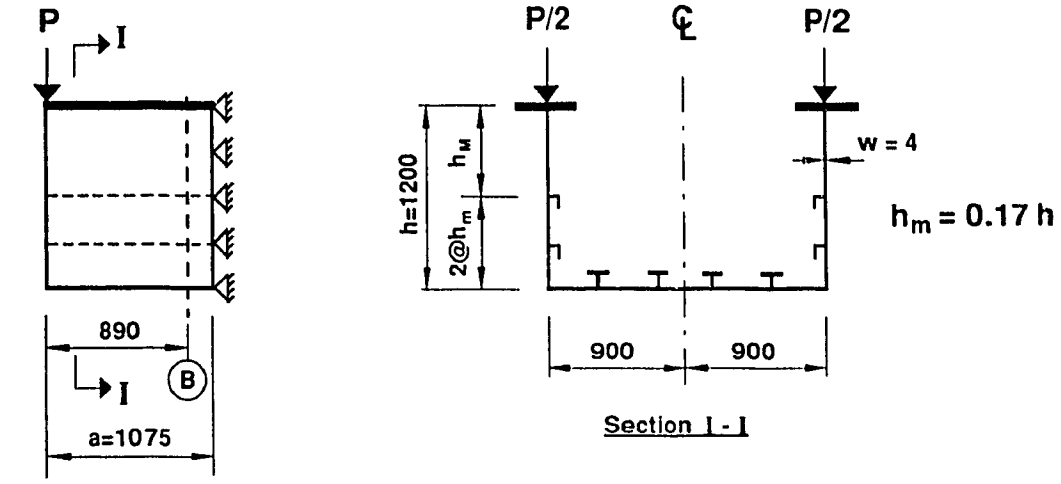

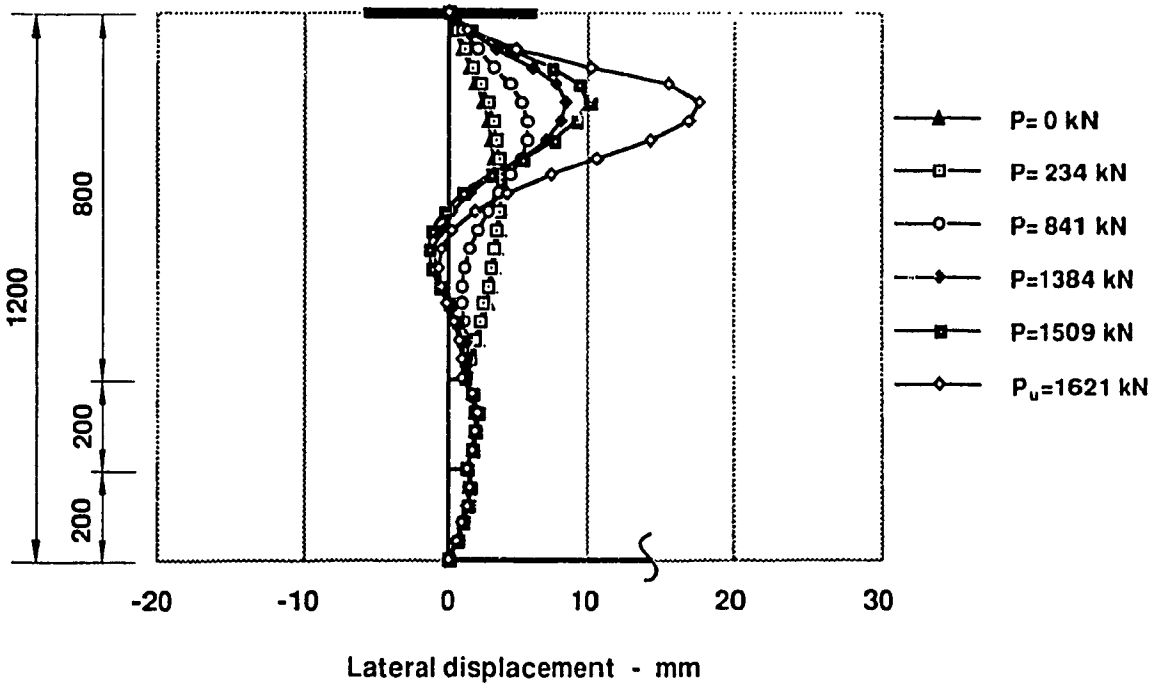

Figure 4.53 Deflection of Web under Loading - Section B
Box Girder Type A. Web Stiffening Type 3.b.(ii)

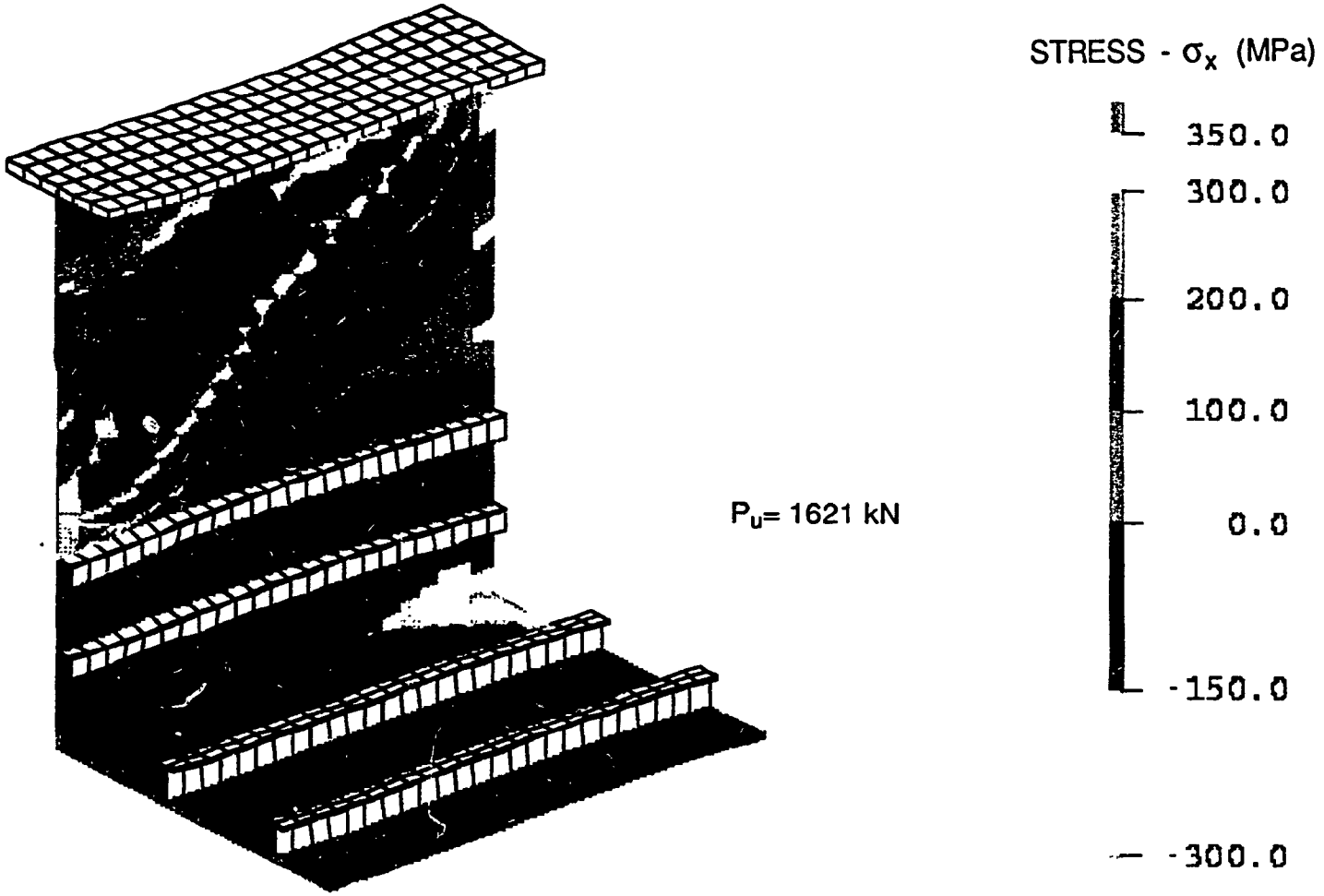

Figure 4.54 Normal Stress Distribution
Box Girder Type A. Web Stiffening Type 3.b.(ii)

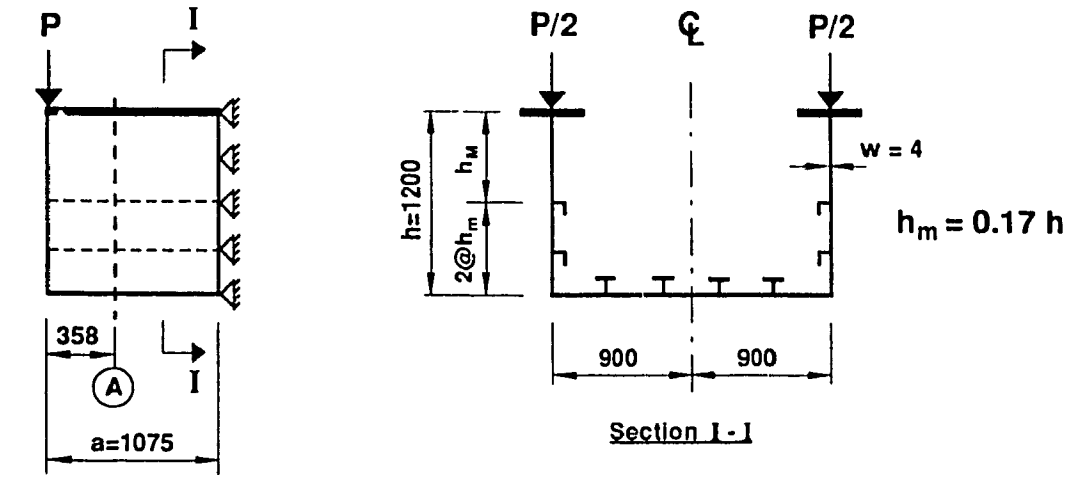

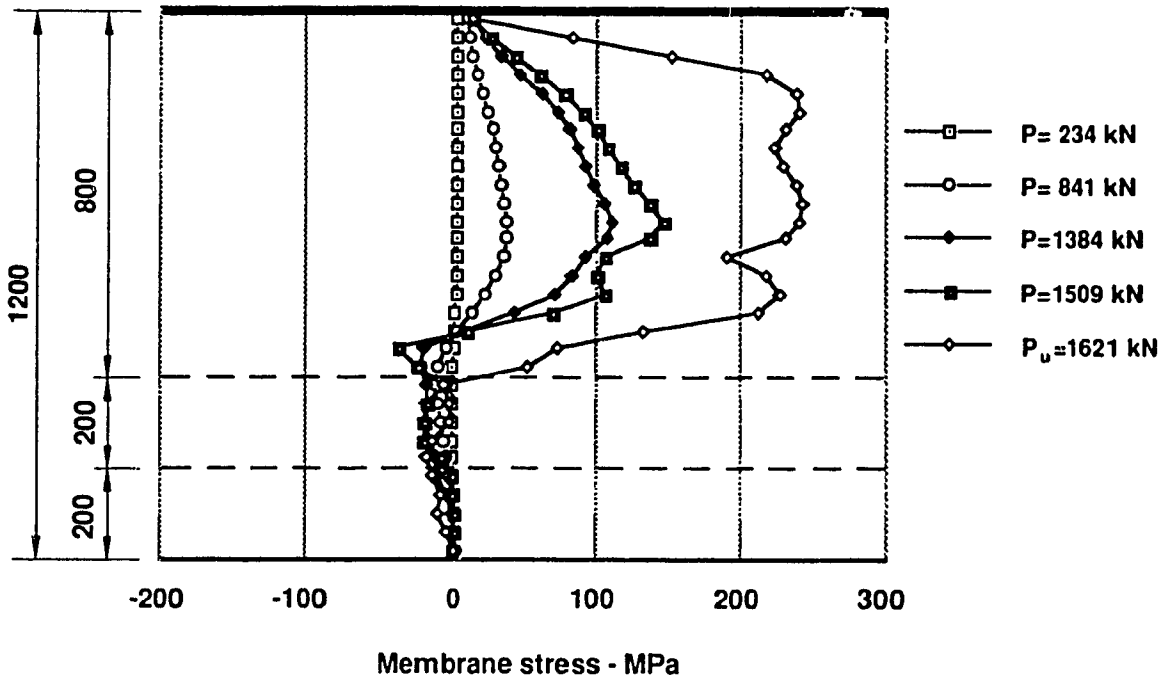

Figure 4.55 Distribution of Membrane Stresses - σ_x in the Web at Section A Box Girder Type A. Web Stiffening Type 3.b.(ii)

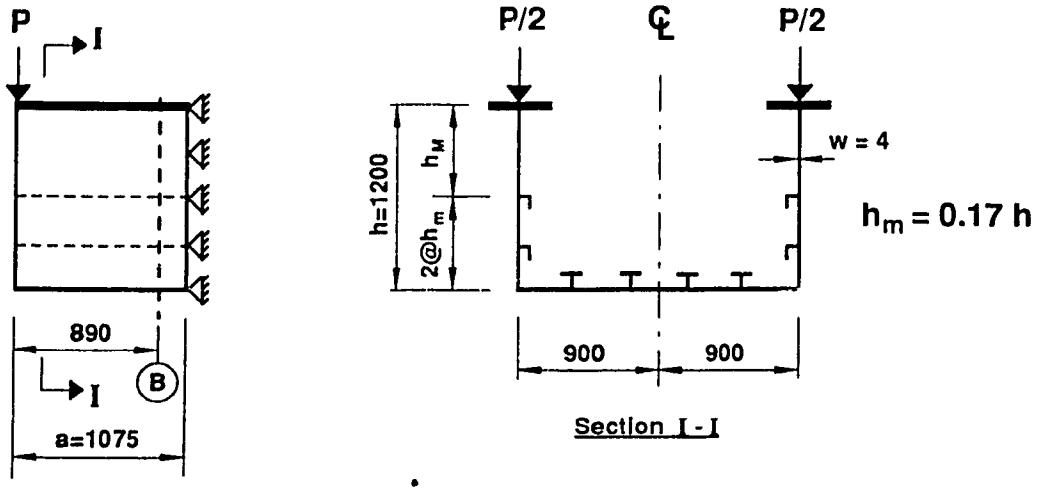

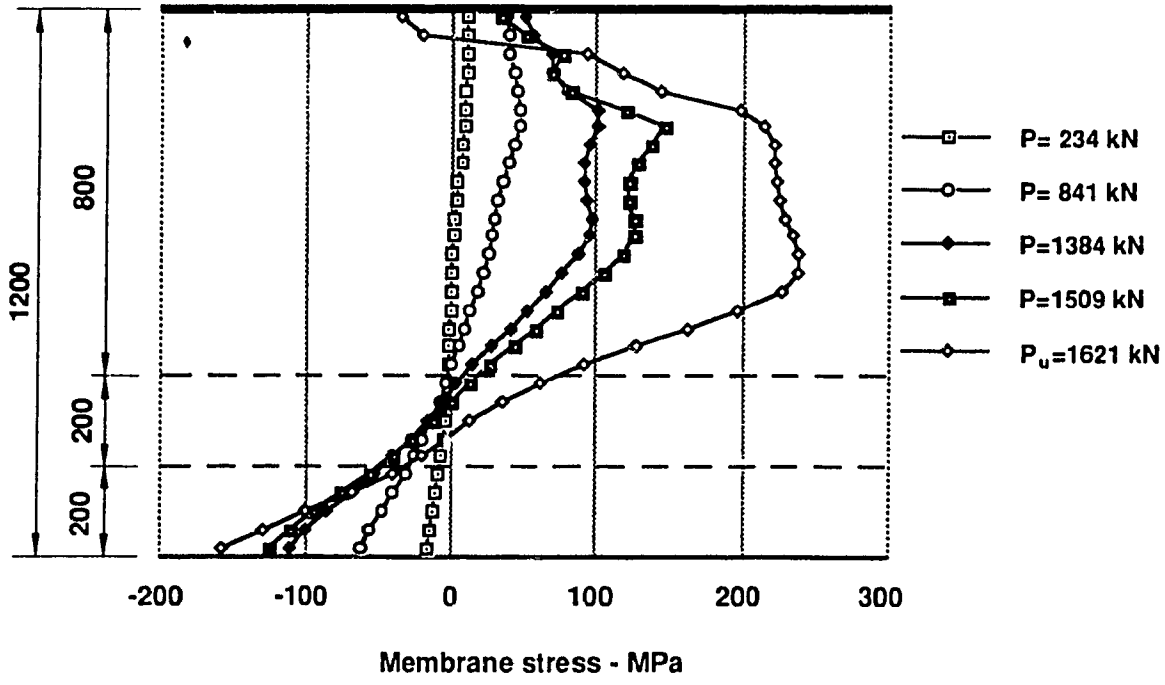

Figure 4.56 Distribution of Membrane Stresses - σ_x in the Web at Section B Box Girder Type A. Web Stiffening Type 3.b.(ii)

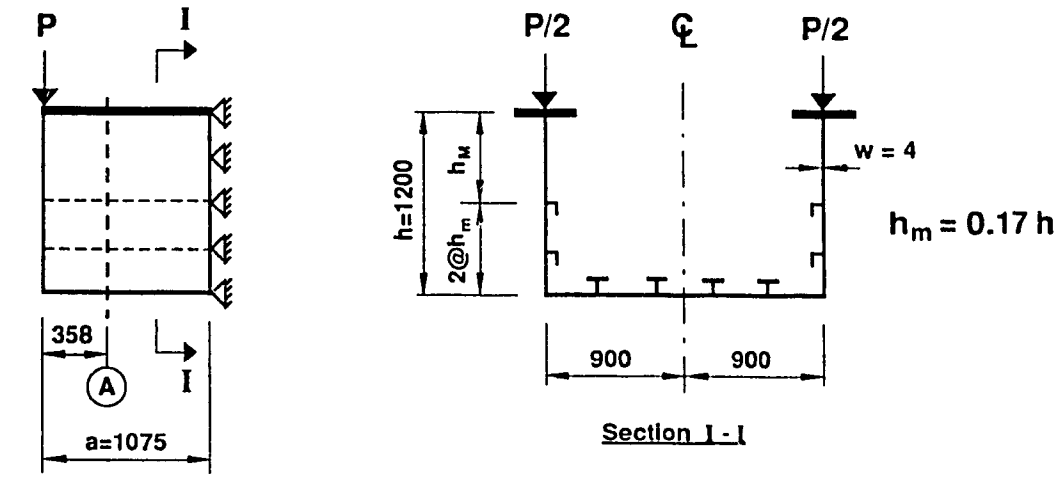

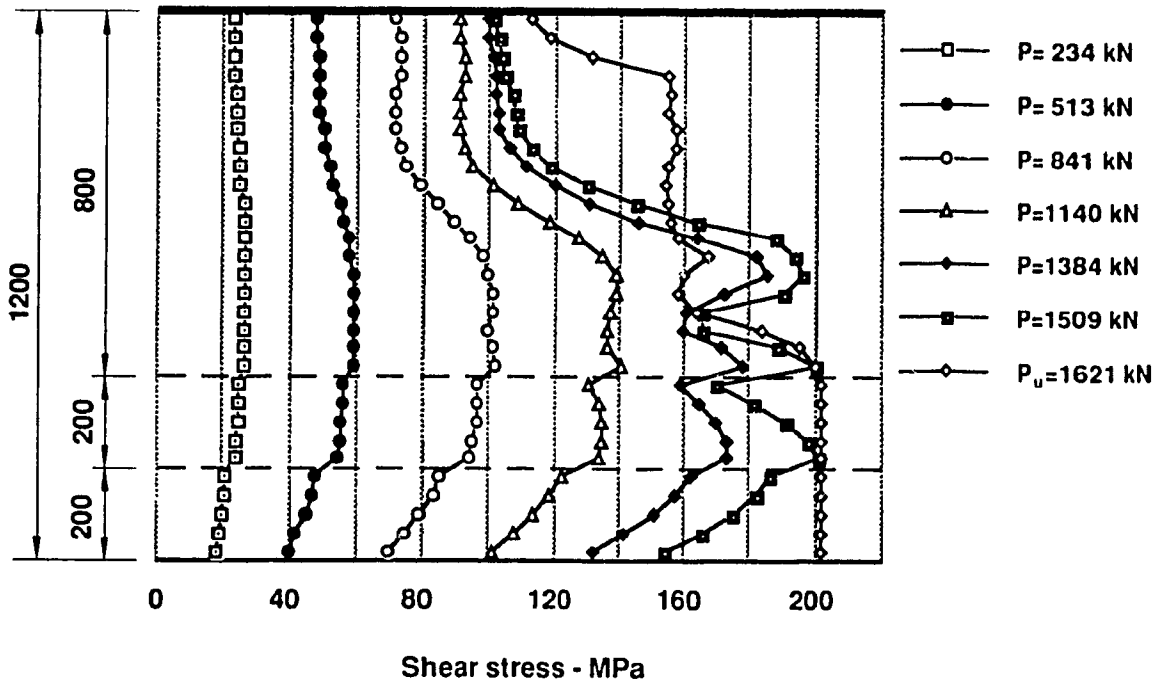

Figure 4.57 Distribution of Shear Stresses in the Web at Section A Box Girder Type A. Web Stiffening Type 3.b.(ii)

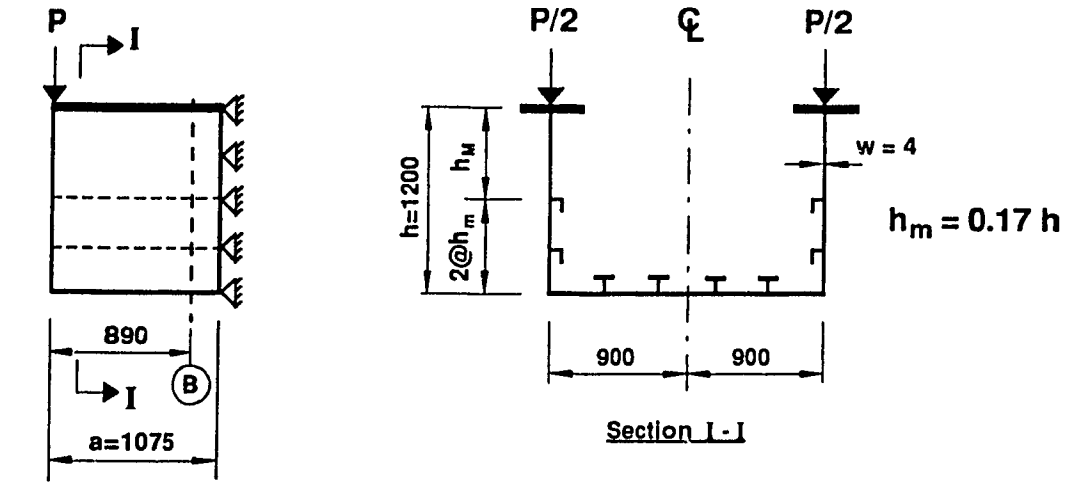

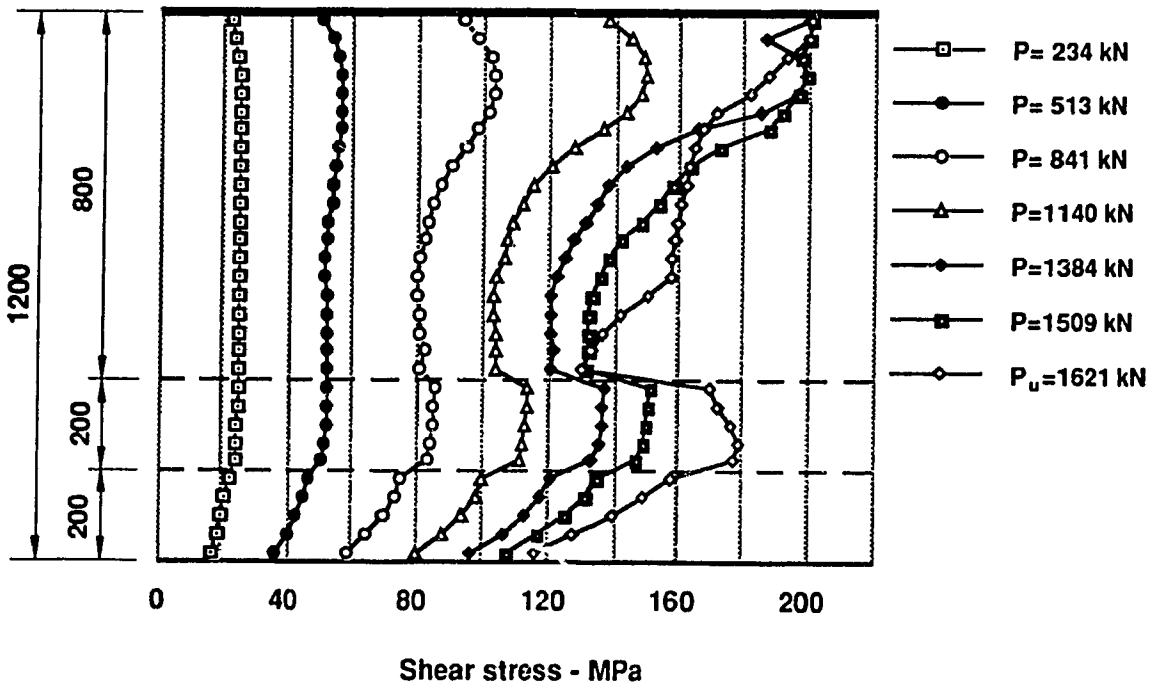

Figure 4.58 Distribution of Shear Stresses in the Web at Section B Box Girder Type A. Web Stiffening Type 3.b.(ii)

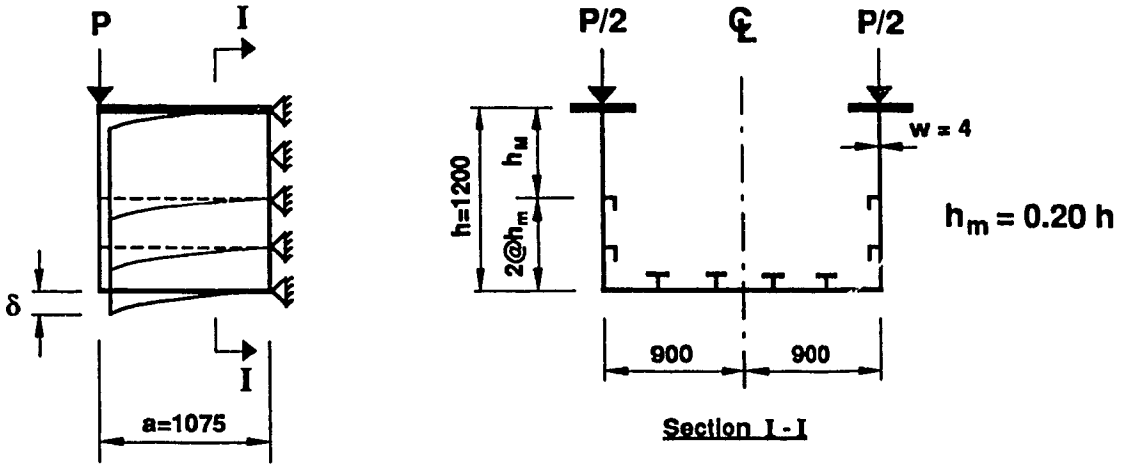

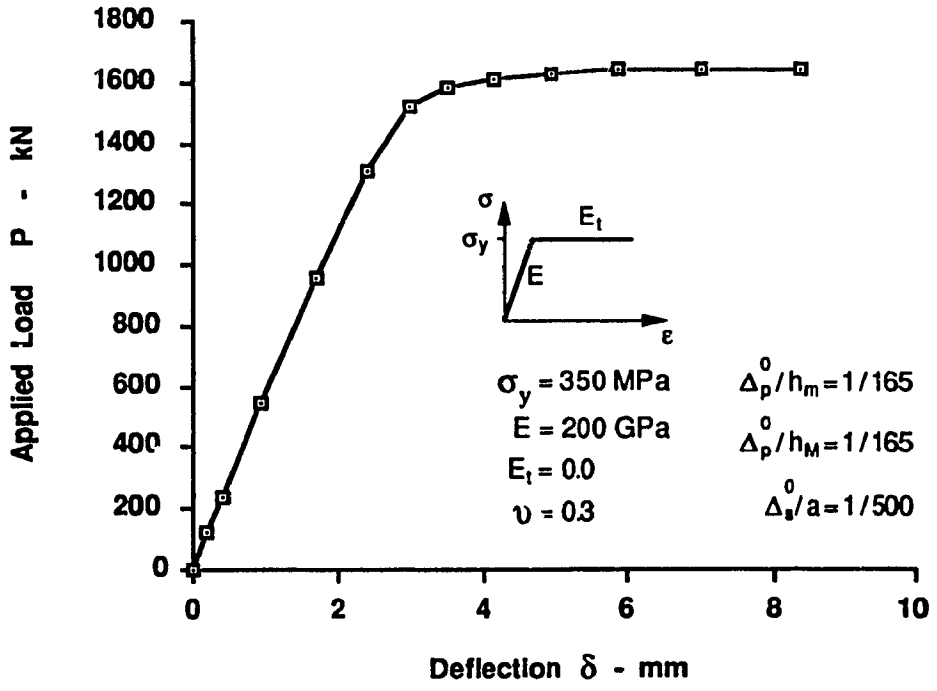

Figure 4.59 Load - Deflection Curve for Box Girder Type A. Web Stiffening Type 3.c.(ii)

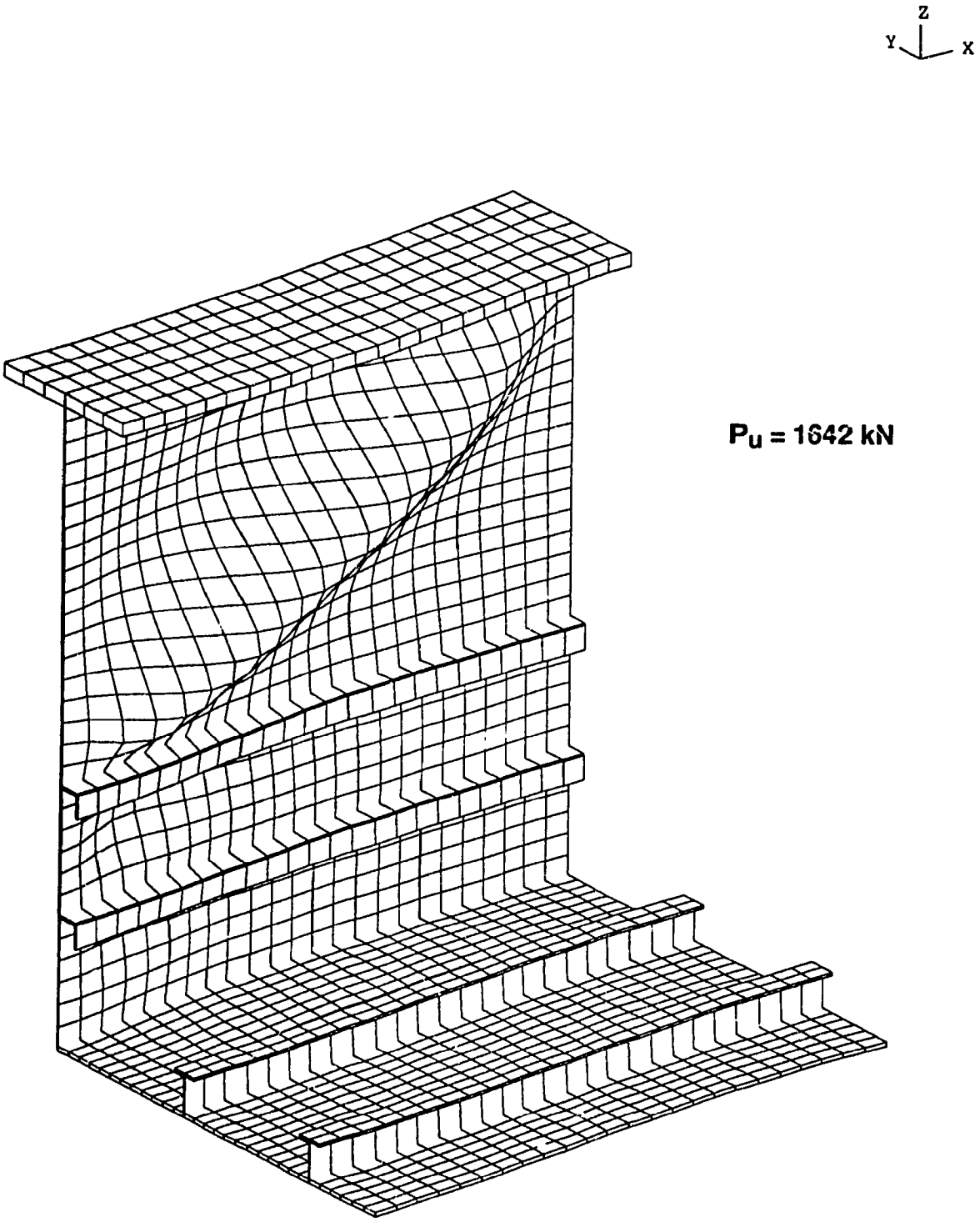

Figure 4.60 Web Buckling of Box Girder Type A.
Web Stiffening Type 3.c.(ii)

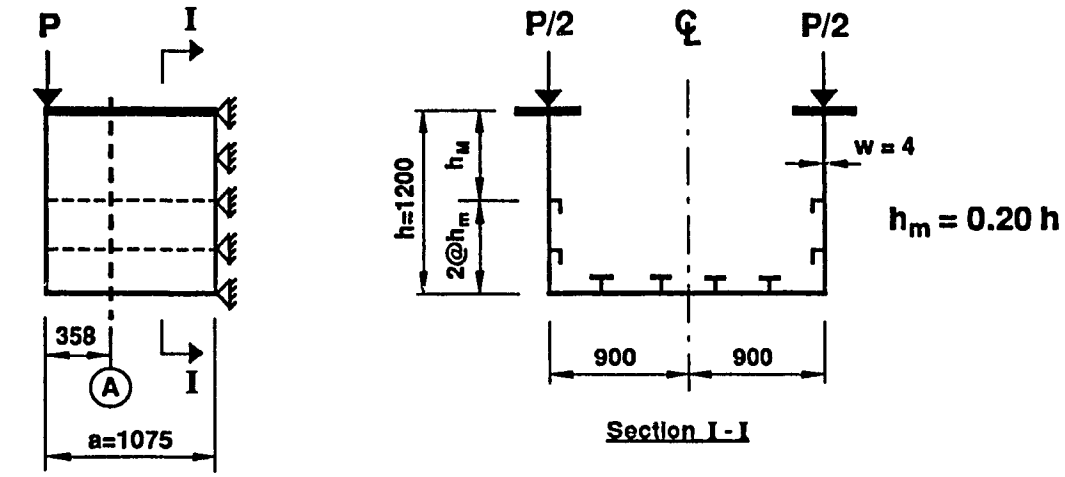

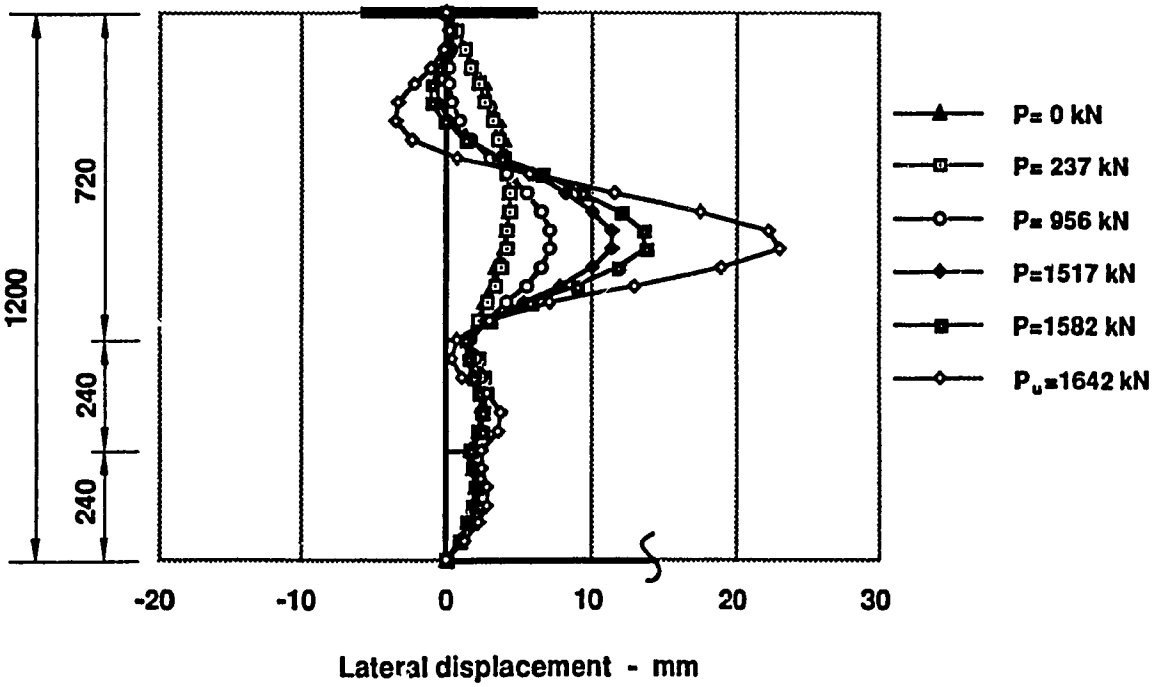

Figure 4.61 Deflection of Web under Loading - Section A
Box Girder Type A. Web Stiffening Type 3.c.(ii)

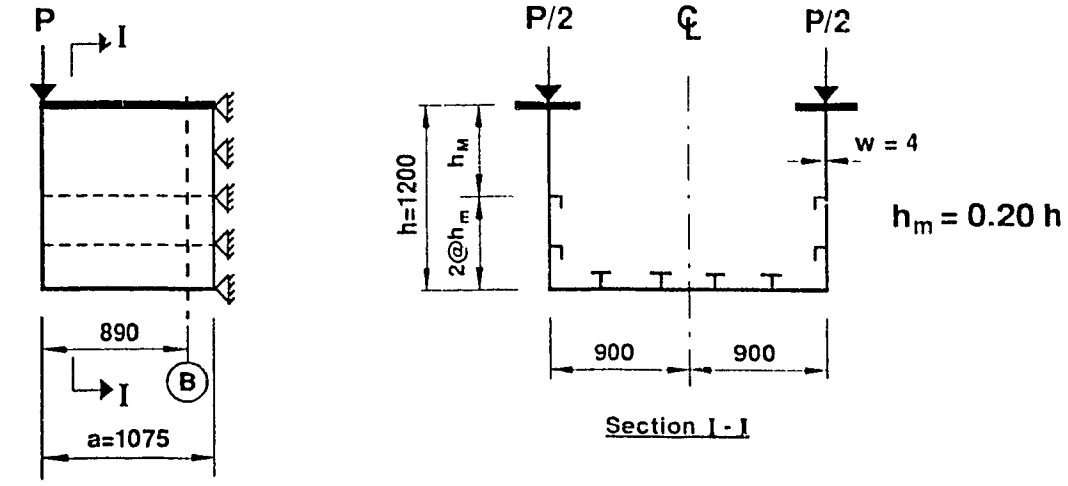

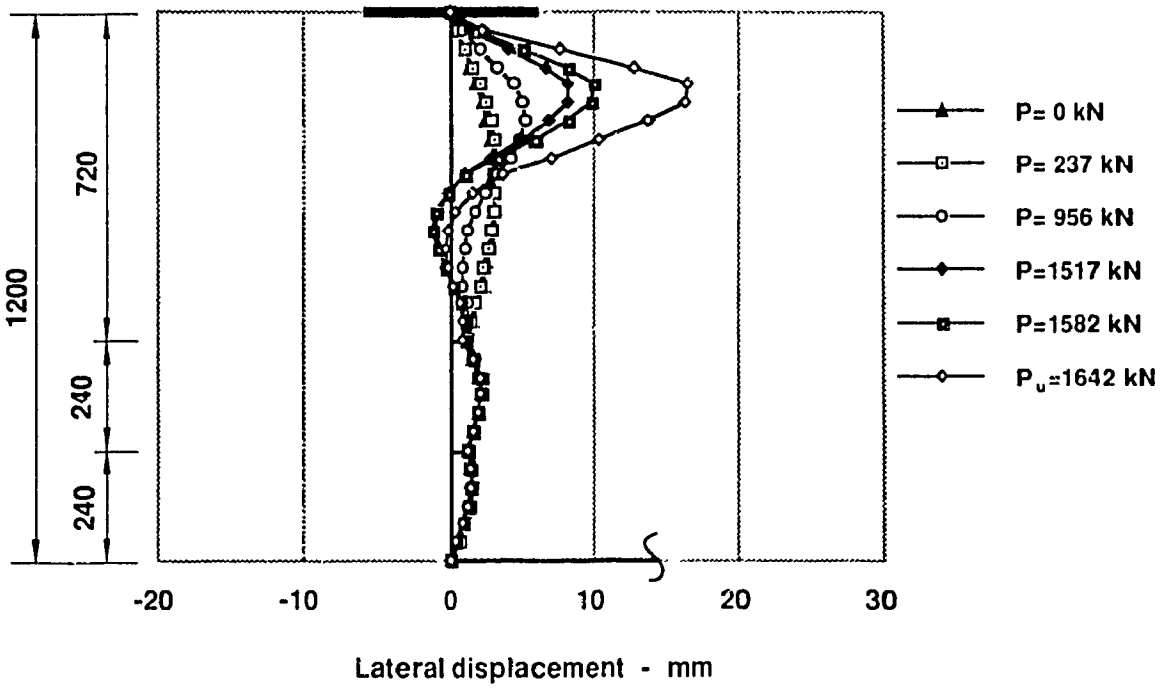

Figure 4.62 Deflection of Web under Loading - Section B
Box Girder Type A. Web Stiffening Type 3.c.(ii)

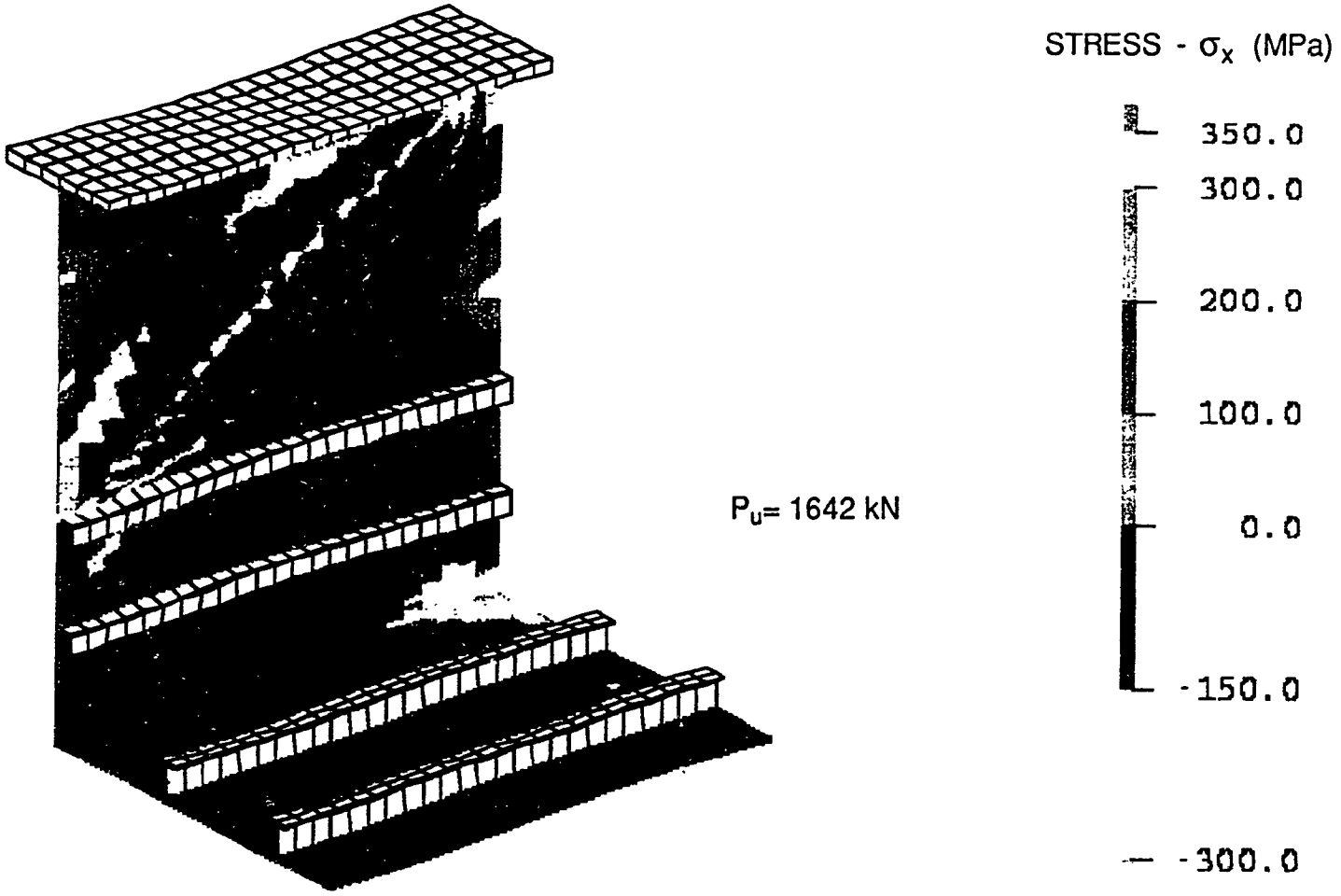

Figure 4.63 Normal Stress Distribution
Box Girder Type A. Web Stiffening Type 3.c.(ii)

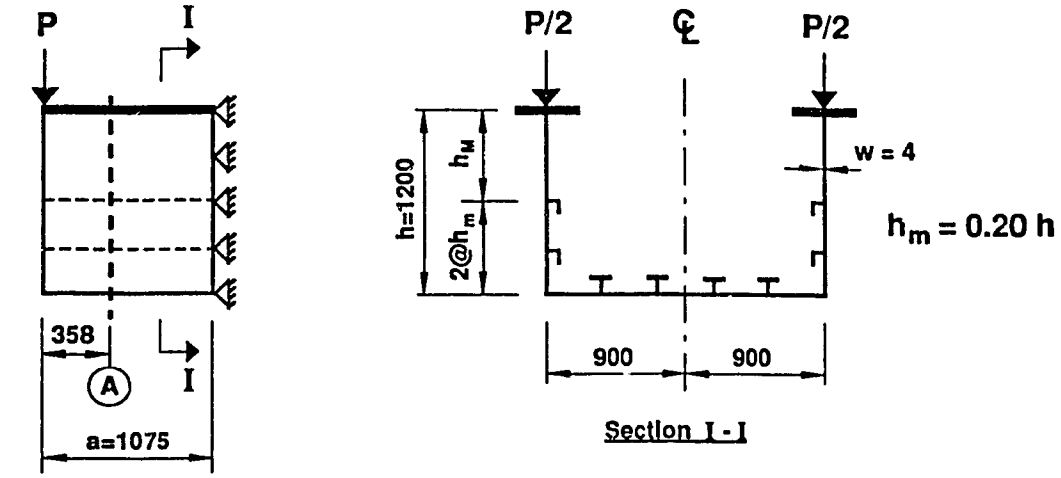

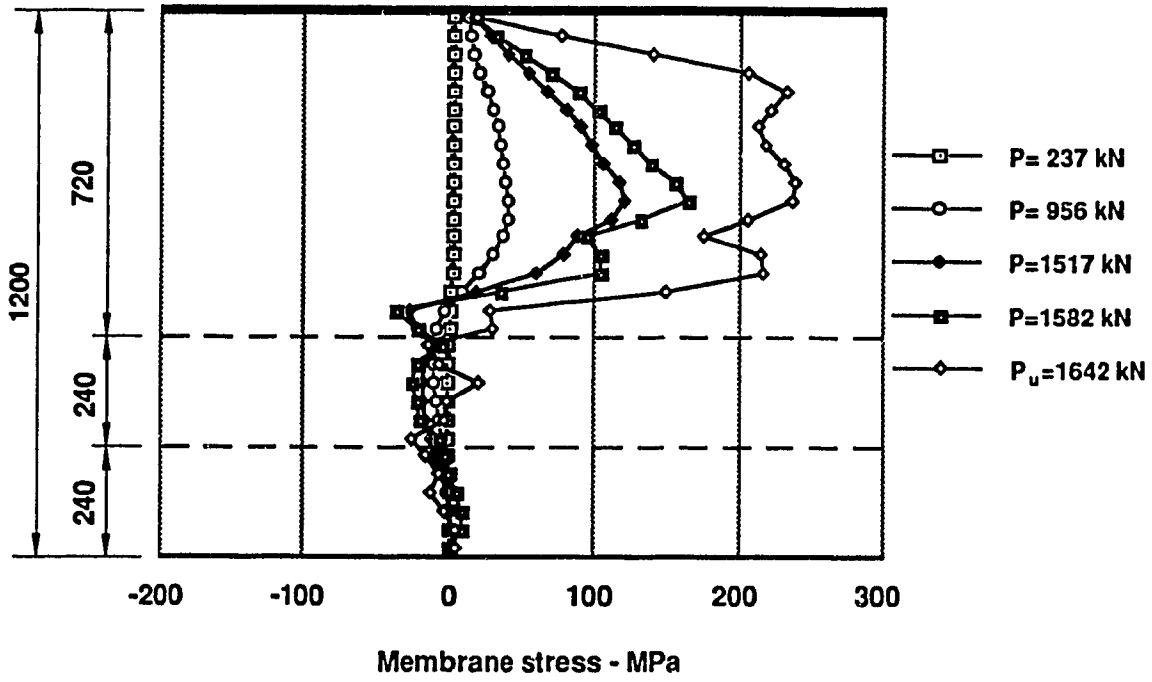

Figure 4.64 Distribution of Membrane Stresses - σ_x in the Web at Section A Box Girder Type A. Web Stiffening Type 3.c.(ii)

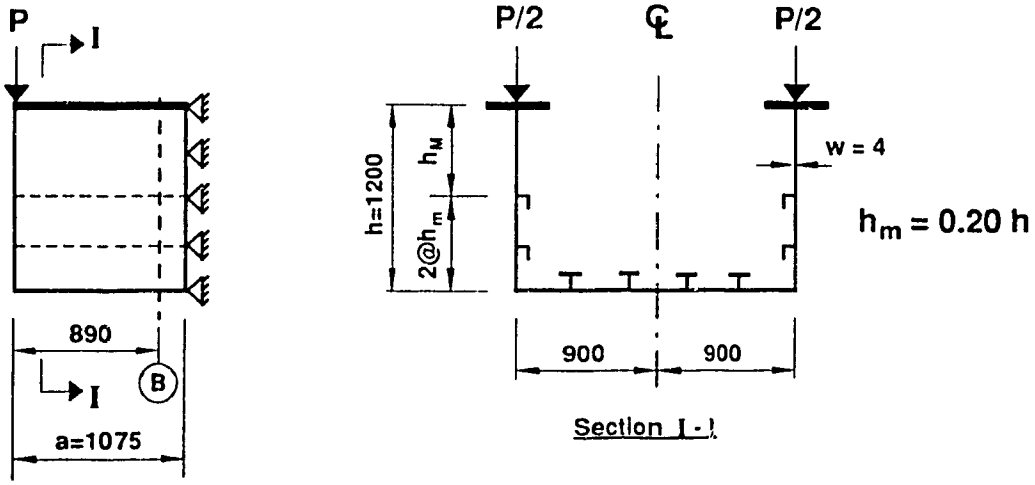

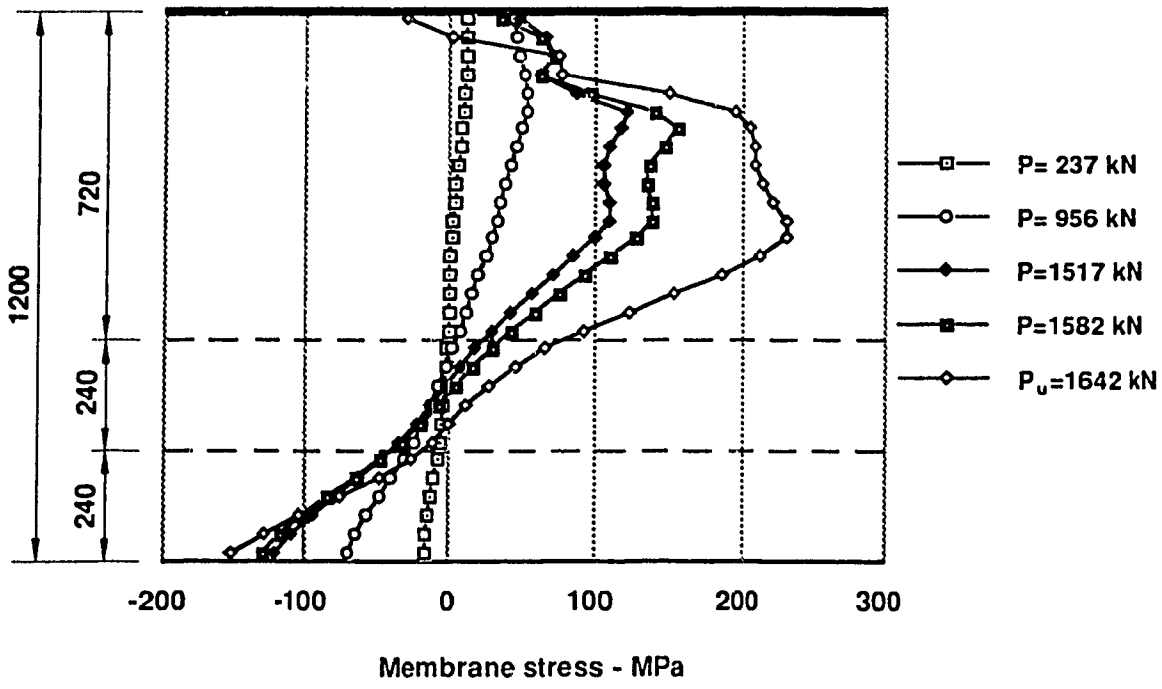

Figure 4.65 Distribution of Membrane Stresses - σ_x in the Web at Section B Box Girder Type A. Web Stiffening Type 3.c.(ii)

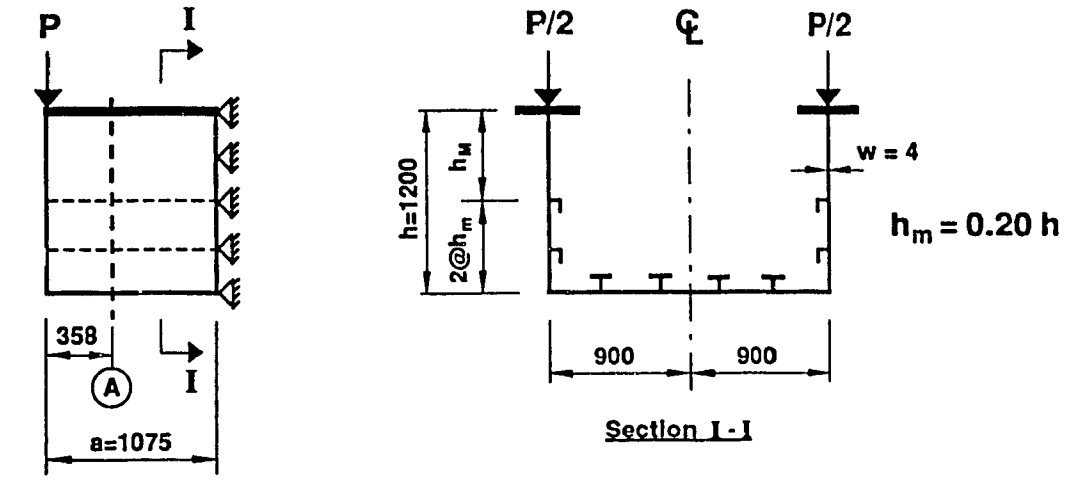

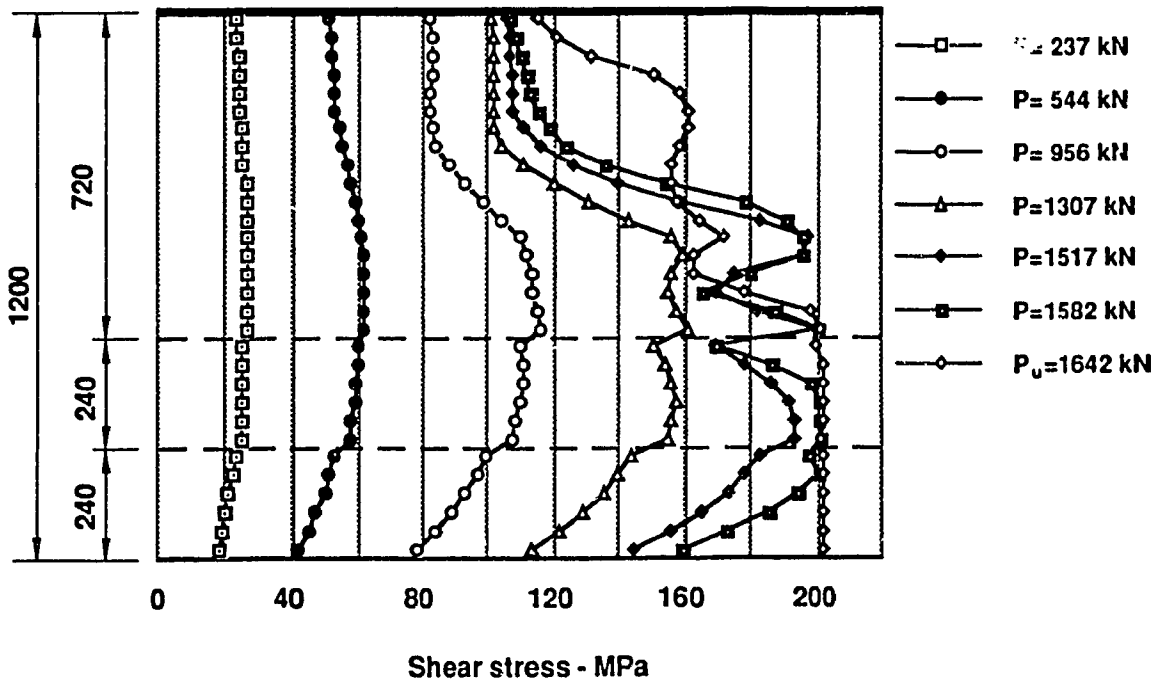

Figure 4.66 Distribution of Shear Stresses in the Web at Section A Box Girder Type A. Web Stiffening Type 3.c.(ii)

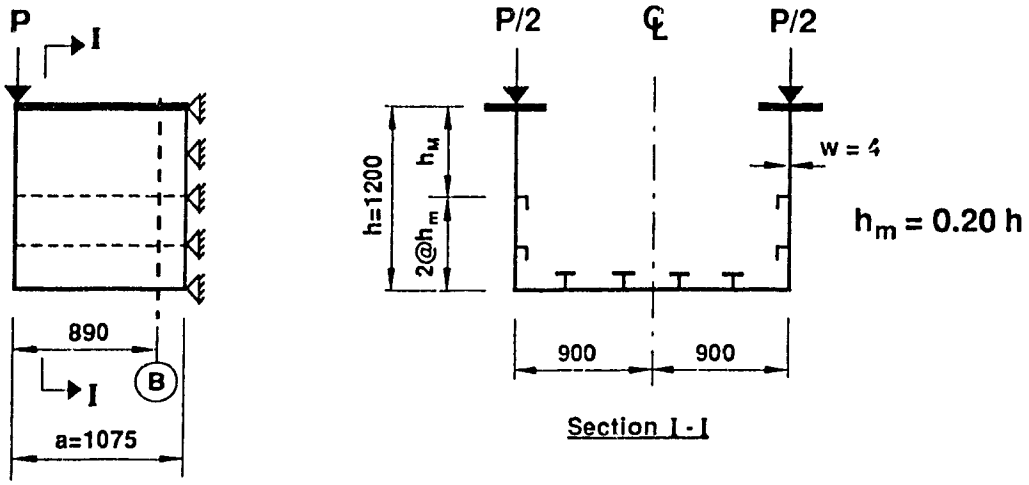

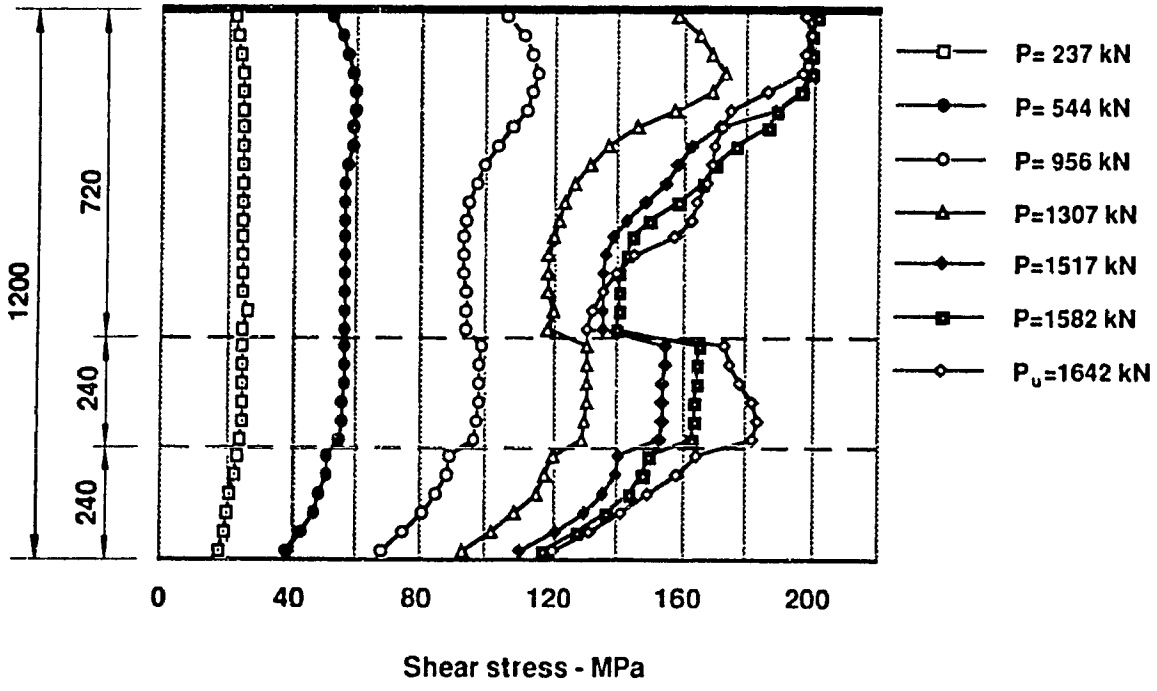

Figure 4.67 Distribution of Shear Stresses in the Web at Section B
Box Girder Type A. Web Stiffening Type 3.c.(ii)

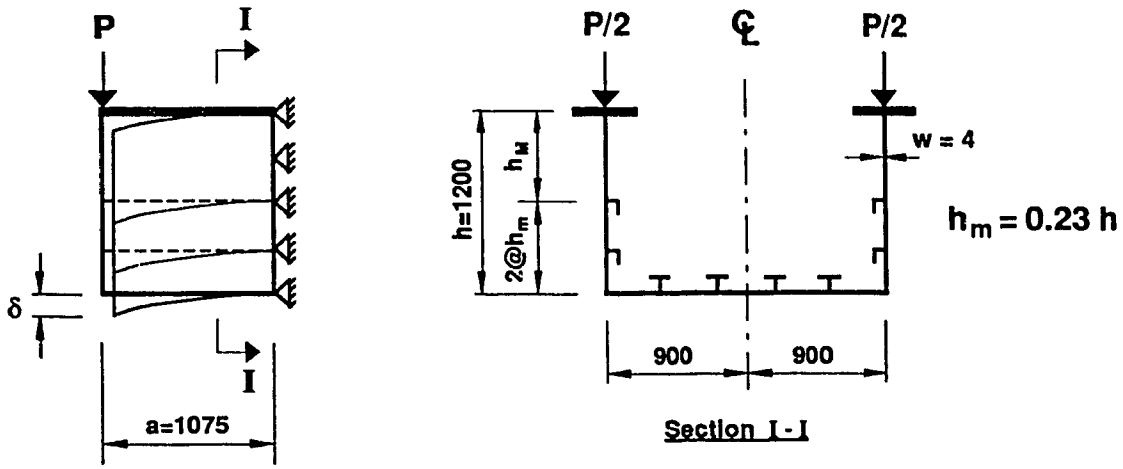

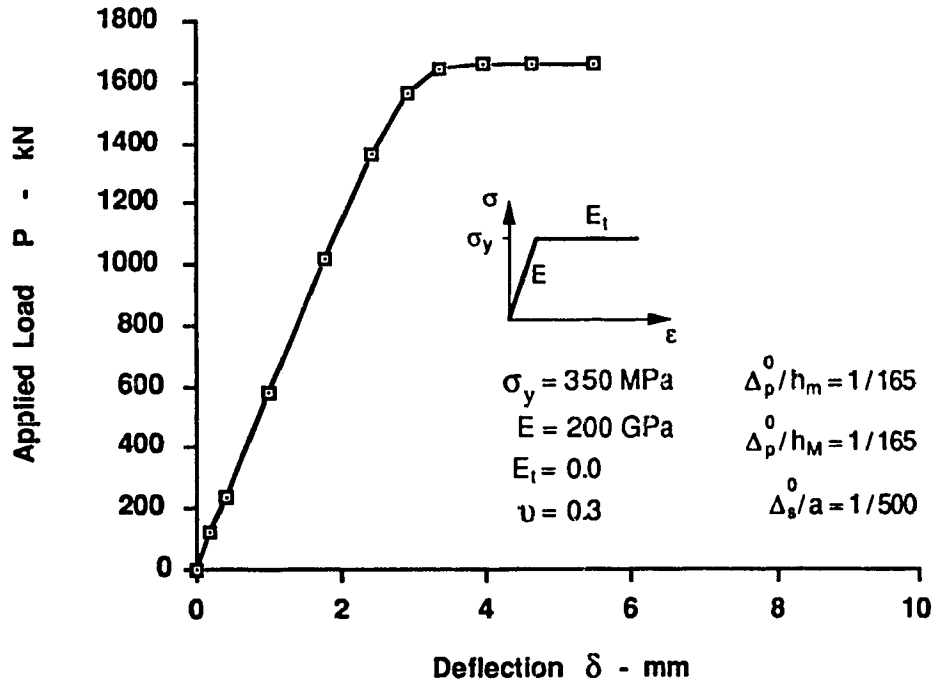

Figure 4.68 Load - Deflection Curve for Box Girder Type A. Web Stiffening Type 3.d.(ii)

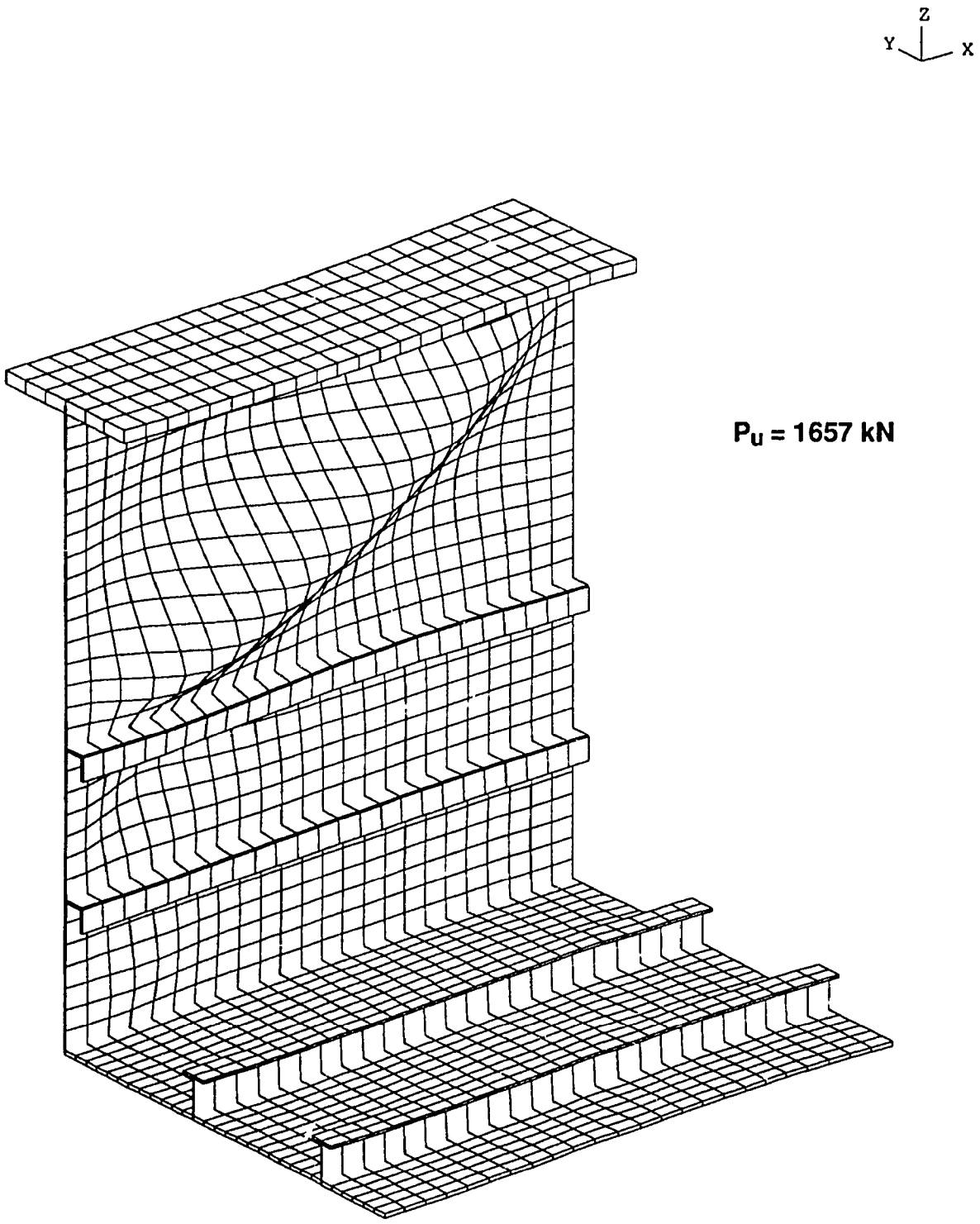

Figure 4.69 Web Buckling of Box Girder Type A.
Web Stiffening Type 3.d.(ii)

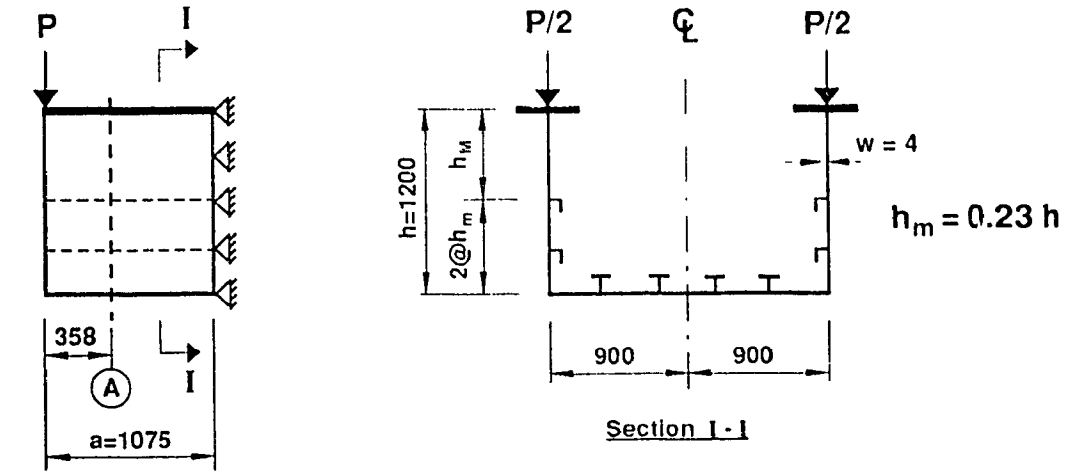

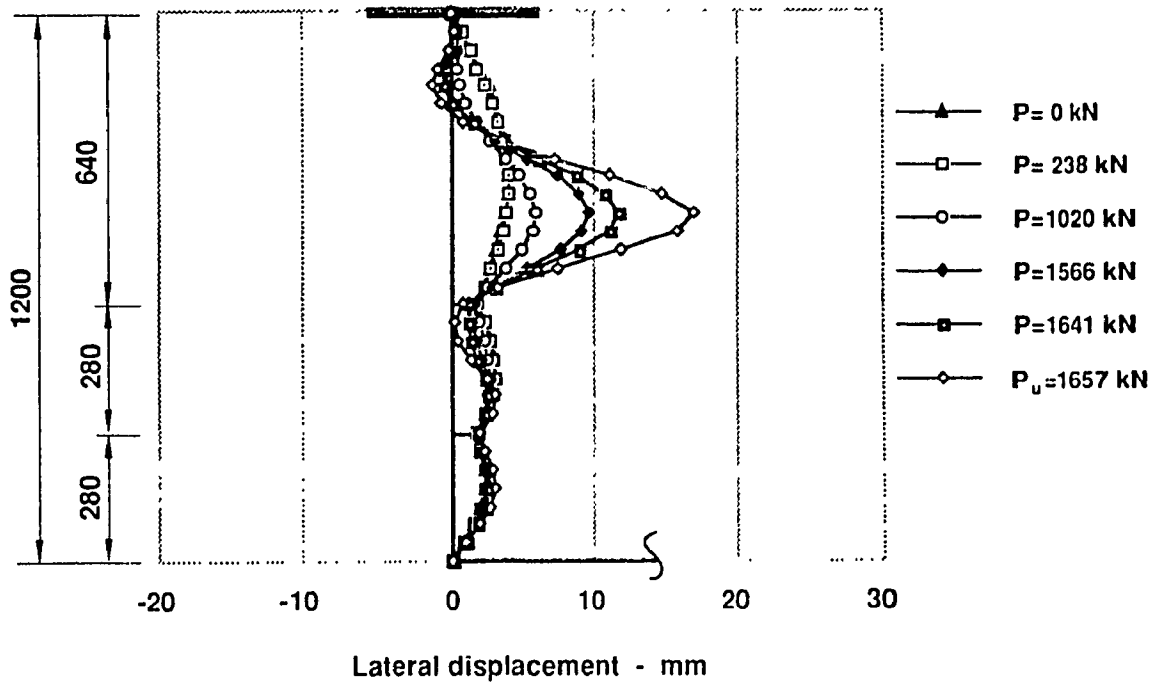

Figure 4.70 Deflection of Web under Loading - Section A
Box Girder Type A. Web Stiffening Type 3.d.(ii)

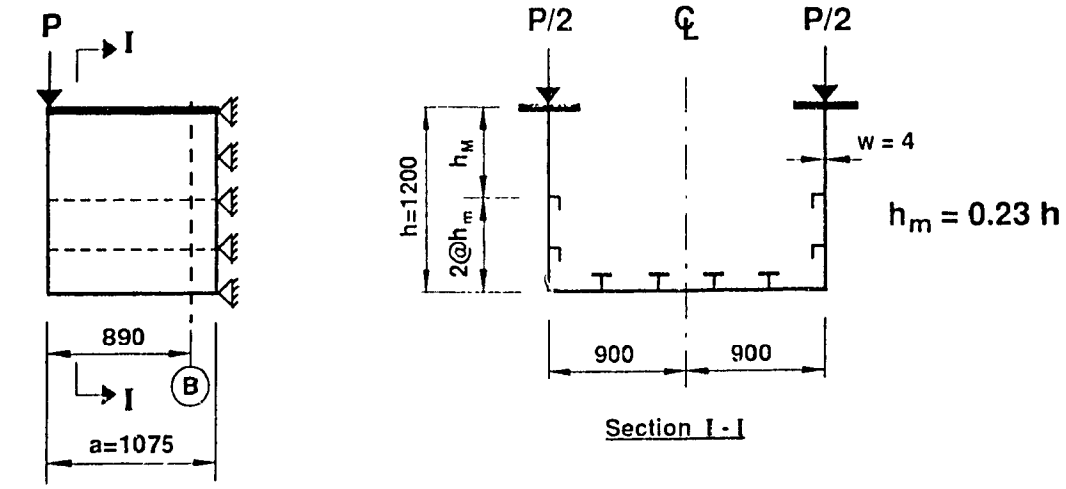

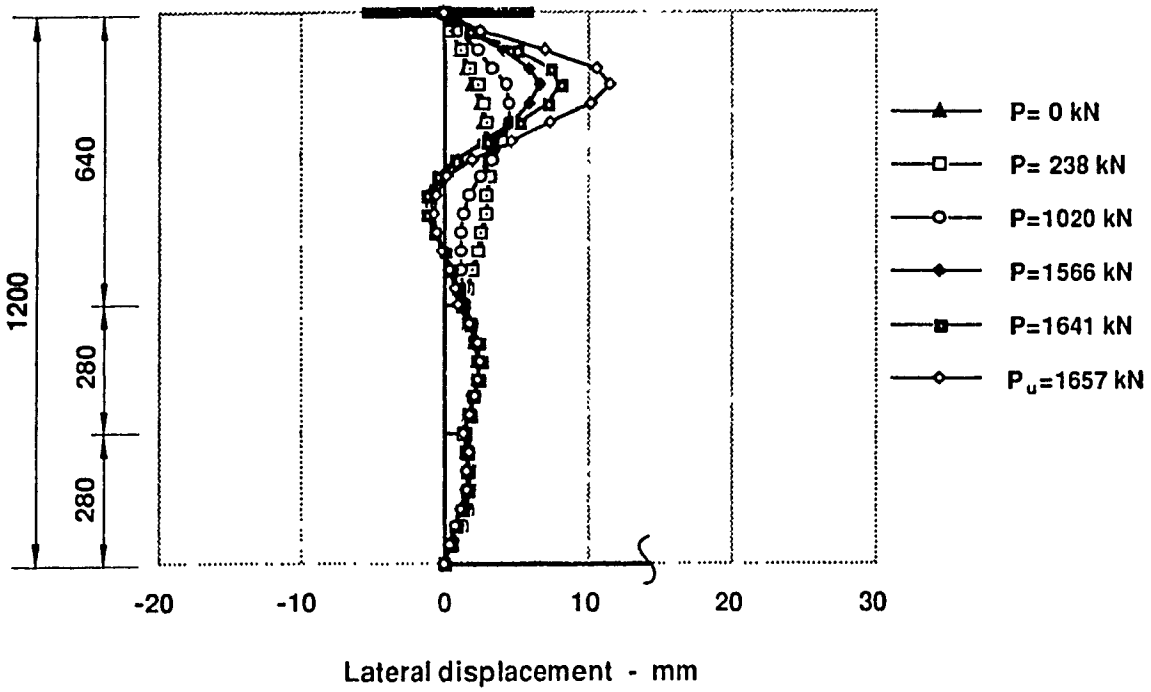

Figure 4.71 Deflection of Web under Loading - Section B
Box Girder Type A. Web Stiffening Type 3.d.(ii)

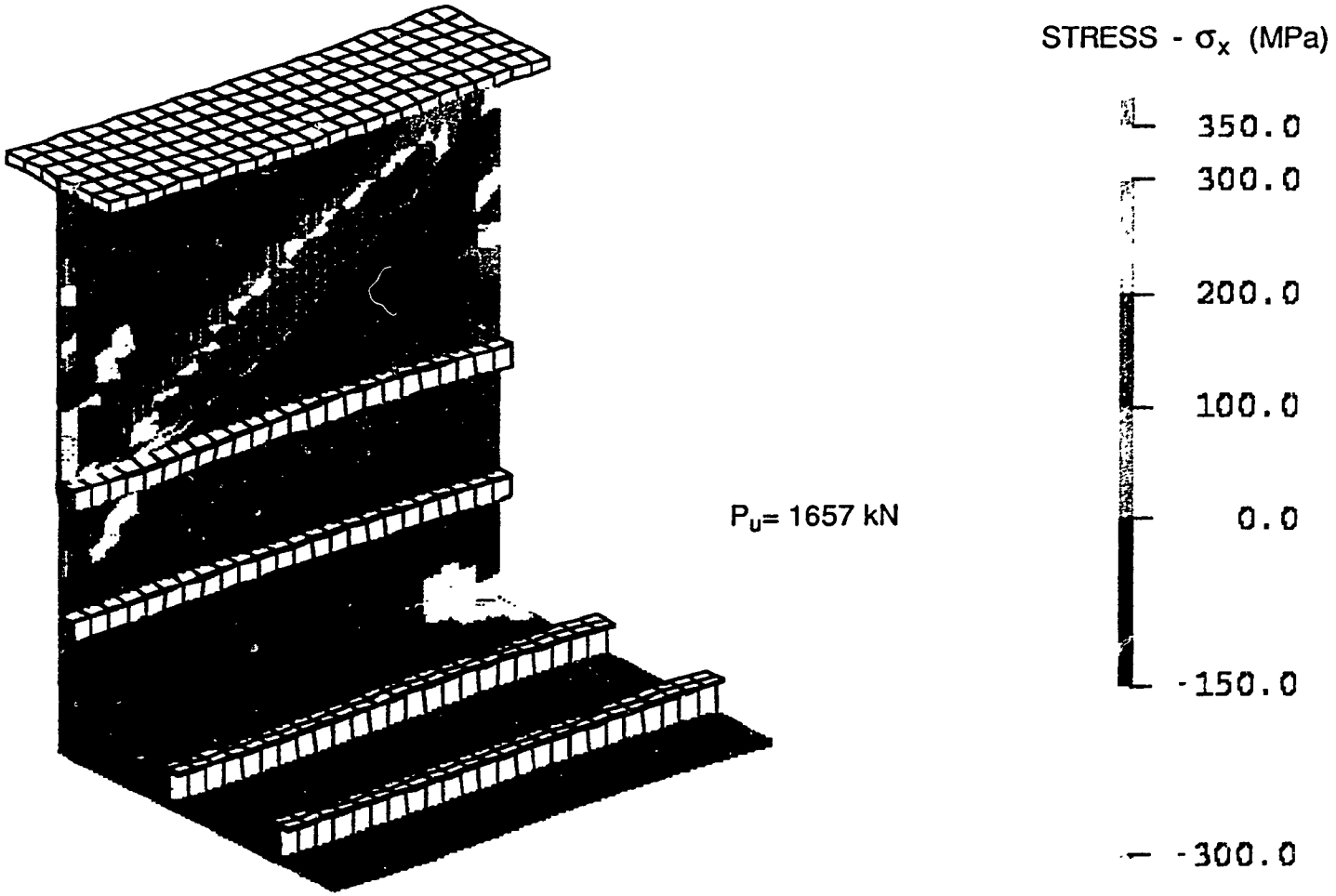

Figure 4.72 Normal Stress Distribution
Box Girder Type A. Web Stiffening Type 3.d.(ii)

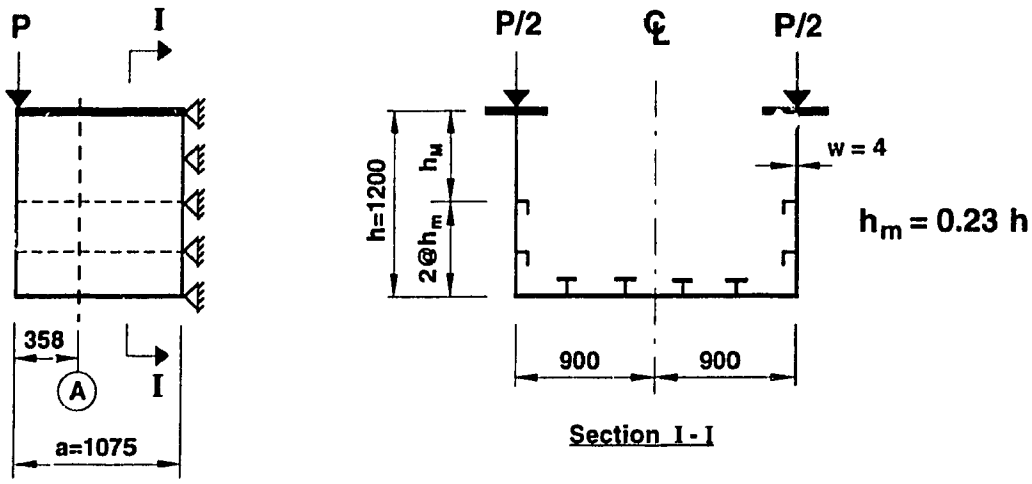

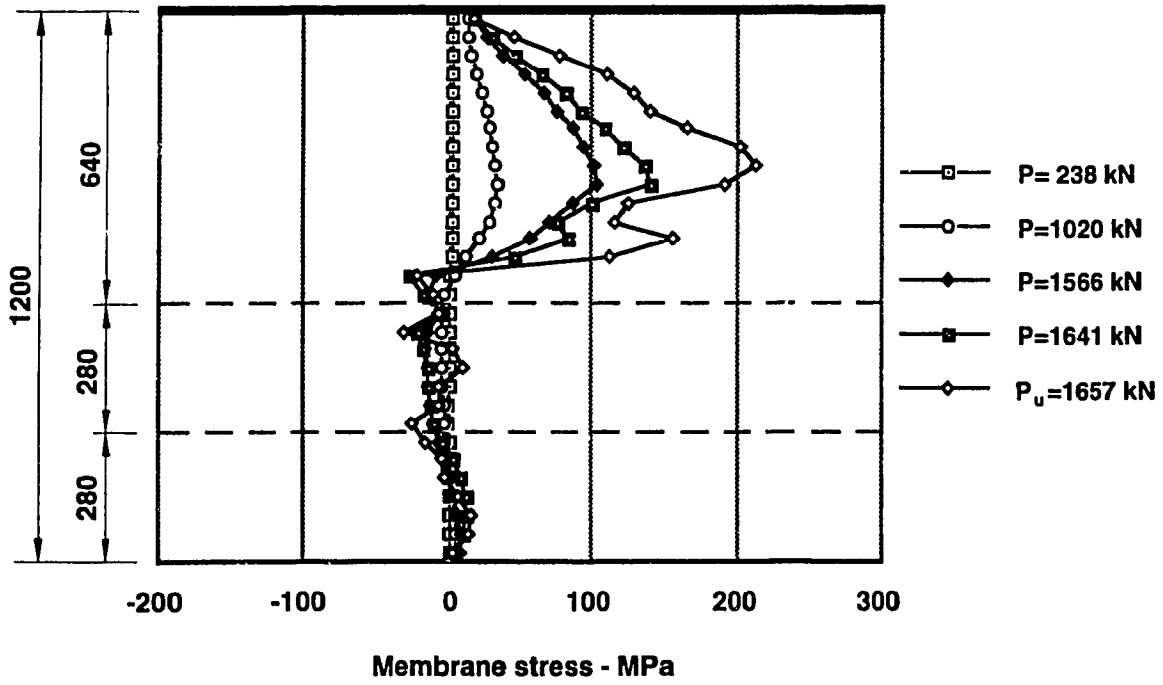

Figure 4.73 Distribution of Membrane Stresses - σ_x in the Web at Section A Box Girder Type A. Web Stiffening Type 3.d.(ii)

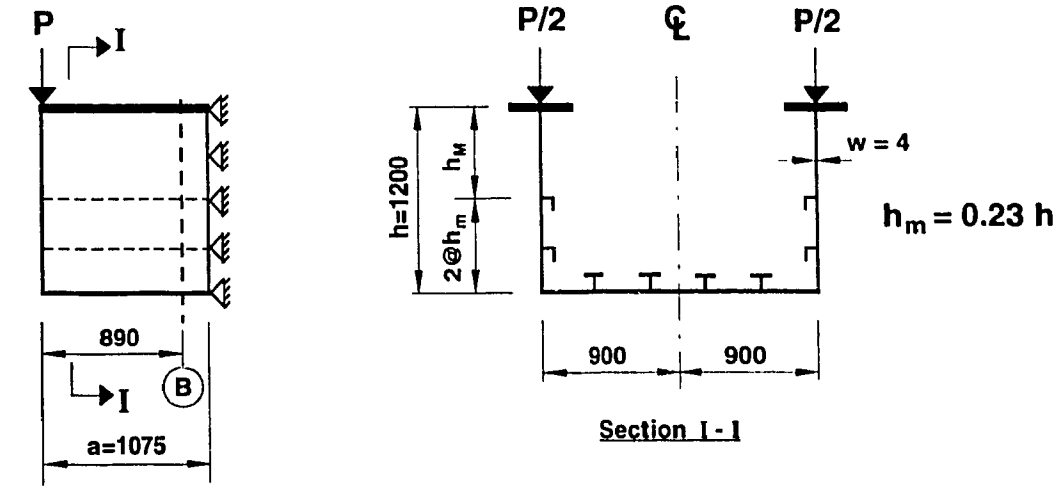

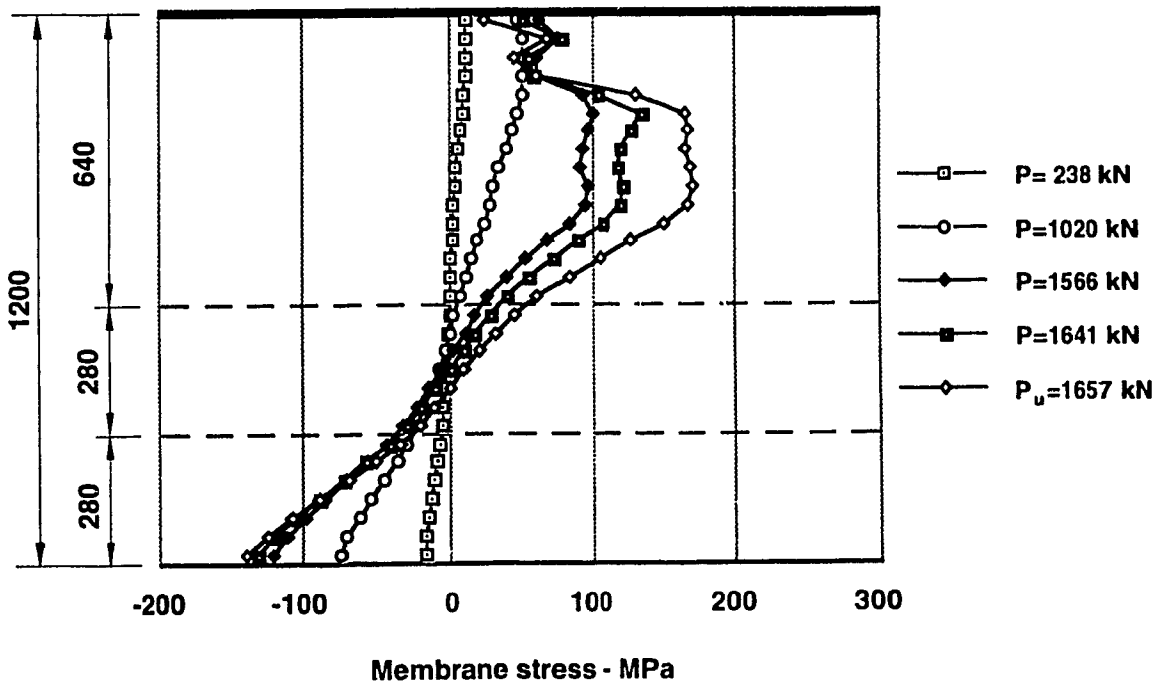

Figure 4.74 Distribution of Membrane Stresses - σ_x in the Web at Section B Box Girder Type A. Web Stiffening Type 3.d.(ii)

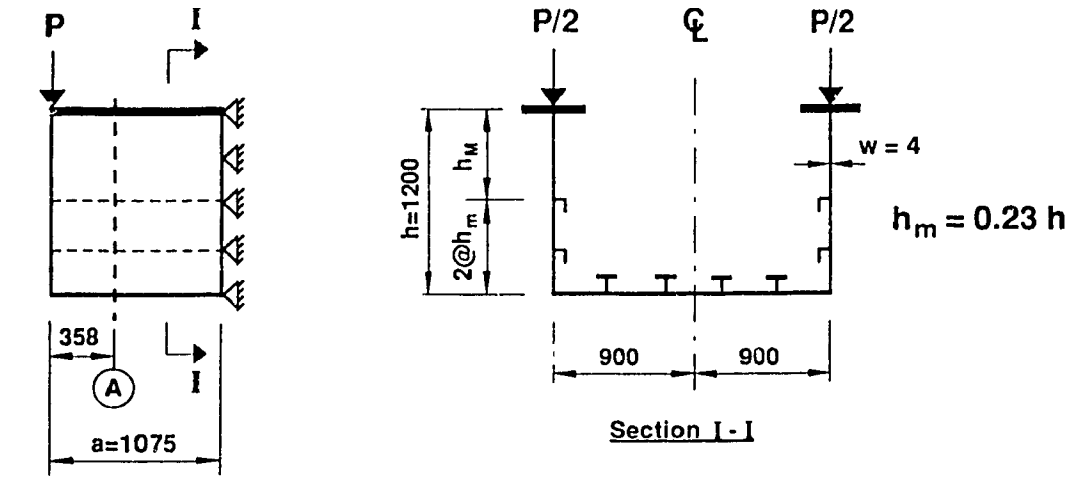

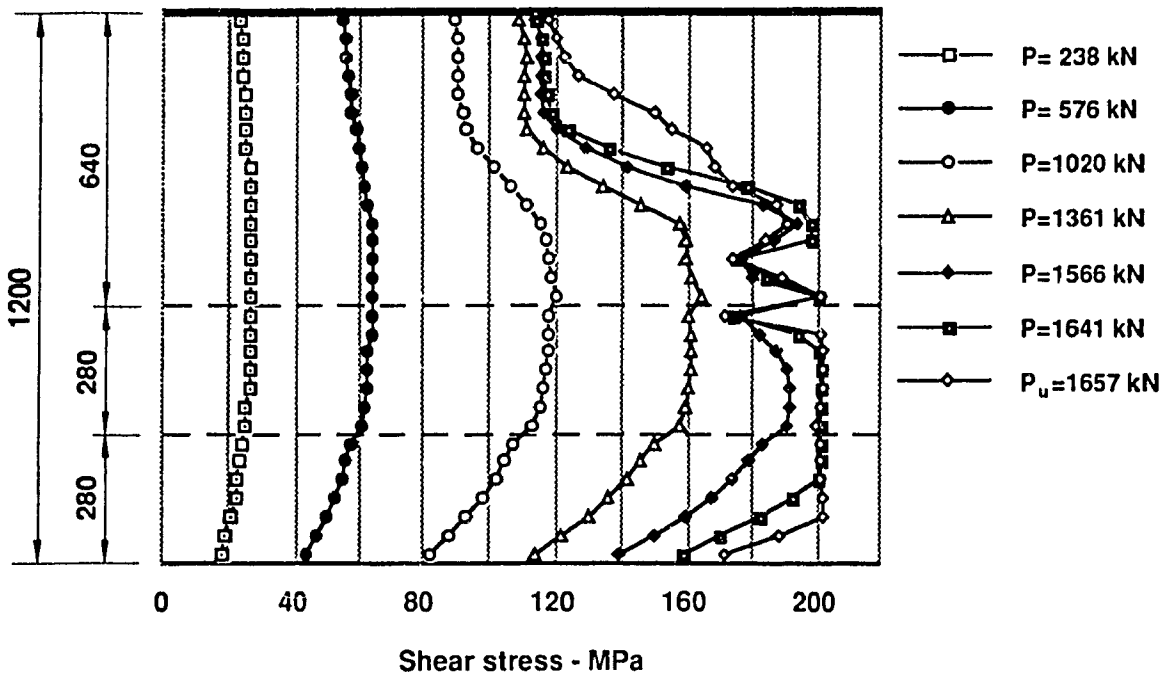

Figure 4.75 Distribution of Shear Stresses in the Web at Section A Box Girder Type A. Web Stiffening Type 3.d.(ii)

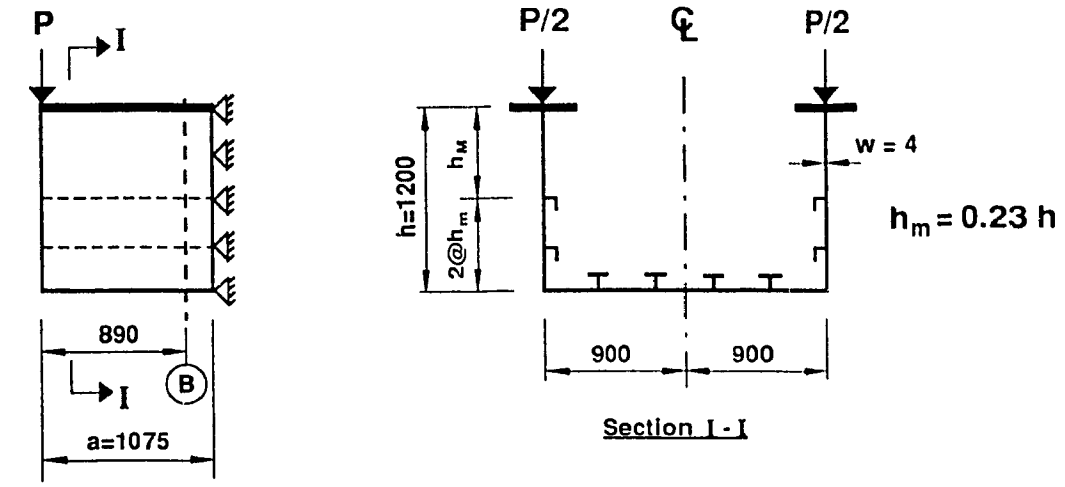

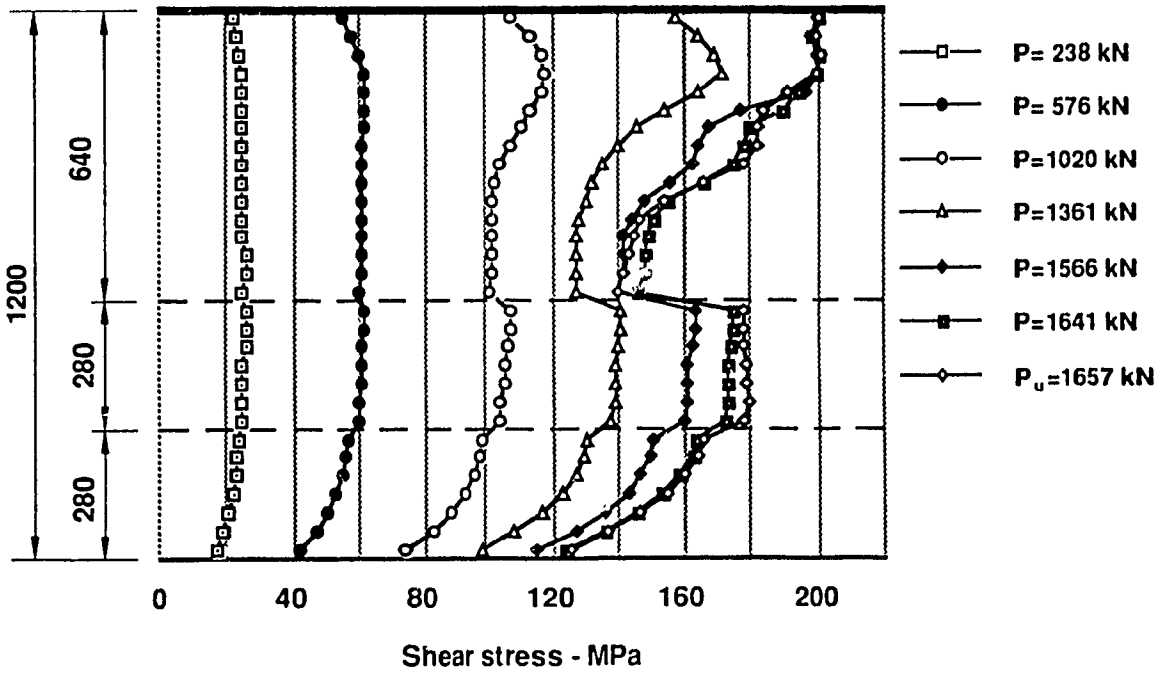

Figure 4.76 Distribution of Shear Stresses in the Web at Section B Box Girder Type A. Web Stiffening Type 3.d.(ii)

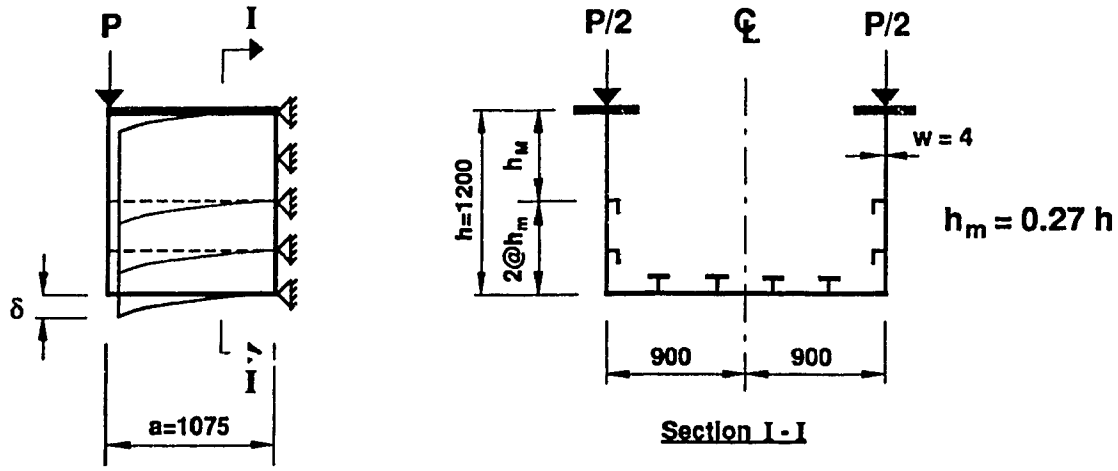

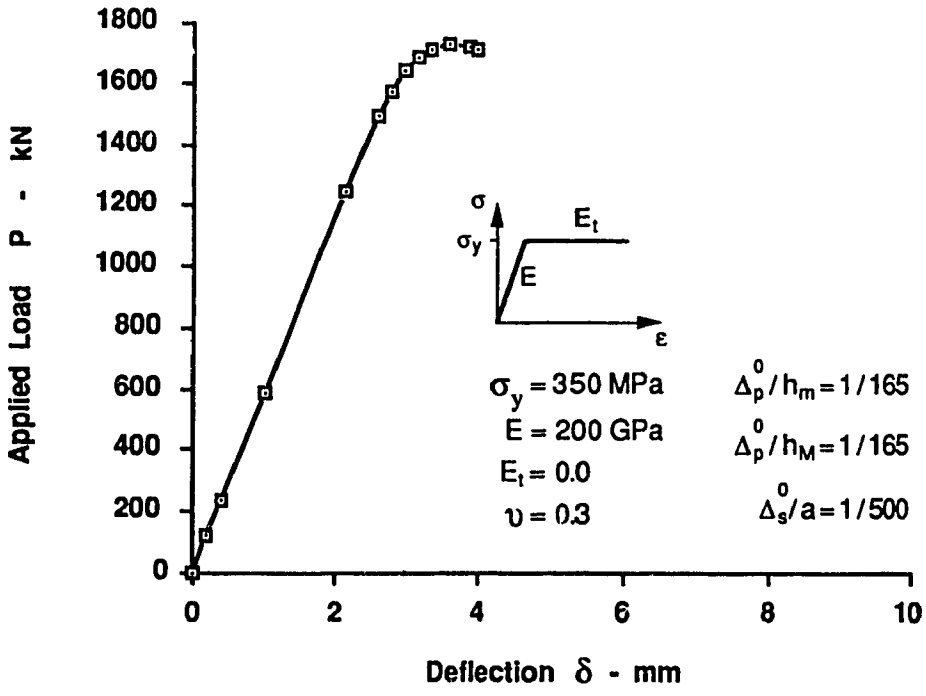

Figure 4.77 Load - Deflection Curve for Box Girder Type A. Web Stiffening Type 3.e.(ii)

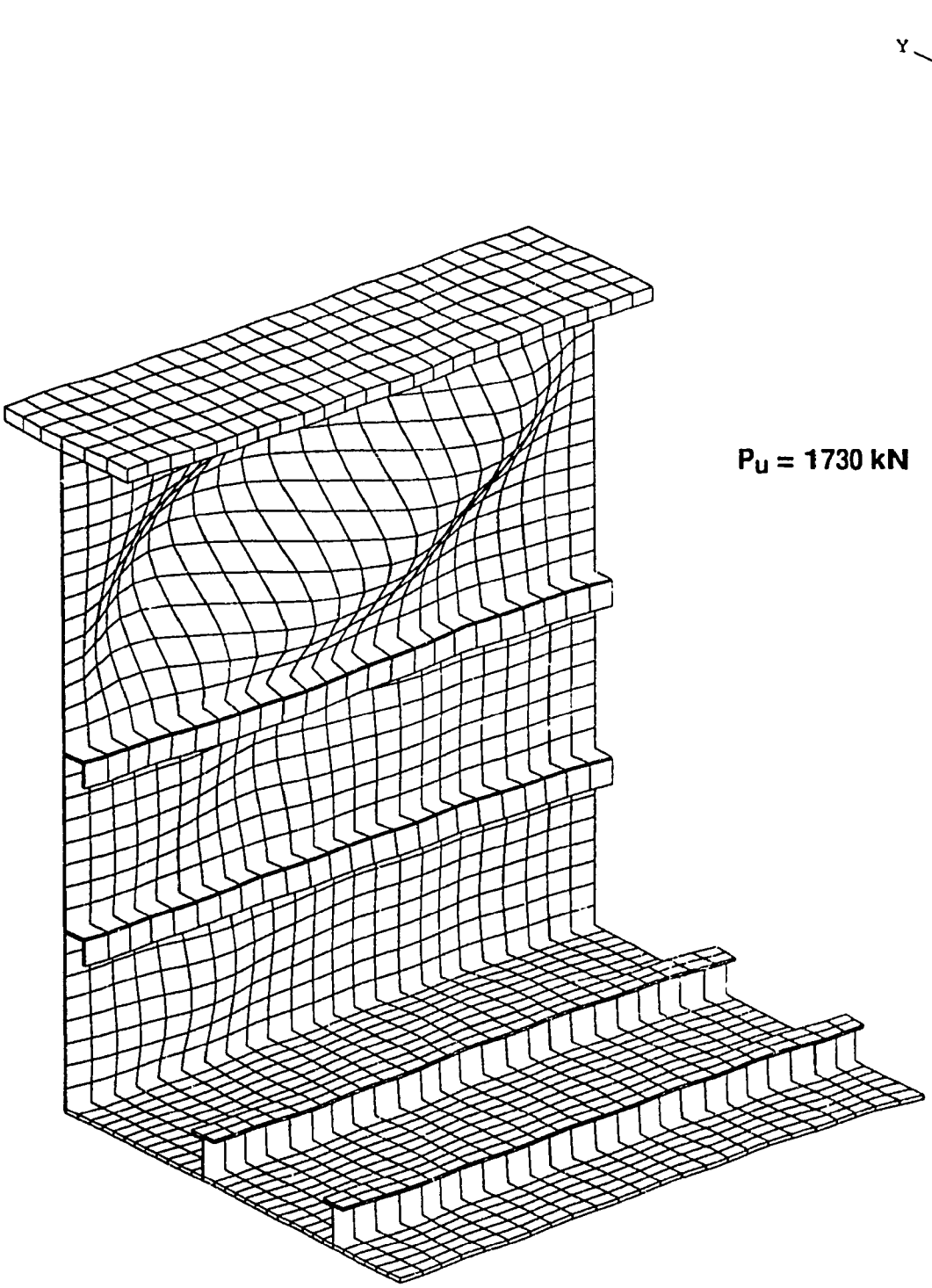

Figure 4.78 Web Buckling of Box Girder Type A.
Web Stiffening Type 3.e.(ii)

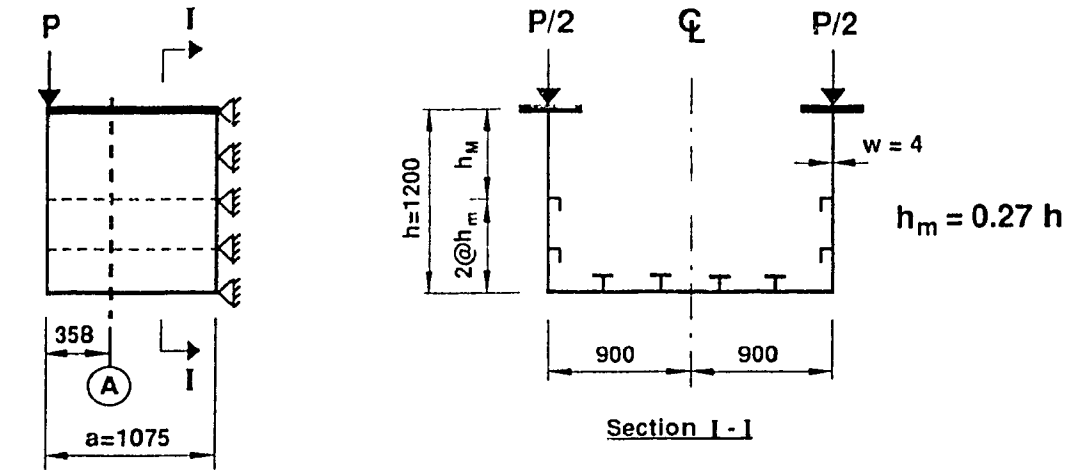

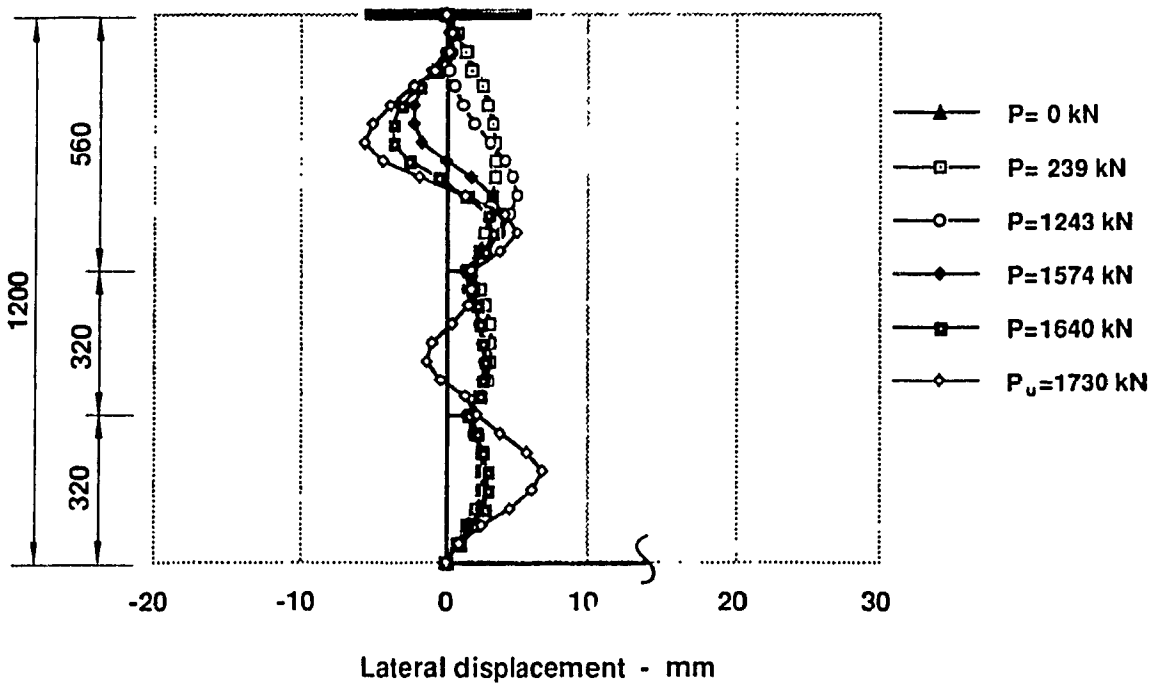

Figure 4.79 Deflection of Web under Loading - Section A
Box Girder Type A Web Stiffening Type 3.e.(ii)

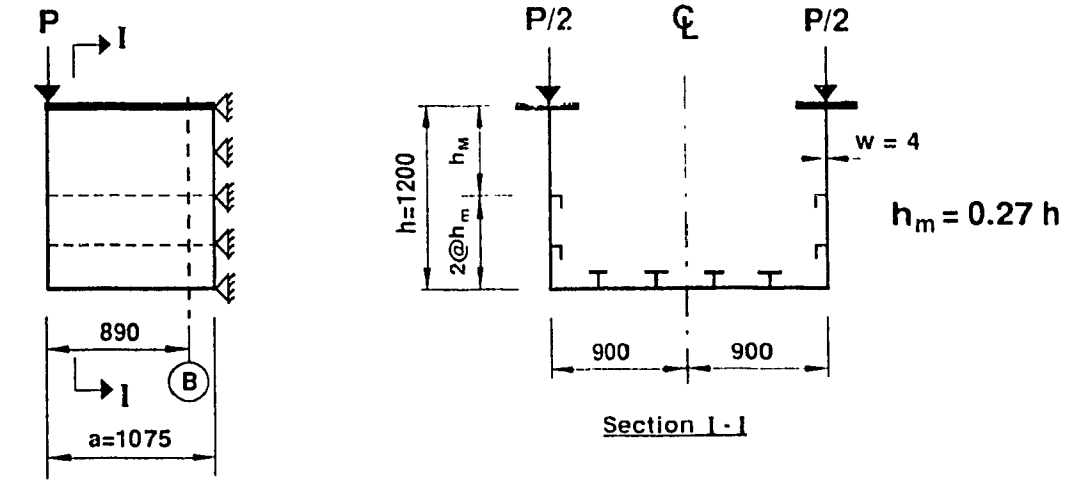

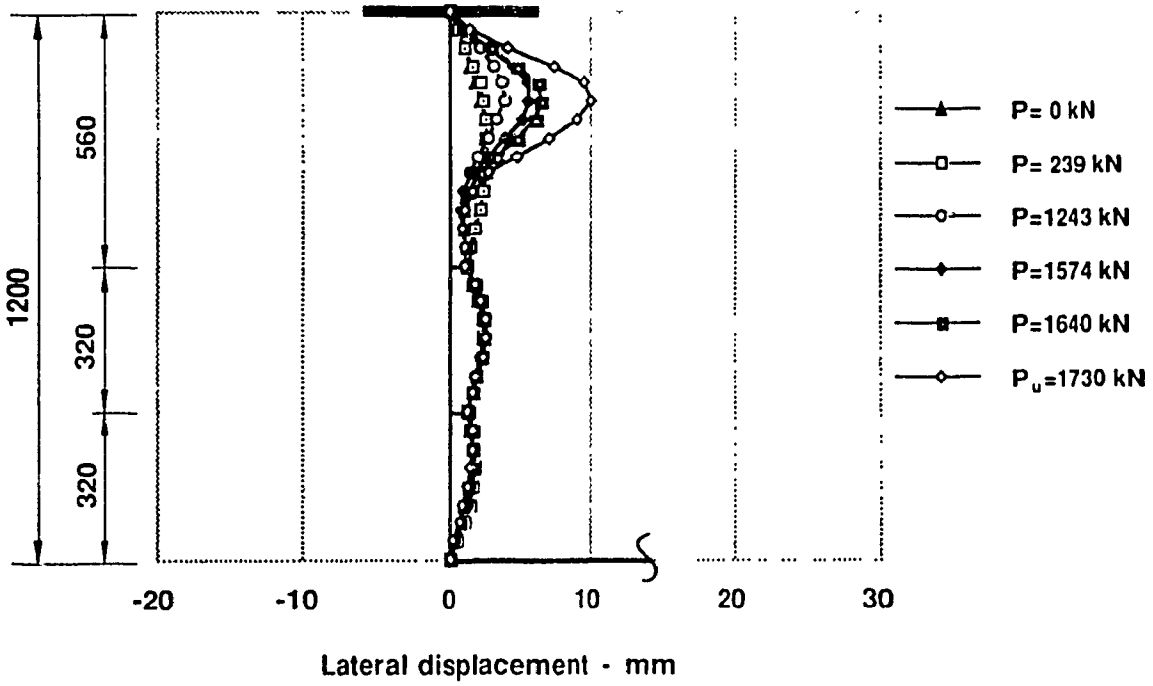

Figure 4.80 Deflection of Web under Loading - Section B
Box Girder Type A. Web Stiffening Type 3.e.(ii)

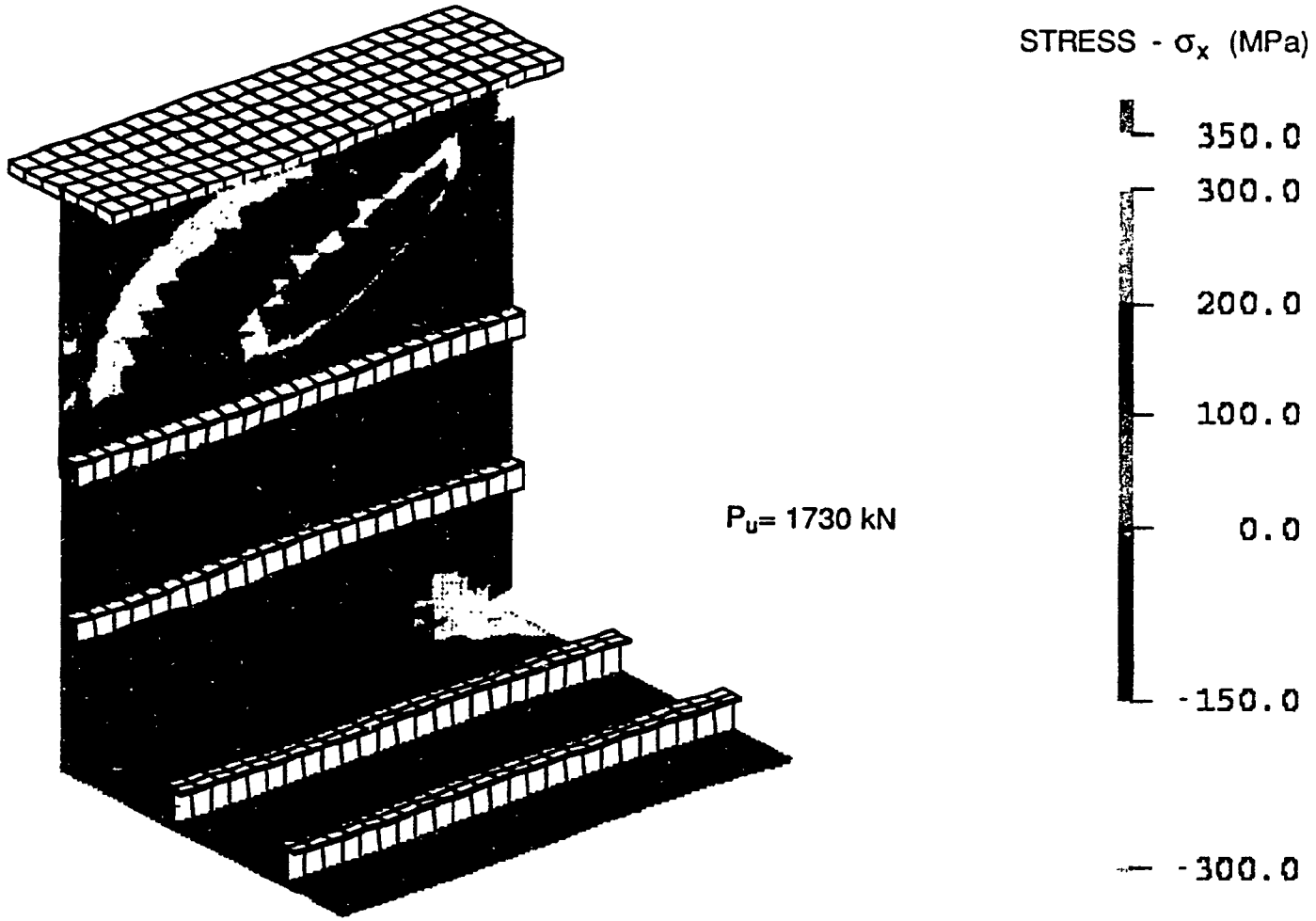

Figure 4.81 Normal Stress Distribution
Box Girder Type A. Web Stiffening Type 3.e.(ii)

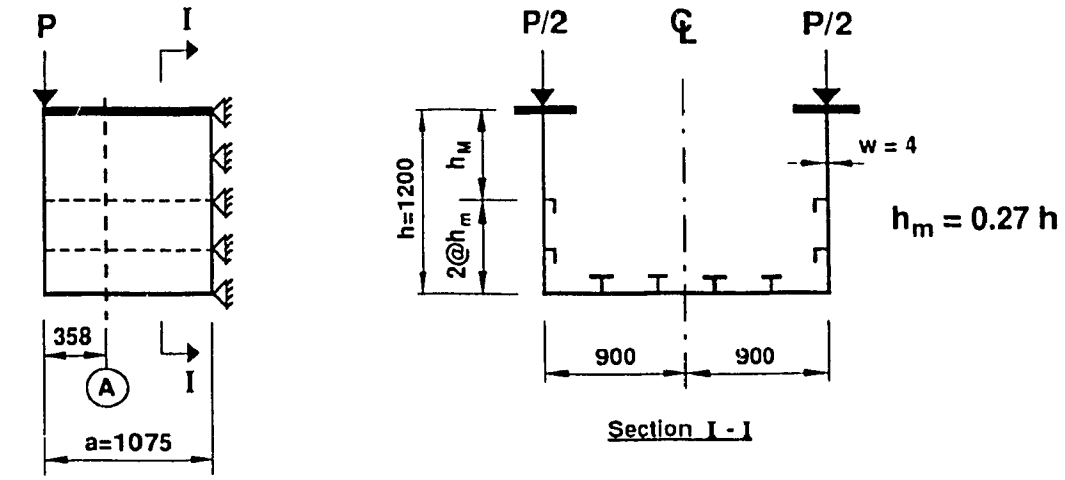

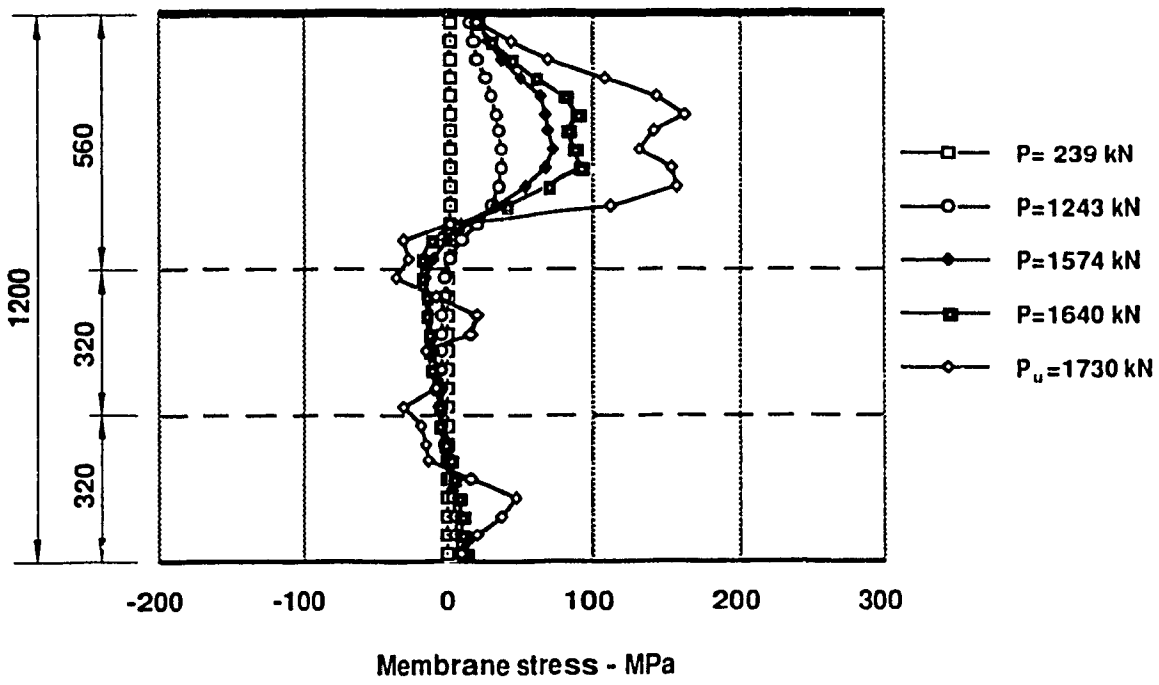

Figure 4.82 Distribution of Membrane Stresses - σ_x in the Web at Section A Box Girder Type A. Web Stiffening Type 3.e.(ii)

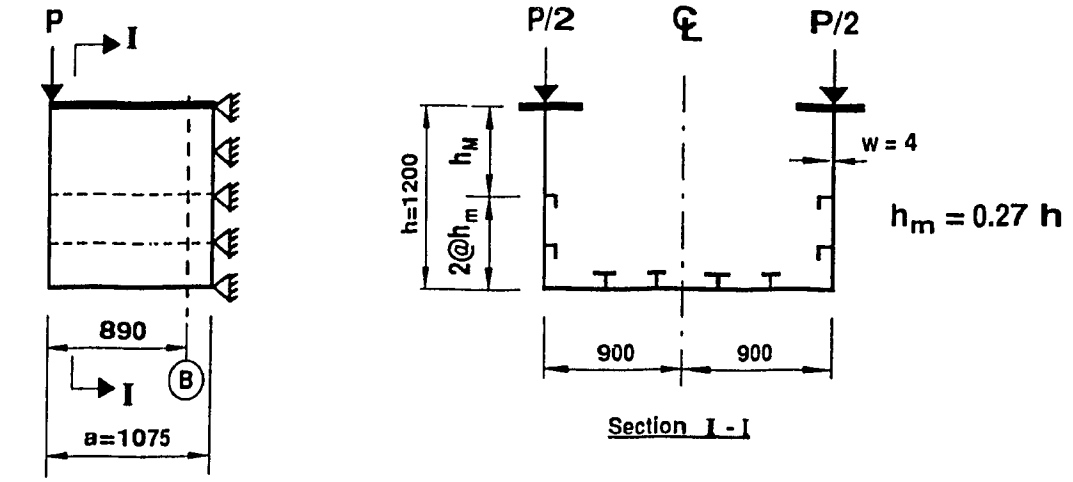

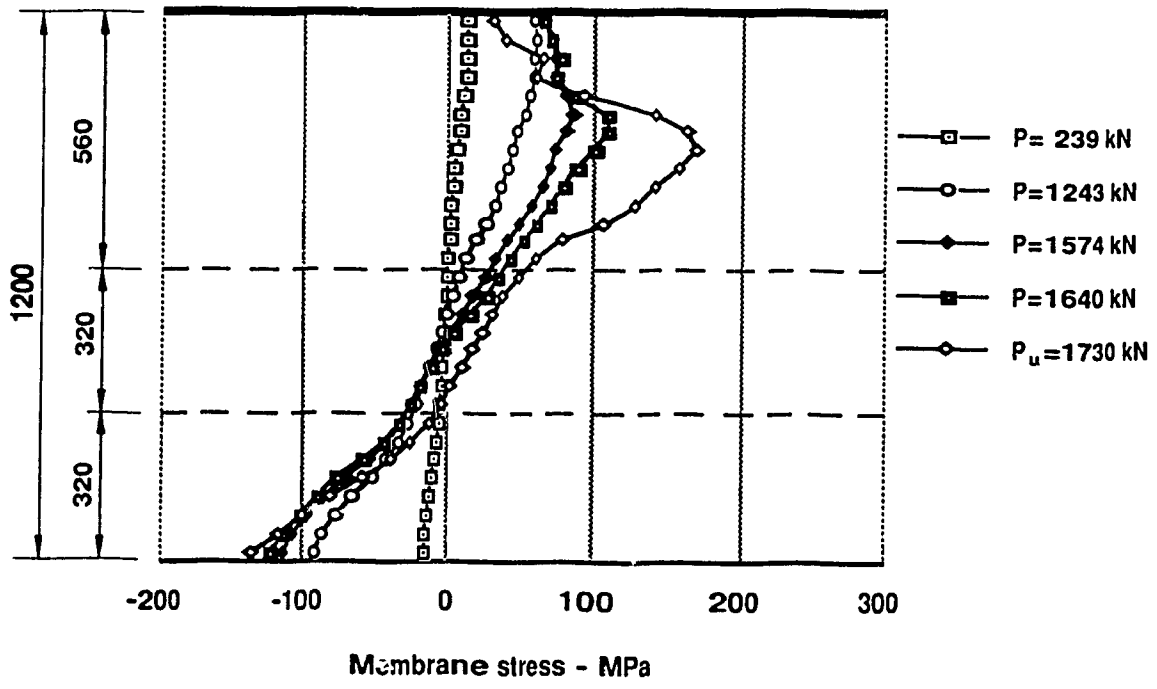

Figure 4.83 Distribution of Membrane Stresses - σ_x in the Web at Section B Box Girder Type A. Web Stiffening Type 3.e.(ii)

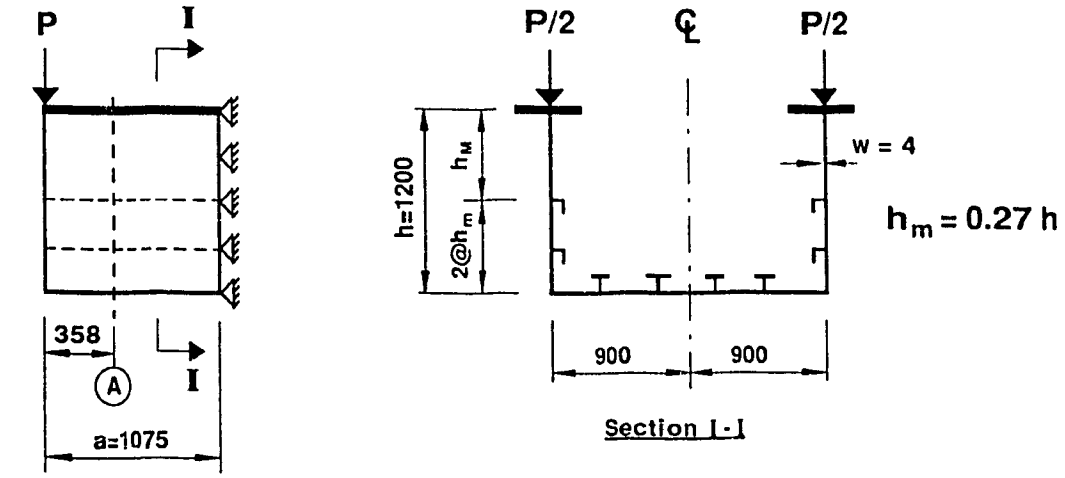

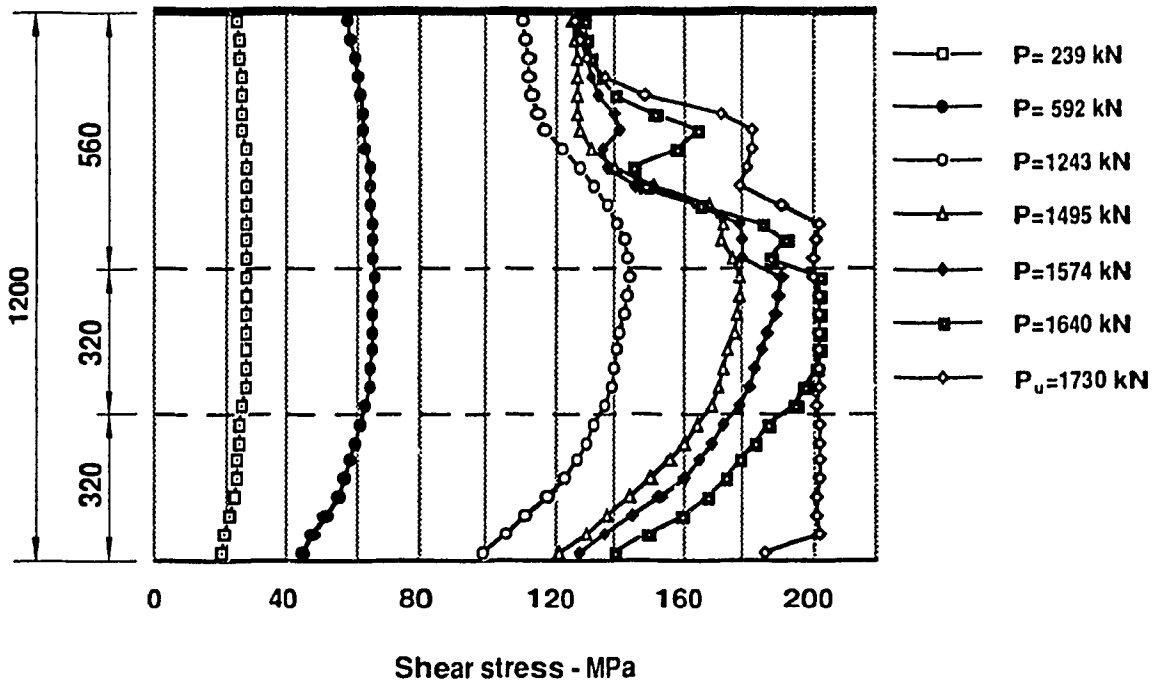

Figure 4.84 Distribution of Shear Stresses in the Web at Section A Box Girder Type A. Web Stiffening Type 3.e.(ii)

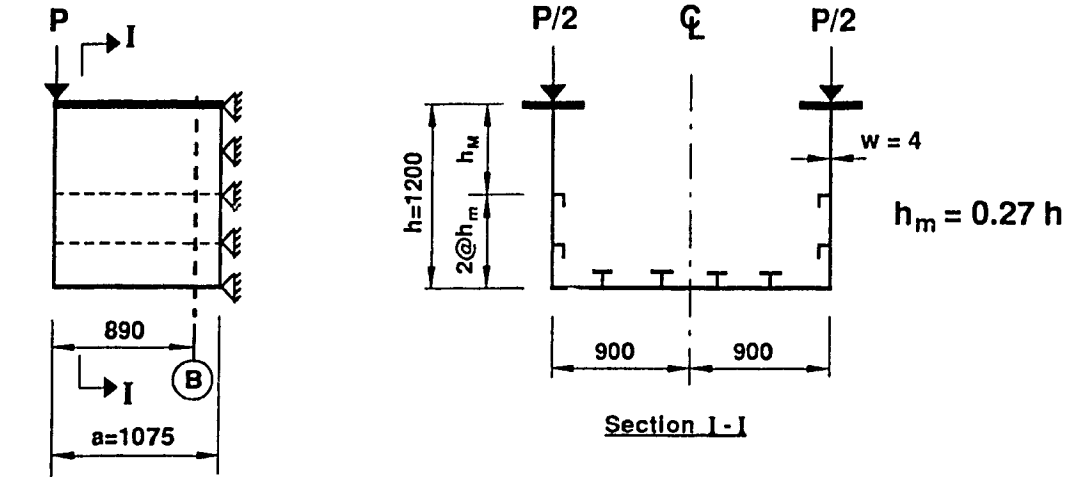

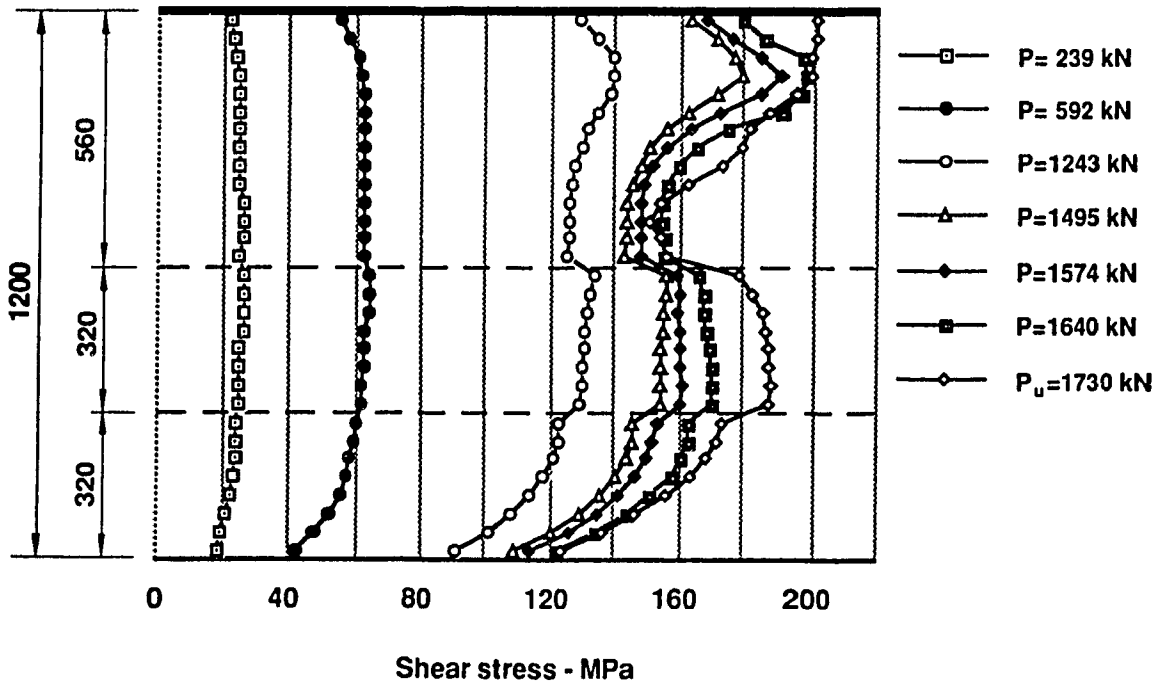

Figure 4.85 Distribution of Shear Stresses in the Web at Section B
Box Girder Type A. Web Stiffening Type 3.e.(ii)

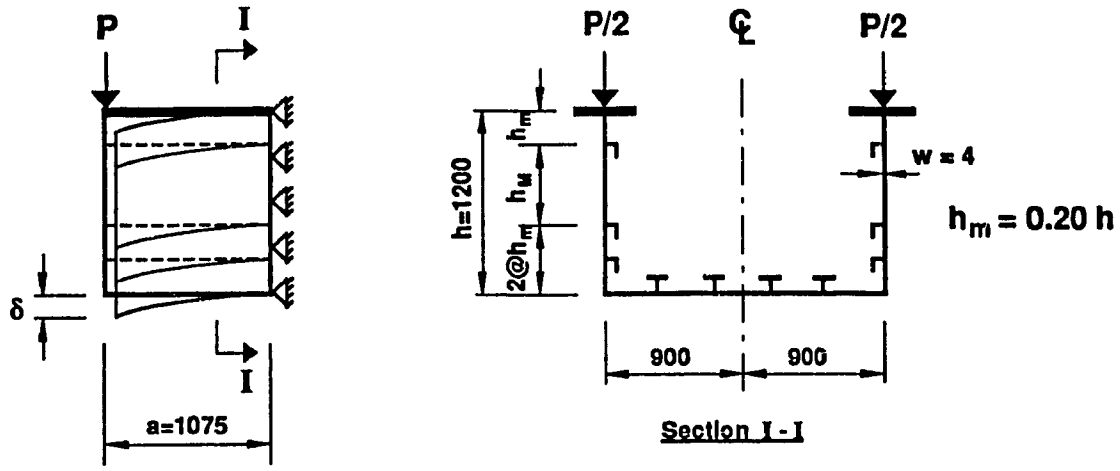

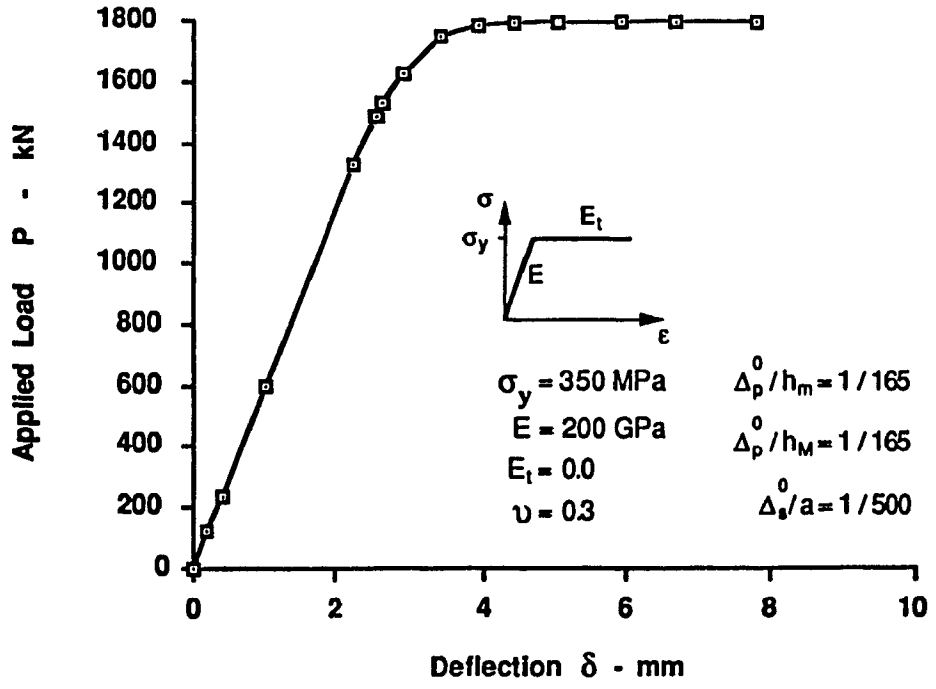

Figure 4.86 Load - Deflection Curve for Box Girder Type A. Web Stiffening Type 4.(ii)

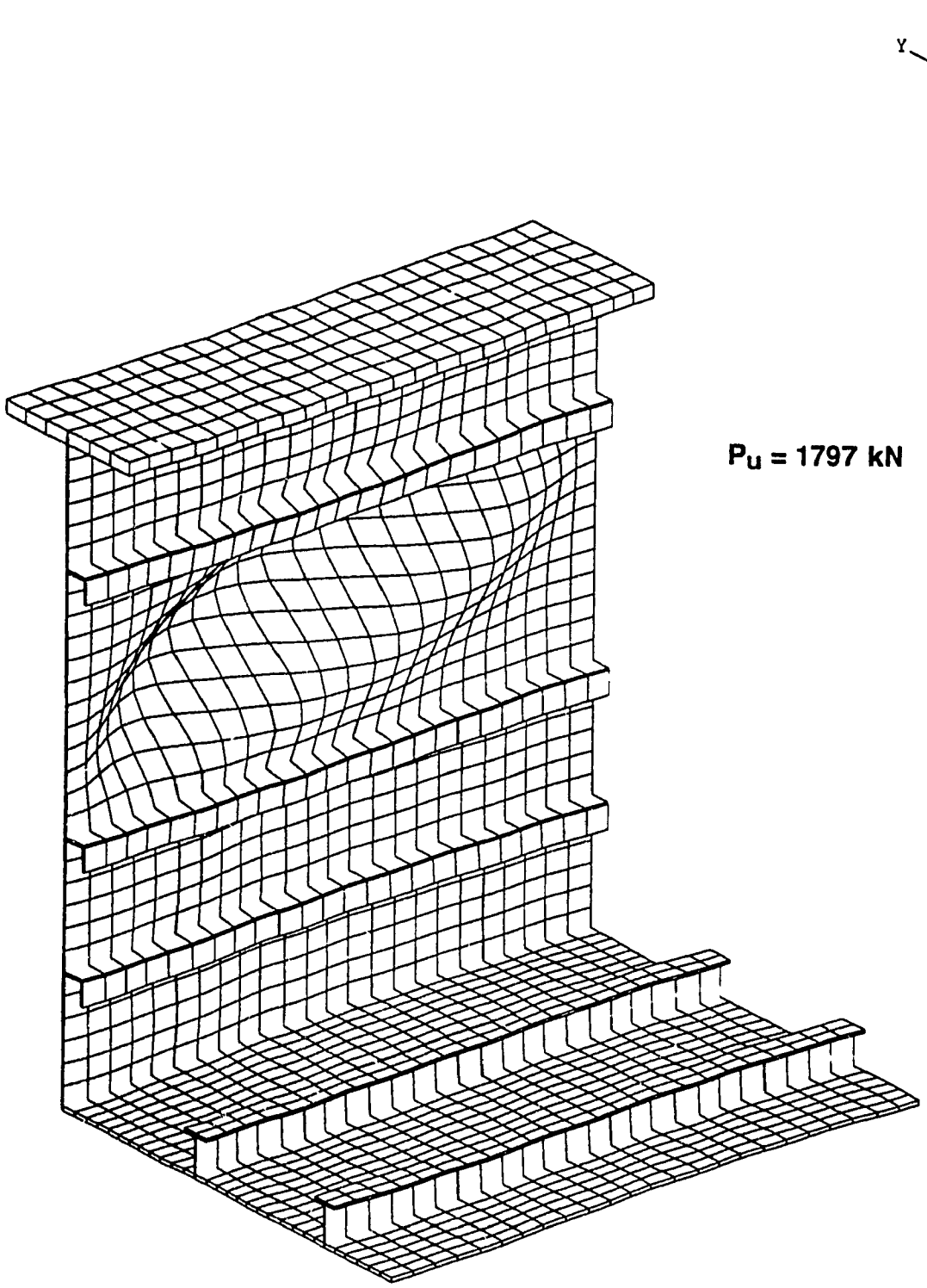

Figure 4.87 Web Buckling of Box Girder Type A.
Web Stiffening Type 4.(ii)

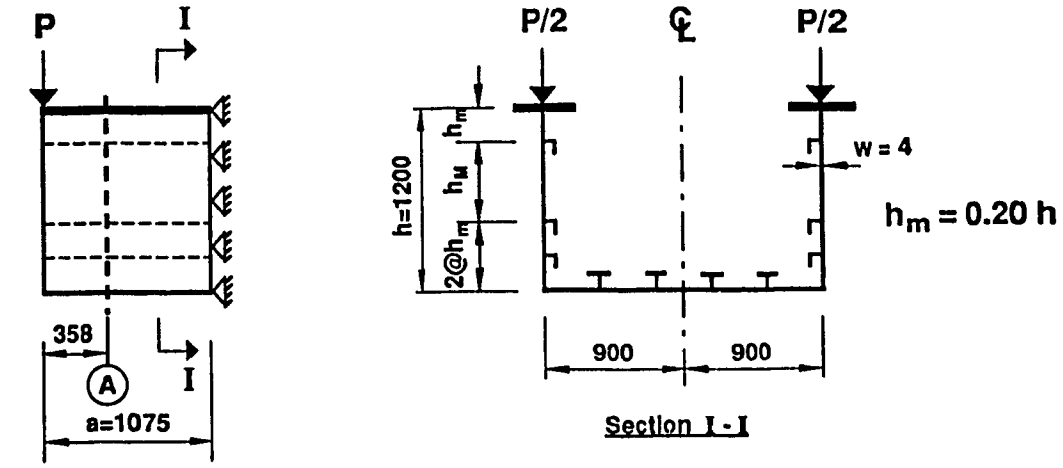

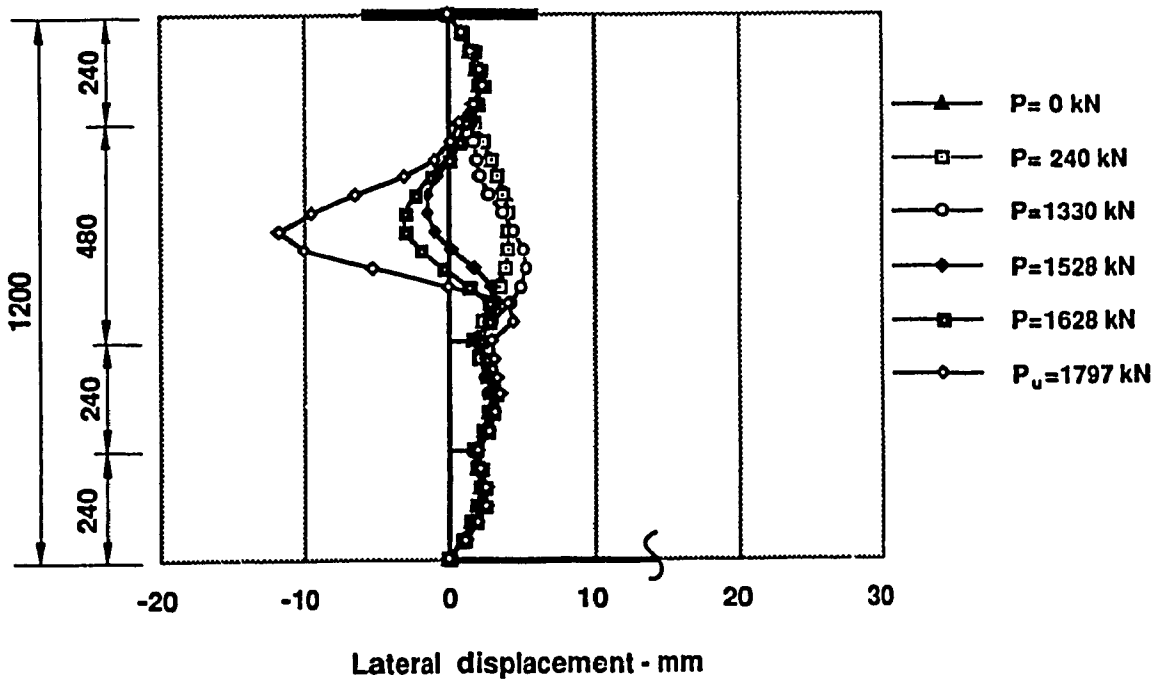

Figure 4.88 Deflection of Web under Loading - Section A
Box Girder Type A. Web Stiffening Type 4.(ii)

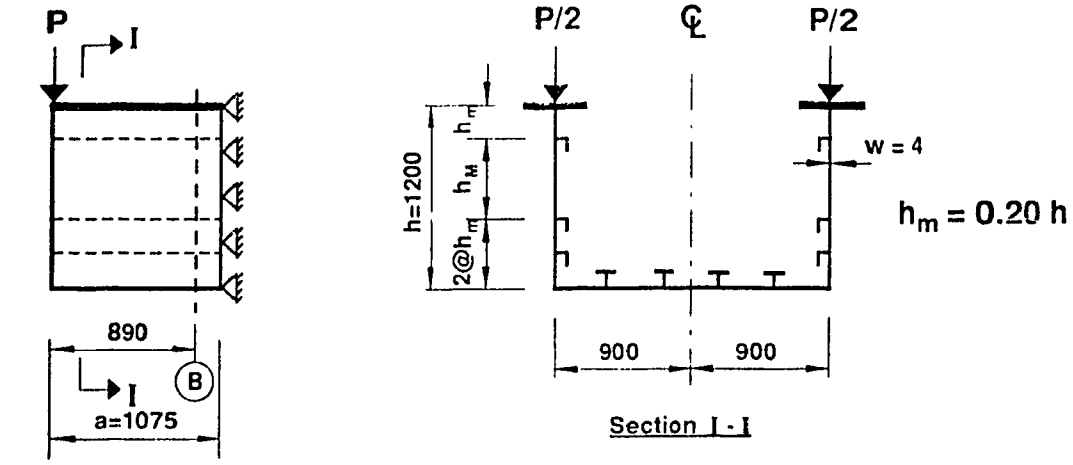

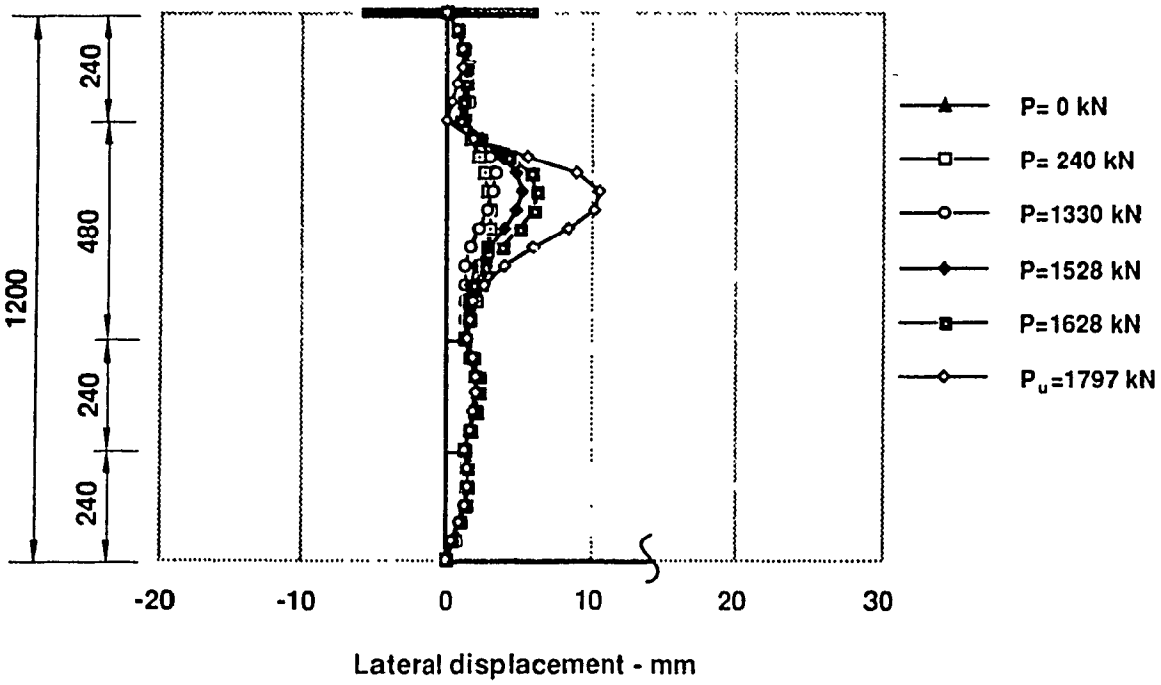

Figure 4.89 Deflection of Web under Loading - Section B
Box Girder Type A. Web Stiffening Type 4.(ii)

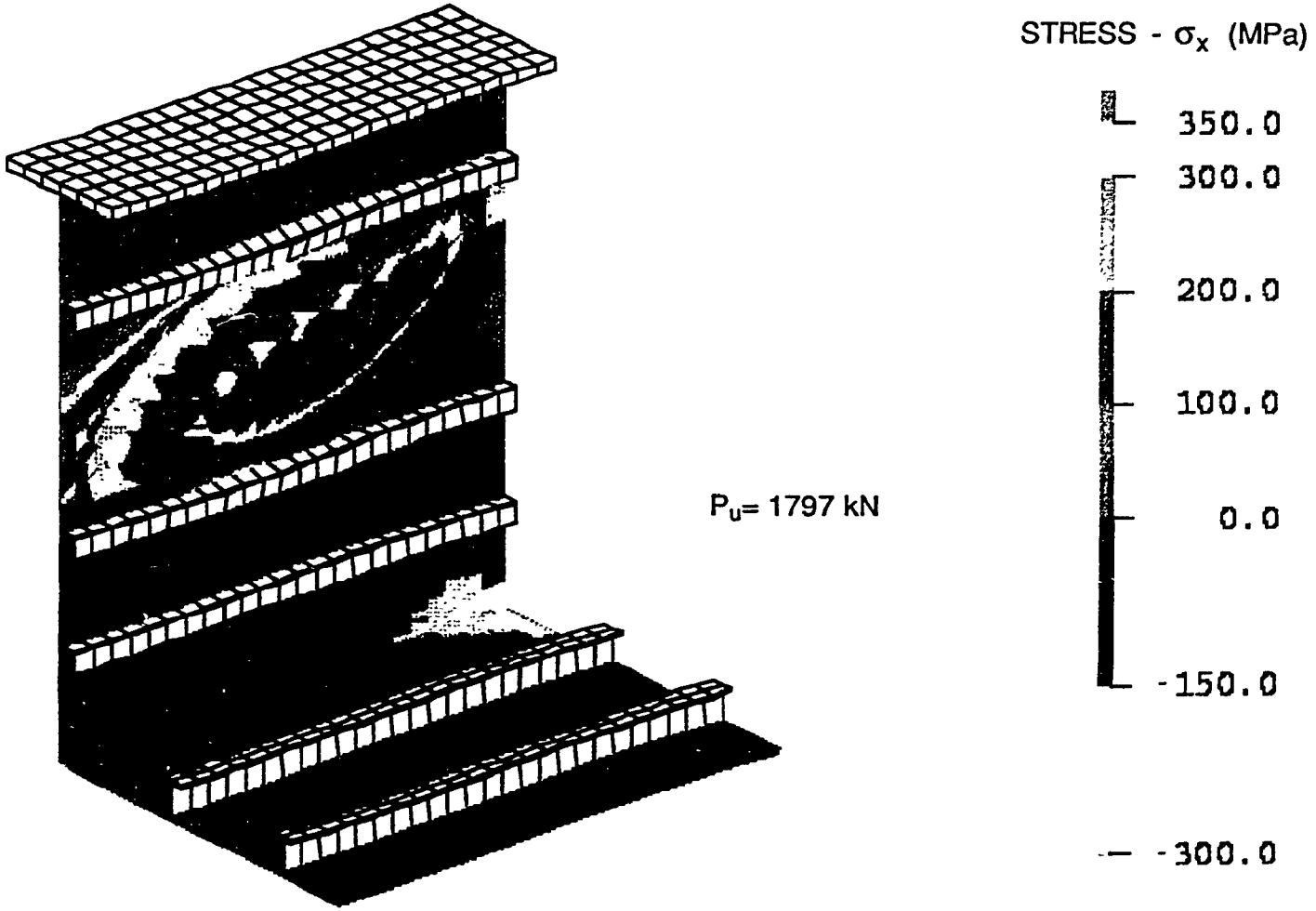

Figure 4.90 Normal Stress Distribution
Box Girder Type A. Web Stiffening Type 4.(ii)

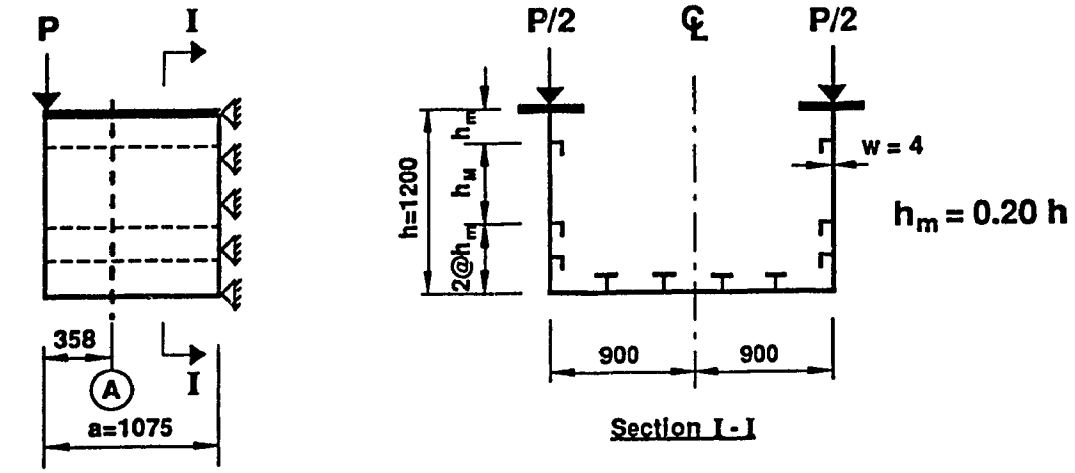

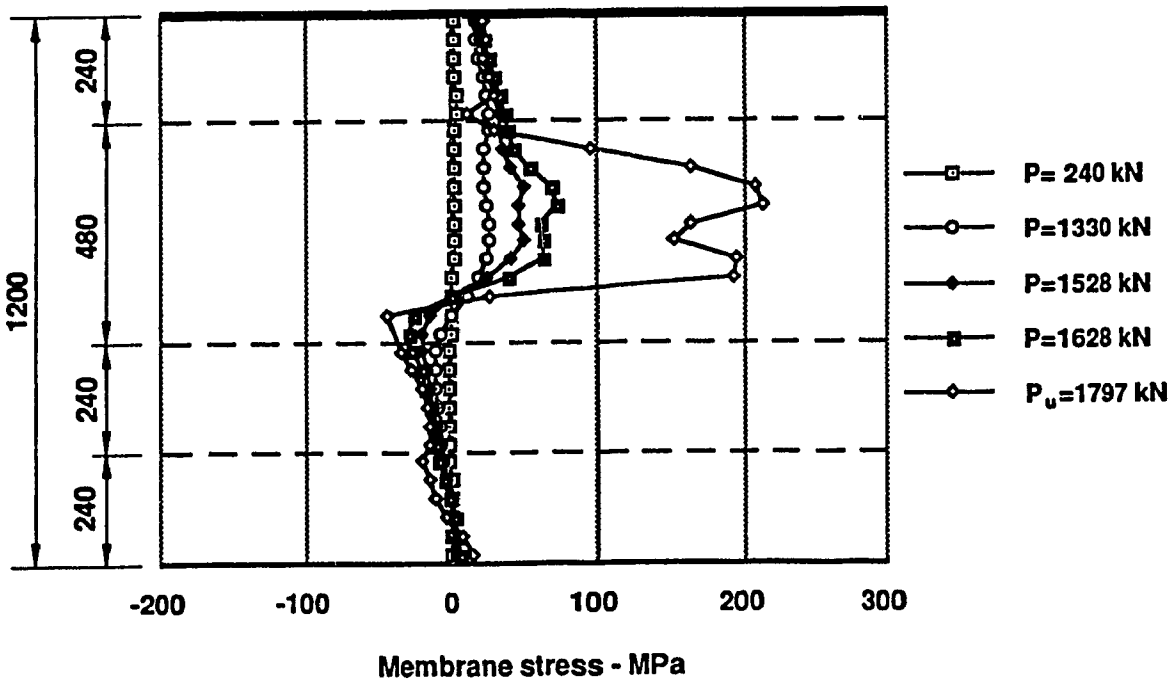

Figure 4.91 Distribution of Membrane Stresses - σ_x in the Web at Section A Box Girder Type A. Web Stiffening Type 4.(ii)

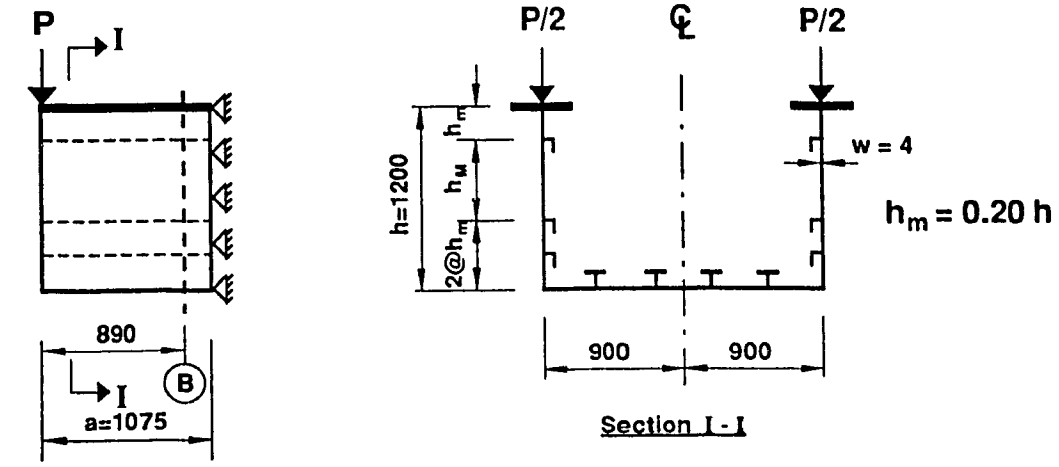

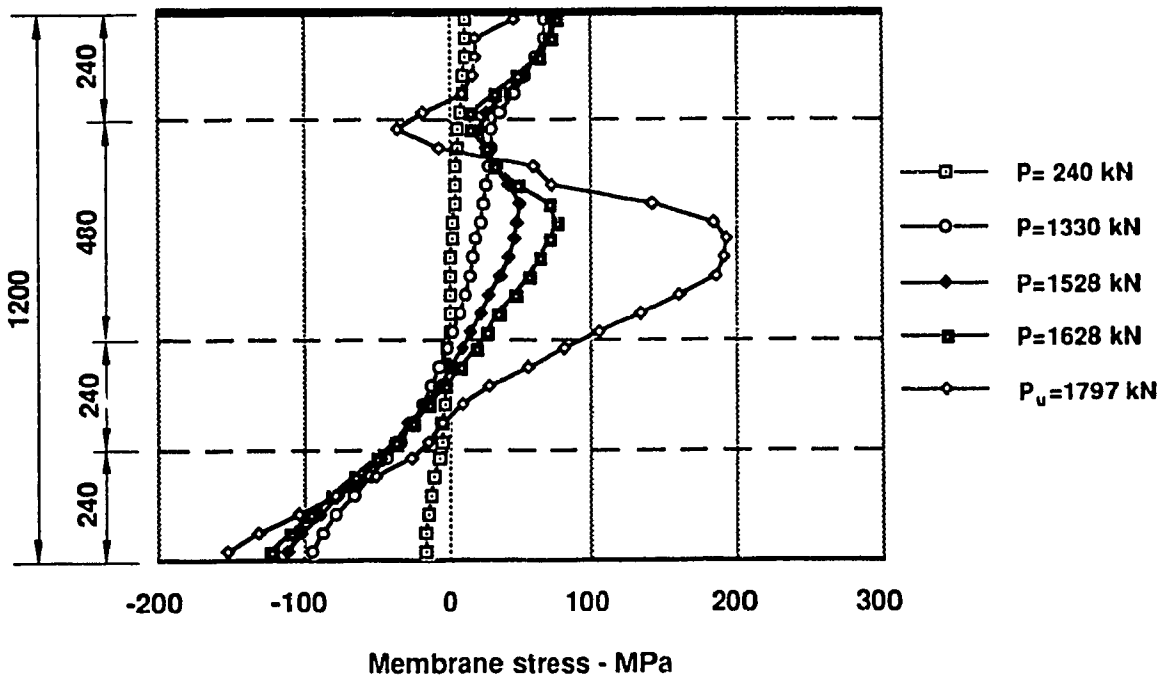

Figure 4.92 Distribution of Membrane Stresses - σ_x in the Web at Section B Box Girder Type A. Web Stiffening Type 4.(ii)

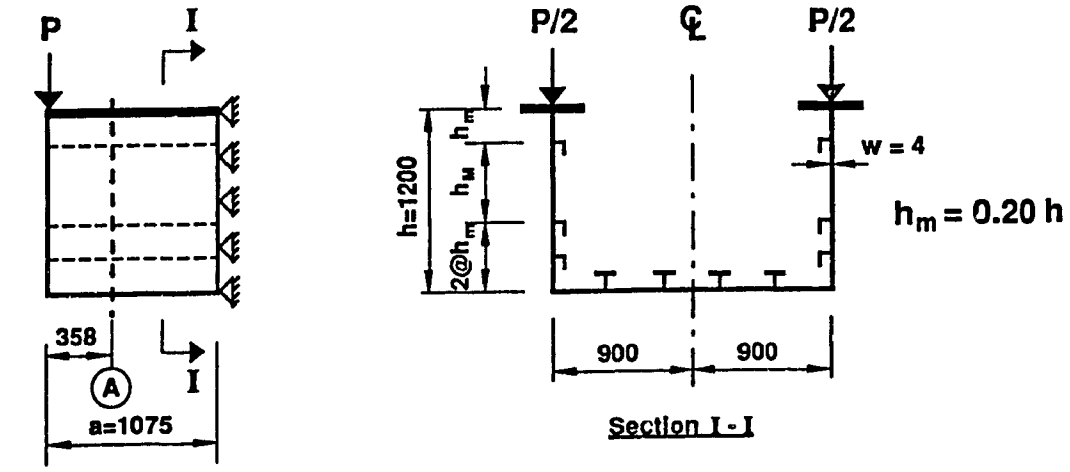

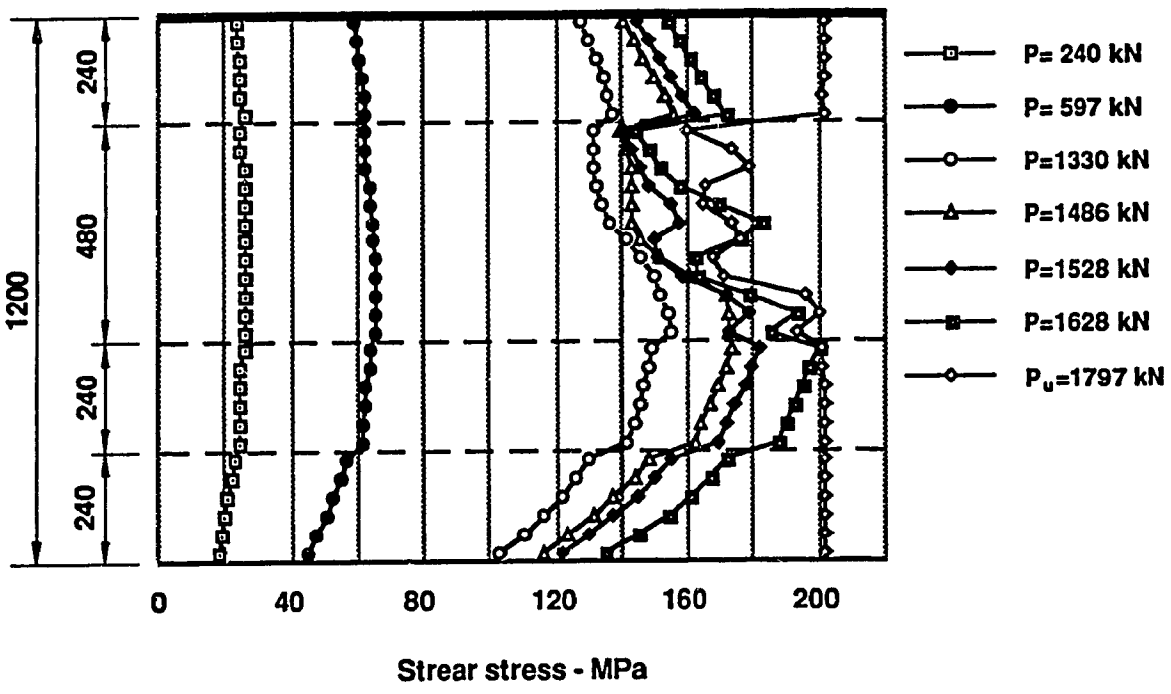

Figure 4.93 Distribution of Shear Stresses in the Web at Section A Box Girder Type A. Web Stiffening Type 4.(ii)

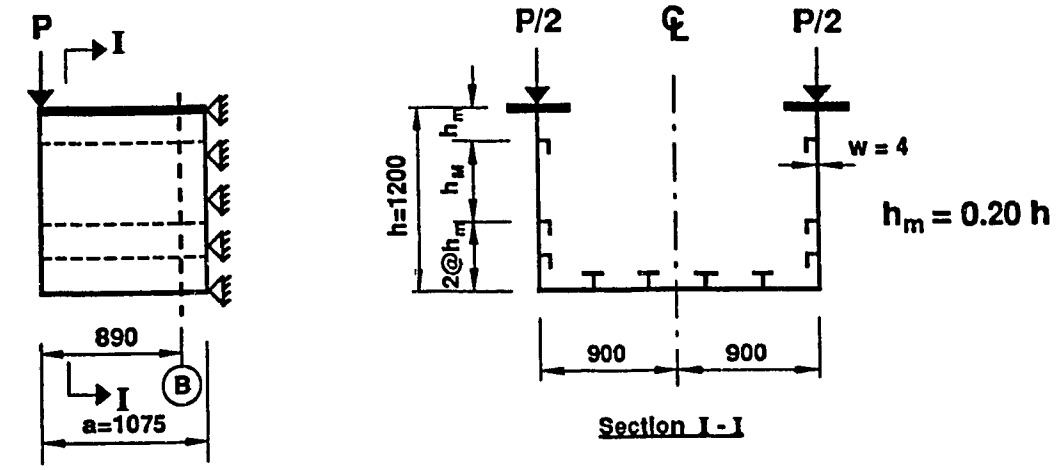

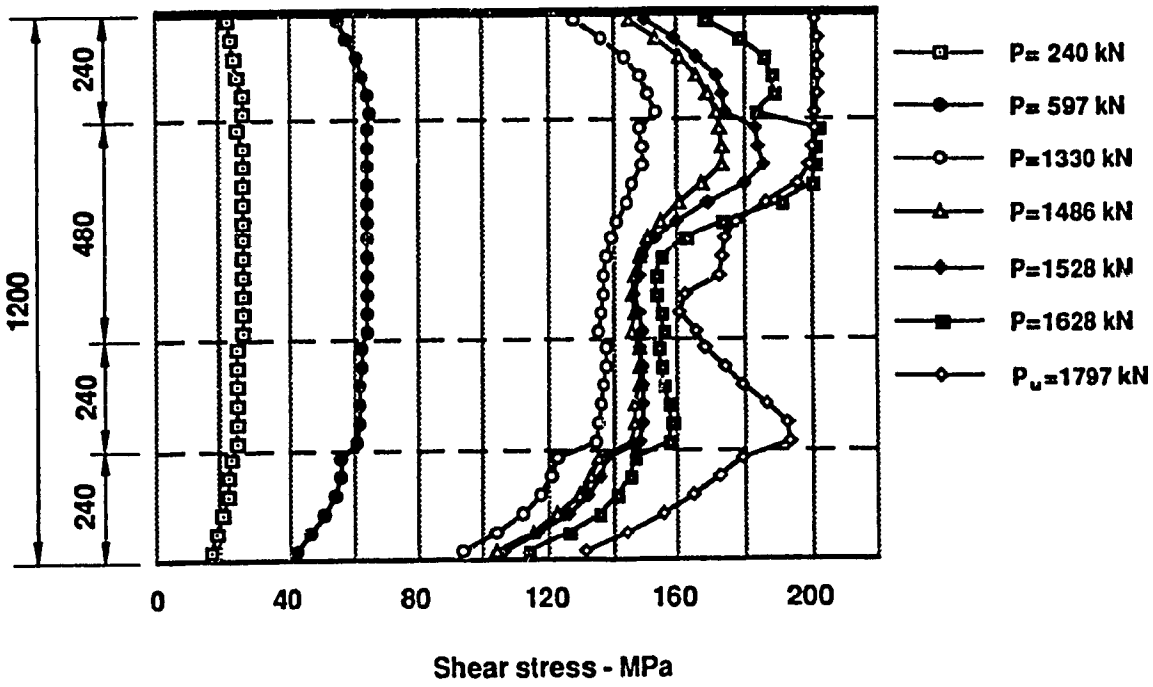

Figure 4.94 Distribution of Shear Stresses in the Web at Section B Box Girder Type A. Web Stiffening Type 4.(ii)

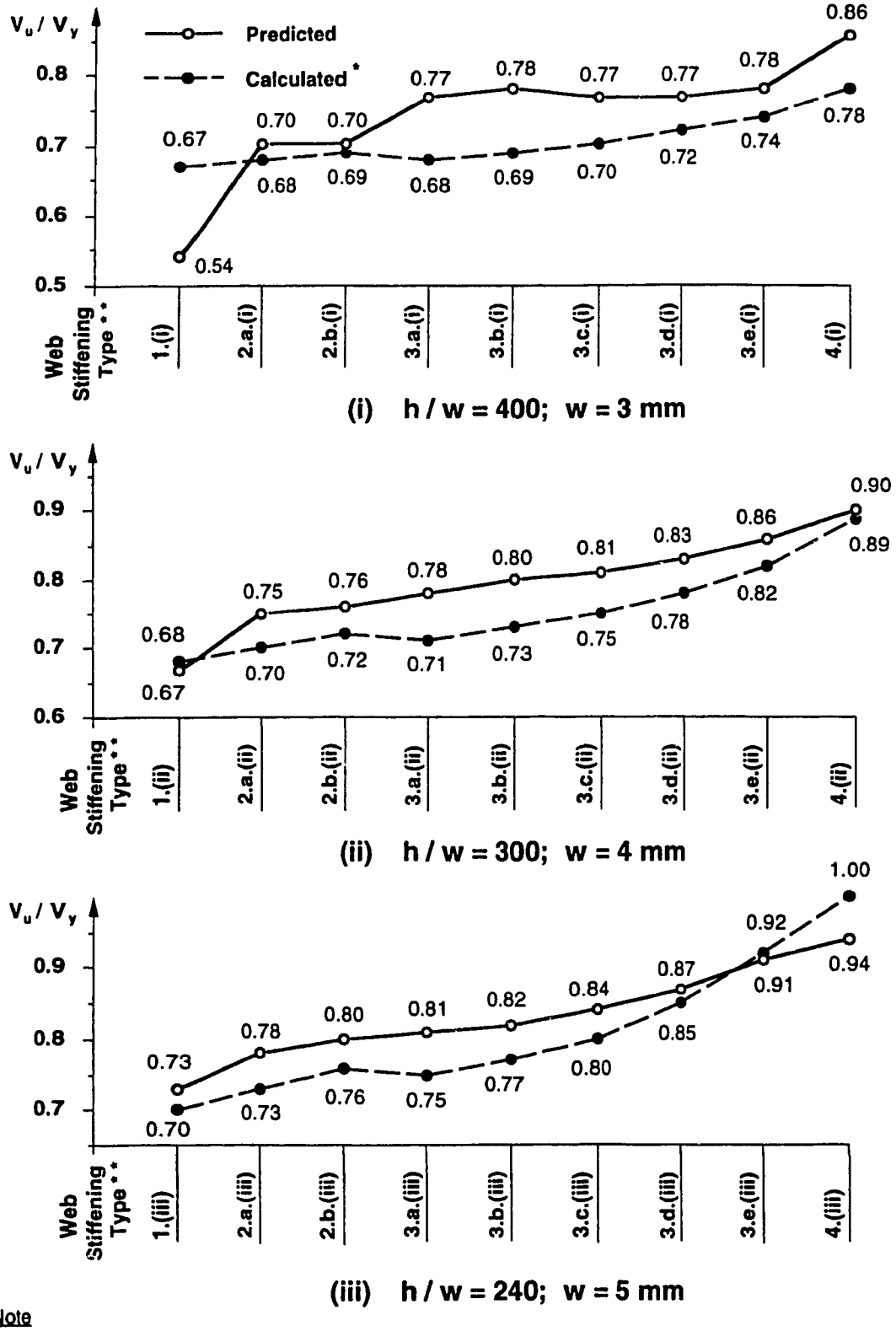

Note

* See "Note" - Table 4.6.

** For "Web Stiffening Type" see Figure 4.2.

Figure 4.95 Predicted and Calculated Ultimate Shear Resistance of Box Girder Webs

CHAPTER 5

SUMMARY AND CONCLUSIONS

5.1 Summary

Results of an extensive parametric study on buckling behaviour and ultimate strength of longitudinally unstiffened and stiffened box girder webs subjected to shear and combined shear and bending was presented.

Formulation of a numerical model for analyzing the large deflection elasto-plastic response of stiffened webs has been successfully accomplished. Both residual stresses and initial geometric imperfections specific to Canadian practice were included. Von Mises yield criterion and an associated flow rule were adopted and finite element method used to solve the plate equations. A total Lagrangian formulation was employed throughout this study, together with the full Newton method. The soundness of the present approach was checked against other existing methods by comparing the results from each method, and a very good correlation was found.

The superiority of the discretely stiffened plate approach in prediction of the buckling behaviour and ultimate strength of box girder webs was proved by comparison with experimental data and the results obtained by using some of

the simplified analytical models. Analytical predictions of the behaviour and strength of box girder webs were carried out on simulated box girders of the experimentally tested box girder model. Based on a very good agreement between the numerical predictions and the results of tests on two cantilever beams, where differences of only 2 and 6 percent were found, an extensive parametric study on box girder webs was carried out. Practical levels of residual stresses and initial geometric imperfections likely to be encountered in steel box girders built in Canada were considered. Plate panel/subpanel aspect and slenderness ratios in the range currently used in design of these bridge structures were also employed as parameters.

To complete the picture of box girder webs behaviour, an extension to slender webs was done and the results are worth noting.

Ultimate load curves applicable to design of box girders were defined for each type of stiffening.

5.2 Conclusions

This study on ultimate strength and behaviour of box girder webs adds to the limited basic data on the subject and contributes towards a better understanding of the collapse behaviour of steel box girders. Information gained on the interaction of the compression flange with the adjacent web considered in the analytical model makes this study unique at the present time. This has lead to a very good agreement between the predicted and experimentally determined behaviour and ultimate resistance.

From the parametric study the following conclusions were drawn:

1. Compression flanges of box girders of thickness comparable with that of webs provides a lower axial and bending rigidity than the thicker and narrower tension flange.

2. Longitudinal stiffeners bounding the large web panel must be designed for the reactive compressive force created by the unbalanced shear stress acting on each side of the stiffener.

3. New and useful data on the behaviour and ultimate strength of box girder webs subjected to shear and combined shear and bending have been generated.

4. The ultimate resistance of box girder webs subjected to shear is practically not affected by the presence of residual stresses even though the stiffness of the web subpanels is reduced in the early stages of loading.

5. Although the expressions do not model the true behaviour, the ultimate shear resistance of box girder webs calculated using the empirical design formulas specified for plate girders in Canadian bridge design code are generally in good agreement with the predicted ones under the condition that: elastic critical buckling shear stress of the web subpanel of maximum slenderness ratio is used in conjunction with the hypothetical tension-field postbuckling stress corresponding to the overall web panel.

6. For box girder webs subjected to combined shear and bending in which $V_u / V_y > 0.6$ the interaction starts at $M_u / M_y = 0.6$ and consequently a new interaction design formula is proposed.

5.3 Future Work

As further experimental data on ultimate resistance of box girder webs become available it could be useful to correlate these results with the ones predicted by the present study.

A more detailed parametric study on box girder webs subjected to combined shear and bending is considered as absolutely necessary. This will lead to a more complete understanding of the box girder behaviour at the ultimate loads so that simple but rational rules can be developed for the design of these structures.

The effect, if any, of sloped webs on the buckling behaviour and the ultimate strength of box girders should be examined because of their extensive use in box girder bridges.

REFERENCES

1. Dowling, P. J. et al. 1973. Experimental and predicted collapse behaviour of rectangular steel box girders. Proc. Intl. Conf. Steel Box Girder Bridges, ICE, London, pp. 77-94.

2. Flint, A. R. and Horne, M. R. 1973. Conclusion of research programme and summary of parametric studies. Proc. Intl. Conf. Steel Box Girder Bridges, ICE, London, pp. 173-192.

3. Horne, M. R. 1976. Ultimate capacity of longitudinally stiffened plates used in box girders. Proc. Inst. Civ. Engrs., Part 2, vol. 61, pp. 253-280.

4. Thimmhardy, E. 1988. Influence of residual stresses and geometric imperfections on buckling strength of stiffened compression flanges of steel box girder bridges. Ph.D. Thesis, Concordia University, Montreal, Quebec, Canada.

5. Rockey, K. C., Evans, H. R. and Porter, D. M. 1973. The ultimate load capacity of stiffened webs subjected to shear and bending. Proc. Intl. Conf. Steel Box Girder Bridges, ICE, London, pp. 45-61.

6. Dowling, P. J. et al. 1973. The behaviour up to the collapse of load bearing diaphragms in rectangular and trapezoidal stiffened steel box girders. Proc. Intl. Conf. Steel Box Girder Bridges, ICE, London, pp. 95-117.

7. Massonnet, Ch. and Maquoi, R. 1973. New theory and tests on ultimate strength of stiffened box girders. Proc. Intl. Conf. Steel Box Girder Bridges, ICE, London, pp. 131-144.

8. Korol, R. M., Thimmhardy, E. G. and Cheung, M. S. 1987. An experimental investigation of the effects of steel box girders. Canadian Journal of Civil Engineering, Vol. 15, pp. 443-449.

9. Thimmhardy, E. G. 1991. Nonlinear analysis of buckling behaviour of steel box girder components. Computers & Structures, Vol. 40, pp. 469-474.

10. Timoshenko, S. P. and Gere, J. M. 1961. Theory of elastic stability. Second edition, McGraw-Hill.

11. Basler, K. and Thurlimann, B. 1961. Strength of plate girders in bending. Journal of Structural Division, Proceedings, ASCE, August, pp. 153-181.

12. Basler, K. 1961. Strength of plate girders in shear. Journal of Structural Division, Proceedings, ASCE, October, pp. 151-180.

13. Basler, K. 1961. Strength of plate girders under combined bending and shear. Journal of Structural Division, Proceedings, ASCE, October, pp. 181-197.

14. Basler, K. et al. 1960. Web buckling tests on welded plate girders. Welding Research Council Bulletin. No. 64, September.

15. Rockey, K. C. and Skaloud, M. 1968. Influence of flange stiffness upon the load carrying capacity of webs in shear. Proc. 8th Congress IABSE, New York, pp. 429-439.

16. Rockey, K. C., and Skaloud, M. 1972. The ultimate load behaviour of plate girders loaded in shear. The Structural Engineer, vol. 50, pp. 29-47.

17. Chern, C. and Ostapenko, A. 1969. Ultimate strength of plate girders under shear. Fritz Engineering Laboratory Report No. 328.7. Lehigh University, USA.

18. Komatsu, S. 1971. Ultimate strength of stiffened plate girders subjected to shear. Proceedings of IABSE Colloquium, London, pp.49-65.

19. Porter, D. M., Rockey, K. C. and Evans, H. R. 1975. The collapse behaviour of plate girders loaded in shear. The Structural Engineers, Vol. 53, pp. 313-325.

20. Rockey, K. C., Evans, H. R. and Porter, D. M. 1978. A design method for predicting the collapse behaviour of plate girders. Proc. Instn. Civil Engineers, Part 2, vol. 65, pp. 85-112.

21. Horne, M. R. and Grayson, W. R. 1983. The ultimate load behaviour of longitudinally stiffened web panels subjected to shear stress. Proc. Instn. Civil Engineers, Part 2, vol. 75, pp. 175-203.

22. Horne, M. R. and Grayson, W. R. 1983. The ultimate load behaviour of stiffened web panels subjected to combined stress. Proc. Instn. Civil Engineers, Part 2, vol. 75, pp. 635-656.

23. Marsh, C. 1982. Theoretical model for collapse of shear webs. ASCE, Journal of The Engineering Mechanics Division, Vol. 108, pp. 819-832.

24. Marsh, C. 1985. Photoelastic study of postbuckled shear webs. Canadian J. of Civ. Engrg., 12(2).

25. Marsh, C. et al. 1988. Finite element analysis of postbuckled shear webs. ASCE, Journal of The Structural Division, Vol. 114, pp. 1571-1587.

26. Ajam, W., and Marsh, C. 1991. Simple model for shear capacity of webs. ASCE, Journal of The Structural Engineering, Vol. 117, pp. 411-422.

27. Dubas, P. and Gehrin, E. 1986. Behaviour and design of steel plate structures. ECCS Publication. No. 44. TWG 8.3.

28. Vilnay, O. 1990. The behaviour of a web plate loaded in shear. Thin-Walled Structures, Vol. 10, pp.161-174.

29. Rahal, K. N. and Harding, J. E. 1990. Transversely stiffened girder webs subjected to shear loading — part 1: behaviour. Proc. Instn. Civ. Engrs, Part 2, Vol. 89, pp. 47-65.

30. Rahal, K. N. and Harding, J. E. 1990. Transversely stiffened girder webs subjected to shear loading –– part 2: stiffener design. Proc. Instn. Civ. Engrs, Part 2, Vol. 89, pp. 67-87.

31. Rockey, K. C., Valtinat, G. and Tang, K. H. 1981. The design of transverse stiffeners on webs loaded in shear — an ultimate load approach. Proc. Instn. Civil Engineers, Part 2, vol. 71, pp. 1069-1099.

32. Ostapenko, A. and Chern, C. 1970. Strength of longitudinally stiffened plate girders under combined loads. Fritz Engng. Lab. Reported no. 328.10. December.

33. Ostapenko, A. and Chern, C. 1971. Ultimate strength of longitudinally stiffened plate girders under combined loads. Proceedings of IABSE Colloquium, London, Reports of the Working Commissions, Vol. 11, pp. 301-313.

34. Evans, H. R., Porter, D. M. and Rockey, K. C. 1978. The collapse behaviour of plate girders subjected to shear and bending. IABSE Proceedings (P-18/78), Zurich, pp. 1-20.

35. Pulthli, R. S., Supple, W. J. and Crisfield, M. A. 1978. Collapse behaviour of rectangular steel box girders. The Structural Engineer, Vol. 56B, pp. 75-84.

36. Wolchuk, R. and Mayrbaurl, R. M. 1980. Proposed design specifications for steel box girder bridges. Report No. FHWA-TS-80-205, Fed. Highway Admn., Washington, D. C.

37. Mele, M. and Puhali, R. 1985. Ultimate load behaviour of longitudinally and transversally stiffened web plates loaded in shear. Eng. et arch. Suisses. pp. 15-18.

38. Canadian Standard Association. 1988. CAN/CSA-S6-88. Design of highway bridges. Rexdale, Ontaria.

39. Cooper, P. B. 1965. Bending and shear strength of longitudinally stiffened plate girders. Friz Engineering Laboratory Report, No. 304.6, Lehigh University, Bethlehem.

40. Cooper, P. B. 1967. Bending and shear strength of longitudinally stiffened plate girders. Proc. of ASCE, Journal Struct. Div., ST2, pp.419-415.

41. Rockey, K. C., Evans, H. R. and Porter, D. M. 1977. Tests on longitudinally reinforced plate girders subjected to shear. Stability of Steel structures, Second International Colloquium, IABSE, PP. 295-304.

42. Rockey, K. C., Evans, H. R. and Porter, D. M. 1974. The ultimate shear load behaviour of longitudinally reinforced plate girder. Proceedings of Symposium on Structural Analysis. Non-Linear Behaviour and Techniques, TRRL, pp. 163-174.

43. Ostapenko, A. 1980. A shear strength of longitudinally stiffened plate girders. Structural Stability Research Council, Proceedings, New york, pp. 36-40.

44. Evans, H. R. 1983. Longitudinally and transversely reinforced plate girders. Plated Structures — Stability and Strength. Applied Science Publishers, London, pp. 1-37.

45. Dowling, P. J., Harding, J. E. and Frieze, P. A. 1977. Steel plated structures —- an international symposium. Crosby Lockwood Staples, London.

46. Rockey, K. C. and Evans, H. R. 1981. The design of steel bridges. Granada, London.

47. Narayanam, R. 1983. Plated structures — stability and strength. Applied Science Publishers, London.

48. International Association for Bridge and Structural Engineering. 1971. Proceedings of IABSE colloquium, London.

49. Ontario Ministry of Transportation. 1991. Ontario highway bridge design code. 3rd Edition, Toronto, Ontario.

50. American Association of State Highway and Transportation Officials. 1989. Standard specifications for highway bridges. 14th Edition, Washington, DC.

51. British Standard Institution. 1988. BS 5400: Part 3. Code of practice for design of steel bridges, London.

52. Rockey, K. C. 1977. The design of web plates for plate and box girders — a state of the are report. Steel Plated Structures — An International Symposium. Crosby Lockwood Staples, London, pp. 459-485.

53. Bathe, K. J., 1982. Finite element procedures in engineering analysis. Prentice-Hall, Inc., Englewood Cliffs, New Jersey.

54. ADINA-Users Manual. Report AE 81-1, ADINA Engineering, Sept. 1981.

55. Timoshenko, S. P. and Woinowsk-Kriege, S. 1959. Theory of plate and shells. Second edition, McGraw-Hill.

56. Praeger, W. and Hodge, P. G. Jr., 1973. Engineering plasticity. Van Nostrand Reinhold Co., London.

57. Martin, J. B. 1975. Plasticity: fundamental and general results. the MIT Press, Cambridge, Mass.

58. Johnson, W. and Mellor, P. B. 1973. Engineering plasticity. Van Nostrand Reinhold Co., London.

59. Oden, J. T., 1972. Finite element of nonlinear continua. McGraw-Hill Book Company, New York.

60. Bathe, K. J. 1976. An assessment of current solution capabilities for nonlinear problems in solid mechanics. Numerical Methods for Partial Differential Equations - III, Ed. B. Hubbard, Academic Press, N.Y.

61. Bathe, K. J. and Cimento, A. P. 1980. Some practical procedures for the solution of nonlinear finite element equations. Journal of Comp. Meth. in Applied Mech. and Eng., Vol. 2, pp. 59-85.

62. Bathe, K. J. 1981. Nonlinear finite element analysis and ADINA. Computers and Structures, Vol. 13, No. 516.

63. Levy, S. 1942. Bending of rectangular plates with large deflections. NACA Report No. 737, Also NACA Tech. Notes No. 846.

64. Von, K. T. 1910. Festigkeitsprobleme in Mashinenbau. Encyklopadie der Mathematishen Winssernchaften, Vol. 4, B.G. Teubner, Leipzig, pp. 348-351.

65. Crisfield, M. A. 1975. Collapse analysis of box-girder components using finite elements. TRRL Supplementary Report 164 U.C., Dept. of Environment, pp. 45-67.

66. Coan, J. M. 1951. Large deflection theory for plates with small initial curvature loaded in edge compression. ASCE, Journal of Applied Mechanics, Vol. 18, Trans. ASME, Vol. 73, pp. 143-151.

67. Yamaki, N. 1959. Post-buckling behaviour of rectangular plates with small initial curvature loaded in edge compression. Journal of Applied Mechanics, Trans. ASCE, Vol. 26, pp. 407-414, continued in Vol. 27, pp. 335-342.

68. Walker, A. C. 1969. The post-buckling behaviour of simply supported square plates. Aero Quarterly, Vol. 20, pp. 203-222.

69. Marcal, P. V. 1969. Large deflection analysis of elastic-plastic plates and shells. Proc. First Int. Conf. in Pressure Vessel Tech., ASME/Royal Netherlands Engineering Society, Delft, pp. 75-87.

70. Maxham, K. E. 1971. Theoretical prediction of the strength of welded steel plates in compression. Cambridge Univ., Dept. of Eng., Report CUED/C-Struct/TR2.

71. Maxham, K. E. 1971. Buckling tests on individual welded steel plates in compression. Cambridge Univ., Dept. of Eng., Report CUED/C-Struct/TR3.

72. Thimmhardy, E. and Korol, Robert M. 1987. Geometric imperfections and tolerances for steel box girder bridges. Canadian Journal of Civil Engineering, Vol. 15, pp. 437-442.

73. Harding, J. E. et al. 1977. Ultimate load behaviour of plate under combined direct and shear in - plane loading. Steel Plated Structures — An International Symposium. Crosby Lockwood Staples, London, pp. 369-403.